Benjamin Samuel Lutz

Smart Manufacturing System for Process Optimization Regarding Deviations among Material Batches

FAU
University Press

Benjamin Samuel Lutz

Smart Manufacturing System for Process Optimization
Regarding Deviations among Material Batches

FAU Studien aus dem Maschinenbau

Band 432

Herausgeber/-innen:

Prof. Dr.-Ing. Jörg Franke
Prof. Dr.-Ing. Nico Hanenkamp
Prof. Dr.-Ing. habil. Tino Hausotte
Prof. Dr.-Ing. habil. Marion Merklein
Prof. Dr.-Ing. Sebastian Müller
Prof. Dr.-Ing. Michael Schmidt
Prof. Dr.-Ing. Sandro Wartzack

Benjamin Samuel Lutz

Smart Manufacturing System for Process Optimization Regarding Deviations among Material Batches

Dissertation aus dem Lehrstuhl für Fertigungsautomatisierung und Produktionssystematik (FAPS)
Prof. Dr.-Ing. Jörg Franke

Erlangen
FAU University Press
2024

Smart Manufacturing System for Process Optimization Regarding Deviations among Material Batches

Intelligentes Fertigungsassistenzsystem für die Prozessoptimierung hinsichtlich Abweichungen zwischen Materialchargen

Der Technischen Fakultät
der Friedrich-Alexander-Universität
Erlangen-Nürnberg

zur
Erlangung des Doktorgrades Dr.-Ing.

vorgelegt von

Benjamin Samuel Lutz, M.Sc.

aus Lauf an der Pegnitz

Als Dissertation genehmigt
von der Technischen Fakultät
der Friedrich-Alexander-Universität Erlangen-Nürnberg

Tag der mündlichen
Prüfung: 25.07.23

Gutachter: Prof. Dr.-Ing. Jörg Franke
                    Prof. Dr.-Ing. Prof. h.c. Dirk Biermann, TU
                    Dortmund

Preface

This thesis was written in the context of my employment as a research scientist at the corporate technology team T REE MDM FMP-DE at Siemens AG and my PhD student work at the Institute for Factory Automation and Production Systems (FAPS) of Friedrich-Alexander-Universität Erlangen-Nürnberg (FAU).

My special thanks goes to Prof. Dr.-Ing. Jörg Franke, head of the chair and my doctoral supervisor, for his trust in me and for giving me the opportunity to pursue my doctorate. His constant support and scientific advice not only made a great contribution to this work, but also helped me advance personally.

Furthermore, I would like to express my thanks to Prof. Dr.-Ing. Nico Hanenkamp as chairperson of the examining committee, Prof. Dr.-Ing. Prof. h.c. Dirk Biermann for providing the second review, and Prof. Dr.-Ing. Dietmar Fey as the additional member of the examining committee.

I would also like to thank my colleagues both at Siemens and at FAPS for the engaging and helpful scientific exchange. In particular, I would like to thank my supervisors at Siemens, Dr. Carsten Schuh and Daniel Regulin, my research sector director at FAPS, Jonathan Fuchs, as well as my colleagues and friends, Dominik Kisskalt, Fabian Hartner, Tobias Hauser, Philipp Breese, Matteo Pantano, Raven Reisch, Alexander Schmidt, Stefan Seebauer, and Tobias Gaag. Furthermore, I would like to thank the remaining staff at FAPS and colleagues at the various T REE MDM research groups for the good and collegial collaboration and support of my research, which I have greatly appreciated.

Additionally, I would like to thank my parents, Dr. Claudia Buerhop and Dr. Norbert Lutz, my sister Judith Lutz, and my grandparents Christa and Dr. Hans Buerhop for sparking my curiosity and encouraging me to investigate the world from an early age. Last but not least, I have to express my gratitude to my partner Katrina Lutz, who has made a significant contribution to this work, through her never-ending support and by providing me with the space I needed as well as strengthening my confidence in my career.

Contents

List of Symbols and Abbreviations

List of Abbreviations

Abbreviation	Description
2D	two-dimensional
3D	three-dimensional
AE	acoustic emission
AI	artificial intelligence
ANN	artificial neural network
API	application programming interface
AutoML	automated machine learning
BBI	batch behavior index
BUE	built-up-edge
CCD	charge-coupled device
CFRP	carbon fiber reinforced plastics
cGAN	conditional generative adversarial network
CMOS	complementary metal-oxide-semiconductor
CNN	convolutional neural network
DSLR	digital single lens reflex
DT	decision tree
DTW	dynamic time warping
GAN	generative adversarial network
G-Code	machine control instructions
GPU	graphics processing unit
GUI	graphic user interface
HMI	human machine interface
ID	identifier
IoT	internet of things
IoU	intersection over union
kNN	k-nearest-neighbor
LIBS	laser-induced breakdown spectroscopy

Abbreviation	Description
LR	logistic regression
mIoU	mean intersection over union
ML	machine learning
NB	Naïve Bayes
NC	numeric control
OES	optical emission spectrometer
OSS	open source software
PCA	principal component analysis
PLC	programmable logic controller
PMI	positive material identification
png	portable network graphics
ReLU	rectified linear unit
RF	random forest
ROI	region of interest
SMaPOMBa	smart manufacturing system for process optimization regarding deviations among material batches
SVM	support vector machine
TCM	tool condition monitoring
WAAM	wire arc additive manufacturing
XRF	X-ray fluorescence

List of Symbols

Symbol	Unit	Description
a_p	mm	cutting depth
$\mathcal{B}$		material batch
$\widehat{\mathcal{B}}$		predicted material batch
$\mathcal{C}$		set of cutting parameters
f	mm	feed rate
F_a	N	active force

Symbol	Unit	Description
F_c	N	cutting force
F_f	N	feed force
ϕ		feature map
Φ		set of feature maps
FN		false negatives
FP		false positives
F_p	N	passive force
F_z	N	machining force
$\mathcal{H}$		historic data
$\mathcal{M}$		machining state
$\boldsymbol{\mathcal{M}}$		set of machining state
M		type of classification model
$\mathbf{M}$		set of classification model types
MRR	$cm^3\,min^{-1}$	material removal rate
NCR	$cm^3\,min^{-1}$	net chip rate
n_{tc}		number of tool changes
P		model hyperparameter
$\mathbf{P}$		set of model hyperparameters
p		pixel-of-interest
ψ		BBI entry
r		reference image
$\mathcal{S}$		scene
T	min	tool life
$\mathcal{T}$		tolerance for data selection
$\boldsymbol{\mathcal{T}}$		set of tolerances for data selection
t_c	min	tool change time
t_m	min	machining time
TN		true negatives
t_n	min	non-productive time
TP		true positives

Symbol	Unit	Description
t_p	min	production time
t_{tc}	min	time per tool change
U		set of images
u		image
V	cm³	to-be-machined-volume
v		preprocessed image
VB	µm	flank wear width
v_c	m min⁻¹	cutting speed
w		ground truth masks
$\widehat{w}$		predicted mask
W		set of ground truth masks
X		feature vector
$\tilde{X}$		processed feature vector
y		label
$\hat{y}$		predicted label

List of Figures

List of Tables

1   Introduction

Subtractive manufacturing is one of the main manufacturing technologies used today for the production of various components. Due to this, there is a constant drive to improve subtractive manufacturing processes, which aim at improving product quality and productivity, while minimizing costs. To achieve this, tool degradation needs to be minimized while maximizing the material removal rate (MRR). Thus, the optimization of cutting parameters and therefore the prediction of tool life is crucial.

One prevailing challenge is the strong dependency of the manufacturing process on the workpiece material, specifically its machinability. Thus, when dealing with multiple materials of different machinability, flexible solutions are needed that can adapt the cutting process to each individual material. This can be seen for the machining of multi-material workpieces, where optimized machining can only be carried out when adapting the cutting parameters regarding the respective material being machined [1]. With the recent advances in additive manufacturing of combining multiple materials in the building process of metal parts, the task of post-processing these with subtractive manufacturing processes will be of great interest. A similar challenge is posed when machining materials with strong batch-specific characteristics. In such cases, the material properties might vary significantly among material batches [2, 3]. This can lead to the real behavior of a specific material batch not matching the expected, batch-agnostic, material behavior [4] as well as parts manufactured from different batches showing different behavior in their material properties [5] and intended use [6]. Even small deviations, such as a change in chemical composition within the nominal specifications, can significantly impact the consecutive manufacturing process [7, 8]. Thus, batch-specific process adaptation and parameter optimization is needed for the efficient production of high-quality parts [8].

While adapted machining is needed for both multi-material parts and differently behaving material batches, the characteristics of each situation differ. When machining multi-material workpieces, the number of different materials, their behavior, and their design are generally known. However, based on the impacts of the fabrication procedure [9] or due to geometrical complexity [10], the exact material transition point might be unknown. Contrarily, for material batch-related machinability deviations, neither the number of unique behavior patterns nor their explicit behavior is known. Furthermore, while for multi-material parameter optimization, the scope of the problem is fixed during operation, this is not the case when dealing with material

batches, as new batches with novel characteristics and behavior might be encountered during operation.

Besides, with the recent trend of Industry 4.0 and the progress in information technology, advanced data analytics through means such as machine learning (ML) become a promising tool for optimizing machining processes [11]. This manifests in the emerging research field of smart machining, which is searching for procedures to adapt machining processes based on acquired data to achieve a given objective. These objectives include purposes such as machine health monitoring [12], predictive maintenance, process parameter optimization, and improvement of product quality. [13]

Goal

Thus, the goal of this research is to leverage the potential of advanced data analytics to derive a smart manufacturing system, capable of identifying the machinability behavior of the currently machined material. Subsequently, corrective actions on how to optimize the process in regard to the detected machinability should be suggested. Thereby, the decision-making process of the operator can be supported and improved. Furthermore, as the number of batches are not known prior to operation, the system must detect such situations and interpolate information from the existing material batches. Throughout operation, ground-truth data should be gathered automatically to characterize novel batches and integrate them in the system, so that they will be correctly optimized for subsequent runs. Furthermore, the huge variety of cutting operations needs to be considered, requiring the solution to be flexible enough for easy adaptability to new environments. To enable a broad adoption of the derived solution, requirements regarding additional hardware for sensing and computation should be kept to a minimum while utilizing existing platforms.

Such a concept builds a fundamental building block of the factory of the future, as machine tools are made aware about the context they are working in. By acquiring detailed information about the machinability of the respective to-be-machined material, optimized cutting parameters are found, and by evaluating the cutting process after completion, ground-truth data for self-improvement is gathered. Thereby, the autonomy of machine tools is further increased.

Approach

To achieve this goal, the characterization of material batches should only be carried out once for novel material batches. Material batches behaving

similar to ones machined in the past, however, should be machined with the optimized parameters found while characterizing the respective most-similar historic material batch, thereby eliminating redundant material characterization. To enable automated material characterization, TCM systems are deployed. Through TCM, the condition of the cutting tool can be determined for given situations. Thus, it is possible to generate ground-truth data about the tool degradation and thus the tool lifetime, which is used to characterize novel materials.

Furthermore, a data-driven approach is realized, using the process data that can be acquired through the machine tool's numeric control (NC), to identify the currently being machined material as either novel or as any of the material batches encountered in the past. For the second case, existing information regarding process optimization should be stored and adapted to the current machining situation, thus allowing the recommendation of optimized cutting parameters. Due to the high variety of different machine tool types, the NC is the common denominator among these and is used as primary data supplier. As the NC does not offer enough computational power for the execution of advanced algorithms, edge devices and cloud computing will be utilized. To convey the computed information to technical systems as well as human users, technical interfaces and graphical user interfaces are needed.

Requirements for an Automated Process Optimization Regarding Material Batches

Based on the situation presented above, these general requirements for such a smart manufacturing system can be derived:

R1   Subtractive manufacturing processes should be optimized regarding deviations in machinability among material batches.

R2   Novel material batches must be detected as such, whereas known ones should be identified correctly.

R3   The number of material batches is not known prior to operation and can continuously increase throughout operation.

R4   Even without ground truth data for the machinability of a material batch, a limited process optimization should at least be possible.

R5   Novel materials should be characterized and integrated automatically.

R6   Throughout operation, the models should improve continuously.

A tool condition monitoring system will be integrated in the proposed system to assess the tool condition and to enable automated characterization of novel materials. As such a system is sophisticated on its own, further specific requirements are defined:

R7   Different types of wear defects should be detected and differentiated.

R8   The adaptation of the method to new environments needs to be effective.

To enable the proposed solution to be applied in industrial settings, it needs to be compatible with common shop floor scenarios. Thus, certain requirements are derived for the implementation and operation of the smart manufacturing system:

R9   The modules of the approach should be able to run individually.

R10   The system should be integrated effectively into modern machine tools.

Structure of the Thesis

Based on the approach and the defined requirements, the structure of this thesis, see Figure 1, is derived. In Chapter 2 the fundamentals of and the state of the art for the defined requirements are introduced, enabling the derivation of suitable methods from related approaches. Furthermore, research gaps are identified as research needs. Based on these research needs, concepts and methods are proposed in the following three main chapters. Chapter 3 investigates the topic of effective image segmentation, Chapter 4 details the research regarding material batch identification, and Chapter 5 adds process optimization while also combining all individual subtopics into an overarching smart manufacturing system and detailing the prototypical implementation. Using the implemented system, a validation of the proposed methods is carried out on multiple scenarios in Chapter 6. The thesis is concluded in Chapter 7 with a summary of the conducted research activities and an outline of future research activities.

Chapter 1: Introduction

Chapter 2: Derivation of the Need for Research in Material Batch-specific Process Optimization

Chapter 3: Image Segmentation for Low Volume and Highly Diverse Datasets	Chapter 4: In Situ Identification of Material Batches	Chapter 5: Smart Manufacturing System for Process Optimization Regarding Deviations among Material Batches

Chapter 6: Validation

Chapter 7: Summary and Outlook

Figure 1: The thesis is structured in three main chapters to derive a smart manufacturing system for batch-specific process optimization.

2 Derivation of the Need for Research in Material Batch-specific Process Optimization

In order to derive a smart manufacturing system for process optimization regarding the deviations among material batches, it is important to understand the underlying processes. Thus, in Section 2.1 the fundamentals of steel manufacturing and machining are introduced. Here, the importance of material machinability on the cutting process is shown. Consecutively, the concept of machinability is detailed and it is shown how there is variation not only between materials, but also between material batches.

After discussing the reason for machinability deviations among material batches, approaches for handling these deviations are reflected in Section 2.2. Subsequently, methods for the direct assessment of machinability as well as the identification and differentiation among different categories of materials are introduced and summarized.

The analysis of related material identification approaches highlights the importance of data-driven approaches and ML analysis. Thus, in Section 2.3 the concept of smart machine tools is analyzed in regard to their general architectures, sensing capabilities, and service distribution. Here, the concept of TCM in particular is reviewed as such systems seem promising for automated material characterization. Furthermore, the fundamentals and recent advances in the field of ML are introduced in Section 2.4. Finally, the relevant state of the art found is compared to the requirements to derive solution approaches and define research needs (Section 2.5).

Some aspects of this chapter were already discussed in student works supervised by the author [S1–S6]. Furthermore, central findings were made available to the scientific community in [P1].

2.1 Machinability Deviations among Material Batches

In this section, the fabrication procedure from iron ore to finished part is introduced (Section 2.1.1). Furthermore, the fundamentals of machining are touched briefly in Section 2.1.2 and the concept of machinability is detailed in Section 2.1.3. Thereby, the relation between deviations in the fabrication procedure and differences in machinability among material batches can be drawn (see Section 2.1.4).

2.1.1 Steel Fabrication Fundamentals

The first step in the steel manufacturing procedure is a primary forming process [14]. In general, three process alternatives can be differentiated (see Figure 2). In the first alternative, *casting to semi-finished parts*, technologies such as *ingot casting* and *continuous casting* are used to produce steel, which is consecutively fabricated using *metalworking* technologies to adjust shape and material properties, such as *rolling* and *forging*, before a subsequent machining process to produce the desired shape takes place. In the second alternative, *near net shape casting*, and third alternative, *powder metallurgy*, parts are produced close to their desired shape which can directly be post-processed in a machining step. [14] When comparing the popularity of each alternative, continuous casting is most ubiquitous with 85% of steel worldwide being produced with this methodology [15]. Furthermore, *heat treatment* steps are used to adjust material properties.
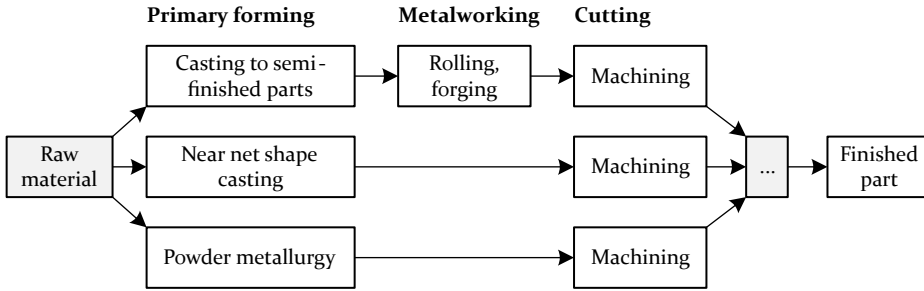
Figure 2: Simplified and generalized alternatives for manufacturing procedures, adapted from [14].

Forming

Steel is produced from iron ore in combination with coke and other supplements, which are melted and processed in blast furnaces, thereby producing pig iron [15]. To convert pig iron into steel, the carbon content needs to be reduced, unwanted elements need to be removed, and the desired alloying elements need to be adjusted as required by the specific steel grade [16]. The most common smelting process is the usage of blast furnaces, which can be seen in Figure 3 [16]. The smelting process requires three material groups: [17].

- iron ore
- fuel and reductants, such as coke
- slag former, such as limestone
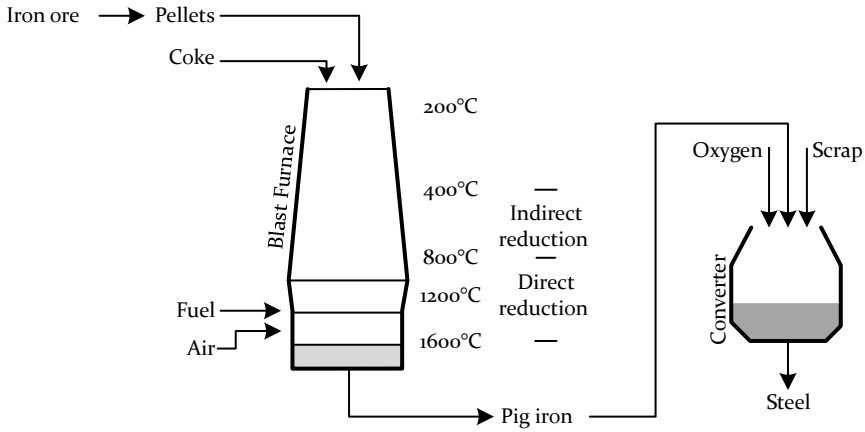
Figure 3: Simplified procedure of the blast furnace route, adapted from [15, 16].

The blast furnace uses hot air inserted at the bottom which moves to the top, thereby reacting with the materials and becoming furnace gas. Contrarily, the ore is reacting and undergoes reduction while making its way from the top to the bottom of the furnace. [17] Thus, the required iron ore needs to be pre-manufactured to pellets, as all products need to be fragmented to allow for gas flow through the furnace.

Indirect reduction with carbon monoxide (see Equations 1, 2, and 3) and direct reduction with carbon (see Equation 4) take place at temperatures between 400°C and 800°C, and between 800°C and 1200°C, respectively [15].

$$Fe_3O_4 + CO \rightarrow 3FeO + CO_2 \tag{1}$$

$$FeO + CO \rightarrow Fe + CO_2 \tag{2}$$

$$Fe_3O_4 + 4CO \rightarrow 3Fe + 4CO_2 \tag{3}$$

$$Fe_2O_3 + 3C \rightarrow 2Fe + 3CO \tag{4}$$

The pig iron produced by the blast furnace is now processed to produce steel at the desired material grades. The consecutive processes can be divided in primary metallurgy and secondary metallurgy. Primary metallurgy takes place in the *converter* with the goal of carbon-content reduction, removal of unwanted elements, and adjustment of the desired alloy composition. [17] To remove unwanted elements, the process of indirect oxidation is used [15]. Secondary metallurgy includes methods such as *vacuum metallurgy* and remelting processes with the goal of homogenization and further adjustment of alloy composition [15].

Heat Treatment

The primary microstructure of the material develops after the initial solidification of the melt, while the secondary microstructure is defined by the subsequent post-processing procedures, such as shaping and heat treatment [16]. Through heat treatment, the microstructure can be adjusted [16], and the material properties optimally fine-tuned [15]. Heat treatments typically consist of three phases: An initial heating, a holding period, and a cooling phase [16]. There are several heat treatment techniques including *hardening*, *tempering*, *annealing*, and *normalizing* [18].

In a typical hardening process, metal is initially austenized by heating and holding at a certain temperature and a consecutive quenching process for rapid cooling to avoid the formation of pearlite microstructures [16]. Thereby, the hardness and strength, but also the brittleness of the material are increased. To reduce the brittleness, which limits a steel's usability, tempering is used. In tempering, the material is heated at lower temperatures than during hardening, allowing the relief of internal stresses. Annealing methods are used similarly to improve a material's ductility, microstructure refinement, and a relief of internal stresses. To achieve this, the material is cooled down at an extremely slow rate after being heated to a desired temperature. Annealing allows for both the improvement of the material's machinability and the reduction of undesired effects of previous manufacturing steps [16]. While normalizing also involves the relief of internal stresses, normalized steels are typically harder and stronger compared to annealed steels. In this type of heat treatment, the material is heated to a temperature higher than the other alternatives, held until it is heated throughout, and finally cooled down in air. [18]

Metalworking

Through *metalworking* operations, the shape, surface, and material properties of metallic workpieces can be adjusted. The main criteria for shape change is plastic deformation, which happens if the shear stress exceeds the yield strength of the material. Based on the temperature, the two metalworking types *cold working* and *hot working* can be differentiated. [19] In cold working, the ambient temperature is below the material's recrystallization temperature, leading to an increased dislocation density and therefore hardening, also known as *work hardening* [16, 19]. In hot working, the temperature is set above the material's recrystallization temperature, which allows the adjustment of grain size through working at a certain temperature and subsequent cooling. [16]

Metalworking processes are defined by a variety of factors such as workpiece, tool, lubricant, temperature, and many more, which influence the change in material properties throughout and after the metalworking process [19]. Typical processes encountered are *rolling* and *forging*. In rolling, hot rolling operations are generally carried out first to allow for increased shape change at lower forces, with an optional subsequent cold rolling processes to further adjust the desired material properties [19].

2.1.2 Machining Fundamentals

The group of cutting technologies combines methods for the shape change of solid bodies by reducing local cohesion [20]. Machining, DIN 8589, is one of the main technologies used for metal cutting, which aggregates the specific technologies *turning*, *milling*, and *drilling* among others. In machining, the product is shaped by a mechanical metal removal process of a cutting tool, removing material layers as chips by a cutting motion [21]. The cutting tools are well-defined regarding the number of cutting edges, their shape, and their positions [20]. Machining processes can be defined clearly by their cutting parameters, technological-physical parameters, and chip-related parameters [22]. For example, the three cutting parameters found for turning operations are: cutting speed (v_c), feed rate (f), cutting depth (a_p).

Shape change is realized by a relative movement between the tool and the workpiece [23]. Chip formation is caused by advancing a cutting wedge through the material causing an initial elastic deformation. With sufficient force being exerted by the cutting tool, the material's yield strength is exceeded, causing plastic deformation, which leads to fracture and material separation due to shear forces. [21, 23, 24] On a microscopic level, five different zones of material deformation can be differentiated (see Figure 4). In the primary shear zone (①), chip formation occurs due to shearing. In the secondary shear zones at the rake face (②, ④), the friction forces between tool and workpiece cause plastic deformation of these areas. At the stagnation zone (③), the deformation and separation of the material takes place. Finally, the preliminary deformation zone (⑤) is defined by chip formation-induced stresses, leading to elastic and plastic deformation. [20]

As the material is resisting the tool's intrusion, force needs to be exerted to enable machining. These observable forces are typically used to describe the machining process. The different types of cutting forces can be seen in Figure 5 exemplarily for the longitudinal cutting operation. The cutting force (F_c) is applied tangentially against the direction of the cutting motion, the passive force (F_p) perpendicular to the cutting force, and the feed force (F_f) against the feed direction. The cutting force and the feed force are aggregated
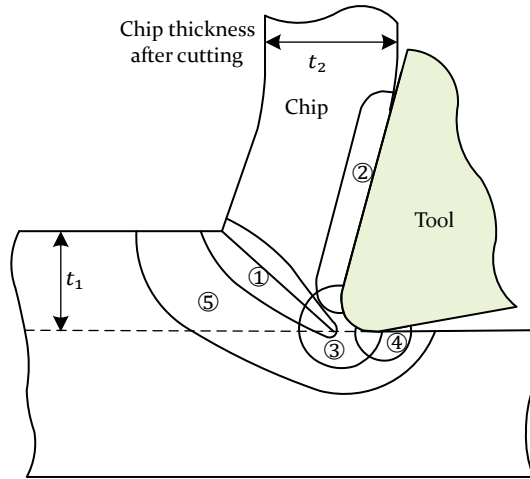
Figure 4: In the chip formation process in machining, different material deformation zones are found, adapted from [21, 25].

as active force (F_a) while all forces are summarized as machining force (F_z) (see Equation 5). [20]

$$F_z = F_a + F_p = F_c + F_f + F_p \tag{5}$$
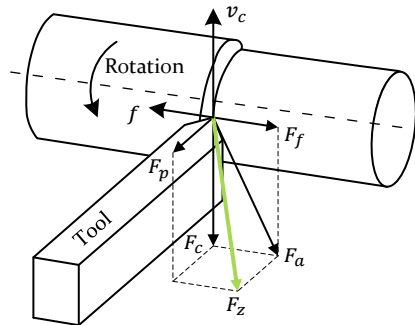
Figure 5: The machining force F_z can be decomposed into the force components F_c, F_f, and F_p for turning operations, adapted from [26].

The cutting force is used to overcome the resistance of the workpiece against the rotation and is thus typically the highest of all forces, accounting for over 98% of the total power consumption. Similarly, the feed force is the resistance against the feed direction, with magnitudes typically at 50% of the cutting force. The passive force does not contribute to the material removal process

as there is no velocity in the radial direction, but is important for dimension accuracy [20]. [21]

The expected cutting forces are directly related to the cutting parameters and follow characteristic non-linear relations [22–24]. However, the cutting forces and the machining process itself is not only influenced by the cutting parameters, but also by the workpiece material [24]. This material impact is described by the concept of machinability.

2.1.3 Machinability

The machinability of a material is a measure of its ability to be machined. Typically, a high machinability is desired, which allows for higher cutting speeds and reduced tool wear, thus increasing productivity while reducing costs [27]. *Machining steels* are known for rather high machinability, while *tool steels* and *heat-resistant steels* show low machinability. Machinability is typically expressed in relation to a reference material [28].

Based on SCHNEIDER, the machinability of a given material is influenced by the condition of the work material as well as its physical properties. The factors determining the condition of the work material are the *chemical composition*, the *microstructure*, the *grain size*, the *heat treatment*, the *fabrication process*, the *hardness*, the *yield strength*, and the *tensile strength*. [28] These can be further grouped into the groups *basic material properties*, *refinement and specialization*, and *mechanical properties* [S1]. The basic material properties define the boundary conditions for the properties of the respective material. The second group summarizes the methods that are used to create and modify the basic material properties, while the third group describes the mechanical properties resulting from the combination of basic material properties.

The **chemical composition** is a central aspect for a material's machinability. Based on the chemical composition of steels, certain generalizations can be made in regard to its machinability. However, as the nature of element interaction is complex, effects might be unclear. In general, it can be said that elements such as phosphor (>0.1 wt.%), chromium, molybdenum, tungsten, nickel, silicon, titanium, and vanadium decrease machinability, while the elements phosphor (<0.1 wt.%), manganese, sulfur, lead and suited deoxidants result in increased machinability. These impacts are made either due to a change in microstructure such as the formation of abrasive or lubricative inclusions [26]. As an example, sulfur forms soft inclusions with manganese which breaks chips during machining [16]. Furthermore, non-metallic inclusions can reduce the shear strength in the cutting area, cause a lubrication

effect, or form a protective layer on the cutting tool [29], and thereby improve machinability [30–32]. [28]

The **microstructure** is determined by the chemical composition, including the carbon-content, and the mechanical and thermal processing. *Ferrite* typically leads to adhesion, and thus the formation of built-up-edge (BUE) on the cutting tool. *Cementite* has a high hardness and brittleness, rendering it essentially not machinable. *Perlite* also has increased hardness and reduced forming abilities, and thus strong abrasive wear of the cutting tool, high cutting forces but also beneficial chip forms and increased surface finish. *Austenite* shows high formability, toughness and low heat conductivity, thus resulting in an increased adhesion, work hardening and high temperature wear at the tool's cutting edge. *Martensite* exhibits low machinability, high abrasive wear of the cutting tools and high mechanical and thermal load due to its high hardness and brittle behavior is expected. Finally, for *bainite* similar behavior to *martensite* or *pearlite* can be expected based on the temperature. [S1] Based on the direct impact of the material microstructure on the material's machinability, simulation models are proposed to predict the machinability for different states of C60 steel [33].

The **grain size** is significantly influenced by the number of nucleii and the cooling rate [16]. Small grains lead to an increased strength, ductility, and toughness, as grain boundaries hinder dislocation movements [34]. Thus, the machinability increases with larger grains.

The **fabrication procedure** significantly impacts microstructure, grain size, and grain orientation, and therefore hardness, ductility, and strength of the material. Typical fabrication procedures include: hot rolling, cold rolling, forging, and casting. [28]

Heat treatments enable the adjustment of mechanical properties before and after the fabrication procedure. Through heat treatments, hardness, strength, and grain size can be adapted. [28] While diffusion annealing reduces local variations of the chemical composition, coarse-grain annealing leads to a microstructure of large grains, which exhibit good machinability. Normalizing aims at reaching a continuous, small-grain-sized microstructure with worse machinabilities than coarse-grain or soft annealing. Hardening leads to a diffusionless phase transformation of austenite resulting in a martensitic or bainitic microstructure. Tempering, however, increases ductility, thus increasing machinability. [S1]

The **hardness** of a material depends both on the chemical composition and the microstructure of a material. With increased hardness, tool degradation

due to abrasion increases and machinability reduces. The **yield strength** and **tensile strength** behave similarly [28]. [S1]

2.1.4 Deviations among Material Batches

Industrial materials are specified by standards, such as the DIN EN 10027, UNS, ASME, and BSi specification standards. Based on the respective material grade, the nominal specifications can be found. However, due to fluctuations in the manufacturing process, materials can vary within their nominal specification or the tolerance limits provided by their supplier [6], resulting in differently behaving material batches. [5] Furthermore, the actual material properties can deviate from those acquired from samples, which are typically used to validate the compliance to the specification, as samples have simple geometries, a simple stress distribution, a homogeneous nature and are tested under laboratory conditions [16]. Thus, machinability variations among material batches can be mostly related to fluctuations in *chemical composition*, *heat treatment* and the resulting *microstructure* including the *grain size*.

In Figure 6, the measured chemical compositions of samples from different batches of the same material grade are shown for data acquired in this study (Figure 6 - a) and published data in [27] (Figure 6 - b). While the measured values are close to the specified values, a spread in element composition can be observed. In their study, BREZOCNIK ET AL. acquire a dataset of 146 material batches for 18 different steel grades with measured chemical compositions and respective machinability. It can be seen that slight deviations in chemical composition among the material batches for a single material grade impact the respective machinability. [27] Furthermore, [35] show that the machinability of the nickel alloy Inconel 718 can be improved by adapting the aluminum percentage within its nominal specification. In regard to non-metallic inclusions, JEON ET AL. investigate three material batches with varying amounts of sulfur contents. It can be seen that the machinability depends significantly on the amount of non-metallic inclusions. [36]

Heat treatment is especially important for deviations among material batches, as deviating heat treatments can lead to different machinability. Also, treatment types such as case-hardening and nitriding lead to a change in microstructure and chemical compositions only at certain positions of the workpiece [28], thus inducing different behavior among material zones. A similar effect can be seen for water quenching, as the microstructure might be different from the outer surface to the material core due to different cooling rates [37]. In [38], reduced machinability of SAE1050 steel samples was observed when applying the heat treatments annealing and normalizing.
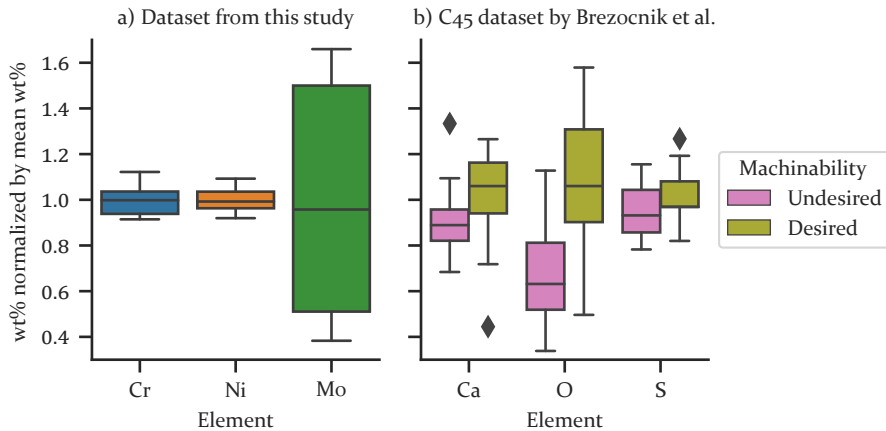
Figure 6: The chemical compositions vary among samples of the same material grade for data investigated in this study a) as well as for publicly available datasets [27] b).

Different microstructures among material batches are formed by different cooling rates after hot rolling [33]. It has been found that the sample with a higher percentage of ferrite and larger grains exhibits higher machining forces and reduced tensile strength. Furthermore, [37] investigate the effect of several heat treatments after an initial austenitizing and show that only water quenching leads to martensitic microstructure, while annealing, normalizing, and oil quenching of the investigated AISI 1045 samples all show a ferrite-pearlite microstructure. The effect of grain size variations among material batches on machinability can also be seen in the samples investigated in this work. While the material batch with rather large grain sizes, see Figure 7 (a), exhibits high machinability, the material batch with smaller grain sizes, see Figure 7 (b), has a reduced machinability in direct comparison. Another effect is that material batches of different purity levels but of the same grade show different hardening behaviors [16]. In [39] it is shown that for a given hardness, the material's microstructure has a significant impact on its machinability.

2.2 Approaches for Handling Machinability Deviations

As shown in Section 2.1 fluctuations in the material manufacturing process lead to deviations in properties among material batches and thus to different machinability. This prompts the investigation of established practices for handling these deviations (Section 2.2.1). Furthermore, the different approaches for assessing a material's specific machinability are introduced (Section 2.2.2)
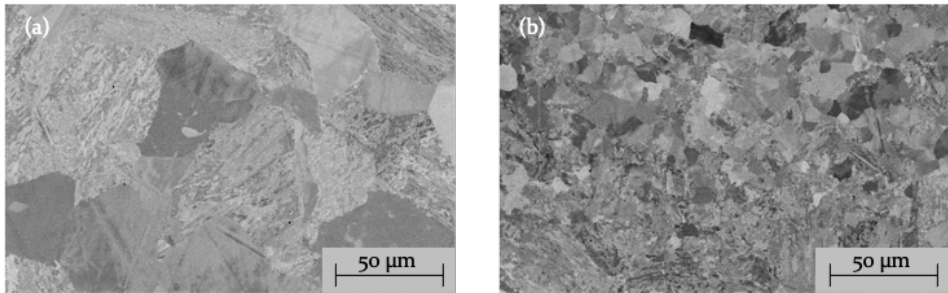
Figure 7: The two material batches a) and b) show differently sized grains.

and the general area of material identification is reviewed (Section 2.2.3) to draw similarities for material batch identification.

2.2.1 Solutions for Handling Material Deviations

There are several solutions for handling machinability deviations among material batches. These include:

- Tighter tolerances
- Usage of generally applicable cutting parameters
- Material testing and machinability characterization for every batch
- Simulation

By **tightening** the tolerances of the material specifications, the expected deviations among material batches can be minimized. However, there might be a technological limit as not all influencing factors causing the deviations can be controlled to the most accurate level. Furthermore, with tighter tolerances, the material costs increase as the effort for material manufacturing rises [40], while the amount of suppliers that can deliver their material up to the specified standard diminishes.

Alternatively, in a naive approach, machinability deviations among material batches can be ignored, by finding a set of **generally applicable cutting parameters**, which work sufficiently well for all machinability variations of the respective material grade. In this approach little effort has to be put into material characterization. However, the cutting parameters need to be selected in a conservative way such that they account for batches with bad machinability. Therefore, the process is running mostly at non-ideal conditions.

To enable machining at ideal conditions, the machinability of the to-be-machined material batch needs to be known. To do this, one can carry out

material testing and material characterization for every new material batch to establish optimized machining strategies. Such an approach can be seen in [8] for laser cutting of five material batches of X5CrNi18-10, with some chemical elements deviating up to 40% from the mean. By finding material-batch specific cutting parameters, good quality can be reached for all material batches [8]. For the machining of different material grades DENKENA ET AL. find optimized sets of cutting parameters for each material [9], reducing the cutting time significantly [1]. While this allows for optimized machining, and thus the lowest machining costs, there are significant testing efforts involved. For the in-depth analysis of a novel alloy with the goal of finding optimized machining strategies and cutting tools, over 300 cutting experiments were conducted [41]. In a typical industrial scenario, fewer experiments are needed. In a simplified, general manner, the cutting depth is optimized first, followed by the feed rate and finally the cutting speed. These experiments involve manual process observation by visual and acoustical means as well as the assessment of machinability by tool life.

A different alternative is the field of **simulation**. EVANS states that "batch to batch variation will contain both a systematic and a random component" [5]. Thus, they investigate the usage of *theta methodology* for the random component [42] and the *Wilshire equation* for the systematic component [5] for their investigation of creep life. Similarly, in [4] a strategy of combining an offline simulation [43] with an online adaptation is proposed, which can adapt to long term changes, such as a change in material behavior throughout time.

In Table 1 the different approaches are compared qualitatively, based on impacts on material costs, testing costs, and machining costs. It can be seen that through tight tolerances and extensive material testing the problem of material batch deviations can be compensated. However, these approaches lead to an increase in material costs and testing time. Through means of simulation, especially long-term effects, such as seasonal trends, might be modeled and compensated. This method is not suited to represent the stochastic nature of batch deviations due to manufacturing fluctuations as there is no known pattern that can be modelled efficiently. Using a fixed set of parameters for a given material grade, while ignoring material batch deviations, has normal material costs and low testing costs. However, due to the more conservative nature of the parameters, the machining costs rise for differently behaving material batches. Finally, the method of testing every material batch allows for the determination of the exact machinability and, thus, low machining costs due to ideal cutting parameters for every material batch. Even though this enables the most cost-efficient machining during operation, the associated costs of extensive material testing might outweigh the benefits.

Table 1: The different strategies for handling material batch deviations are compared in regard to the associated manufacturing costs.

Strategy	Material costs	Testing costs	Machining costs
Tight tolerances	high	low	low
Default parameters	medium	low	high
Testing all	low	high	low
Simulation	medium	medium	medium

2.2.2 Methods for Material Characterization

To characterize a material batch, its machinability needs to be determined. This can either be done by analyzing all influencing factors on the machinability, see Section 2.1.3, or by judging the machinability through an indirect method.

Monitoring of Influencing Parameters

There are several advances in the monitoring of the machinability's influencing factors and the consecutive machinability prediction. Given the chemical composition of a material, methods such as genetic programming [27] or artificial neural networks (ANNs) [44] are investigated for machinability prediction. ABOURIDOUANE ET AL. propose the usage of the *representative volume element* technique for predicting machinability based on the material's microstructure [33]. The required microstructure can be measured using microscopes, however there is a sophisticated sample preparation process required, rendering it infeasible for in-process analysis. Similarly to the microstructure, the grain size can be determined using microscopes prior to the machining process [45]. While ML-methods can be used for automated grain size determination [46], the samples still need to be prepared outside the machining process. In [47], both acoustic emissions and cutting forces are investigated to identify the heat treatment condition, annealed or tempered, of the work material. Audio signals can also be used to detect hardness variations during milling [48]. However, similar hardness does not necessarily correspond with similar machinability as the remaining factors might differ.

In summary, it can be said that there are approaches to monitor some of the factors influencing machinability during machining. However, for the detailed analysis of most parameters, time-consuming preprocessing steps are needed to acquire the data needed for machinability determination. Thus, the

factors influencing the machinability are not suited for an online monitoring of a material batch's machinability.

Machinability Monitoring

Machinability can not be determined directly, but is typically assessed through one or multiple criteria. These include the *tool life*, the *tool forces and power consumption*, the *surface finish*, and the *chip form* [28]. Advanced methods integrate multiple factors such as hardness, strength, toughness, cutting force, thermal conductivity, cutting temperature, tool life and surface roughness for machinability assessment [49].

Tool life refers to the time during which a tool can execute machining operations at the desired quality [50]. Materials that are machined without causing a lot of tool wear are considered to have good machinability [28]. Among all machinability assessment alternatives, tool life is the most popular one [24]. As a challenge, tool life is very sensitive to other influencing factors, such as tool material and cutting parameters [28]. To predict the expected tool life at specific cutting parameters for a given work material - tool material combination, tool life models are used. JOHANSSON ET AL. compare the commonly used *Taylor* model [52], its extended version [53], the *Coromant turning model version 1* model and the *Colding* equation [54] for tool life prediction. While the best performances are achieved using the Colding equation, the standard Taylor model and its extended versions are especially feasible for industrial applications due to their limited number of coefficient parameters [51].

The investigation of **machining forces** originates in the understanding of machinability as the ease of cutting, which "implies that a metal through which a tool is easily pushed should have a good machinability rating" [28]. Among all machining forces, the cutting force is investigated most often. In general, harder-to-machine materials require higher cutting forces [24]. Therefore, cutting forces appear to be suitable as an indirect measure of machinability [55]. However, the cutting force does not only depend on the material's machinability, but also on other factors such as the condition of the cutting tool as well as the cutting parameters.

Surface finish is determined by elastic and plastic deformation at the minor cutting edge. Furthermore, surface roughness is caused by the formation and detachment of BUE parts on the cutting tool, which are more commonly observed when machining soft and ductile materials [28]. Surface roughness can be measured using technologies such as *ultrasonic sound* [56] or *angular-speckle correlation* [57]. Using the surface finish as a machinability index is

only viable for certain cutting conditions and the results might deviate from those acquired using tool life and machining forces [28].

Lastly, machinability can be judged by the **chip form** [58], which impacts both the machining process and the chip handling [50]. Thus, materials with desired chip forms would receive a high machinability rating. As the chip form needs to be judged manually by the operator, the rating is of a rather qualitative nature. Applications are found mostly in drilling [28] and for limited chip space [50]. [28]

In their research, JAWAHIR ET AL. further investigate the different criteria, establish interrelationships among them, and derive the need for considering all factors in an integrated machinability approach [59, 60]. Such a concept is later introduced as *total machining performance* consisting of the five factors surface finish, tool wear rate, dimensional accuracy, cutting power, and chip breakability, which can be quantified by using fuzzy logic [61] or genetic algorithms [62]. Based on this concept, a comprehensive methodology is proposed combining analytical, empricial, numerical and AI-based models in a hybrid approach for machining performance assessment [63].

2.2.3 Material Identification Methods

Material identification methods enable production systems to gain information about the material being processed. The general architecture of material identification systems is shown in Figure 8. The to-be-identified material is observed by one or multiple sensors. These either monitor passive signals or, optionally, use active signals induced by an actuator. The acquired signals are preprocessed before making a decision.
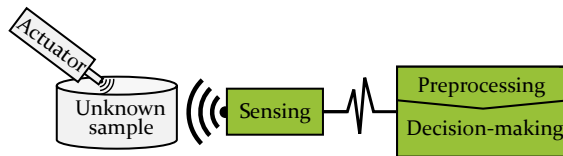
Figure 8: Material identification systems typically consists of a sensing unit, a data preprocessing module, a decision-making system and optionally an actuator for active sensing approaches, adapted from [P1].

Degree of Similarity

For material identification, a dependency from the difficulty of the identification task to the level of similarity among the to-be-identified specimens can be seen. For the identification of several wood types and wood classes,

PIURI ET AL. show that the identification of the exact type, such as *wild cherry* or *oak chestnut,* is more challenging than the sole identification of the wood classes, such as *conifer* or *broad-leaved* [64]. Similarly, DENKENA ET AL. study the classification between two different steel alloys as well as the classification between one aluminum and one steel sample. While the steel and the aluminum sample can be differentiated clearly, the two types of steel are significantly harder to differentiate due to similar cutting forces [65]. Thus, it is necessary to assess the level of similarity among the to-be-identified samples for an initial judgment of the material identification task. To achieve this, STRESE ET AL. propose a taxonomy for the detailed labeling of investigated samples [66], which is extended in [P1] to match all scenarios typically encountered in material identification for smart manufacturing systems. This taxonomy consists of the five levels *major material, material sub-class, specific material, material grade*, and *material batch* (see Figure 9).
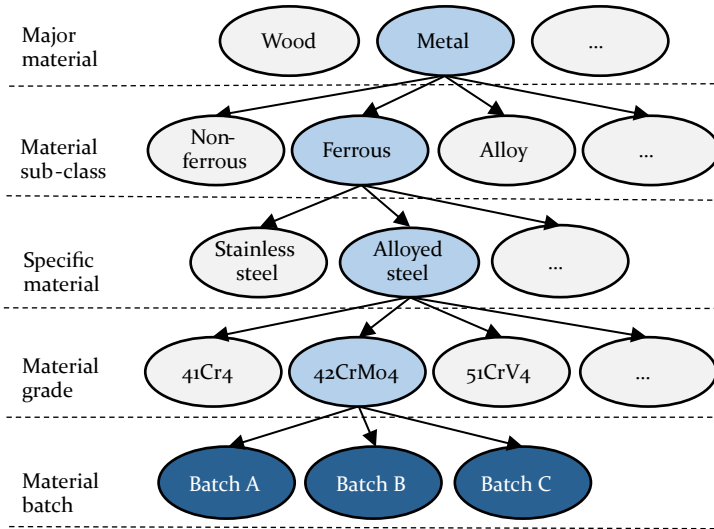
Figure 9: The taxonomy allows an initial estimation of the difficulty of the material identification task based on the similarity of the to-be-identified specimens, adapted from [P1].

Integration in Manufacturing Systems

Material identification is typically carried out either as *process monitoring* or as *offline identification* [P1]. While the alternative of process monitoring takes place in situ during machining, offline identification is carried out as an auxiliary process step before the main process. As a consequence, process monitoring solutions are desired due to no negative effects on the cycle times, while offline identification methods have greater flexibility regarding the sensing approach as no interference from the manufacturing process is

present and active actions such as knocking on [67, 68] or moving over [69] the sample can be conducted.

Signal Sources

To enable material identification, a great variety of signals are investigated. These include visual images [70], infrared images [71–73], tactile images [74], cutting forces [9], spindle torques [9], friction forces, structure-borne sound, air-borne sound, vibrations, color measurements [75, 76], fluorescence [64], electric impedance [77], temperature measurements [78–81], density measurements [66] and simulation data [9]. Among these, [P1] find that the groups of *surface images*, *force and torque* signals, and *vibration* data are most commonly used (see Figure 10, a). Typically, not a single data source is used, but multiple sensors are integrated, combining the information of the various modalities [82], which often leads to improved identification accuracies [S2].
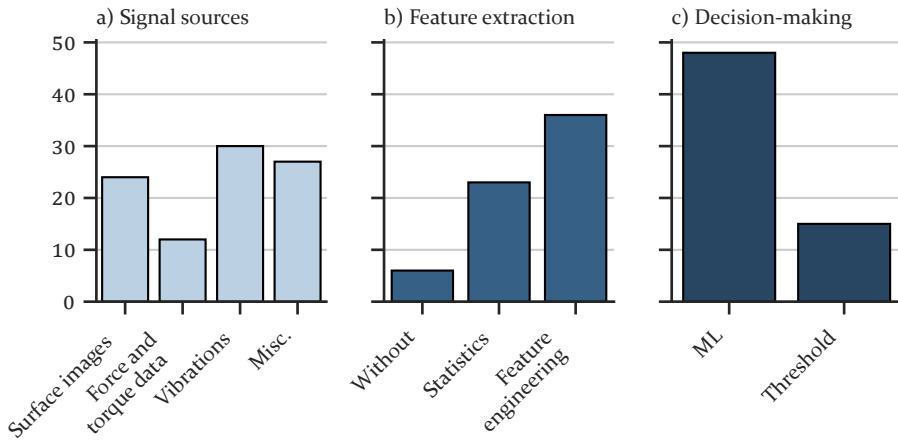
Figure 10: Among all investigated studies for material identification for smart manufacturing systems, trends regarding signal source, data preprocessing, and decision-making can be observed.

To find out which feature has the highest impact, feature ranking methods such as the *joint-mutual information method* can be used [65]. Regarding the effectiveness of the different signals, varying observations are made. While in some studies force data contains more information than vibration data [1, 83], in other studies all samples can be classified only with vibration data, but not with forces [84]. As a further challenge, [67] notice that vibration data strongly depends on the shape and volume of the to-be-identified sample.

Feature Extraction

The acquired signals are either analyzed directly as raw data, or preprocessed into features through general statistical methods or expertise-specific feature engineering methods. Simple feature extraction includes the computation of features that are generally used, such as the signal's mean or standard deviation [83]. While these are most commonly applied to time-series signals, methods like pixel averaging can also be applied to image data [70]. Feature engineering describes the process of deriving specific features characteristic for the respective application. These include the *histogram of oriented gradients* [85], material-specific frequency bands [86], and bio-inspired tactile features [74], among others [66, 69, 87]. When comparing the popularity of the different alternatives (see Figure 10, b), it can be seen that only a few approaches analyze raw data directly, while most approaches use simple feature extraction methods or some form of engineered features [P1].

In direct comparison of different feature extraction alternatives, it can be seen that in general worse results were seen when analyzing raw data compared to preprocessed data [78]. However, in certain cases, the usage of raw data in combination with sophisticated decision-making systems outperforms manually crafted features [66, 88].

Decision-making

Decision-making systems are used to derive a label describing the specimen under investigation based on the available data. Here, both rule-based systems and ML-approaches are used most often [P1]. Within ML, both supervised and unsupervised approaches are utilized. Rule-based systems typically aggregate the observed information through data preprocessing into a characteristic feature. This feature is then compared to a set of rules, such as a predetermined threshold, to decide whether a certain material is present. In the binary case with only two materials present, typically a single threshold is used [9, 86, 89], while for multiple material classes, ranges are defined for each material [67]. In supervised ML, a classifier is trained to predict the sample's label based on the available features. Among all reviewed studies, a variety of different models is investigated. These include k-nearest-neighbor (kNN) [90, 91], ANN [92, 93], general Markov models [94], support vector machine (SVM) [79, 95], Bayesian models [96, 97], decision tree (DT) [71], dictionary learning [69, 77], random forest (RF) [70], and logistic regression (LR) [70]. Furthermore, approaches such as one-shot learning are investigated in particular for the application with small-sized datasets [98]. Especially for such data driven approaches, the sampling strategy must be correctly chosen [99].

In unsupervised learning, no distinct labels describing the data are available, but rather the samples need to be grouped into groups of highest similarity, such as similar colors. This can be achieved by using a k-means clustering algorithm to find clusters in existing data. These clusters can consecutively be used as a classifier to assign novel materials to one of the found clusters, see Figure 11. [100]
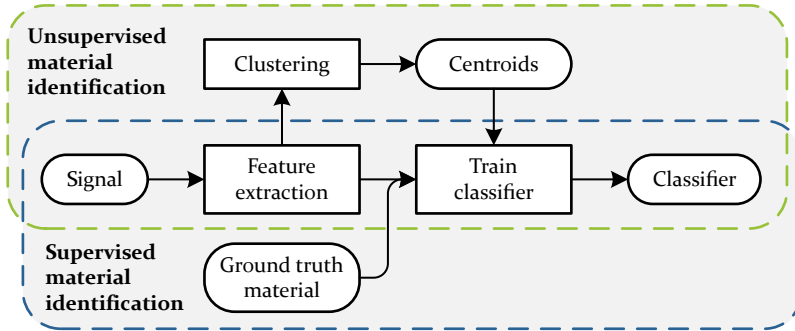
Figure 11: Difference between supervised and unsupervised material identification, adapted from [100].

Rule-based systems are less complex and easy to understand, and are well suited if both materials can be clearly distinguished, such as by an absolute signal difference [9]. When those differences diminish, i.e. when considering tool condition, such rule-based systems were found unsuitable [101]. Comparing the popularity of the investigated decision-making systems, see Figure 10, it can be observed that ML-approaches are used in the majority of all studies. Among these ML-methods, especially ANN, SVM, and kNN are popular choices as they are investigated in a quarter of all studies. However, depending on the available dataset, other algorithms such as boosting [96] or Bayesian approaches [64, 80, 97, 102] outperformed the popular choices. For image analysis in particular, the usage of CNN was found as a promising alternative, slightly outperforming other algorithms while also reducing the data preprocessing effort [66, 103, 104]. When classifying among the different material types of aluminum and steel, DENKENA ET AL. find all investigated algorithms to be suitable, but when evaluating the same algorithms for the detection of two different steel grades, only the kNN algorithm showed acceptable results [65]. Thus, it can be seen that for each dataset a variety of algorithms need to be investigated to find the one most suitable.

Application-specific Trends

Material identification systems are investigated for various applications such as remote operation [71, 94], waste management [67], construction [75],

additive manufacturing [73], and subtractive manufacturing. The major applications in subtractive manufacturing can be found as positive material identification (PMI), monitoring the turning of compound parts [9], and monitoring the drilling of multi-material stacks [89]. Further approaches in subtractive manufacturing are the grinding of compound parts [86] and the milling of woods [84]. In Figure 12, the trends are shown for the most relevant applications of preproces PMI, monitoring turning processes, and monitoring drilling processes.
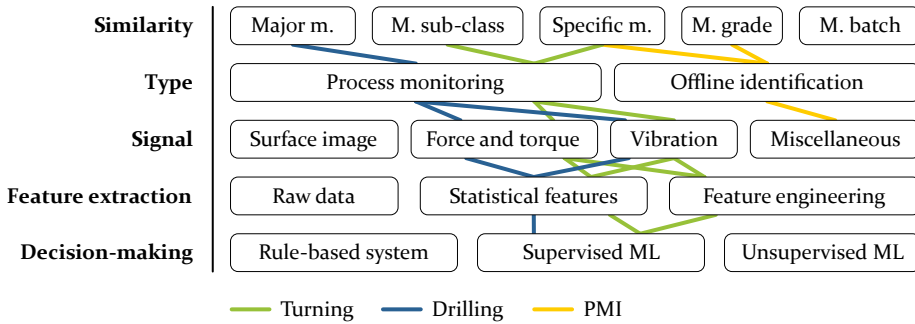
Figure 12: Comparing common approaches for material identification in turning, drilling, and PMI, trends are observed regarding the categories sample similarity, type, signal, feature extraction, and decision-making.

In subtractive manufacturing, material identification is carried out as process monitoring to detect the transition zone from one material to another. [9] propose a method for the identification of steel and aluminum zones in friction welded hybrid workpieces. The cutting force is acquired through a dynamometer and the spindle torque is measured by the NC. Consecutively, monitoring parameters are computed by relating the measured signals to the current material removal rate computed by simulation. They show that once these parameters cross a defined threshold, the material transition happens. [65] investigates cutting forces measured with a dynamometer, current and torque signals from the NC, and acceleration data for the identification of aluminum and steel in hybrid workpieces. The raw signals are preprocessed into various features. To reduce complexity, the joint mutual information method is investigated for feature selection. Out of all features, great importance is especially placed on the cutting force, feed force, passive force, and motor current related to the passive force. All investigated classification approaches, SVM, DT, ANN and kNN are capable of differentiating between the classes *no material interaction*, *steel*, and *aluminum*. In their consecutive study, [83], they further investigate the usage of ANNs for material classification. They find that when training a classifier for one cutting condition the network performs poorly for other points of operation. However, when including the new

parameters in the training dataset, the algorithm is capable of performing well also for novel combinations of those parameters. Comparing the need for the various data sources, they conclude that acceleration sensors or internal machine data alone provide worse results, but together they eliminate the need for dynamometer-based force measurements. In a different scenario, TETI ET AL. investigate the identification of the heat treatment type through acoustic emissions and cutting force data for aluminum alloys [47].

Process monitoring for detecting the transition point from one material to another is a central challenge in the machining of multi-material parts. The identification of the major material groups *metal* and *composites* is broadly investigated in regard to aircraft manufacturing as many holes need to be drilled in stacks of metal and carbon fiber reinforced plastics (CFRP) for the subsequent riveting process. As signals, both acoustic emissions [10, 89, 101, 105] and cutting forces [101] are investigated. Even though threshold-based systems can be used for material identification [89], when considering tool degradation, such systems are found to become unsuitable [101].

In industrial applications, the term PMI refers to a variety of spectral methods used typically in handheld devices for non-destructive testing of metal materials to identify the material grade and its chemical composition. These are based on several methods such as *laser-induced breakdown spectroscopy (LIBS)* [106], *X-ray fluorescence (XRF)* [107], *OES*, and *fourier transform infrared spectroscopy* [108]. In their study, SHER AFGAN ET AL. use a handheld LIBS device to analyze the chemical composition of steel samples with low absolute measurement errors [109]. Additionally, the usage of XRF and LIBS in challenging environments is investigated in [110] for material recycling. It is shown that while industrial available instruments provide information about the chemical composition of various alloys, the data is not reliable enough to meet the requirements for a reporting tool.

2.3 Smart Machine Tools

While the concept of intelligent machine tools is not a novel one [111], the recent advances in information and communication technologies allow for increased smartness of manufacturing systems [112]. There is no central definition of smart manufacturing, but it can be described as "a collection and a paradigm of various technologies that can promote a strategic innovation of the existing manufacturing industry through the convergence of humans, technology, and information" [113]. Key enabling technologies include internet of things (IoT), cyber-physical production systems, big data, artificial intelligence (AI) and ML, cloud computing, and digital twin [114]. In [115] central pillars of smart manufacturing are defined, including man-

ufacturing technology and processes, materials, and data, while MITTAL ET AL. name context awareness and process parameter adaptability as central characteristics associated with smart manufacturing [116]. The concept of cognitive awareness for machine tools is explained in [117], with adaptive machining [118] as an example of process adaptability. Besides smart manufacturing, intelligent manufacturing, advanced manufacturing, cyber-physical production, cloud manufacturing, and digital manufacturing are other manufacturing paradigms with many similarities [114]. Thus, the desired task of adapting machining processes based on observed material batch characteristics can be considered a step towards smart manufacturing.

When mapping the concepts of smart manufacturing onto machine tool research, similar developments are found. Here, various terms such as *Industry 4.0 Machine tool* [119], *intelligent machine tool* [120–122], *smart machining system* [123, 124], *Machine Tool 4.0* [125], *Cyber-Physical Machine Tools* [126], *Smart Machine Tools* [127], *Smart Machine Tool System* [128] and *Feeling machine* [129] are used. In Figure 13, common building blocks found in most concepts are shown. These consist of physical devices such as the machine tool itself, the cutting tool, and the to-be-machined workpiece. Through the NC or other data acquisition devices, process data can be observed, stored, and analyzed using various algorithms. Cloud computing technologies provide the necessary computational power for big data analytics. Furthermore, human machine interfaces (HMIs) are needed to convey information from the digital world to the machine operators.
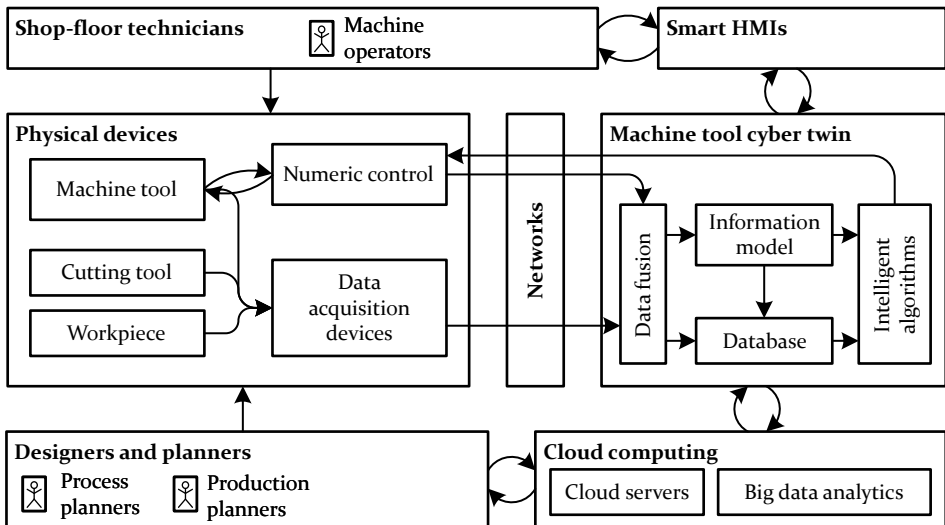
Figure 13: Generalized and simplified framework of a smart machine tool systems, adapted from [126].

Another trend besides smart machine tools are smart components, such as smart spindles [130], smart feed-drives [131], smart tool holders [132], and smart cutting tools [133]. These components include additional sensors, communication, and computation capabilities to provide detailed data to other smart systems as well as consuming such data themselves to improve their functionality [119].

2.3.1 Sensors and Data in Machine Tools

Sensor systems provide the necessary data needed by process monitoring and process optimization systems for decision-making. The most common sensors are *dynamometers*, *accelerometers*, *acoustic emissions* sensors, and *current* sensors [134]. Further sensor systems include *roughness* sensors, *thermal cameras*, *ambient condition* sensors, *tool probes*, and *thermocouples* [135]. When comparing sensors regarding their costs, intrusive nature and signal reliability, [136] find that while dynamometers are the most reliable they come with highly intrusive nature and increased costs. Using current and power sensors, however, attributes to the least intrusive nature and costs as the sensors are easy to retrofit if not already integrated and available in modern control systems, and are thus suitable for operational use [135].

The drives and spindles in machine tools provide the necessary force for material removal. The drive control power can either be measured using external sensors, or acquired by accessing internal control data [137], as the power measure is internally needed by the machine's NC for the drive control loop [138]. When using internal signals, the motor itself is used as an indirect sensor of the cutting force, as the motor armature current is proportional to the torque, which itself is proportional to the cutting forces [136]. As the inertia of the motor's rotor acts as a low-pass filter, there is limited sensing bandwidth, making it hard to observe high-frequency signal components [139].

Besides the current, power, and torque data, typical NC systems provide additional signals, such as the speed as well as the designated and measured position of each axis. Due to the high requirements regarding resolution, photoelectric scanning methods are used most commonly for position measurement [140].

2.3.2 Tool Condition Monitoring Systems

In subtractive manufacturing the production costs and the quality of the produced part rely on the condition of the cutting tool used. While it is important to use cutting tools for their full useful life to save tool costs [141],

severe tool wear needs to be avoided as it might lead to increased costs and decreased product quality [142], or even damage to and breakdown of the machine tool [143]. Furthermore, worn out tools produce parts with low surface quality that might need to be reworked, and invoke opportunity costs due to unproductive machining time during tool replacement [144].

Studies found that cutting tool failures contribute to 20% of a machine's downtime [143], and between 3% and 12% of the total production costs can be allotted to wear and breakage based tool failures for composite machining [145]. Furthermore, manual tool wear assessment using a toolmaker's microscope takes place while the tool is resting and can take between 5 and 30 minutes [146].

Thus, TCM systems are needed to monitor the wear of the cutting tool during operation. Thereby, the tool can be used to its full extent, while preventing tool breakage and damage to the workpiece and machine tool [147, 148]. Despite a recent study finding most tool wear inspections still being carried out manually [149], the recent technological advances in hardware development and signal processing [150] justify the intense research done for automated TCM systems.

Wear mechanisms

Tool wear can be attributed to four common wear mechanisms: *abrasion*, *adhesion*, *fatigue*, and *oxidation*.

Wear by **abrasion** is a solely mechanical wear mechanism, caused by the intrusion of hard particles or rough workpiece materials [26] in the softer tool surfaces [151, 152]. These particles include microchips, lubricant impurities, precipitants [153], and material inclusions [153]. As a result, microdeformation and micromachining can be observed for ductile materials, and cracks and grooves for brittle materials [152]. While it is not possible to avoid this type of wear mechanism, it is especially common at low feed rates and cutting speeds [151].

Adhesion refers to the formation of atomic bonds between metallic homogeneous surfaces due to high local forces [152]. Besides chemical adhesion, there is also mechanical adhesion, caused by mechanical interlocking at high temperatures [154]. With particles permanently adhering to the cutting tool, a material layer is formed on top of the original surface, altering the tool geometry [151], which leads to the wear defect known as BUE [21]. This results in a reduced surface quality and increased flank wear.

Changing mechanical loads cause **fatigue** at the load-bearing areas of the cutting tool's surface. Contrarily to other wear mechanisms, fatigue wear has a long incubation phase during which cracks form and spread before they break loose, and the wear phenomena becomes observable. [152, 155] Fatigue wear can be reduced by using specific tool coatings and lubricants [S7].

Oxidation refers to the formation of undesired coatings and particles on the cutting tool's surface. Thereby, the properties of the boundary layer change [26]. Depending on the hardness of the formed particles, tool wear is negatively or positively impacted [154–156]. Furthermore, oxidation can cause a chain reaction of other wear mechanisms, as the formed oxide particles can adhere to or grind on the tool's surface, causing further adhesion and abrasion wear [152].

Overview TCM Systems

TCM systems are typically realized using either direct or indirect observation methods, but there are also approaches combining both through sensor fusion [S4, 157]. KURADA ET AL. define several requirements for a successful tool wear sensor including accurate assessment of the tool condition, no interference with the machining process, contact-freeness, and a fast response [143].

A detailed review of indirect measurement methods can be found in [147, 148]. These methods include the monitoring of burr formation [158], the analysis of chip shapes using a three-dimensional (3D) scanning electron microscope [159], vibrations [160, 161], acoustic emissions [48, 162], power [162], current [160, 163], torque [164], the analysis of surface images [165, 166], or the combination of multiple sensors [167, 168]

While indirect methods are easy to integrate into manufacturing processes, they are prone to noise from the environment, resulting in reduced prediction performance [169, 170]. In contrast, when using direct measurement methods, specifically computer vision, the actual geometric changes of the cutting tool due to wear effects can be measured [143, 171, 172], and contact disturbance is avoided [173]. Due to this, they generally show better detection rates.

Within direct TCM, a variety of different sensors and sensing approaches are investigated. These include *charge-coupled devices (CCDs)* [174] and *complementary metal-oxide-semiconductor (CMOS)* [175] cameras, *laser scanning confocal microscopy* [176], and *infrared sensors* [177]. While typically a single camera is used, YAMASHINA ET AL. propose a setup of two visual cameras, one having a global view detecting the orientation and position of the tool, the other focusing on the wear region of interest (ROI) [178].

Such approaches are extended to enable not only 2D measurements, but also 3D measurements of the wear defects. This can be achieved by using multiple cameras for stereo vision [179, 180] or by using multiple cameras for computing disparity maps [181]. Instead of using multiple cameras, SZYDŁOWSKI ET AL. use a single movable camera, taking images at different focal planes, which are combined to compute a depth map [182]. Other approaches include the usage of *white light interferometry* [151, 183, 184], *coherent light interferometry* [185], and *knife-edge diffraction interferometry* [186, 187]. Besides, the usage of *structured light* is investigated for reconstructing the 3D shape of wear defects [188, 189]. Similarly, WANG ET AL. explore a TCM-method of projecting fringe patterns on the cutting tool for 3D reconstruction [190]. The assessment of the wear profile is also investigated by ČERČE ET AL. using laser profile scanners [191], and extend their analysis approach by a finite element stress simulation in [192].

Components of a direct TCM system

The typical components of a direct TCM system are shown in Figure 14. The ROI, e.g. the flank of the cutting tool insert or the face of a face-mill, is positioned in front of the image acquisition unit at a known position [175]. Direct artificial illumination, such as light-emitting diode rings [175], or back-lighting technology [193] are used for optimized illumination of the ROI. Furthermore, jets of compressed air supplied by an air nozzle are used to clean of remaining chips and lubricants from the tool [194]. The image of the cutting tool is then taken by the respective sensor and processed in a connected processing unit. The computed results can be communicated to the operator using a GUI [195]. As an enhancement, THAKRE ET AL. propose the usage of a known reference body within the image area for automated pixel calibration [196].
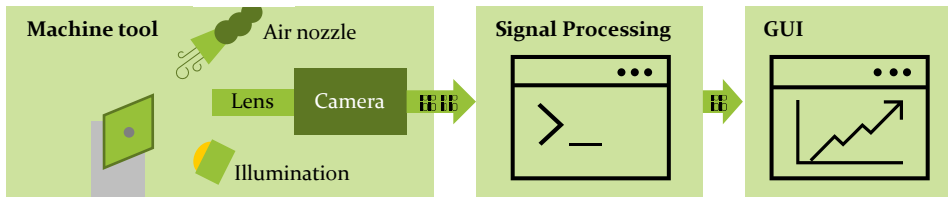
Figure 14: The basic framework of visual TCM systems consists of an image acquisition unit integrated into the machine tool containing a camera, artificial illumination, an air nozzle, a signal processing unit, and a GUI.

While in [197] methods are proposed for quantifying two wear mechanisms, most approaches focus on predicting general wear metrics. The most popular

metrics, as specified in ISO3685, are flank wear width (*VB*) and crater wear depth. Studies found, however, that especially the flank wear area is an important indicator of the condition of the cutting tool [170, 198, 199]. Furthermore, the centroid of wear [200], burr shape [201], radial wear [170], and diameter wear [170] are used as wear metrics. When using 3D measurement technology, not only the shape of tool wear, but also the depth can be assessed. Thereby, the crater wear depth [180], and subsequently the wear volume [180, 185, 191, 192] can be measured and used as metrics for tool wear.

With the variety of metrics describing the state of wear, FADARE ET AL. propose a combined tool wear index to represent the overall tool condition [200]. A similar approach is proposed by KWON ET AL., suggesting a different tool wear index based on the detected flank wear area for an accurate representation of tool condition [202].

While most approaches focus on flank wear and crater wear, LANZETTA proposes a wear defect classification system with suitable features and decision rules to classify the various defects present in an image [203]. In a more simplified classification system, SUN ET AL. identify the different wear types *fracture, BUE, chipping* and *flank wear* [204].

Integration in a Machine Tool Environment

In research settings, cutting tools are typically removed manually from the machine tool for taking the necessary images. As an alternative, jigs are proposed to enable a flexible and easy installation [205].

For operational use, it is necessary to integrate the sensing unit into the machine tool, so that measurements can be taken automatically. This can be achieved by placing the sensing unit so that it faces the typical working region of the tool, e.g. next to the main spindle [174, 204, 206] or above the tool center point [207, 208]. As an alternative, MIAO ET AL. position the camera so that it faces the tool revolver, thus taking images of the cutting tool while it is in its resting position [209]. Besides these static approaches, methods are investigated to position the cutting tool and sensing unit in front of each other. While BAGGA ET AL. mount the sensing unit at a fixed position in the machine tool and move the cutting tool to the sensing unit [175], DAI ET AL. mount the sensing unit on a movable platform, controlled by the NC, which is moved to the cutting tool [170].

In addition to the physical integration, the logical integration needs to be discussed as well. GARCÍA-ORDÁS ET AL. consider their approach an online approach, as no intervention for extracting the tool inserts from the toolholder is needed [144]. More differentiated, ZHANG ET AL. define a *real-time* mode

and an *in-process* mode of online measurement. In the real-time mode, image acquisition needs to take place during operation without stopping the machine tool, while the in-process mode takes images when the cutting process is halted [210]. For real-time measurement, WANG ET AL. propose a measurement system acquiring images during spindle rotation [211]. Similar approaches are presented in [212, 213], which have the cutting tool slowly rotate in-front of the image acquisition unit. However, all approaches are not true real-time, as no cutting operation takes place during measurement. Thus, most approach can actually be categorized as in-process measurement.

For the integration into the machining process, static or dynamic triggers are used. In [214], the cutting process is interrupted at regular intervals for image acquisition. For a more flexible approach, YANG ET AL. integrate the camera control into the programmable logic controller (PLC), thus allowing flexible triggering [206]. A similar idea of automated cooperation between the TCM system and the machine tool's control is proposed in [170]. As an alternative to online measurements during the machining phase, RUITAO PENG ET AL. integrate the image acquisition phase at the end of every cutting operation [174] and MOLDOVAN ET AL. suggest taking images once the tool is placed back in the magazine [215].

Image Analysis Methods

Early works of visual tool inspection can be found by GIUSTI ET AL., using cameras for flank and crater wear analysis [216, 217]. The typical steps for image processing include "image enhancement, image segmentation, breakage detection and tool wear parameter derivation" [143].

Initial preprocessing steps such as filtering and morphological operations are typically carried out to remove image noise [207, 208]. Furthermore, through image processing the effects of chips and cutting fluids can be cut down [181]. Especially the usage of *morphological component analysis* has been investigated to decompose a cutting tool image into background, noise, and object of interest, thereby allowing the noise and background effects to be filtered out [199, 218].

The approaches for deducing the tool condition from wear images are manifold; however, many use image processing techniques to produce binary images for tool condition analysis [219]. A common procedure is to use a defined gray-level threshold to segment out areas of interest, such as the flank wear region. Here, SUN ET AL. investigate defect-specific thresholds, so that different types of wear can be identified [204]. These regions can then be converted to wear metrics by pixel counting [220] or the average wear width

by averaging the width of the detected wear area at multiple positions [196]. Another approach is presented by CASTEJÓN ET AL., using the segmented flank wear region to compute several descriptors, such as the *eccentricity*, the *extent*, and the *solidity*, which are analyzed using a *finite mixture model* approach to classify the tool condition as low wear, medium wear, or high wear [221]. For thresholding, especially the usage of *Otsu's method*, allowing automatic image thresholding, is commonly investigated [173, 222–224]. ONG ET AL. combine such a segmentation procedure with the measured surface roughness and the current cutting conditions to predict the tool wear degree using an ANN [224].

In [225], a procedure is proposed for the extraction of wear profiles in drilling, which consists of a threshold-based image segmentation step combined with edge detection for refinement, allowing for sub-pixel accuracy. Similar procedures are presented in [175, 194], while in [173] the usage of *Zernike* moments is investigated for sub-pixel edge detection.

As an alternative, edge detection methods are used for finding the wear area [198, 226–228]. While needing manual corrections, KWON ET AL. use the wear area segmented in such a way to develop a novel tool wear index representing the condition of the tool [202]. In [229], the drill edges are segmented by edge detection, allowing for the computation of the *deviation from linearity* metric, which is a well-suited indicator of drill wear. An approach combining *Hough transform* and edge detection for finding the wear area is proposed in [223], subsequently integrating Otsu's method-based thresholding for analyzing multiple views of the cutting tool with view-specific procedures [230]. The combination of contour-based and threshold-based segmentation for drilling is investigated in [231]. For edge detection, especially the usage of *Sobel filter* [223, 232], *Canny edge detection* [223, 229], *statistical filtering* [233], and *moment invariance* [234] are researched.

Texture-based segmentation approaches for wear segmentation are proposed in [235, 236]. A more complex approach is proposed by GARCÍA-ORDÁS ET AL. The cutting edge is extracted from the cutting tool image and divided into multiple subregions. For each of these regions, texture descriptors based on *Local Binary Pattern* are computed, which are classified by an SVM to decide whether the cutting tool can be used further. [144]

Another method for segmenting the wear area is *region growing*. Such an approach can be found in [237] using the segmented image to compute several descriptors based on statistical moments for wear classification. ZHU ET AL. combine region growing with morphological component analysis to segment the wear area, producing rotation-invariant features [199]. In [174], a procedure to compute flank wear width and flank wear area is proposed

combining Hough transform for the horizontal orientation of the cutting edge, region growing, and Canny edge detection.

Besides these primary methods, a variety of other approaches exist. These include the usage of *Markov Random Fields* for tool wear segmentation [238, 239], *Bayesian Inference* for recreating the original cutting boundary [149], *adaptive connecting domain labeling* for wear segmentation [240], and the usage of a statistical shape model [241].

While the segmented images can be used for the direct assessment of flank wear metrics by the means of pixel counting, a different group of approaches extracts features from raw or segmented images, which are used to deduce the wear state by a classifier. CHETHAN ET AL. show this procedure using preprocessing and segmentation steps for computing a binary image, which is used to extract three features that are used to decide whether a tool is worn out or serviceable [242]. Further features are proposed in [200]. In their study, GARCÍA-ORDÁS ET AL. investigate several contour descriptors. The authors extend their procedure by including shape descriptors and texture descriptors in their consecutive publications [144, 243]. Contour signatures are also investigated in [244]. Another approach is presented in [245] and [246] using *active contour models* to extract image features. Comparing several descriptors, CASTEJÓN ET AL. find the *eccentricity*, *extent*, and *solidity* to carry the most information [221], BARREIRO ET AL. achieve the best results using *Hu* and *Legendre* descriptors [247], and ALEGRE ET AL. get the least errors using *Zernike* and *Legendre* descriptors [237]. Furthermore, in [248] a method is proposed using *edge-labeling graph neural networks* for tool condition classification, which utilizes an embedding network to extract features from the original images. The authors state that this method showed promising results, especially for small-sized datasets.

Another research direction is the incorporation of reference images to derive the tool condition. Thereby, the data from an unworn tool is used as a reference and compared to the actual image acquired during machining [184]. As it is essential to realign the worn images with the reference images taken before operation, image registration techniques are researched [249, 250]. Therefore, it is possible to overlay both images and find the difference. SAWANGSRI ET AL. develop such a system by finding the tool pixels in both the reference image and the current image, stating that the difference of both is a suitable indicator for the occurred wear [219]. A similar approach is shown for drilling in [251]. The wear area is also analyzed by ZHANG ET AL. in such a procedure, finding the tool tip before performing column scanning [210]. Besides subtracting both images from each other, *cross-correlation* technology is investigated to compare fresh and worn tools [186, 187]. By using this method,

FONG ET AL. compute the similarity between both images, measuring the relative displacement, which serves as an indicator for wear degree [195]. They suggest that the correlation pattern contains information indicating the different types and sizes of wear defects [195]. Further approaches of including reference images are proposed, comparing the pixel distributions of both images [252], as well as matching the numbers of pixels found [253].

Besides analyzing a single image or comparing the current image to a reference image, PFEIFER ET AL. propose a method of taking a series of images at varying illumination settings, which allows effective contour filtering [254]. A method combining both successive image analysis and the usage of a reference image is proposed in [211], and LINS ET AL. present an in-process TCM system for analyzing image sequences taken during operation [213].

The reviews by REHORN ET AL. and SIDDHPURA ET AL. find that ML-methods are receiving increased attention in TCM research [147, 255]. Early approaches date back to 1994, investigating the usage of ANN for remaining useful life prediction by analyzing image data, material hardness, machinability, and cutting conditions [256].

Within the general scope of ML, unsupervised clustering methods, such as *k-means clustering*, are investigated by FERNÁNDEZ-ROBLES ET AL. to identify clusters of worn regions [223, 230]. Supervised classifiers are mostly used to classify tools as worn based on features extracted from preprocessed tool wear images. This is shown in [244, 257] using a *kNN*, by GARCÍA-ORDÁS ET AL. using an *SVM* [144], or by YANG ET AL. using *fuzzy statistical learning* [206].

However, most approaches are focusing on the usage of *ANNs* [147]. YANG ET AL. use a mathematical tool model for feature extraction and neural network training, allowing for the classification of 15 types of abnormalities [258]. In the study [215], the authors compared both the direct image analysis using an ANN and the analysis of calculated image features by ANN, with the latter achieving better results. Other approaches of ANNs for tool wear classification can be found in [214] and [257]. A further procedure is proposed by D'ADDONA ET AL., combining an ANN with molecular biology inspired genetic approach to predict tool wear based on features extracted from segmented images [201, 259].

Specific types of ANNs investigated for tool wear detection include *edge-labeling graph neural networks* [248], *pulse-coupled neural networks* [260], *wavelet neural network* [224], and *CNNs* [212, 261]. In their study, MAREI ET AL. further investigate the pretraining of networks on unrelated datasets, transferring the learned knowledge to the tool wear identification problem [261].

For the task of not only identifying the state of the cutting tool, but also to segment the current shape of the wear region, specific segmentation networks are researched, which yield a mask of the desired area of interest. MIKOŁA-JCZYK ET AL. suggest the usage of a *single category-based classifier type neural network* for the segmentation of the flank wear region [262]. The same authors extend their approach by a second ANN to predict the remaining tool life under constant cutting conditions [263]. Another approach can be found by BERGS ET AL. using the popular *U-Net* architecture for image segmentation. They find that training separate models for each type of cutting tool investigated might be beneficial over training a generic model for all types of cutting tools. [264] Furthermore, they extend their work by integrating a rule-based wear metric calculation to derive wear metrics from the segmented images [265]. The approach of using U-Net is further investigated by MIAO ET AL., proposing the incorporation of deep supervised learning to address the problem of small sample sizes as well as the usage of *Matthews correlation coefficient* loss to address the problem of data imbalance [209]. Similarly, U-Net is used for not only the identification of flank wear, but also the defects chipping and BUE in [266], further enhancing the classification approach by an uncertainty assessment enabling a human oracle to annotate low-quality predictions. Another novel segmentation method is proposed by REN ET AL., combining *active, incremental fine-tuning*, the *SegNet* architecture, and *conditional random fields*. They also use model pretraining on large datasets, such as the publicly available *ImageNet* dataset [268], with consecutive adaptation to the relevant, small-sized TCM dataset. Thereby, training speed and memory consumption can be reduced. [267]

Model Adaptation

Especially with the rise of ML for decision-making in TCM, attention has to be given to the necessary model training, as many approaches require annotated training data. The required effort for training data generation further increases when training many application-specific models, rather than a single generic model, which is found to produce more accurate results in [264].

As a solution, transfer learning is proposed [261, 267], pretraining the respective models on an unrelated dataset, thereby reducing the number of annotated images from the target application. Another approach is the adaptation of existing training data between applications, known as *domain adaptation*. Such approaches have been investigated for indirect sensing approaches. LIU ET AL. use *adversarial discriminative domain adaptation* for knowledge transfer from a pretrained network of one cutting tool to a new

domain with a different cutting tool [269]. A similar methodology is applied by ZHAO ET AL. to vibration data [270].

2.3.3 Distributed Logic Execution

Cloud computing can be considered a new computing paradigm [271] that shares similarities of time-sharing computers from over 60 years ago [272]. The term *cloud* refers to the ubiquitous availability and accessibility of computing capabilities through the internet [273, 274]. Through cloud computing, hardware and software services are virtualized and rented out to customers [275]. Central aspects include the on-demand service provisioning, an infinite resource pool, a guarantee of service quality, no need for up-front commitment, as well as increased availability, scalability, and flexibility [271, 276]. The provided services can be grouped in categories such as *Infrastructure as a Service*, *Platform as a Service*, and *Software as a Service* [277]. While public clouds provide cloud services on pay-per-use basis to customers, private clouds refer to internal data centers [276]. Therefore, customers have access to a large amount of computing power at reduced costs [278]. In their study regarding cloud computing adoption among the manufacturing industry, OLIVEIRA ET AL. find that these cost savings are one of the major drivers for using cloud technology [279]. One challenge, however, is the delay caused from data generation to decision-making and execution when using cloud systems [280].

With increased data volume and increased cloud computing capabilities, the data transportation speed has become a bottleneck for cloud computing [281]. Thus, **edge computing** emerged, also known as *cloudlets* [282], *fog computing* [283] or *mobile computing* [284], which aims at computational data, applications, and services to be executed at the edge of a network rather than cloud servers [285]. Thereby, edge computing takes place in between local IoT services and cloud computing for both upstream and downstream data [286]. For the integration of edge computing in manufacturing, CHEN ET AL. propose the integration on either equipment level, control level, or workshop level, enabling intelligent services to be executed close to the manufacturing unit while meeting key requirements [287]. Similar to cloud computing, edge computing devices can run arbitrary code, typically using isolation technologies, such as virtual machines or containers [288]. General advantages of edge computing are reduced network bandwidth consumption [275], low latency [289], the resulting shorter response times [281], proximity to the user [289], and better reliability [281]. In contrast to cloud computing, edge computing has local computing devices and a reduced chance of data en-route attacks while having a more limited scope and less scalability [285].

Both cloud computing and edge computing technologies can be combined for the usage in the manufacturing domain. Such systems can be separated into a *physical layer* containing the hardware, such as sensors and actuators, a *cyber layer*, which handles data preprocessing, data storage and decision-making for both edge and cloud computing, and an *application layer*, which includes the actual data-driven applications [290, 291]. VATER ET AL. conduct expert interviews to derive requirements and potential solutions for an information technology architecture following the main requirements of production process control and model recalculation for adaptations throughout time. They find both the usage of HMIs and service-based architectures as promising solutions and propose a reference architecture that leverages cloud computing for model recalculation as well as long-term data storage and edge computing for the storage of operationally needed data (see Figure 15). [292] The interaction between edge and cloud computing is investigated by LIU ET AL., proposing an orchestration with four different types of processing logic: sole cloud computing, sole edge computing, cloud computing to edge computing, and edge computing to cloud computing [290]. LOU ET AL. propose such a cloud edge collaboration system. The cloud system is used for data storage, big data analysis, and model algorithm optimization, while the edge device focuses on data fusion tasks, logic control, as well as the execution of lightweight model algorithms. For the model execution on edge devices, [293] show that edge devices provide sufficient computational resources for the inference of deep neural networks, naming the technologies of *kernel pruning* and *weight quantization* for further model complexity reduction.
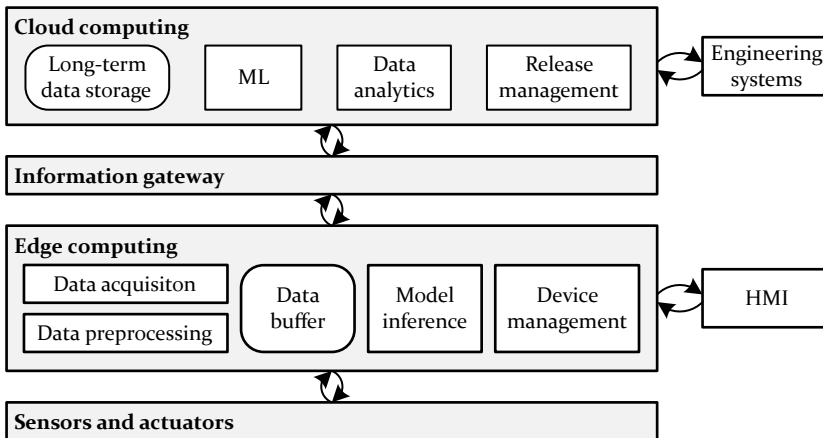
Figure 15: Collaboration of cloud and edge computing systems, modified from [292].

Among the technologies of cloud computing, edge computing, and IoT, the paradigm of **service-oriented architectures** [294] receives increased atten-

tion. Reviewing recent studies on service-oriented architectures, NIKNEJAD ET AL. find that while there is no clear definition, most authors agree that service-oriented architectures "can be defined as an architectural concept that promotes loose coupling, reusability, interoperability, agility, and efficiency, with a focus on breaking each business process into smaller blocks of tasks and functions such as services" [295]. Thereby, monolithic systems can be broken up into a network of many distributed and interconnected services [296]. These services can be designed using microservices, which are light-weight entities performing specific tasks [297]. Combining multiple such specialized microservices, specific functionalities of an application can be realized. In [296], a holistic service architecture is proposed for such a decomposition of software-based industrial services. Applications of this concept can be found both for process optimization in maintenance [298] as well as engineering configurators [299, 300].

2.4 Data-driven Decision-Making

In their review, TETI ET AL. name the sequence of central activities for process monitoring in machining as firstly, *sensorial perception* of process variables, secondly, *data processing and feature extraction*, thirdly, *cognitive decision-making*, and lastly, *action* [138]. With *sensorial perception* discussed in the previous sections, this section focuses on the *data processing and feature extraction* (Section 2.4.1) as well as the *cognitive decision-making* (Sections 2.4.2, 2.4.3, and 2.4.4). For data analysis and decision-making ML in particular has become a popular technology in industrial applications [P2], as the bottleneck of expertise-based, hand-crafted features is removed when using ML instead of traditional feature-based approaches [301]. With the high sensor integration and large data volume, especially machining processes are a promising technology to be further optimized using ML-methods [302].

2.4.1 Feature Extraction and Selection

Initially, *analog signal filtering* can take place. Consecutively, *digital filtering* and *data cleaning* is carried out to reduce noise and improve the signal quality. Based on the cleaned signal, the segments of interest are selected during *segmentation*, discarding the remaining signal parts. These segments are used for *feature generation*, including a *preprocessing* step, and the following *selection* of the most relevant feature set. [136, 303] These steps of data preparation are of great importance due to the impurity of real-world data and the improvement in pattern quality [304].

Standardization is a common data preprocessing method applied to multi-scale data for data normalization [303]. In standardization, the distribution of a feature X is scaled to a standard distribution with a mean of zero and a variance of one (Equation 6), which is supposed to improve model training [305] as the imbalance of features spanning large value ranges can be compensated.

$$X_i' = \frac{X_i - \mu}{\sigma} \tag{6}$$

When working with categorical values, such as batches $\mathcal{B}_1$, $\mathcal{B}_2$, and $\mathcal{B}_3$, encoding needs to be carried out during data preprocessing. In *one-hot* encoding, categorical variables are converted to binary representations such that each category is represented by a specific bit (see Table 2).

Table 2: Using the one-hot encoding method, the binary representation of batch $\mathcal{B}_1$ can be found as $\langle 1, 0, 0 \rangle$.

Categorical value	Binary representation		
	Bit $\mathcal{B}_1$	Bit $\mathcal{B}_2$	Bit $\mathcal{B}_3$
Batch $\mathcal{B}_1$	1	0	0
Batch $\mathcal{B}_3$	0	0	1

Further preprocessing steps might be necessary when dealing with multivariate data. These include data alignment strategies for aligning data points from sensors with different sampling rates, as well as dimensionality reduction methods to reduce the complexity of a dataset.

Simple approaches for aligning one signal to another include *interpolation*, *resampling*, and signal *stretching*. When both signals are aligned in general but sample data points at different times, interpolation methods [306] can be used to find the expected values of the first signal at the sample times of the second signal. Resampling refers to an alignment procedure of two time series with different frequencies. Here, the objective is to adjust the data points of both signals to a common frequency using interpolation methods to fill in gaps. In signal stretching, the timestamps of one signal are scaled linearly to match the timestamps of the other signal. Such methods work well only when considering simple and linearly scaled time series without noise [S8]. Thus, non-linear approaches for data alignment are researched. These include methods such as *dynamic time warping (DTW)* [307], *DTW Barycenter Averaging* [308], and *Diffeomorphic Temporal Alignment Nets* [309].

Given two sequences a and b with respective lengths n and m, the DTW method can be used to find best alignment by computing the $n \times m$ matrix M, with each element $M_{i,j}$ corresponding to the squared distance of a_i and b_j as:

$$M_{i,j} = (a_i - b_j)^2 \tag{7}$$

The optimal alignment between both sequences can now be found as the path through the matrix M that minimizes the total aggregated distance. [310]

With the preprocessed and aligned sensor signals, features can be extracted from the time series signals, describing relevant information in regard to the desired prediction target. Common features in machining include the arithmetic mean and average value, variance, skewness, and kurtosis. Further features include the signal magnitude, signal power, peak-to-peak amplitude, crest factor, and signal ratios. [138] Furthermore, *feature engineering* describes the procedure of creating custom features, characteristic for a given problem, by combining original features through transformation functions based on domain expertise [311].

Based on the number of signals and feature extractions, the resulting number of features can be rather large. Among these, it is likely that only a few contain the majority of the information. As model training becomes more challenging with higher amounts of features [312], it is thus advised to select a subset of the most important features. Feature selection methods include the computation of an importance metric for each feature, selecting the n most important, or the usage of greedy methods for selecting a subset of n features that together have the best prediction results. For feature importance calculation, metrics such as the *Pearson correlation coefficient* between feature and response variable [313], the *coefficient of determination* [314], the *statistical overlap factor* [315], or *joint mutual information* [65] exist. Furthermore, one can train a surrogate model that allows the assessment of feature importance and uses these for feature selection [305]. To find the best subset of features one can differentiate between the two iterative procedures *forward selection* and *backward elimination*. In forward selection, a feature search starts with an empty set of features, adding the feature that brings the most information to the set each iteration. Contrarily, in backward elimination the process is started with all features and the feature with the least information gain is removed each iteration. [316]

As an alternative to feature selection, *dimensionality reduction* methods can be used to transform "high-dimensional data into a meaningful representation of reduced dimensionality" [317], thereby reducing complexity, increasing computational efficiency, and improving accuracy. Popular methods include

singular value decomposition [318] and *principle component analysis* [319]. More recently, VAN DER MAATEN ET AL. proposed the *t-SNE* method for 2D or 3D visualization of high-dimensional data [320].

2.4.2 Machine Learning Fundamentals

AI refers to the intelligence of machines by perceiving their environment and taking actions to optimize a specified goal [321]. As a field of AI, ML describes methods through which computers can learn patterns in data without explicit programming [322].

Categorization of Learning Task

Within the area of ML, one can differentiate between *supervised* learning, *unsupervised* learning, and *reinforcement* learning. In supervised learning, algorithms are trained with sets of feature vectors and the respective target values, with the goal of finding the mapping between both. This mapping can then be used to predict the expected outputs for unseen data. [323] In unsupervised learning there is no target data. It is rather the job of the algorithm to find patterns within the provided data [324]. Finally, reinforcement learning is characterized by an agent taking actions in an environment in order to maximize a specific reward. Through this, the agent has to explore novel actions and thereby learns which actions lead to the highest rewards for each situation faced. [325]

ML-problems can be grouped based on the learning task. In *classification* tasks, the objective is to classify samples as one of many distinct categories. Contrarily, *regression* problems aim at predicting a continuous response variable based on the input data. *Segmentation* tasks are mostly seen in image data but can also be applied to time series data. Segmentation describes the challenge of associating every pixel of an image or value of a time series with its respective meaning. In *novelty detection*, the target is to identify novel samples that are outside the expected distribution of the data, also known as outliers. This can be achieved by training the algorithm with data only from the expected distribution. *Domain adaptation* refers to the task of adapting data from one domain to another, which proves useful for efficient model training. A further task is *metric learning*, which aims at computing a metric indicating the similarity of two samples [326]. Finally, *active learning* follows the idea of the ML-algorithm learning from fewer, but more significant samples, needing an information source, such as a human, for labeling relevant, but so far unlabeled, data [327].

Algorithms

Due to the large number of algorithms and methods proposed for ML, a comprehensive review is not feasible within this study. Instead, the main concepts used in this work are introduced briefly.

One of the most basic ML-algorithms are **decision trees** [328], which are sequential models. Each sequence consists of a simple test, such as the comparison of a feature value to a predefined threshold, for splitting the search space. This procedure is repeated recursively, until a terminal node, also known as leave node, is reached. A greedy search algorithm is used to find the best split at each node. [329] The best split is defined as the combination of splitting feature and splitting value that maximizes the purity of the two resulting subsets. For regression trees, the *squared-error* metric is used as node impurity measure, whereas classification trees utilize the *misclassification error*, *Gini index*, or *cross-entropy* as an impurity measure. [330] Popular decision tree algorithms are *C4.5* [331] and *CART* [332].

Besides using a single classifier, the usage of multiple classifiers, such as **bagging** and **boosting** approaches are found to be successful. The central idea of using multiple classifiers, also known as ensembles, is that many weak classifiers can outperform a single, highly-optimized classifier [333]. In bagging, an ensemble of identical classifiers is built using different subsets of the training data [334]. Building on the idea of bagging, *random forest (RF)* adds algorithm randomization by learning many different base-level classifiers [335], which is considered one of the best performing ensemble classifiers [329]. Similar to bagging, boosting approaches also train several identical model instances on different training data subsets. However, instead of a random subset selection, the performance of the learning algorithm is tracked, and further subsets are drawn favoring inaccurately learned instances. [336] Methods utilizing boosting are *AdaBoost* [336], *XGBoost* [337], and *Boosted Regression Trees* [338].

For the task of novelty detection LIU ET AL. propose **isolation forests**, a specific variation of decision tree ensembles. While traditional novelty detection methods focus mostly on normal instance profiling, isolation forests isolate anomalies. This is achieved using the two main properties of anomalies: the fact that they are in the minority and that they are very different from normal data. Therefore, when constructing decision trees that isolate every instance, anomalies are found closer to the tree root than normal data on average. [339]

SVMs are based on the theories proposed by VAPNIK ET AL. [340]. For given input data and class labels, a hyperplane is determined that best separates the data. This boundary is placed and oriented between the two classes in such a

fashion that the margin among the closest samples of each class is maximized. These closest samples are called *support vectors*. For non-linear classification tasks, kernel functions can be applied. [341] Thereby, the data is mapped into a higher dimensional space with the goal of finding an optimal hyperplane for data separation in that space. Common kernel functions include the *linear* kernel, the *polynomial* kernel, and the *rbf* kernel. [342]

As a specific type of SVM, **One-Class SVMs** are used for novelty and anomaly detection. To do this, the underlying distribution of the normal data is modeled [343]. This can be achieved by finding the boundary around the dataset, which can be described by the trained SVM's support vectors [344].

The **kNN** algorithm is a memory-based classifier that requires no trained model. Given a query point x_0, the k closest points to x_0 from memory are selected and used to classify x_0 using majority voting of the k neighbors found. As data might be from different magnitudes, a prior data standardization is suggested. [330] For the central aspect of distance calculation, a variety of metrics can be used, including: *Euclidean distance, Chebychev distance, city block distance, correlation distance, cosine distance, Mahalanobis distance*, and *Spearman distance* [345].

The **evidence accumulation** clustering algorithm allows for the detection of several clusters without the need for prior specification of the expected number of clusters. To do this, a large number of rather compact clusters are computed initially, using a *k-means clustering* [346]. This procedure is repeated multiple times with random cluster initializations. Subsequently, a voting procedure is used to find the most popular cluster association of each sample among the different random initializations. The resulting co-association matrix is evaluated by a *minimum spanning tree* algorithm [347] to recover natural clusters. [348]

ANNs, specifically feedforward neural networks or multilayer perceptrons, are used to approximate a function f' by finding a mapping $y = f(x; \theta)$ with θ being the set of learned parameters. In feedforward neural networks, there is no information feedback within the model as can be seen in *recurrent neural networks*. The network structure is represented by the sequential application of many functions, such that $f(x) = f^{(3)}(f^{(2)}(f^{(1)}(x)))$ when considering a three layer network. Here, the length of the chain corresponds to the depth of the network. The last layer is called the *output layer* while the remaining layers are called *hidden layers*. The width of each layer is defined by the number of respective *units*, or *neurons*, processing the information of

the previous layer in parallel. [349] Given the input values x_i, their respective weights w_i, and bias b, the output of each unit can be found as:

$$h(x) = \sum_{i=1}^{n} w_i x_i + b \tag{8}$$

Then, an activation function $\varphi(h)$ is applied to the calculated sum to derive the output of that neuron [350]. Thereby, nonlinear functions can be approximated [330]. Common activation functions include *sigmoid* (Equation 9) and *rectified linear unit (ReLU)* (Equation 10), among others [350].

$$\text{sigmoid } \varphi(h) = \frac{1}{1 + e^{-h}} \tag{9}$$

$$\text{ReLU } \varphi(h) = \begin{cases} h, & h > 0 \\ 0, & h \leq 0 \end{cases} \tag{10}$$

ANNs can be trained using *backpropagation* to adjust the weights and bias according to the observed training data. To do this, an error rate, also known as cost function, is computed, judging the prediction of the network based on the ground truth label. The computed error is then cascaded backwards throughout the network, adjusting the weights such that the error rates would decrease in consecutive runs. To do this, optimizers such as *gradient descent* or *Adam* [351] can be used to find the best adjustments of weights and bias per neuron.

Model Lifecycle

Throughout the lifecycle of an ML-model, different phases exist. These phases are formalized as the *CRISP-ML(Q)* process model by STUDER ET AL., expanding the established data mining process model *CRISP-DM* [353] to ML-applications. The sequential steps of the *CRISP-ML(Q)* model are *modeling, evaluation, deployment*, and *monitoring and maintenance*. [352]

Initially, training data needs to be generated. This involves the acquisition of data and the subsequent annotation to enable supervised learning. While for time series classification this involves the assignment of a single label, in semantic image segmentation images need to be annotated pixel-wise. To reduce annotation efforts, weak supervision approaches, which include point clicks [354], bounding boxes [355], and scribbles [356] are researched for creating segmentation masks, however, while these approaches require less human effort they were found to yield reduced prediction accuracies

compared to conventionally annotated images [357]. A more sophisticated procedure is proposed in [358], requiring the user to annotate the images initially with bounding boxes, then automatically converting these into pixel-wise annotations, and finally tasking the user to correct faulty predictions through corrective clicks. Another approach is presented by BRAGANTINI ET AL., dividing each image into subregions, which are subsequently embedded using deep metric learning. Then, the user is shown the representation of the data in the metric space and tasked to assign class labels to the observable clusters which can be applied to all corresponding subregions in the original image space. [359] Thus, using such methods the generation of training data can be made more efficient.

With annotated training data available, a model has to be selected and trained to satisfy the respective constraints and requirements. As there is no model that fits best for all problems [360], model selection needs to be done in relation to the available data. Besides selecting the type of model, model-specific hyperparameters can be adjusted to adapt the respective model towards the data [361]. This procedure of finding the best instance of a model is known as *hyperparameter optimization*. Methods for finding optimized hyperparameters include *grid search* (sampling every specified parameter combination), *random search* (sampling random configurations from defined space) [362], *Bayesian optimization* [363], and *genetic algorithms* [364]. [352]

As an alternative, *automated machine learning (AutoML)* [364] and *neural architecture search* [365] are recent trends in ML, which provide automated frameworks for model selection and hyperparameter optimization and ANN architecture optimization. Using such frameworks, the user needs to formulate the general learning task and provide the required data while the framework handles model selection, optimization, and training, returning a fitted model for inference. Comparing a variety of AutoML tools, EBADI ET AL. find that these are useful but can not replace all human input [366].

In the evaluation phase, the performance of the trained model is validated using a testing dataset, which is a subset of the available data that is not being used for training or hyperparameter optimization. Once trained and validated, the model can then be deployed for operational use. Therefore, hardware needs to be selected that fulfills the computational requirements of model inference. In the final monitoring and maintenance phase, the prediction performance of the model is monitored throughout time. Model updating through retraining can be carried out if a divergence is noticed or if the model needs to be operated outside the conditions it was trained on. [352]

2.4.3 Neural Network Architectures for Image Processing

Especially for the area of image processing, CNNs have become a promising alternative. CNN architectures typically consist of two parts: an initial convolutional part and a subsequent fully connected part. In the convolutional part, alternating *convolution* and *pooling* layers are used which detect translation invariant features, while the fully connected part uses the detected features as inputs for predicting the desired response variable. [367] In convolution layers, trainable kernels, with small spatial dimensionality but spanning the full depth of the input, are iterated over the input data to compute feature maps. Thereby, the trainable parameters are reduced significantly as only the kernel values are trained, and no individual weights are assigned as in fully-connected layers. [368] Here more sophisticated features can be recognized when using a sequence of such convolution layers. In pooling or sub-sampling layers, the complexity for further layers is reduced. This is achieved by dividing the image into subregions and computing a value for each region such as the maximum or average value. [369]

Image Segmentation Networks

For image segmentation tasks, specific types of CNNs emerged that predict not a single class, but a semantic label mask, which contains information about the class membership of each input pixel. These architectures typically consist of an encoder-decoder architecture.

The **U-Net** model was proposed for small-sized datasets such as seen in biomedical imaging and is named after its U-shape. The network contains an encoder part and a symmetric decoder part, with skip connections, which concatenate entire feature maps from the encoder part to the upsampled data of the decoder part. Thereby, context information is obtained, improving the localization of high-resolution features. [370] Based on the original U-Net architecture, several extended networks such as *U-Net++* [371] and *attention U-Net* [372] are proposed.

The **LinkNet** architecture was developed with a light-weight structure for usage in mobile devices and real-time segmentation. Therefore, its encoder uses the *ResNet18* architecture [373] with fewer parameters than other segmentation approaches. The novel encoder-decoder architecture incorporates spatial information from the encoder directly into the decoder. Thereby, accuracy and computational performance are increased. [374]

The **PSPNet** architecture is a novel architecture containing a *pyramid pooling module* for better utilization of global scene information. The usage of context information in deep neural networks is indicated by the size of the

receptive field, which is found to be smaller than theoretically assumed for CNNs, especially for high-level layers [375]. Thus, ZHAO ET AL. propose the usage of a hierarchical global prior, which contains information at different scales and different subregions, known as the pyramid pooling module. In their proposed architecture, a *ResNet* model [373] is used to generate the feature map that is analyzed by the proposed module consisting of four different pyramid scales. Each scale is analyzed individually, and the results are upsampled to the original feature map size using bilinear interpolation and combined as global prior. This prior is concatenated to the original feature map and analyzed by a subsequent convolution layer. Thereby, the final feature map is generated, which leverages contextual information obtained at different scales. [376]

DeepLabv3 uses atrous convolution [377] for the extraction of dense feature maps. Through different atrous rates, sampling rates, and field-of-views, multiscale information is encoded. [378] This approach is extended as the **DeepLabv3+** architecture, which combines the advantages of spatial pyramid pooling and encoder-decoder methods. To achieve this, an encoder-decoder architecture is used with a simple decoder module and original DeepLabv3 model as the encoder module. The features generated by the encoder are bilinear upsampled by a factor of four and concatenated with the respective low-level features from the encoder layer at the same resolution. These low-level features are flattened using a 1x1 convolution. Subsequently, 3x3 convolutions are carried out before another bilinear upsampling of a factor of four to derive the segmentation result. [379]

Generative Adversarial Networks

Generative adversarial networks (GANs) were first introduced by GOODFEL-LOW ET AL. for data generation and can be used to generate artificial data for training subsequent ML-models [381]. They consist of a generator model G with the goal of capturing the data distribution to generate synthetic data and a discriminator model D, which estimates the probability of a sample being generated by G or from the training dataset. Thereby, both algorithms are trained in parallel as a *min-max* game, leading to the generator generating better data and the discriminator getting better at finding generated samples. When using multilayer perceptron networks for G and D, backpropagation can be used for training. [380]

While GANs allow the generation of synthetic data, there is no control of which type of data is generated. When desiring the creation of specific type of data, such as images corresponding to a specific class label, the model can be conditioned with such additional information to steer the data generation

process. This is achieved in conditional generative adversarial networks (cGANs), using extra information, such as the class label, as an additional input for both the generator and the discriminator model. [382] In *image-to-image* translation, the objective is the translation of one image representation (source) to another (target). This translation can be learned using cGANs. To do so, the generator is fed with the source images instead of random noise, while the discriminator needs to distinguish between target images and the generated images. [383]

The **pix2pix** architecture is such an image-to-image translation network using GANs in a conditional setting. The generator and discriminator architectures are based on [384] using modules of type *convolution-BatchNorm-ReLu* [385]. In general, to avoid the single bottleneck layer of traditional encoder-decoder networks, a U-Net-based structure with skip connections is used for the generator. Furthermore, the discriminator is designed such that only patch-scale structures are penalized. [383] As an extension, WANG ET AL. propose the **pix2pixHD** architecture for the translation of high-resolution images, featuring a novel adversarial loss as well as optimized multiscale generator and discriminator architectures. For the generator functionality, two subnetworks are used: the global generator network G_1 and the local enhancer network G_2, both operating at different image resolutions. During training, G_1 is trained first, followed by G_2 and a final fine-tuning step of both networks together. As discriminator, three identical sub-discriminators D_1, D_2, and D_3 are used, which analyze the image at the original scale (D_1) as well as downsampled by a factor of two (D_2) and four (D_3). Thereby, both the generation of globally consistent images and creation of fine details can be achieved. [386]

2.4.4 Performance Evaluation

Performance metrics are used to evaluate the prediction performance of the respective model. Based on the learning task, different types of metrics are commonly used.

Given the number of true positives (*TP*), false positives (*FP*), false negatives (*FN*), and true negatives (*TN*), classification metrics for binary classifications can be computed. These include the *accuracy*, *recall*, *precision*, and *F1 score*.

$$\text{Accuracy} = \frac{TP + TN}{TP + FN + FP + TN} \tag{11}$$

$$\text{Recall} = \frac{TP}{TP + FN} \tag{12}$$

$$\text{Precision} \ = \frac{TP}{TP + FP} \tag{13}$$

$$\text{F1 Score} \ = 2 * \frac{\text{Precision} \ * \text{Recall}}{\text{Precision} \ + \text{Recall}} \tag{14}$$

For image segmentation the prediction of each pixel is classified as TP, FP, FN, or TN. Thereby, the *pixel-wise accuracy* can be computed as shown in Equation (11). As the pixel-wise accuracy is not robust regarding imbalanced datasets, the *IoU* and *mIoU* scores are more commonly used in image segmentation [387]. The IoU score of class i is defined as the intersection of the predicted area and the actual ground truth area, divided by the union of predicted and ground truth area (see Equation 15).

$$\text{IoU} = \frac{TP}{TP + FP + FN} \tag{15}$$

Given the IoU scores of all n classes, the mIoU score can be calculated as:

$$\text{mIoU} = \frac{1}{n} \sum_{i=1}^{n} \text{IoU}_i \tag{16}$$

2.5 Research Outline

As seen in the previous sections, deviations among material batches of the same specified grade are expected due to in-tolerance deviations in the manufacturing process, leading to deviations in machinability. As shown in Table 1, page 17, individual testing is required for optimized machining but the required efforts for material testing make it infeasible. Analyzing the various material identification systems, it is shown that while there is no research for material batch identification in machining, the general identification of different materials is possible as process monitoring. As the impact of a degrading tool condition on the machining signals is expected to be more significant than a change in material batch machinability, TCM systems are reviewed for tool condition assessment. It is found that especially image segmentation using ML-approaches is a promising choice, however, there is little research on effective mutliclass wear defect identification considering not only the image segmentation, but also the involved data annotation and model adaptation to new environments. Furthermore, for operational use, strategies need to be derived that allow for efficient retraining when the environmental conditions change. Thus, based on the solution approaches found, Figure 16 shows the identified research needs for addressing the requirements defined in Chapter 1. Aggregating the individual research needs, the central

research question can be worded as: *Is it possible to identify deviations in machinability among material batches in situ and optimize the machining process accordingly using machine learning?*

Requirement		Research need		Section
R1:	Process optimization regarding machinability deviations among material batches	**N1:**	Routine for batch adaptive machining	5.1 5.2.1
R2:	Detection of novel batches and classification of known batches	**N2:**	Classification algorithm for in situ material batch recognition using ML	4.2.2
		N3:	Novelty detection approach for identification of novel material batches	4.2.1
R4:	Process optimization without available ground truth data	**N4:**	Unsupervised learning for material batch assessment	4.2.3
R5:	Automated characterization and integration of novel batches	**N5:**	Characterization routine using TCM for in situ machinability assessment	5.2.2
R3:	Unknown number of batches	**N6:**	Model retraining routine for continuous model improvement and adjustment of to - be-predicted material batches	5.2.3
R6:	Continuous model improvement			
R7:	Detection and differentiation of various wear defects	**N7:**	Methods for multi-class image segmentation using ML	3.2
R8:	Effective adaptation to new environments	**N9:**	Few-shot learning for data annotation	3.3
		N8:	Synthetic training data generation	3.4
R9:	Individually usable modules	**N10:**	Creation of a service-based architecture	5.3
R10:	Effective integration into modern machine tools	**N11:**	Data handling and feature generation pipeline to utilize internal machine signals	4.1

Figure 16: Based on the requirements and the solution approaches found research needs can be identified.

Solution Overview

To solve the research question, a smart manufacturing system capable of executing the necessary routines is needed. In Figure 17 an overview of the proposed system is shown. A TCM system is used prior to machining to assess the initial tool condition, thereby allowing for elimination of the tool condition's impact on the machining signal. During machining, the internal machine data is observed and preprocessed to extract generalized and information-dense features. These are used to initially decide whether the current material batch is a novel one, and subsequently to carry out material batch classification for known batches and material batch clustering for unknown ones. Finally, this information is used to assess historic knowledge associated with the identified material batch, transferring it to

the current cutting operation for the recommendation of corrective actions to the operator.

For novel material batches, an automated material batch characterization routine is carried out. This involves two machining operations at different cutting parameters to assess the respective tool life and to construct a machinability model. Similarly, this procedure can be used for continuous model improvement by using tool life as groundtruth machinability data.

Both for the material characterization as well as for the parameter recommendation, the condition of the cutting tool plays a central role. Thus, an advanced TCM system is constructed using a CNN to assess cutting tools regarding various types of defects. For an efficient model adjustment process to new environments, domain adaptation and effective annotation methods are proposed, which reduce the required manual effort for training data generation.
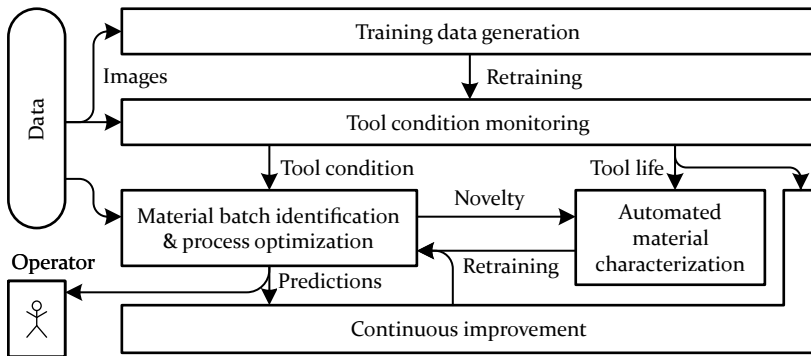
Figure 17: Overview of the needed components.

Differentiation

The topics of process monitoring and tool condition monitoring are researched intensively by a variety of researchers. In both areas, especially the usage of ML has become a popular trend in recent years. Thus, there are several publications and research fields closely related to this work. However, there is no approach that investigates the topic of a smart system for material batch identification as presented in this work, which is shown in Table 3.

Among the TCM research, BERGS ET AL. propose the usage of U-Net for image segmentation of cutting tools [264] and rule-based wear metric calculation [265]. They find, that while this model yields good prediction results, it is better to train individual models for different types of cutting tools rather than a generic model for all types. In their study, they hint towards the

Table 3: Certain aspects of the defined research needs are investigated in related studies [1, 9, 65, 83, 100, 264, 265, 267, 269].

Research Need	BERGS ET AL.	TREISS ET AL.	REN ET AL.	LIU ET AL.	DENKENA ET AL.	LIN ET AL.	LUTZ
N1: Routine for batch adaptive machining	○	○	○	○	◑	◑	●
N2: Classification algorithm for in situ material batch recognition using ML	○	○	○	○	◑	◑	●
N3: Novelty detection approach for identification of novel material batches	○	○	○	○	○	○	●
N4: Unsupervised learning for material batch assessment	○	○	○	○	○	●	●
N5: Characterization routine using TCM for in situ machinability assessment	○	○	○	○	○	○	●
N6: Model retraining routine for continuous model improvement and adjustment of to-be-predicted material batches	○	○	○	○	○	○	●
N7: Methods for multi-class image segmentation using ML	◑	●	◑	○	○	○	●
N8: Synthetic training data generation	◔	○	◑	●	○	○	●
N9: Few-shot learning for data annotation	○	◔	○	○	○	○	●
N10: Creation of a service-based architecture	○	○	○	○	○	○	●
N11: Data handling and feature generation pipeline to utilize internal machine signals	○	○	○	○	●	○	●

usage of GANs for data generation without showing concrete concepts or actual results. Furthermore, their analysis is limited to the detection of flank wear. [264]

A further step is taken by TREISS ET AL., who use the U-Net architecture for the segmentation of the three different wear defects flank wear, BUE, and chipping. Besides the investigation of U-Net for multi-class segmentation, they propose the integration of an uncertainty estimation, enabling a human expert to manually annotate and assess images with estimated low prediction quality. The proposed human-in-the-loop procedure could be considered a data annotation method, however, the primary purpose of the study is to increase model transparency rather than improving the task of data annotation. [266]

Another TCM research is presented by REN ET AL. They use ML-based image segmentation for the binary segmentation of flank wear. Furthermore, they utilize transfer learning by pretraining their networks on public datasets to improve the training speed. [267]

Domain adaptation using deep adversarial transfer learning is proposed by LIU ET AL. While they focus on predicting the remaining useful life as part of TCM, they are using time series data rather than image data. [269]

Regarding the topic of material identification process parameter identification, active research is carried out by DENKENA ET AL. In their research, they investigate process monitoring systems for the identification of different material pairs: two steels of different grades and aluminum-steel. They achieve promising results with a variety of ML-methods and propose optimized cutting parameters for the identified materials, allowing for material-adaptive machining [1]. In their research, the challenges associated with material batches such as novelty detection are not considered. [9, 65, 83]

Finally, an approach for unsupervised material batch classification is proposed by LIN ET AL. for the classification of similar wooden boards based on color. Similarities can be drawn from the unsupervised approach, however the scope of the study is limited to the material identification method. [100]

Research Overview

In the following chapters, approaches are presented to satisfy the defined research needs. Initially, in Chapter 3, methods for efficient image segmentation are proposed. These include methods for multi-class image segmentation as well as procedures for efficient model training. Subsequently, Chapter 4 introduces the methods for handling time series data including the approaches for novel material identification, batch classification, and batch clustering. With the findings of both previous chapters, Chapter 5 proposes the central smart manufacturing system with several routines for parameter recommendation, continuous retraining, automated material characterization, and novel scene adaptation after introducing the batch-specific parameter optimization procedure.

3 Image Segmentation for Low Volume and Highly Diverse Datasets

In this chapter, a novel method for effective image segmentation is proposed. This method does not only include the segmentation model to derive a semantic label mask based on the raw image supplied by a camera itself, but also proposes necessary methods for effective training data annotation and efficient adaptation to novel scenes through domain adaptation.

In Section 3.1 the architecture of the visual TCM system is introduced. Furthermore, the available data and its variance is detailed regarding both the different types of semantic labels visible and the influence of external factors. Thereby, the term *scene* is derived, specifying a set of constant influencing factors. In the following section, image segmentation methods that focus on the different aspects *accuracy* and *computational efficiency* are shown. Thereby, a target-specific procedure can be derived. These methods are adapted for the detection of all defined semantic labels. In Section 3.3, methods are proposed for an efficient data annotation process. This involves a procedure to support a process expert while annotating images. In the final section, methods are proposed to leverage existing training data when training a model for a novel scene.

These results were also investigated in student works supervised by the author [S3–S5, S7, S9, S10]. Furthermore, the following patent applications were submitted [P3–P5] and parts of the proposed methods were made available through scientific publications [P6–P9].

3.1 Visual Tool Condition Monitoring

As described in Section 2, the usage of optical data is a viable alternative for TCM systems, enabling detailed wear analysis. For this procedure, a visual TCM system consisting of a microscope camera with integrated illumination to take a micrograph of the cutting tool is used. The camera is connected to a computation unit to analyze the micrograph, which provides an interface to a human operator or other technical systems for showing the computed information. The technical details are shown in Chapter 6.

In this section, the TCM domain is analyzed further to derive relevant semantic classes. Additionally, environmental factors influencing the visual appearance of a tool's micrograph are detailed.

3.1.1 Domain Analysis

In subtractive manufacturing various types of tool degradation can be observed. For the defect categorization, the approach proposed by LANZETTA is used: The different wear morphologies are grouped into wear defects and breakage defects. The wear defects include the classes: *inner and outer chip notch, flank wear, crater wear, peening wear, BUE, primary and secondary groove*, and *chip breaker groove wear*. The breakage defects include the types: *degeneration of wear, catastrophic failure, breaking, thermal softening and plastic flow*, and *chipping*. [203] With the addition of the generic class *background* representing any object visible in the background of the image and the class *tool* representing the undamaged part of the cutting tool, all areas of an image of a cutting tool can be sufficiently described (see Figure 18).
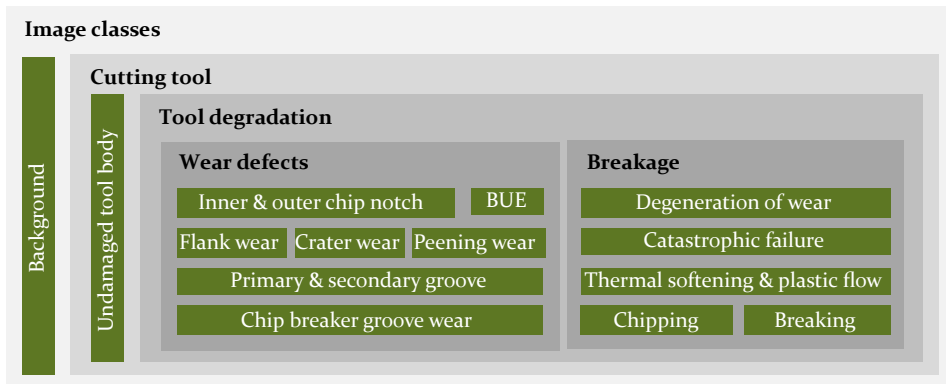
Figure 18: Hierarchy of all defect classes.

The **background** of the image contains mostly areas of uniform color. In some cases, the shadow of the cutting tool insert can be seen in the background. Also, structures from elements in the back of the scene might be visible in this region. Due to the short focal depth of the used cameras and the focus on the flank of the cutting tool, any structures in the background are typical very blurrily depicted and no sharp edges can be made out.

In contrast, the **undamaged cutting tool** itself is mostly in the focal plane and thus depicted sharply. This class represents the areas of the cutting tool that do not show any wear defects. Artefacts, such as chips or residue from the machining process that are visible on the cutting tool, are considered part of this class. Thus, the class consists of large and homogeneous faces and small freckled areas.

The different **wear defects** usually span medium to small areas within the image. While some defects such as *flank wear* or *crater wear* form a connected

wear region, other defects such as *BUE* might appear multiple times, scattered along the cutting edge. Typically, wear defects are visible near the cutting edge with each type of defect appearing on a characteristic face of the cutting tool. Wear defects have their own distinct visual appearance based on the underlying wear mechanisms.

Breakage defects are partly invisible, as parts of the cutting tool might be broken away, thus showing the background of the scene instead. Furthermore, with parts of the cutting tool breaking away, the new surface of the cutting tool might be recessed further, causing them to be out of focus and appear blurry. Generally, the various breakage defects can be described as merging with the background and are identified by unusual borders. Breakage defects are especially apparent when comparing the image with a reference image of a fresh cutting tool.

Figure 19: The different image regions have their distinct visual appearance.

3.1.2 Analysis of TCM Domain Divergence

In this study, a *scene (S)* refers to a series of images taken at the same settings, such as the field of view, camera, and illumination. Thus, images of the same scene should only vary in the degree of wear while otherwise having a similar visual appearance. In Figure 20 sample images from various image segmentation scenarios (scene A - C) can be seen. While the images within the same scene show rather similar visual characteristics, only varying in the degree of wear, significant differences can be observed when comparing images from different scenes.

In this section, potential environmental factors influencing the visual properties of the images within a scene are investigated and detailed. Thereby, scene-specific data adaptation is enabled, allowing for artificial manipulation of the detected factors, which will be detailed in later sections.
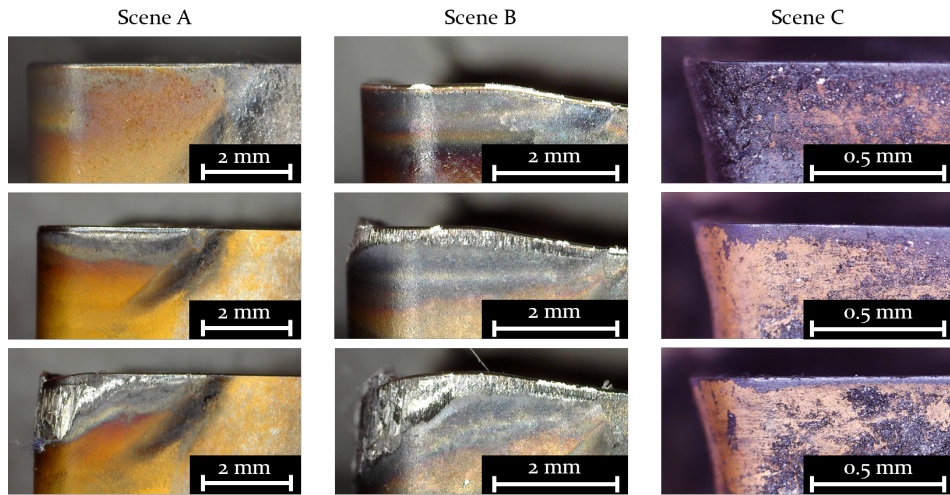
Figure 20: Within TCM, distinct similarities can be seen within a scene while the visual appearance between scenes varies significantly.

Analyzing the domain of cutting tool images, a variety of factors influencing the visual appearance of cutting tool images can be found (see Figure 21). These factors can be broadly grouped in categories, including *cutting tool*, *machining process*, and *image acquisition*. [P8]
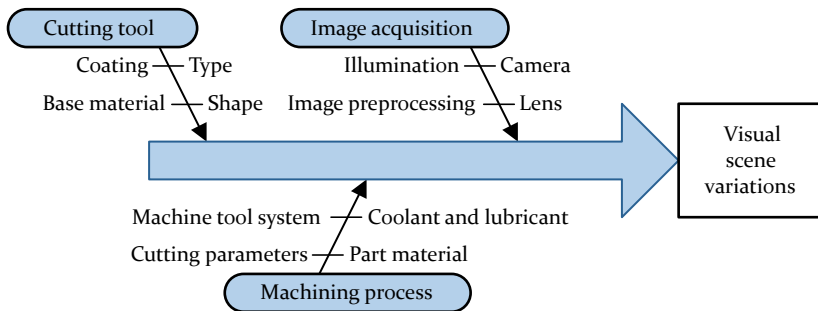
Figure 21: Factors influencing the visual characteristics of cutting tool images, adapted from [P8].

The **cutting tool** significantly impacts the visual appearance due to the main criteria of type of tool, tool shape, tool material, and tool coating. There are different types of cutting tools, such as drills, milling tools and cutting tool inserts, which can be used for a variety of operations. The shape of cutting tool inserts is defined in the industrial standard DIN1832, specifying several tool geometries. Furthermore, the tool material and the tool coating impact the appearance. Among the different coatings, the main groups are uncoated

cutting tools, coatings using chemical vapor deposition, and coatings using physical vapor deposition. [S7]

The influence of the **machining process** can be seen in different ways. Firstly, the type of cutting operation, the respective cutting parameters, and the selected material influence the type and magnitude of the different wear mechanisms and, thus, the expected tool defects (see Section 2.3.2). Depending on the depth of cut and orientation of the cutting tool, the relative position of the flank wear width and its extent might differ. Secondly, factors of the machining process such as the coolants and lubrication influence the scene differently. As the viscosity of the selected liquid can vary significantly, different levels of residue remaining on the cutting tool can be expected [S7]. Other interfering objects can include chips [388] produced by the machining operation. Thirdly, the technical image acquisition system might change between scenes regarding its positioning in the machine tool environment, visible background, and orientation in relation to the cutting tool. Furthermore, the optional presence of a tool cleaning system, such as compressed air, influences the cleanliness of the cutting tool, avoiding partial defect masking by residue.

Besides its placement, the actual **image acquisition** system itself is a major influencing factor on the visual appearance. This unit typically contains a camera, a lens, and an illumination. These all have properties influencing how the cutting tool is portrayed. Main characteristics include the image's resolution, the focus distance, the perspective, and the effects of illumination such as reflections and color shifts. Here, aspects such as limited installation space leading to worse illuminations were noticed [209]. As part of the image acquisition pipeline, respective preprocessing steps can also be noted. These might include cropping, rotating, and zooming to a defined region of interest.

3.2 Image Segmentation Methods for Detection of Different Types of Tool Wear

As shown in Section 3.1.2, a variety of defects can be observed in the micrographs of cutting tools, which all might convey different information to the operator and allow for a more detailed representation of the complex wear mechanisms. While *classification* models would only allow for the decision of whether a sample as a whole belongs to one of many classes and *regression* models would only allow for the prediction of predefined metrics, *segmentation* models offer the greatest level of detail, which can be further processed for a variety of application-specific metrics (see Figure 22). Thus, for holistic condition and defect analysis, image segmentation must be used. Specifically,

semantic image segmentation describes "the task of clustering parts of images together which belong to the same object class" [387]. Adapting the semantic segmentation task to TCM, the objective is to find each pixel's semantic label, with the semantic labels being *background*, *undamaged part of tool*, or any defect described in Section 3.1.1.
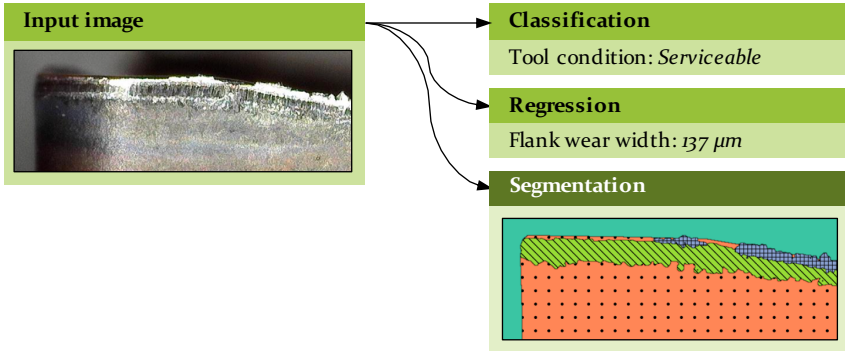
Figure 22: Compared to classification and regression models, segmentation models offer the greatest level of detail.

While the integration into the smart manufacturing system and prototypical implementation will be detailed in Chapter 5, this section introduces the proposed data processing pipeline for semantic image segmentation, which can be seen in Figure 23. In Section 3.2.1, the usage of a reference image in conjunction with the actual micrograph is introduced. Consecutively, in Section 3.2.2 the image analysis using one-pass segmentation networks and in Section 3.2.3 the image analysis using a window-based approach are shown. Both alternatives are compared quantitatively and qualitatively in Section 3.2.5, deriving an optimized method. Furthermore, Section 3.2.4 details how different condition metrics can be computed from the derived semantic masks.
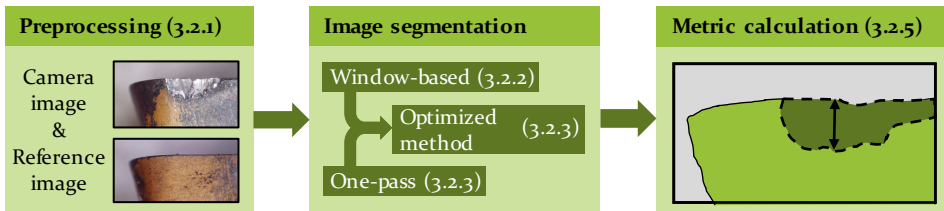
Figure 23: The camera image is preprocessed by adding a reference image. Consecutively, the semantic label mask is derived by an image segmentation model, which is used to calculate several wear metrics.

3.2.1 Reference Image Integration

As shown in Section 2.3.2, data from unworn tools was found as an important source of information for deriving a tool's condition, especially considering that the original tool boundary might be partially gone [149]. However, necessary fine adjustments for reducing mapping errors, as needed for traditional computer vision approaches, make it infeasible [149]. Here, a method is proposed for incorporating reference images in the image analysis pipeline not to provide a pixel-accurate difference, but rather to give context about the expected visual appearance in a given region, see Figure 24.
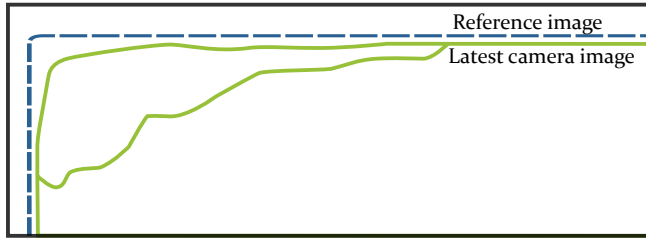
Figure 24: Visualization of the tool contours for an undamaged reference tool (blue) and a to-be-evaluated used tool (green).

To achieve this, a reference image (r) is taken of each new cutting tool before the start of operation, using the same image acquisition procedure used to take images throughout operation. Thereby, it can be ensured that the visual appearance of both images are as similar as possible. This reference image is now appended to each image (u) taken throughout operation for analysis. For a given scene, the assumption can be made that the absolute position of the cutting tool in respect to the camera is always known, as the tool is mounted to a toolholder, which is controlled by the machine's NC. Therefore, the position of the cutting edge within the acquired micrographs is known. Thus, with a defined reference orientation and placement it is possible to adjust potential misalignment through translation (17) and rotation (18) so that the reference image matches the orientation and position of the actual micrograph.

A necessary translation motion of pixel p with coordinates p_x and p_y by an offset of Δ_x and Δ_y can be expressed as:

$$\begin{pmatrix} p'_x \\ p'_y \end{pmatrix} = \begin{pmatrix} p_x \\ p_y \end{pmatrix} + \begin{pmatrix} \Delta_x \\ \Delta_y \end{pmatrix} \tag{17}$$

and a rotation by θ degree as:

$$\begin{pmatrix} p'_x \\ p'_y \end{pmatrix} = \begin{pmatrix} \cos(\theta) & -\sin(\theta) \\ \sin(\theta) & \cos(\theta) \end{pmatrix} \begin{pmatrix} p_x \\ p_y \end{pmatrix} \tag{18}$$

Once both images are aligned to each other, the data of the reference image is stacked with the data of the original image. Thus, when using RGB images, the preprocessed image (v) can be expressed as a six-dimensional vector with the RGB values of the to-be-evaluated image (u) and the RGB values of the reference image (r). These contextualized images can now be analyzed by segmentation algorithms to derive the semantic label mask.

$$v = \begin{pmatrix} u_{\text{red}} \\ u_{\text{green}} \\ u_{\text{blue}} \\ r_{\text{red}} \\ r_{\text{green}} \\ r_{\text{blue}} \end{pmatrix} \tag{19}$$

3.2.2 One-pass Image Segmentation

As shown in Section 2.3.2, *One-pass image segmentation* methods, methods which segment the image with one forward pass through the neural network, show high potential for image segmentation in TCM. These networks typically consist of an encoder-decoder structure with one input neuron for every pixel in the raw image and one output neuron for every pixel in the mask representing the found class (see Figure 25).
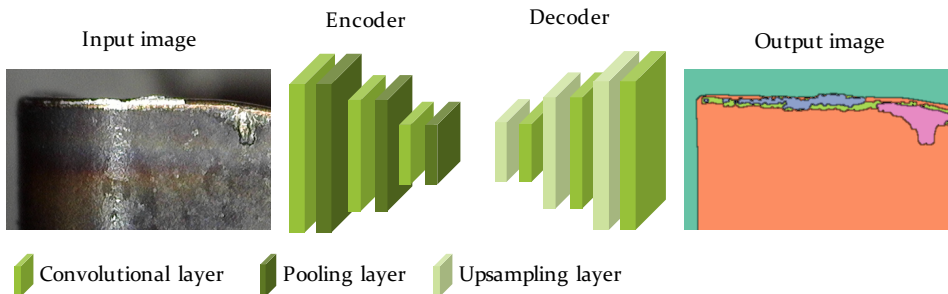
Figure 25: Encoder-decoder structure of a typical one-pass segmentation network.

Within this field of image segmentation, a variety of network architectures are proposed (see Section 2.4.3). These networks are trained while feeding the network with pairs of images and their respective masks. Here it is important that all images are of the same size, thus a resizing operation is needed to ensure this property. As the cutting edge is rather horizontally shaped, a size of 1024x256 pixels is used. Preliminary experiments reveal that especially *LinkNet* and *DeepLabV3Plus* show great potential for image segmentation of the cutting tools investigated in this work [P6, P8]. Compared to other segmentation networks they showed the best overall mIoU score, as well as high IoU for the present defect classes *flank wear* (IoU_{fw}), *groove* (IoU_{groove}), and *BUE* (IoU_{BUE}). For their investigations of only segmenting flank wear, other authors found good results with the *U-Net* [209, 264, 266] and *SegNet* [267] architectures.

However, one challenge seen when using such one-pass segmentation networks is that while the classes *background* and *tool* are identified with high IoU scores for all algorithms, the defect classes, which are especially important, have a significant lower identification accuracy. Other investigated network architectures, such as *FCN* and *SegNet*, were not able to detect the defect classes at all. [P6]

3.2.3 Window-based Image Segmentation

In contrast to one-pass image segmentation, an iterative method based on sliding windows is proposed. The general procedure of the algorithm can be seen in Algorithm 1. In an initial step, the contextualized image v is analyzed pixel by pixel. For each pixel-of-interest (p) p_{ij}, a feature map (ϕ) is created based on the surrounding pixels within the window of size s. This feature map is then analyzed by the classifier $g(\phi)$, predicting the class of p_{ij}. Thereby, the predicted mask ($\widehat{w}$) is filled iteratively. In a second step, image post-processing is carried out to remove noise from $\widehat{w}$.

Algorithm 1 Window-based image segmentation procedure

---

  procedure SEGMENTATION(v, g, s)
    for all $p_{ij} \in v$ **do**   ▷ Iterative segmentation
      $\phi \leftarrow$ GENERATE FEATURE MAPS(v, p_{ij}, s)
      $\widehat{w}_{ij} \leftarrow g(\phi)$
    end for
    $\widehat{w}' \leftarrow$ DENOISE($\widehat{w}$)   ▷ Noise removal
    return $\widehat{w}'$
  end procedure

Generation of Feature Maps

The feature map describes the area of the image surrounding the pixel-of-interest that is used as input for the classifier g to determine the class of the pixel-of-interest. Thereby, not only the information about the pixel-of-interest is taken into consideration, but also neighboring information allowing for an evaluation of patterns nearby. Thus, for a window of size s, the feature map of pixel p_{ij} is defined as:

$$\phi = v_{\substack{i-s/2<x<i+s/2 \\ j-s/2<y<j+s/2}} \tag{20}$$

As the feature map definition allows for values outside the normal area of the image, the border handling needs to be defined. Here, the border values are extended outwards to fill in missing values. For a given p with coordinates x and y, the respective values can be found as:

$$p_{xy} = p_{\min(\max(x,x_0),x_{\max}),\min(\max(y,y_0),y_{\max})} \tag{21}$$

The proposed concept of feature map generation and value padding at the image borders is shown in Figure 26.
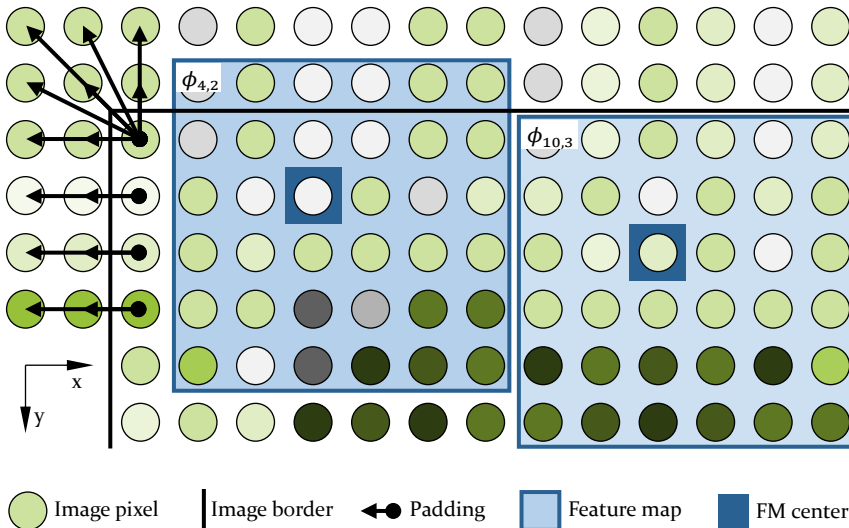
Figure 26: Value padding and feature map generation.

Class Prediction

The prediction of the class label can be carried out by a manually optimized classification algorithm or by using automated approaches such as AutoML and neural architecture search.

A CNN is used to predict the class of each p using the information of the feature map (see Figure 27). In preliminary studies, a network consisting of an initial convolution part followed by a fully connected part was found to show good prediction results [P7]. In the first part, *convolutional* and *pooling* layers are used in an alternating fashion. The network is designed such that every convolutional layer consists of twice the number of filters as the previous convolution. Furthermore, the size of the kernels is set to 3 by 3 pixels. In the fully connected part, two hidden layers are used. All layers have *ReLU* activation functions with the last layer using a *softmax* activation function. Analyzing various hyperparameters in a grid-search manner, it is shown that the highest accuracies are achieved using either four convolutional layers with 16 kernels in the first layer, 128 neurons in the hidden layer, and a window size of 64x64 pixels; four convolutional layers with 64 kernels in the first convolutional layer, 128 neurons in the hidden layer, and a window size of 48x48 pixels; or five convolutional layers with 16 kernels in the first convolution layer, 32 neurons in the fully connected layer, and window size 48x48 pixel. As smaller windows result in smaller computing times, the window size 48 is preferred [P7].

Contrarily to manually designing the network architecture and optimizing its hyperparameters, *automated machine learning (AutoML)* provides methods for automating this process. Thereby, the machine learning expert only needs to specify the learning task and provide the data and the respective labels, while the AutoML-framework carries out network selection and hyperparameter optimization, returning a trained and optimized model for operational use. However, one of the limitations of AutoML is the restriction to the learning tasks that the respective framework offers. These are mostly regression and classification tasks, but not image segmentation.

In this study, AutoML can thus be used for class prediction in the sliding window approach. Thereby, AutoML frameworks offering image classification tasks can be utilized. The procedure is similar to the one shown in Figure 27. However, instead of using a custom CNN network, the black box model provided by the AutoML framework is used for class prediction. [P6]
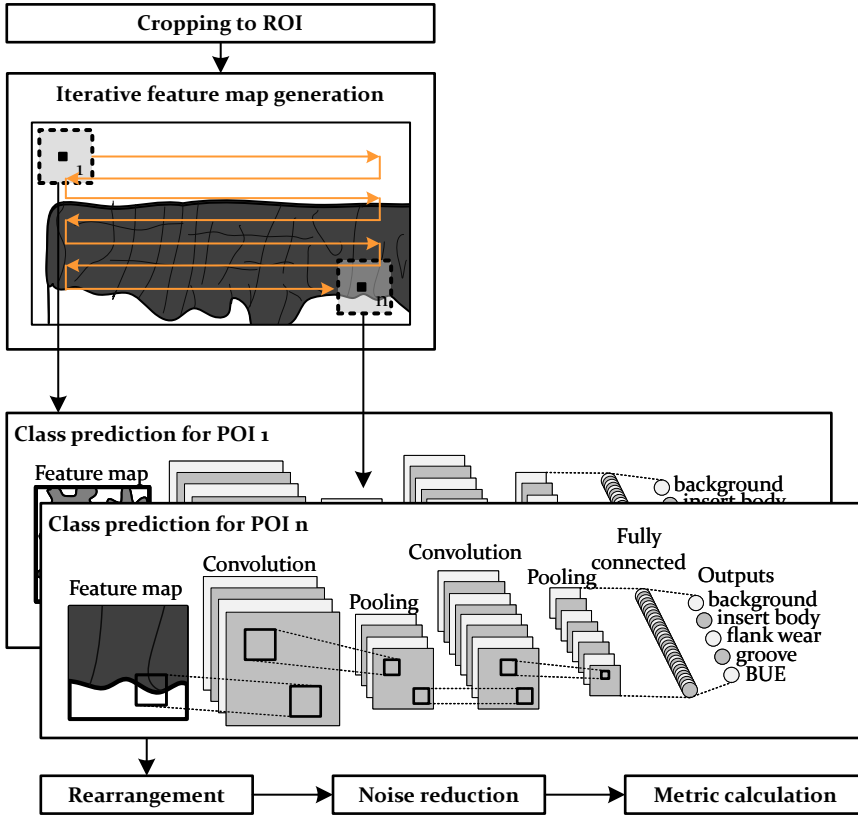
Figure 27: Procedure of the window-based image segmentation approach using a custom CNN, adapted from [P7].

Post-processing

Once the algorithm is executed for all frames, the resulting predictions are recombined to the original shape of the image. Since the image is not analyzed as a whole, but each frame is analyzed independently of its neighboring frames, noise is expected. Thus, the morphological operations *closing* and *opening* are used to reduce noise in the resulting image. These are carried out using an elliptically shaped kernel element *e* of size 7 by 5, see Equation 22. [P7]

Training Procedure

Within the area of TCM, data imbalance is a common problem, as faulty regions, the different wear defects, are less common than unworn regions. Preliminary studies investigating the class distribution within a standard TCM

use-case show that the classes *background* and *tool* appear in every image and have rather high areas within those images, see Table 4. Contrarily, the defect classes *flank wear*, *groove*, and *BUE* are not visible in every image and make up for less than 10% of all pixels combined. [P7] Thus, a balancing operation is needed during the training of such a model so that it only considers equal amounts of feature maps from each class in the training data set. With $C(x)$ being the number of samples of class x, the smallest occurrence of a single class d_{min} can be computed. Now, d_{min} samples are randomly drawn from all classes, thus generating a balanced training dataset of feature maps Φ' with the respective labels C'. [P7]

$$
e = \begin{bmatrix} 0 & 0 & 0 & 1 & 0 & 0 & 0 \\ 1 & 1 & 1 & 1 & 1 & 1 & 1 \\ 1 & 1 & 1 & 1 & 1 & 1 & 1 \\ 1 & 1 & 1 & 1 & 1 & 1 & 1 \\ 0 & 0 & 0 & 1 & 0 & 0 & 0 \end{bmatrix} \tag{22}
$$

Table 4: Exemplary distribution of wear defects in a typical TCM dataset in regard to the percentage of pixels showing the respective defect (pixel percentage) and the ratio of images containing each defect independent of its size (image percentage), adapted from [P7].

	Back-ground	Tool	Flank wear	Groove	BUE
Pixel percentage	39%	54%	6%	1%	1%
Image percentage	100%	100%	97%	37%	65%

To train the window-based image segmentation model, a training dataset of images U_{train} and their respective semantic label masks W_{train} is needed. These label masks need to be created by a process expert. Furthermore, a reference image (r), as well as the values specifying the potential misalignment between reference image and actual images Δ_x, Δ_y, and θ are needed. With these, the training procedure, see Algorithm 2, can be executed. For each training image u supplied, context is added by stacking the reference image yielding the contextualized image v. Each of these images is now analyzed pixel-by-pixel to create feature maps of size s. Both the feature map and the class of the respective pixel w_{ij} are appended to the global set of feature maps (Φ) and respective classes C. After all available images are analyzed, the lowest occurrence of a single class d_{min} is computed, and Φ and C are randomly sampled so that they only contain d_{min} samples of each class. Using

these balanced sets Φ' and C' the selected image segmentation model, either a custom created CNN or an AutoML pipeline, can now be trained, yielding a trained classifier g'. When using the CNN network, the model is trained using the *Adam optimizer [351]* for 200 epochs with a 0.001 learning rate. For the usage of the AutoML alternative, no hyperparameters need to be specified for model training.

Algorithm 2 Training procedure for window-based image segmentation

---

  procedure TRAIN WINDOW SEGMENTATION($g, U_{\text{train}}, W_{\text{train}}, r$)
    for all $u \in U_{\text{train}}$, $w \in W_{\text{train}}$ **do**
      $v \leftarrow$ ADD CONTEXT(u, r) $\triangleright$ Add reference image
      for all $p_{ij} \in v$ **do**
        $\phi \leftarrow$ GENERATE FEATURE MAPS(v)
        $\Phi \leftarrow \Phi \cup \phi$ $\triangleright$ Append feature map
        $C \leftarrow C \cup w_{ij}$ $\triangleright$ Append class of central pixel
      end for
    end for
    $d_{\min} \leftarrow \min C(D)$ $\triangleright$ Find minimum distribution of samples
    $\Phi', C' \leftarrow$ SAMPLE$(\Phi, C, d_{\min})$ $\triangleright$ Undersample training data
    $g' \leftarrow$ TRAIN(Φ', C') $\triangleright$ Train classifier
    return g'
  end procedure

3.2.4 Metric Calculation

Procedure 3 shows the process for deriving wear metrics M from the predicted semantic label mask $\hat{w}$. The most important metric used is the flank wear width (*VB*). It can be computed from the segmented image using a pixel counting procedure. First, the image is rotated in such a manner that the upper cutting edge is horizontally aligned. Second, the image is analyzed column by column, finding the number of *flank wear* pixels for each column. The average flank wear width VB_{avg} is calculated as the median flank wear width of all columns containing flank wear, while the maximum flank wear width VB_{max} is computed as the 90-th percentile of all flank wear widths. Thereby, the robustness of the metric increases as potential outliers are ignored. For all other defect classes, their number of occurrences is computed. Furthermore, for all defect classes including flank wear the total area of the image showing that defect is computed as the number of pixels of the respective class. Finally, all metrics are converted from pixel units to SI units using the calibrated conversion factor c of the image acquisition system.

Algorithm 3 Metric calculation

---

procedure CALCULATE METRICS($\widehat{w}, c$)
    for all $i \in \widehat{w}$ **do**

$$wp \leftarrow \sum x \text{ with } x = \begin{cases} 1, & w_{ij} = C_{\text{flank wear}} \\ 0, & \text{else} \end{cases}$$

    end for
    $VB_{\text{avg}} \leftarrow \text{median } WP * c$
    $VB_{\text{max}} \leftarrow \text{percentile}(WP, 90) * c$
    $VB_A \leftarrow \sum WP * c^2$
    $M \leftarrow (VB_{\text{avg}}, VB_{\text{max}}, VB_A)$
    for all d **do**

$$A_d \leftarrow c^2 * \sum x \text{ with } x = \begin{cases} 1, & w_{ij} = C_d \\ 0, & \text{else} \end{cases}$$

        $M \leftarrow M \cup A_d$
    end for
    return M
end procedure

3.2.5 Assessment of Different Segmentation Approaches

To compare the effectiveness of the proposed approaches, a preliminary set of experiments is carried out [P6]. The algorithms to compare are the sliding window approach using the optimized CNN architecture shown in Section 3.2.3, the sliding window approach in combination with the AutoML classifier[1], and the best found one-pass image segmentation architecture *LinkNet*. In Table 5 a qualitative benchmark of the different methods can be seen. Regarding the complexity, both the sliding window approach with custom CNN and the one-pass segmentation approaches involve building a ML model, and thus are of high complexity. For the AutoML however, only a data preprocessing step is needed, so the complexity of AutoML frameworks is rather simple from a user's perspective. This comes with a cost in explainability, as no insight into the trained model is possible. This, however, depends on the chosen framework. While open source software (OSS) frameworks, such as *Auto-sklearn* [389] or *Auto-keras* [390], offer insight into the selected and trained models, commercial solutions typically allow no such insight and only provide an interface for inference. The *flexibility* of a model describes how easy it can be adapted to changing situations such as a different camera setup with different image data. Here, both sliding window approaches show advantageous characteristics, as those can handle different image sizes easily without retraining, while the one-pass segmentation approaches require a retraining of the model for different resolutions, or cropping and reshaping to the resolution it was trained on with potential loss of information. Finally,

---

[1] Both approaches are trained using sliding windows of size 48 by 48 pixels

both approaches with manually coded classifiers require higher setup times due to the manual network creation, in contrast to the AutoML approach.

Table 5: Benchmark of the different image segmentation alternatives regarding prediction accuracy, complexity (Comp.), flexibility (Flex.), explainability (Expl.), setup time (t_{setup}), and inference time ($t_{inference}$), adapted from [P6].

	Accuracy	Comp.	Flex.	Expl.	t_{setup}	$t_{inference}$
CNN	★★★	★	★★★	★★	★	★
AutoML	★★★	★★★	★★★	★	★★	★
OnePass	★★	★	★	★★	★	★★★

As both the sliding window approach and the one-pass segmentation approach show beneficial behavior, a method is derived combining both alternatives for their respective strengths. In Figure 28 an overview can be seen. As the sliding window approach has the highest accuracy with the drawback of long inference times, it is used in cases where results are not needed urgently, for example when a tool is being put back in the toolholder and a different tool is used to continue machining. However, if a result is needed urgently, such as analyzing a tool before a machining operation starts, the one-pass segmentation approach is chosen instead.
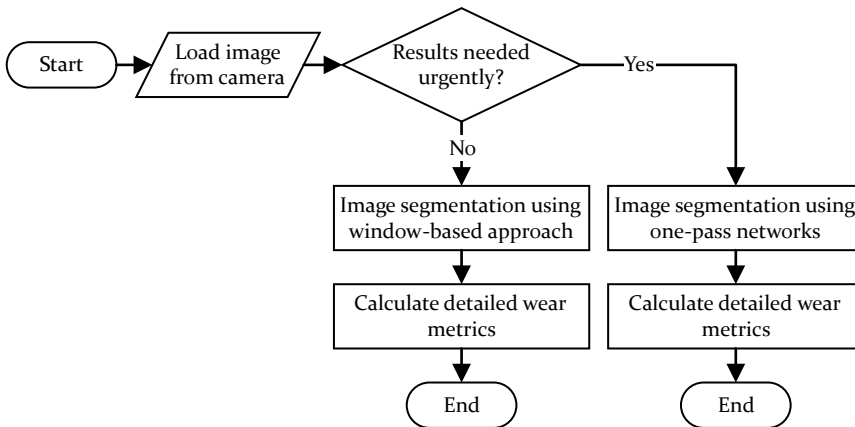
Figure 28: Based on the urgency of the result delivery, either the window-based image segmentation or the one-pass image segmentation is used.

3.3 Strategy for Effective Training Data Annotation

One of the main challenges in supervised ML is the need for labelled training data. While these labels needed are rather easy to acquire in image classi-

fication problems, e.g. assigning each image to the category *serviceable* or *disposable* [144], these labels are more sophisticated in image segmentation. In scope of this work, it was found that the manual labeling process, referred to as data annotation, took between five and ten minutes for a single image. Thus, significant costs are involved in creating sufficiently large training datasets.

As a solution, a novel active learning approach is proposed, incorporating unsupervised learning into the data annotation process, which is shown in Figure 29. This method consists of a *superpixel generation* step, which divides the image into multiple subregions, known as superpixels. These superpixels are then analyzed in an unsupervised manner using metric learning to find the most similar match within a given reference set to provide the expert with an initial suggestion of the respective class label per superpixel. Next, domain-specific logical constraints are used for an automated correction of the generated mask. These aim at filtering out predictions made that are not realistic to appear within the TCM domain. Subsequently, the human is asked to check the resulting mask for faulty annotations and to manually correct them. The final mask can then be used to train a semantic segmentation model. Furthermore, all corrections made by the human will be used as additional reference data for the similarity detection step to label the next image. With every iteration, the automatically generated mask will become progressively better while reducing the human effort, enabling continuous improvement. [P9]

3.3.1   Superpixel Generation and Similarity Determination

A superpixel can be defined as a group of pixels in an image that share common characteristics and are bordering each other. In this work, an algorithm generates superpixels by clustering pixels based on their color similarity and proximity in the image plane. In specific, the *Superpixel Sampling Network* [391] is used, combining the benefit of the established *SLIC* algorithm [392] for superpixel generation with a deep network. Its main benefit is that it can be trained with images and their semantic masks to later generate class-specific superpixels and thereby outperform traditional superpixel algorithms. The number of superpixels needed for accurate representation of small sized defects is determined iteratively based on the image resolution. [P9]

After the superpixels are generated, they can then be compared to a reference dataset, finding the closest match. This is achieved using distance metric learning, specifically deep metric learning, for similarity calculation. A CNN model is used to extract features from the superpixel image snippets. These features, known as embeddings, are subsequently projected into an
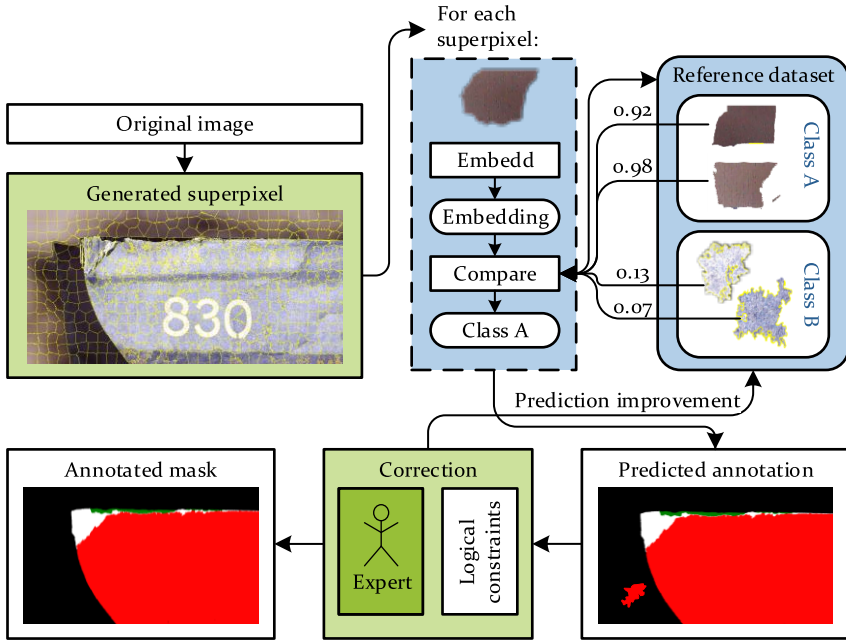
Figure 29: Concept for data annotation using superpixels and deep metric learning for unsupervised class estimation, adapted from [P9].

embedding space, which minimizes the distance between related vectors while maximizing the distance among unrelated ones [393]. The similarity of two superpixels can then be found as their distance in the embedding space. The class of the superpixel with the most similar encoding is then used to annotate the superpixel with the corresponding class. This procedure is repeated iteratively for every superpixel in the image, generating an initial mask. [P9]

Both of the above-mentioned models need to be trained before they can be used. For that some training data is needed in advance. First the Superpixel Sampling Network has to be trained with images and their ground truth masks to generate class-specific superpixels. The class specific superpixels generated from the same training data can then be used to train the deep metric learning-based superpixel embedding. [P9]

3.3.2 Logical Constraints

To refine the initial prediction by the unsupervised method, domain expertise is utilized to derive constraints to judge whether certain classifications are

realistic or not. For the investigated application of monitoring the flank of the cutting tool, the following constraints are derived:

C1   The class *background* covers the region and any objects visible in the background of the image. Thus, this class spans rather large continuous areas. Any single superpixel classified as *background* that is not bordering another *background* superpixel is thus considered a wrong classification.

C2   Furthermore, areas of multiple superpixels that are classified as *background* that are fully engulfed by defect classes or the class *tool* are also considered misclassifications.

C3   Contrarily, any group of superpixels that is fully surrounded by only *background* superpixels must be of the class *background* as well.

C4   Flank wear is a rather large and continuous region. Single superpixels of class *flank wear* are therefore considered misclassifications.

C5   Similar to **C3**, any region fully engulfed by the breakage defects or chipping defect categories must be of that same category.

3.4   Integration of Domain Expertise in Data Adaptation

Observing the sample images shown in Figure 20, page 58, for multiple investigated applications of visual TCM, distinct characteristics of each scene can be noticed. Therefore, images within the same scene exhibit a rather similar visual appearance, while images from different scenes vary significantly. Even though the influencing factors on visual appearance are defined as constant for a given scene (see Section 3.1.2), leading to this effect, there are some inter-scene variations. These include the degradation of the cutting tool, the randomness of visible defects regarding type, size, and location, and the randomness of remaining residue and other artefacts on the cutting tool.

This observed phenomena of intra-scene similarity and inter-scene dissimilarity leads to a decreased prediction accuracy in image segmentation, when combining data from multiple scenes compared to training specialized models for each scene[2], even though the total training volume increases [S3]. Similar conclusions are drawn by [264], showing that having a specific network trained for scenes of different cutting tool types performs better than a single network trained combining all training data. Thus, it is advantageous

---

[2]   The comparison of scene-specific and scene-agnostic models was carried out using the sliding window segmentation model and training data from two different scenes. With the two scene-specific models prediction accuracies of 0.66 mIoU were achieved while the single scene-agnostic model, trained on data from both scenes, reached an accuracy of 0.63 mIoU. [S3]

to train separate models for each scene, rather than one generic model for all types of cutting tools.

Training new model instances for each scene, however, requires the necessary training data of that specific scene. Therefore, the increase in prediction performance comes at a cost of increased labelling efforts. Thus, to enable scene-specific segmentation models with the least amount of training samples needed, methods are proposed for reusing existing training data while minimizing the amount of new annotated data.

As a common solution, transfer learning strategies are used to transfer learned knowledge from other, potentially unrelated, scenes to a novel target scene [394]. However, preliminary experiments reveal that the standard approach of both pre-training an image segmentation model on publicly available datasets as well as pre-training the model on TCM data from other scenes results in low prediction performances[3] [S3]. Thus, advanced strategies need to be researched for transferring existing knowledge to a new target scene.

In this section, a method is proposed for adapting existing training data to the visual appearance of a novel scene, so that the historic data can indeed be used for pre-training an image segmentation model for the new scene. This procedure is shown in Figure 30. Initially, a small amount of training data from the new scene S_N is needed. These are used to automatically characterize the scene regarding certain influencing factors described in Section 3.1.1, deriving a transfer function $f(v, w)$. This transfer function can now be applied to the pairs of historic images and their respective semantic-label-masks from all historic scenes S_i to adapt their original appearance to the appearance of S_N. Lastly, both the synthetic dataset and the few samples provided from S_N are combined and used to train the image segmentation approach for S_N as described in Section 3.2.

The central aspect of the data adaptation procedure is the transfer function f, allowing the adaptation of images v and their respective masks w from any scene S_i to be changed such that they match the visual appearance of a target scene S_t, see Equation 23. This adaptation procedure can be broken down into two aspects:

1. The adaptation of the shape of the cutting tool, which applies both to the actual image and the respective semantic label mask

---

[3] Pre-training the segmentation model on the public ResNet-18 dataset yielded a prediction performance of 0.57 mIoU for the novel scene while pre-training on data from other TCM scenes yielded a prediction performance of 0.12 mIoU.
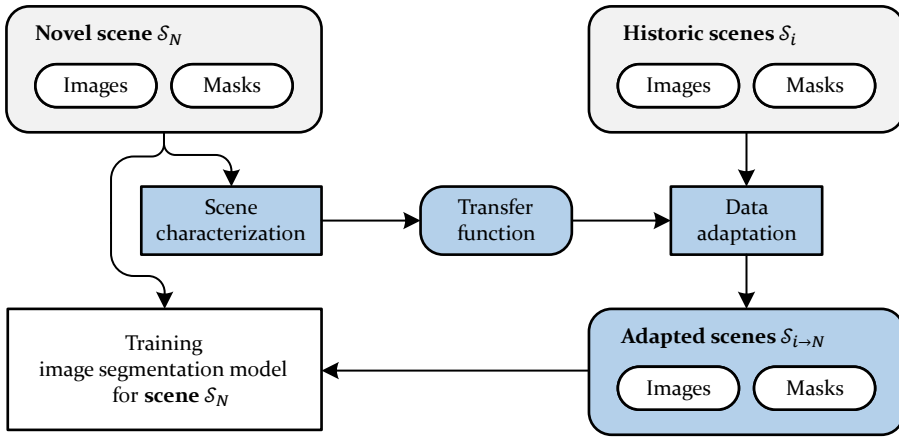
Figure 30: Historic training data can be reused for training a novel scene's segmentation model by adapting the historic data to the visual appearance of the novel scene.

2. The adaptation of the color and texture of the depicted objects, which applies only to the image data

$$(v_{S_i \to S_t}, w_{S_i \to S_t}) = f(v_{S_i}, w_{S_i}, C_t) \qquad (23)$$

3.4.1 Method for Tool Shape Adaptation

As described in the previous section, the shape of the cutting tool and therefore the shape of the cutting edge varies between different types of cutting tools. For cutting tool inserts, the shape of the cutting edge is defined by multiple parameters. As the shape thus does not depend on statistical influences, but is a defined property, image warping can be applied to modify a given shape into a desired shape.

The general procedure of image warping can be seen in Algorithm 4. Given the shape of the cutting tools in S_t and the shapes of the historic data S_i, the images and masks of S_i can be distorted in such a way they match the new shape in S_t. First, the available data is used to extract the shape of the cutting edge for each scene. Subsequently, the images are checked for horizontal alignment of the cutting edge. If this is not the case, image rotation is carried out. Thereby, it is ensured that all images and masks are oriented in such a fashion that the main cutting edge is oriented horizontally with the flank of the cutting tool below. Furthermore, using the metadata available, all images are cropped so that the cutting tools are shown in similar scales. Second, feature points are selected at regular intervals on the cutting edge, the body of the cutting tool, and the edges of the image. This is carried out

for the reference image of each historic scene as well as for one image of $\mathcal{S}_t$, ideally the reference image. The computed feature points can now be connected in a third step to form triangles using the *Delauny triangulation* algorithm [395]. Finally, for each triangle, image warping is carried out to warp and interpolate each given triangle from its feature point coordinates in the historic scene to the respective coordinates in the target scene. This geometrical transformation is carried out using *affine transformations* to retain the relations within each triangle. [S3]

Algorithm 4 Shape Adaptation

procedure AUGMENT TOOL SHAPES(g, I_{train}, M_{train})
    for all $\mathcal{S} \in \mathcal{S}_t \cup \mathcal{S}_i$ **do**
        edge $\leftarrow$ FIND EDGE($\mathcal{S}$)
        FP $\leftarrow$ GENERATE FEATURE POINTS(edge, r_s)
    end for
    FP2Triangle $\leftarrow$ DELAUNY TRIANGULATION(FP$_{\mathcal{S}_t}$)
    Triangle$_{\mathcal{S}_t} \leftarrow$ FP2Triangle(FP$_{\mathcal{S}_t}$)
    $w_{\text{train}} \leftarrow w_{\mathcal{S}_t}$ ▷ Add annotated target masks to training set
    $v_{\text{train}} \leftarrow v_{\mathcal{S}_t}$ ▷ Add annotated target images to training set
    for all $\mathcal{S} \in \mathcal{S}_i$ **do**   ▷ Iterate over historic data for adaptation
        Trinagle$_{\mathcal{S}} \leftarrow$ FP2Triangle(FP$_{\mathcal{S}}$)
        for all $w, v \in \mathcal{S}$ **do**
            $w' \leftarrow$ WARPING(w, Triangle$_{\mathcal{S}_t}$, Triangle$_{\mathcal{S}}$)
            $v' \leftarrow$ WARPING(v, Triangle$_{\mathcal{S}_t}$, Triangle$_{\mathcal{S}}$)
            $w_{\text{train}} \leftarrow w_{\text{train}} \cup w'$ ▷ Add warped masks to training set
            $v_{\text{train}} \leftarrow v_{\text{train}} \cup v'$ ▷ Add warped images to training set
        end for
    end for
    return $w_{\text{train}}, v_{\text{train}}$
end procedure

Tool Flank Extraction

While the shape of the cutting tools of the historic data can be derived from the respective masks, there are multiple alternatives for the shape determination of the new scene. If semantic label masks are available, these can be used. Alternatively, an edge detection algorithm can be used to find the edge of the cutting tool in cutting tool image data. Thirdly, with neither semantic label masks nor image data of $\mathcal{S}_t$ available, the cutting edge can be described mathematically knowing the exact specification of the cutting tool [S7]. [S3]

To extract the cutting edge from semantic label masks, all defect classes and breakage classes are joined with the class of undamaged tool body, thereby creating a binary image consisting of background and condition-independent cutting tool area. Now, the horizontal border between both regions is found

by scanning each column for the transition point between the background class and the joined cutting tool class. This method can be applied for finding the cutting edge for all historic data as well as to the target domain, given that at least one annotated mask is available.

As an alternative, traditional computer vision methods can be used for extracting the cutting edge from a cutting tool image. To do this, the image is converted from RGB color mode to grayscale color mode. Next, the *Canny edge detection* algorithm [396] is applied to detect the main border between the cutting tool and the background. Smaller edges detected are removed using the *erosion* operation while open areas are filled by the *dilation* operation. Finally, a *Gaussian blur* function is applied. [S3]

Lastly, there might be scenarios with neither image annotations nor raw images. This scenario can be seen when adapting an existing image segmentation procedure only by changing the type of cutting tool with otherwise constant environmental influencing factors, or when trying to artificially create a heterogeneous dataset of many potential shapes of cutting tools. As detailed in Section 3.1.1, the shape of a cutting tool can be described by various international standards or specific supplier guidelines. Thereby, a mathematical description $g(x)$ of the ideal shape of the cutting tool can be derived based on its specification, which yields the j coordinate of cutting edge for column i. [S7] The derived cutting edge can then be placed at anchor point $A_{i,j}$. Now, the area under the curve can be considered the tool body for feature point selection purposes. To transfer this theoretical approach into operation, one needs to align the cutting edge placement within the acquired images with the chosen anchor point.

Feature Point Generation

With the detected cutting edge and the tool body, feature points can be assigned. These consist of the four edges of the image, the half-way point of the lower and upper edge, and an adjustable number of points within the image. The determination of these feature points within an image is based on the detected cutting edge and are found in three steps. First, n feature points are placed at regular intervals at the upper cutting edge spanning the full horizontal width covered by the cutting edge. These feature points are pushed upwards by ten pixels such that they are located just above the cutting edge. Next, a second row of n feature points is added with a fixed offset of 50 pixels directly beneath each feature point assigned in the previous step. Thereby, the feature points from step one and two form a band into which most wear defects fall. Finally, a third row of n feature points is added at the half-way point between the last row and the bottom edge of the image. As

image warping will result in image deformation, this proposed procedure ensures that the upper area of the cutting tool, with the highest density of defects, will have the least distortions, while the lower parts of the cutting tool will be more distorted. Furthermore, a set of feature points is added at the left image border on the heights of the first point each layer found by the iterative procedure. Sample images with highlighted feature points can be seen in Figure 31.
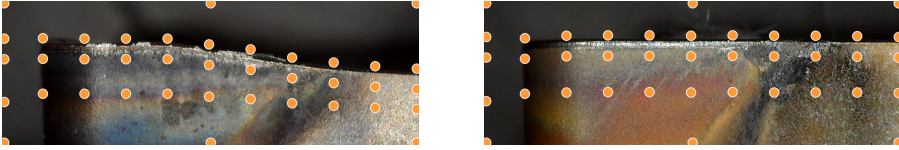
Figure 31: Sample images with feature points highlighted in orange.

Preliminary experiments show that using a sufficient number of feature points is needed for good warping results while too many points cause issues. As a best-practice, between 20 and 50 feature points are found to yield the best results.

Triangulation and Warping

Given the set of feature points, a set of non-overlapping triangles can be found using the Delaunay triangulation method [395]. To ensure the same triangles form in all pictures, the triangulation procedure is executed only for the feature points found for the target scene FP_{S_t}. As each image contains the same feature points independent of its scene with only the relative positions changing between scenes, the triangulation found for S_t can be applied to the remaining scenes by connecting the respective feature points at their scene-dependent position.

Now, image warping is carried out for each triangle found, mapping the points of the original image to the points of the target image. Here, affine transformations such as scaling, rotation, and translation are used. These geometric transformations preserve the relative proportions between points and lines. [S3] The combined procedure of triangulation and image warping can be seen in Figure 32.

3.4.2 Method for Color and Texture Adaptation

While the shape of cutting tools varies in defined characteristics, the color and texture of the cutting tool and the background depend on a greater variety of influencing factors, rendering a traditional approach of changing these characteristics infeasible. Thus, for the adaptation of visual characteristics,
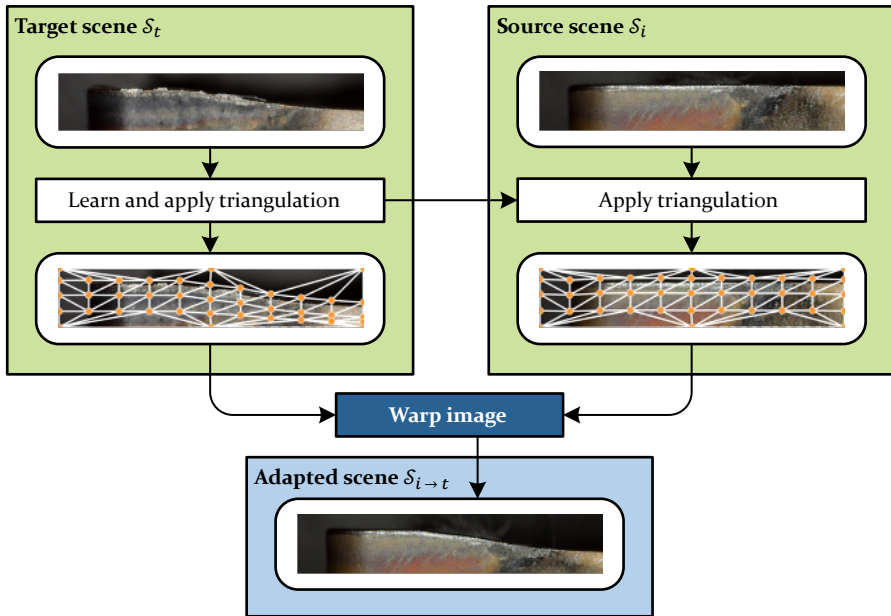
Figure 32: Image triangulation and warping.

GAN networks are researched. These types of neural networks allow for the creation of synthetic images. Especially *image-to-image* translation networks, such as cGAN, are promising, as they provide functions for translating one image to another. Thus, given an image from a source scene $\mathcal{S}_s$ as input to a GAN model trained on a target scene $\mathcal{S}_t$, the model can translate the image to match the visual characteristics expected from images of $\mathcal{S}_t$.

In the scope of historic training data adaptation to new scenes, these networks can thus be used to adapt the visual appearance of existing data to match the expected visual appearance within the new scene, while retaining spatial relations such as the shape of the cutting tool. However, preliminary experiments show that when using cGANs to translate cutting tool images from one scene to another, realistic results could be generated, but the generated images would not align with the original semantic label mask, limiting the benefit of this approach [S3]. Thus, sophisticated image-to-image translation strategies are needed that solve the challenge of mask absence, retaining the mask information needed to train the consecutive image segmentation algorithm.

Region-based Translation

One proposed solution is region-based image-to-image translation. In region-based image-to-image translation the input image is adapted iteratively. Each defect region is analyzed on its own. Thereby, the task of translating a cutting tool image with various defects present is broken down into many smaller subtasks, translating one semantic class as it would appear in scene $\mathcal{S}_s$ to the same semantic class as it would appear in scene $\mathcal{S}_t$. Therefore, separate GAN models need to be trained for each semantic class.

The detailed concept is shown in Figure 33. A grid of width s is applied to the to-be-translated image v_s to generate square-shaped windows of width s. These windows are analyzed iteratively, converting each window to the visual appearance of target scene $\mathcal{S}_t$ while maintaining the class relationship. After each window is analyzed, the generated windows are recombined to form the translated image v_t. For translating the individual windows, two cases need to be differentiated based on the respective semantic label mask snippet of the window. In the first case, only one class is present in the given window. Thus, for a single class c present, the generator model G_c can be used to translate the given window $q_{\mathcal{S}_s}$ to the target scene: $q_{\mathcal{S}_t} = G_c(q_{\mathcal{S}_s})$. In the second case, multiple classes are present in the given window, requiring detailed handling. In this case, each class c_i with $i \in \{1, 2, \dots, n\}$ is handled separately. For a given class c_i, all areas of the window showing different classes are erased, resulting in a partial image of only areas of class c_i. The empty areas are filled in a mirror fashion. Thereby, the window q' is created, containing only class c_i. This window is used as input for the respective generator model G_{c_i} to translate the window to the target scene. The initial semantic label mask is then applied to remove any parts of the image that are not supposed to show class c_i. Once this procedure is executed for all classes, the predicted regions are recombined, forming the translated window $q_{\mathcal{S}_t}$ consisting of multiple translated semantic classes which align with the respective image mask.

Mask-to-Image Translation

As an alternative a *mask-to-image* translation method is proposed, using a domain adaptation model to translate semantic label maps from any source scene to realistic images of the desired target scene. Thereby, existing masks of realistic defect shapes and distributions can be reused for creating synthetic images.

The operational procedure to train a segmentation model for a novel scene using the proposed *mask-to-image* translation procedure is shown in Figure 34. Initially, images from the target scene $\mathcal{S}_t$ need to be acquired representing the
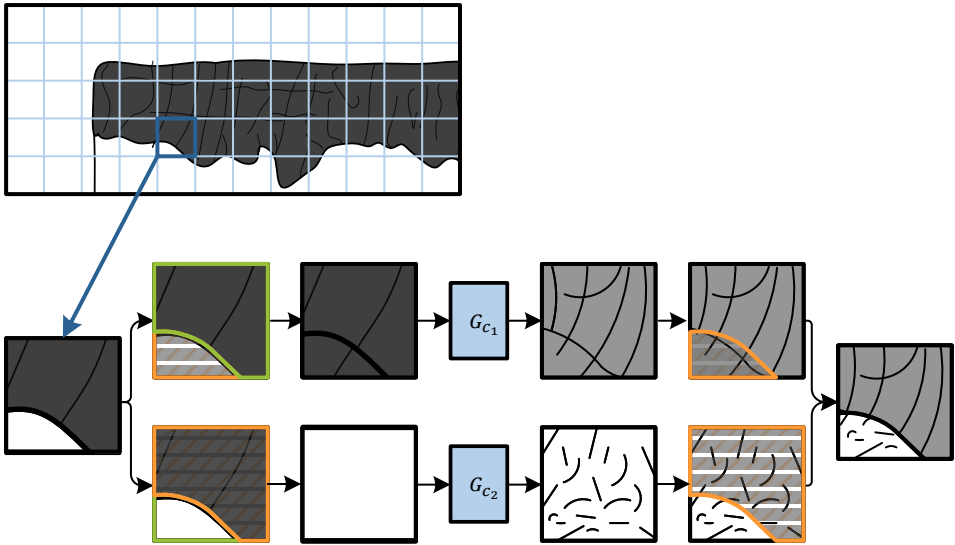
Figure 33: Region-based image-to-image translation concept for windows containing multiple classes.

normal distribution of tool conditions expected in $\mathcal{S}_t$. A few of these images need to be labeled by a process expert to create the *labelled* dataset used for training the domain adaptation procedure, while the remaining images are stored as an *unlabelled* dataset. Furthermore, historic data from other scenes, especially the annotated image masks, are considered as source scenes $\mathcal{S}_i$. In the first step s_1, the *labelled* dataset from $\mathcal{S}_t$ is used to train the domain adaptation procedure, especially the discriminator and generator networks. In the second step s_2, the trained generator of the domain adaptation procedure is now utilized to generate synthetic images from the historic masks of the various source scenes. Thereby, the new *synthetic* dataset in the target scene is created consisting of tuples of the historic semantic maps and the respective created images by the generator network. Now, both datasets in $\mathcal{S}_t$, the initially *labelled* dataset and the *synthetic* dataset, can be used in the third step s_3 to train the image segmentation procedure detailed in Section 3.2. Finally, the trained segmentation procedure can now be used to segment novel images in $\mathcal{S}_t$ during operation. [P8]

In a preliminary set of experiments it is found that the *pix2pixHD* architecture [386] is a promising cGAN for mask-to-image translation in a configuration with three discriminators downsampling the data by factors 2 and 4. It is found to train the model for 800 epochs using the *Adam* optimizer [351] with an initial learning rate of 0.0002 and a momentum beta of 0.5. The
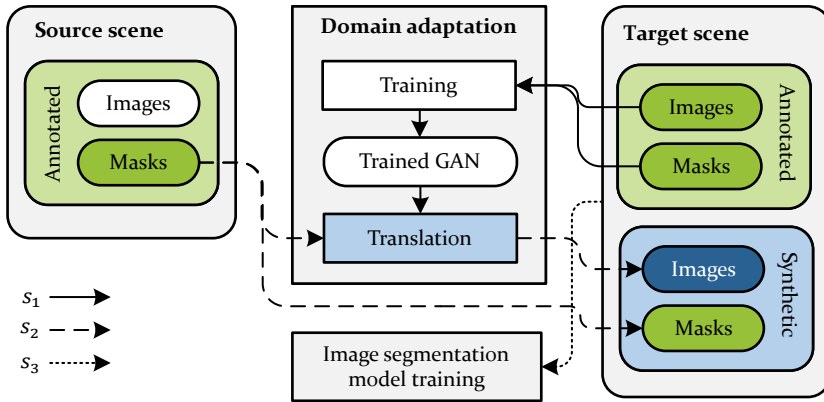
Figure 34: Procedure for automated domain adaptation, adapted from [P8].

training dataset contains pairs of semantic label maps and the corresponding images. [P8]

4   In Situ Identification of Material Batches

While general material information such as the material grade, its expected chemical composition as well as its fabrication procedure are known before machining, fluctuations in any of these properties within its tolerance limits leading to material batch effects can not be predicted. Thus, process monitoring methods are needed that are able to detect these deviations during machining, and inform the operator about the material batch and its expected characteristics so that the machining process can be adapted accordingly.

As the available process data is not only influenced by the machinability of each material batch, but even more by other factors such as the cutting parameters or the tool condition, a sophisticated data handling and preprocessing pipeline is needed (Section 4.1). Specifically, methods are provided to monitor the machining parameters influencing the process data and to compensate for specific effects. Furthermore, the high-dimensional control data used is aggregated into low-dimensional feature vectors.

The computed feature vectors in conjunction with the detected machining state are subsequently analyzed by the material identification routine (Section 4.2). Specific models corresponding to the detected machining state are selected. Initially, it is investigated whether the current material shows a machining behavior similar to material batches machined in the past. If this is the case, the material is classified. Otherwise, an unsupervised approach is used to interpolate information from closely related historic samples.

The implementation of the proposed methods is shown in Chapter 5. Parts of these analyses were supported by student work supervised by the author [S8, S11]. Central findings were already made public to the scientific community in the publications [P10, P11] and patent application [P12] of the author.

4.1   Method for Generating Generalized Features

The continuously monitored process data needs to be evaluated regarding the state of the cutting process, preprocessed to improve data quality, and aggregated into low-dimensional features. As the main data source, the control data of the machine's NC is used. The available data can be classified as *high-frequency* and *low-frequency* data. High-frequency data contains the current, the torque, the speed, the designated position, as well as the measured position at each encoder for each linear and rotary axis of the machine tool. The data is taken at each cycle, thus typically at the cycle frequency of 500 Hz. The low-frequency data contains information such as

the adjusted override or a new line of machining instructions and is published at varying rates. Using these machine-internal signals simplifies scalability to new machines, as these signals are available in most modern machine tools [122]. Besides the control data, other data sources are used for machining state assessment and signal compensation.

In this work, the *machining state* $\mathcal{M}$ refers to the state of the cutting process regarding the type of cutting operation, the respective cutting parameters, the cutting tool, the condition of the cutting tool, and the general workpiece's material. As all these factors strongly impact the machine tools' signals, data from different machining states should be investigated separately. Furthermore, as the machine itself has a significant impact, machine-specific models need to be trained.

The cutting operations can be broadly classified in *no cutting*, for example general tool movements, and *cutting*, which can be further classified in operational types such as *roughing* and *finishing*. Information about the cutting operation can be derived from analyzing the machine control instructions (G-Code). While the G-Code analysis provides the designated cutting parameters, the machine operator can manually adjust the cutting parameters using the override functionality integrated into most machine tool's control panels. Typically, both the cutting speed and the feed rate can be decreased and increased in this manner. The type of cutting tool used is a known information for each specific cut. While the tool types might change for different cuts, they are assumed to remain the same for a given cut. If a tool reaches its defined or unexpected end-of-life, the tool is replaced by another tool of the same type. The condition of the cutting tool is assessed using a TCM system, as proposed in Chapter 3, at the start of each cut. Remaining influencing factors such as the cooling strategy are assumed to be constant for a given cutting operation.

The detailed procedure for determining the machining state for a given time during operation is detailed in Section 4.1.1. In the data preprocessing step (Section 4.1.2) these influences are partially compensated using physical relationships, simulated cutting forces, and data-driven compensation. Finally, information-dense features are extracted from the preprocessed machine data, yielding tuples of feature vectors and their respective machining states (Section 4.1.3).

4.1.1 Data Handling

The high-frequency and low-frequency control data are acquired by connecting to the machine tool's NC. While the high-frequency data contains the

control data at the cycle frequency, it is published at irregular intervals. Thus, the data needs to be realigned in an initial step using the cycle counter of each high-frequency data point which maps the machine data to the exact control cycle it was acquired. Contrarily, the low-frequency data uses timestamps to index the published data. To synchronize the cycle-indexed high-frequency data and the timestamp-indexed low-frequency data, the cycle index and its corresponding timestamp are published as low-frequency data, enabling correct mapping.

In this work, the low-frequency data will be used to segment the continuous signal into individual cuts based on the G-Code and to assign the true cutting parameters, by monitoring the manual override functionality, to each segment. The high-frequency data will be used to derive information-dense features for the subsequent material identification. Besides the internal machine data, other data sources include the measured tool condition from the TCM system, baseline data as reference , and context data such as simulated process forces.

Cut Segmentation

Typical machining programs consist not only of a single cut, but of multiple movement and cutting operations, such as roughing and finishing cuts in basic turning, which are combined to manufacture arbitrary shapes. In this work, the term *cutting operation* or *cut* for short refers to the time between a defined start trigger and its respective end trigger. G-Code analysis is used to segment the continuous process data into the individual cutting operations. Therefore, in an initial step each data point is associated to its cut. In between cutting operations, the machining axis might move, but as they are not in a cutting motion, these general movements are not of interest, therefore they can be discarded.

The segmentation is done by adding or specifying certain G-Code lines, indicating the start and end of each to-be-monitored cutting motion. Now, the process monitoring system can observe the event data stream, waiting for these specified G-Code messages of the respective cutting operation. An example can be seen in Algorithm 5 where the line "N1130 [...]; Cut-start" starts the cutting operation while the cutting operation ends with line "N1140 [...]; Cut-end".

Machining State Deduction

In a connected look-up-table, the planned cutting parameters can be found for each cutting operation indexed by the trigger command, see Figure 35. As the

---

Algorithm 5 Exemplary machine code with trigger

...
N1120 G1 X1=662.649 Z1=-13.057
N1130 G1 X1=662.501 Z1=-226.269; Cut-start   ▷ Start trigger
N1140 G1 X1=667.352 Z1=-228.789; Cut-end   ▷ End trigger
N1260 G1 Z1=-231.503 F0.5
N1270 G1 X1=285.342 Z1=-236.871
...

---

machine operator has the option to manually adjust the cutting speed and the feed rate using the machine override, these effects need to be compensated. The value of both cutting speed and feed rate override as percentages can be read from the low-frequency data stream. Thus, the current values of the override functionalities are monitored and used to correct the planned cutting speed $v_{c\text{plan}}$ and feed rate f_{plan} to the true cutting speed v_c and feed rate f.
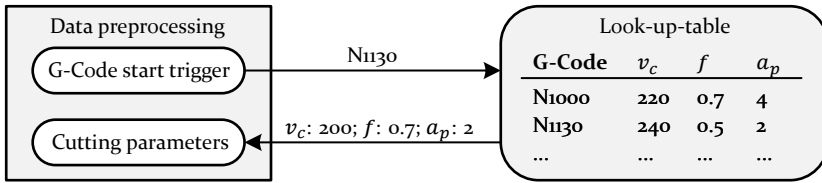
Figure 35: The designated cutting parameters can be found using the machine instructions.

To acquire information about the tool's condition, the flank wear width VB_{t_0} is derived from a TCM system when the tool is entering the process from the tool magazine. Throughout the cutting operation, a batch-agnostic tool life prediction model is used to approximate the continuous degradation as expected for an average batch of the specified material. Here, the Taylor model is used without being adapted for material-batch effects, thus using parameters approximating the general behavior of the material. Given the material-specific parameters c_v and k, the estimated tool condition $VB_{\text{est.}}$ after a machining time of Δt at a cutting speed of v_c can be calculated using Taylor's equation [52] as seen in Equation 24.

$$VB_{\text{est.}} = VB_{t_0} + \frac{\Delta t}{T} \cdot VB_{\text{th.}} = VB_{t_0} + \frac{\Delta t}{c_v \cdot v_c{}^k} \cdot VB_{\text{th.}} \tag{24}$$

While the factors cutting speed, feed rate, and cutting depth are technically continuous variables, in practice only certain values are chosen thus they can be treated as of categorical or discrete type. Similarly, the type of cutting tool is a categorical variable of the machining state. Only the estimated tool

condition shows continuous behavior. Therefore, the machining state would change constantly throughout operation, rendering machining state-specific models infeasible. Thus, it is necessary to discretize the tool condition, expressed as continuous flank wear width VB, to a categorical ordinal value $\widetilde{VB}$, by binning:

$$
\widetilde{VB} = \begin{cases}
0, & 0\mu m \leq VB < 40\mu m \\
1, & 40\mu m \leq VB < 80\mu m \\
2, & 80\mu m \leq VB < 120\mu m \\
3, & 120\mu m \leq VB < 160\mu m \\
4, & 160\mu m \leq VB < 200\mu m \\
5, & 200\mu m \leq VB < 240\mu m \\
6, & 240\mu m \leq VB < 280\mu m \\
7, & 280\mu m \leq VB < 320\mu m \\
8, & 320\mu m \leq VB < 360\mu m \\
9, & 360\mu m \leq VB < 400\mu m \\
10, & 400\mu m \leq VB
\end{cases}
\tag{25}
$$

Windowing

When the respective start trigger triggers the process monitoring algorithm, the system switches to its active state s_A, buffering all high-frequency h and low-frequency l streaming data. This buffer is evaluated once a predefined time of one second passes, or if the operator changes the override, thus changing the machining state. Once either condition is met, the buffered machine data is further evaluated. The buffered values are preprocessed using the data preprocessing routine and subsequently analyzed by the feature extraction routine to aggregate the streaming data into features X. Then, the extracted features with the respective machining state $\mathcal{M}$ can be used for material identification. The full procedure can be seen in Algorithm 6.

4.1.2 Data Preprocessing

The data preprocessing module aims firstly at unfolding the complex process data by reducing process dependencies and secondly enhancing the data through feature engineering. The three steps involved are *baseline compensation*, *context correction*, and *data enrichment* (see Figure 36).

Algorithm 6 Data Handling Pipeline

---

procedure HANDLE DATA(h, l, VB_{t_0})
    $g \leftarrow$ FIND TRIGGER($l_{\text{G-Code}}$)
    if $g \in$ Start Trigger **then**
        global $s_A \leftarrow$ True
        global $t_0 \leftarrow$ TIME
    else if $g \in$ End Trigger **then**
        global $s_A \leftarrow$ False
    end if
    if s_A **then**   ▷ Buffer data when active
        $v_{c_{\text{plan}}}, f_{\text{plan}}, a_p, \text{tool} \leftarrow$ LOOK UP OPERATION(g)
        $v_c \leftarrow v_{c_{\text{plan}}} * l_{v_{c_{\text{override}}}}$
        $f \leftarrow f_{\text{plan}} * l_{f_{\text{override}}}$
        $\Delta t \leftarrow$ TIME$- t_0$
        $VB_{\text{est.}} \leftarrow$ TOOL LIFE PREDICTION($\Delta t, VB_{t_0}$)
        $\widetilde{VB} \leftarrow$ BIN($VB_{\text{est.}}$)
        $\mathcal{M} \leftarrow \langle v_c, f, a_p, \text{tool}, \widetilde{VB} \rangle$
        buffer $\leftarrow$ buffer $\cup\, h$
    end if
    if $\Delta t > 1s \vee \mathcal{M} \neq \mathcal{M}_{n-1}$ **then**
        $\widetilde{\text{buffer}} \leftarrow$ PREPROCESS DATA(buffer, $\mathcal{M}$)
        $X \leftarrow$ FEATURE EXTRACTION($\widetilde{\text{buffer}}$)
        MATERIAL IDENTIFICATION($X, \mathcal{M}$)
    end if
end procedure
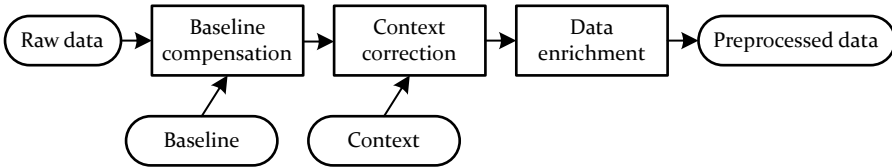
Figure 36: The data preprocessing module can be broken down into three main steps.

Baseline compensation

In baseline compensation, the acquired process data X is adjusted by a base value X_{baseline} to compensate machine or process-induced characteristics. The compensated signal X' can be computed as difference between X and X_{baseline}. Thus, during commissioning the required baseline data, *reference data*, needs to be acquired by observing the process data without any load.

Context correction

Real-life machining operations do not confine to operating at a single machining state and alternate between many machining states throughout operation.

Thus, training machining state specific models becomes infeasible due to the large number of models needed and the reduced volume of relevant historic data for each machining state. This effect can be approached by introducing context information, allowing for a certain level of signal correction and therefore harmonization among machining states.

One manifestation can be found for turning operations with constant cutting conditions but a changing workpiece diameter. These show a significant impact of the diameter d on the data of the spindle $X_{spindle}$, see Figure 37 a). When introducing this diameter as known context, its impact can be compensated as:

$$X'_{spindle} = \frac{X_{spindle}}{0.5 * d} \tag{26}$$

Preliminary investigations have shown that the compensated spindle data is a more generalized feature as it removes the signal dependency on the workpiece's diameter (see Figure 37 b) [P10].
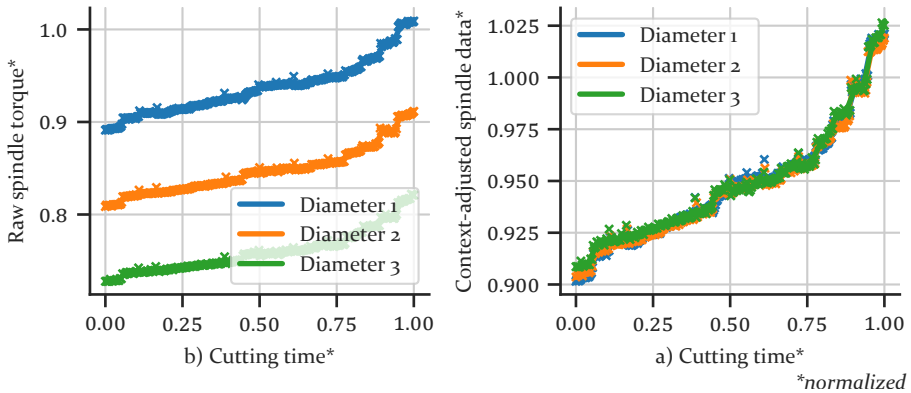
Figure 37: The uncompensated and context-compensated torque data of the spindle is shown for three cutting operations of the same material at different part diameters [P10].

For more complex cutting motions with constantly changing cutting conditions, such as encountered during milling with changing tool engagements, a different context correction strategy is needed. Here, a cutting force simulation model is utilized, which simulates the expected cutting forces considering the true cutting conditions and the general expected material behavior. Using such models the expected process forces can be simulated with errors less than 10% [43]. Specifically, the cutting force simulation functionality of the computer-aided-manufacturing software *NX CAM* is utilized, yielding the simulated forces for a planned machining operation. The expected cutting

forces that do not consider machinability deviations among material batches can now be compared with the process data observed during machining (see Figure 38). By comparing the simulated signal and the baseline compensated process data, an error signal μ can be computed. This error between the expected values and the true encountered values can be used to explain a degrading tool condition or a deviation in machinability among material batches. With the integration of a TCM system, the remaining unknown of the tool's condition can be resolved, thus allowing for the deduction of material batch machinability information.
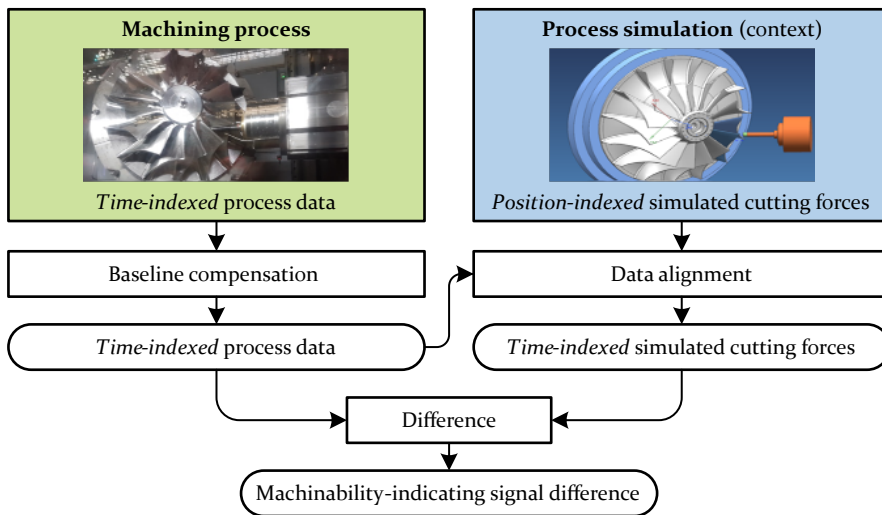
Figure 38: Concept for sophisticated context correction introducing simulated process forces as a reference signal to extract batch-specific signal patterns.

However, the issue of data alignment arises. While the process monitoring data is indexed based on the timestamp of the NC at the respective cycle, the simulated process forces are non-dimensionally indexed, providing tuples of process forces and the respective tool center point. Thus, to calculate the difference of both signals, they first need to be aligned to a common index so that the correct data points can be compared to each other. To do this, the method of dynamic time warping (DTW) is researched, which finds the best non-linear alignment between two signals. In a preliminary set of experiments the parameterization of the DTW method are investigated, finding that the usage of the *global window* hyperparameter and the position signals as matching signals provides the best results with the least overall alignment error [S8].

Data Enrichment

To enrich the available process data, the acceleration $a(t)$, and subsequently the vibration, of each axis is computed as the second derivative of the measured encoder positions $x(t)$ (see Equation 27 and Figure 39) [P10]. While the absolute encoder positions might carry information about the type of cut, but not the machinability of the material batch, vibration analysis is a common measure seen in similar material identification routines (see Section 2.2.3). However, compared to vibration signals acquired with external sensor equipment, the encoder position signals used are assessed with a frequency of 500 Hz. Thus, considering the Nyquist-Shannon sampling theorem [397], only low-frequency vibrations of up to 250 Hz can be observed this way.

$$a(t) = \frac{\mathrm{d}^2 x(t)}{\mathrm{d}t^2} \tag{27}$$
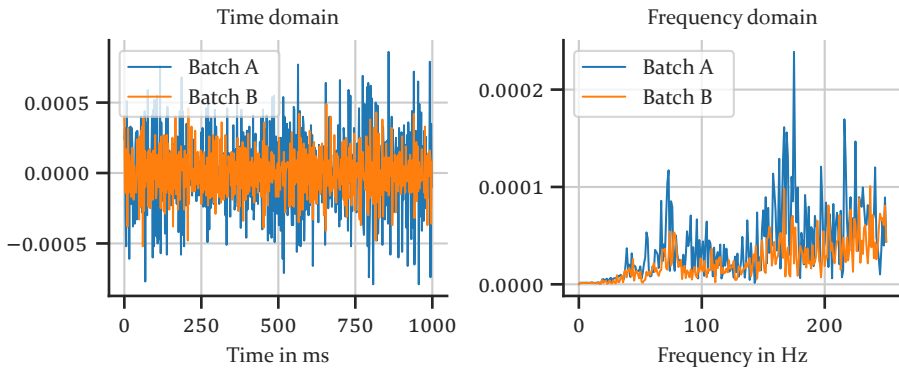
Figure 39: Within the computed vibration signal different behaviors can be seen for two material batches.

4.1.3 Feature Extraction

Using the data preprocessing routine, the vibration and the preprocessed absolute or relative torque signal is available for each feed drive of interest, and the vibration signal and the preprocessed absolute or relative cutting force signal for each spindle. Thus, for a machine tool with three feed drives and a single spindle, a signal window of one second contains 4000 individual signal values, rendering a direct analysis infeasible. Thus, this high-dimensionality needs to be reduced using dimensionality reduction techniques, especially *feature extraction* followed by *feature selection*.

Feature Extraction

In feature extraction, signals are analyzed by predefined formulas to derive feature values. Here, especially statistical features, established metrics from the field of statistics, are commonly used in process monitoring. In particular, in this study, the *mean* (AVG), *standard deviation* (STD), *skewness* (SKEW), and *kurtosis* (KUR) are computed for each window of N samples for signal x as:

$$\text{AVG} = \frac{1}{N} \cdot \sum_{i=1}^{N} x_i \tag{28}$$

$$\text{STD} = \sqrt{\frac{1}{N} \cdot \sum_{i=1}^{N} (x_i - \text{AVG})^2} \tag{29}$$

$$\text{SKEW} = \frac{1}{N} \cdot \sum_{i=1}^{N} \left(\frac{x_i - \text{AVG}}{\text{STD}} \right)^3 \tag{30}$$

$$\text{KUR} = \frac{1}{N} \cdot \sum_{i=1}^{N} \left(\frac{x_i - \text{AVG}}{\text{STD}} \right)^4 \tag{31}$$

These features are computed for each signal individually. To identify each feature, the respective signal that it was computed on is denoted in subscript while the name of the respective drive or spindle is denoted as superscript, e.g. the kurtosis of the acceleration signal from the feed drive X1 is denoted as $\text{KUR}_{\text{acc}}^{X1}$.

Feature Selection

Not all extracted features might carry information about the material batch. Thus, a feature selection method is used to select the n best performing features of all computed features. To do this, all potential combinations X_y^z of feature X for signal y of axis z are computed during model training. Now, *recursive feature elimination* is used to select the n best features. For increased computational efficiency, a *random forest*-based auxiliary model is used for feature selection, as these models were shown to yield high prediction results at low training times for the task of supervised material batch identification [P11]. As machining scenarios might differ in their mechanical

setup, the feature selection procedure is carried out during commissioning and model training, instead of proposing a generic set of features.

As the proposed feature selection method requires the presence of class labels for the calculation of the prediction impact of each feature, it is not suited for unsupervised settings. For these, an alternative strategy is used. This involves the usage of *principal component analysis (PCA)*, which is an unsupervised method of transforming data to linearly uncorrelated dimensions, thereby increasing the information density in lower dimensions. Thus, similar to the recursive feature selection procedure, the PCA method is used to transform the training data into a training dataset of n features for unsupervised tasks.

4.2 Data-driven Material Identification Procedure

The machinability of the current material is determined by utilizing historic process data to find the most similar behaving material batch encountered in the past. Thereby, the knowledge of the measured machinability of the found historic batch can be transferred to the current material batch. Assuming that all potential material batch variations are known, the task can be worded as a supervised classification problem with the goal of finding a function $g(X)$ that predicts a label $\hat{y}$ of potential known labels based on the feature vector X. However, as stated in the requirement **R3**, the number of material batches is not known prior to operation and might increase when material batches of novel machinability are detected. Furthermore, in practice, scenarios might be encountered with unclear associations between individual workpieces and their material batch or without available ground truth data regarding their machinability.

Thus, a novel material identification procedure is proposed consisting of several models to allow for material batch identification under the described constraints (see Figure 40). First, a *novelty detection* algorithm is integrated, capable of identifying whether the machined material has known or novel machinability behavior. Details regarding the novelty detection procedure can be found in Section 4.2.1. Second, for the case of a known material, a *classification* model is used. The classification model classifies the machined material among the material batches encountered in the past, finding the most likely material batch. The respective methodology will be detailed in Section 4.2.2. Third, an unsupervised *clustering* approach is proposed in Section 4.2.3 for an initial machinability estimation. This procedure can be used in situations without ground truth data available for training the supervised classification model as well as for analyzing the case of novel materials.
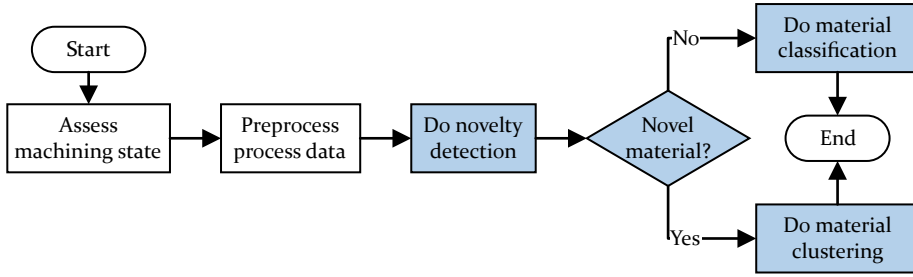
Figure 40: The material identification procedure contains the three main components of novelty detection, material batch classification and material batch clustering.

As the machining state significantly impacts the values of the feature vector, the different machining states need to be investigated separately. This is achieved by training individual instances of each model for each machining state. Thereby, the models can be optimized towards the identification of machinability deviations rather than machining state deviations as root-causes for observed signal deviations. Thus, the instance of the novelty prediction model $f(X)$ for analyzing data at machining state $\mathcal{M}$ is denoted as $f_{\mathcal{M}}(X)$.

4.2.1 Novel Material Detection

As shown in Chapters 1 and 2, the number of differently behaving material batches is not known prior to operation and can increase continuously. Furthermore, while a specific material batch might be encountered in the past, and thus is known generally, historic process data might not be available for the desired machining state. Thus, in this study, a material batch is considered *known* if a material batch with similar machinability was encountered in the past, the machinability of that material batch is characterized, and historic feature vectors for the given machining state are available. If any of these three requirements is not met, the material batch is considered *novel* for the specific machining state.

To predict the novelty of the sample associated to the process data X, a novelty detection model $f(X)$ is used. The novelty detection model is trained on the set of historic data for the respective machining state $\mathcal{M}$ so that $f(X)$ yields high scores for samples that match the distribution of the historic data and low scores for data that does not match its distribution. This computed score is denoted as novelty score s_{novelty}. With the novelty of a sample expressed by the novelty score, the binary decision is made by comparing the novelty score to a predefined threshold, also known as a decision boundary. Novelty scores

above the threshold are within the decision boundary, and are thus considered known, while samples that fall outside the boundary are considered novel.

During model training, the selected historic data can be extended beyond machining state $\mathcal{M}$. Thereby, especially for machining states with low data volume information from nearby, and thus similar, machining states can be utilized. Therefore, a compromise needs to be made between more accurate novelty detection results due to higher data volume versus less accurate detection results due to increased signal influences from machining state deviations. These tolerance limits $\mathcal{T}$ thus need to be adjusted for each machining state individually during model optimization. Given the limits for cutting speed $\mathcal{T}_{v_c}$, feed rate $\mathcal{T}_f$, and flank wear width $\mathcal{T}_{VB}$, the relevant training data X for $\mathcal{M}$ can be found as a subset of all historic data $\mathcal{H}$ as:

$$
\begin{aligned}
X = \big\{ n \in \mathcal{H} \mid\ & (v_{c,\mathcal{M}} - \mathcal{T}_{v_c} \le v_{c,n} \le v_{c,\mathcal{M}} + \mathcal{T}_{v_c}) \wedge \\
& (f_{\mathcal{M}} - \mathcal{T}_f \le f_n \le f_{\mathcal{M}} + \mathcal{T}_f) \wedge \\
& (VB_{\mathcal{M}} - \mathcal{T}_{VB} \le VB_n \le (VB_{\mathcal{M}}) + \mathcal{T}_{VB}) \wedge \\
& (\text{tool}_{\mathcal{M}} = \text{tool}_n) \big\}
\end{aligned}
\tag{32}
$$

Besides optimizing the tolerance values for data selection, the specific novelty detection algorithm and the respective configurable parameters, in this study known as hyperparameters, need to be optimized. In this work, the novelty detection algorithms *One-Class SVM* and *Isolation Forest* [339] are selected.

To adjust a trained model for newly characterized material batches, the model training procedure needs to be executed again. When retraining the model, one needs to consider whether the data volume increased sufficiently, so that the chosen tolerances for sample selection can be decreased. Furthermore, the model could be adjusted regarding its sensitivity throughout operation without the need of retraining by adjusting the threshold of the decision boundary.

4.2.2 Material Batch Identification

With the material batch detected as a material batch of known behavior, the batch classification procedure can be carried out. To do this, a supervised classification model is used for predicting the class $\hat{y}$ based on the feature vector X. The target value, the material batch $\mathcal{B}$, is a categorical value. Thus, it needs to be encoded using one-hot encoding. Furthermore, the feature vectors are scaled to a standard distribution with a mean of zero and a variance of one to improve model training [305]. [P11]

The procedure for model training is shown in Algorithm 7. First, relevant training data needs to be selected from all available historic data (see Equation 32, page 95). Subsequently, the standardization procedure $s(X) = \tilde{X}$ is fitted to the distribution of the training data by computing the mean and standard deviation of the data. Furthermore, the one-hot encoding $e(\mathcal{B}) = y$ is initialized for the unique labels encountered in the training data. Both the fitted standardization model and the encoding model can then be used to transform the features and labels of the training data to their desired formats. These preprocessed features and labels allow the training of the classification model $g(\tilde{X})$. As different machining states $\mathcal{M}$ might exhibit characteristic patterns, machining state-specific models $s_{\mathcal{M}}(X)$, $e_{\mathcal{M}}(\mathcal{B})$, and $g_{\mathcal{M}}(\tilde{X})$ are used. [P11]

Similarly to the procedure described for training the novelty detection algorithm in Section 4.2.1, there are several hyperparameters within the material classification pipeline that can be optimized for each machining state. These include the tolerances $\mathcal{T}$ of training data selection, the type of classification model $M \in \mathbf{M}$ as well as all its model-type-specific hyperparameters P_M. For each machining state, a different set of hyperparameters might perform best. To optimize $\mathcal{T}$, M, and P_M, a range of suitable options is defined for each dimension. Then, a grid-search approach using three-fold cross validation is used to find the best combination among the three categories. While the tolerance limits can be defined independently of the remaining categories, the hyperparameters depend on the selected model type.

Preliminary experiments reveal that tight $\mathcal{T}$ for training data selection, thus only using data points from the same machining state show the best performance when large amounts of training data are available. Contrarily, with less training data available, a significant improvement in prediction performance can be seen with increased $\mathcal{T}$, considering data from nearby machining states [P11]. Evaluating various classification models and training data volumes[1], different behavior can be observed, see Table 6. As expected, more training data yields better prediction accuracies. While SVM and ANN show good performances for both high and low data volume scenarios, RF appears to only perform comparatively well for high data volume and LR only for low data volume scenarios.

During operation, the trained models are used for inference (see Algorithm 7, function *predict*). The fitted classification model and the auxiliary data preprocessing models are loaded. The standardization is used to transform the feature vector. The fitted classification model $g_{\mathcal{M}}(\tilde{X})$ for machining state

---

[1] The datasets considered for high volume scenarios contains 2785 samples on average and for low volume scenarios 1585 samples.

Algorithm 7 Train classification model

---

procedure TRAIN OPTIMIZED MODEL($\mathcal{M}$, $\mathcal{H}$, $\mathcal{T}$, **M**, **P**)
    for all $\mathcal{T} \in \mathcal{T}$, $M \in \mathbf{M}$, $P \in \mathbf{P}_M$ **do**
        $X, \mathcal{B} \leftarrow$ SELECT RELEVANT DATA($\mathcal{H}$, $\mathcal{M}$, $\mathcal{T}$)
        $\langle X_1, \mathcal{B}_1\rangle, \langle X_2, \mathcal{B}_2\rangle, \langle X_3, \mathcal{B}_3\rangle \leftarrow$ SPLIT($\langle X, \mathcal{B}\rangle$) $\triangleright$ 3-fold split
        for $i \in \langle 1,2,3 \rangle$ **do**
            $s, e, g \leftarrow$ TRAIN($X_i \wedge X_{(i+1)\%3}, \mathcal{B}_i \wedge \mathcal{B}_{(i+1)\%3}, M, P$)
            $\widehat{\mathcal{B}} \leftarrow$ PREDICT($X_{(i+2)\%3}, s, e, g$)
            score$_i \leftarrow$ F1 SCORE($\mathcal{B}_{(i+2)\%3}, \widehat{\mathcal{B}}$)
        end for
        score$_{\mathcal{T},M,P} \leftarrow \frac{1}{3}\sum_{n=1}^{3}$ score$_n$
    end for
    $\mathcal{T}', M', P' \leftarrow$ max(score) $\triangleright$ Select parameters of the highest score
    $X, \mathcal{B} \leftarrow$ SELECT RELEVANT DATA($\mathcal{H}$, $\mathcal{M}$, $\mathcal{T}'$)
    $s_{\mathcal{M}}, e_{\mathcal{M}}, g_{\mathcal{M}} \leftarrow$ TRAIN($X, \mathcal{B}, M', P'$) $\triangleright$ Train models for operation
end procedure
function TRAIN($X, \mathcal{B}, M, P$)
    $s \leftarrow$ FIT STANDARDIZATION(X)
    $\tilde{X} \leftarrow s(X)$
    $e \leftarrow$ FIT ENCODER($\mathcal{B}$)
    $y \leftarrow e(\mathcal{B})$
    $g \leftarrow$ INITALIZE CLASSIFIER(M, P)
    $g \leftarrow$ TRAIN CLASSIFIER($\tilde{X}, y$)
    return s, e, g
end function
function PREDICT(X, s, e, g)
    $\tilde{X} \leftarrow s(X)$ $\triangleright$ Standardize feature vector
    $\hat{y} \leftarrow g(\tilde{X})$ $\triangleright$ Predict encoded label
    $\widehat{\mathcal{B}} \leftarrow e^{-1}(\hat{y})$ $\triangleright$ Decode prediction to class label
    return $\widehat{\mathcal{B}}$
end function

$\mathcal{M}$ is used to predict the encoded material batch $\hat{y}$. To decode the prediction, the encoder $e(\mathcal{B})$ needs to be applied inversely so that the predicted material batch $\widehat{\mathcal{B}}$ can be computed as:

$$\widehat{\mathcal{B}} = e^{-1}(\hat{y}) \tag{33}$$

Besides accurate predictions, fast model training and inference times are important for operation. A fast model training time allows the investigation of large model-pipeline hyperparameter space $\mathcal{T}$, **M**, **P** when training and optimizing new models. Fast inference times however improve the usability due to reduced waiting times and enable future integration into smart control systems. Comparing the training times of the different algorithms, see Table 7, it can be observed that all algorithms have fast training times equal or less

Table 6: Prediction performance for material batch classification of different model types considering high and low amounts of available training data, adapted from [P11].

	SVM	RF	NB	kNN	ANN	LR
High data volume	**89.0%**	86.1%	81.2%	82.6%	85.7%	81.7%
Low data volume	70.3%	62.8%	47.3%	63.6%	**71.0%**	68.9%

than 21 seconds[2]. The fastest training times can be seen for the simpler models NB, kNN and LR while the longest training time of the ANN model is several magnitudes larger. In regard to their inference times, all investigated model types take less than 0.25 seconds for execution, with ANN being the slowest option. The models SVM, NB, and LR have the fastest execution times, taking less than one millisecond. Considering both training and inference times, the investigated ANN model type seems the least suited for the given task when comparing computational performance while all the remaining algorithms yield promising results. [P11]

Table 7: Comparison of the investigated model types in regard to their computational performance, adapted from [P11].

	SVM	RF	NB	kNN	ANN	LR
Training time	5.2 s	2.6 s	0.006 s	0.01 s	20.7 s	0.4 s
Inference time	0.7 ms	52.9 ms	0.7 ms	2.3 ms	223.0 ms	0.4 ms

4.2.3 Cluster Analysis

As shown in the previous section, supervised learning can be used for classifying the material batch currently being processed as one of the previously encountered material batches that were present during model training. However, in the case of novel materials, detected by the novelty detection procedure and for scenarios without any material batch information available, a different procedure is needed that can provide information about the machined material without requiring labelled data. Therefore, the usage of unsupervised clustering approaches is proposed.

The proposed concept can be seen in Figure 41. In an initial step, relevant historic data is selected from the database based on the machining state

---

[2] Training and inference times are measured using a machine with Intel Xenon platinum processor running up to 3.1GHz, 8VCPUs, 16GB Ram running Ubuntu 18.05. The datasets used for training contained 2785 samples on average.

$\mathcal{M}$, considering tolerances as shown before (see Equation 32, page 95). The selected feature vectors are now analyzed by a clustering algorithm regarding similar characteristics, assigning them to a cluster subsequently. Now, the available metadata about the samples aggregated in each cluster is associated to the respective cluster. If ground truth labels about the respective material batches are available, these are compared with the clusters found, assigning the label distribution within each cluster as the label of that cluster. Otherwise, the individual metadata such as date and production orders are used as cluster labels. Subsequently, the centroid c of a cluster with N samples is computed as the mean value of each feature vector X:

$$c = \frac{1}{N} \sum_{i=1}^{N} X_i \tag{34}$$
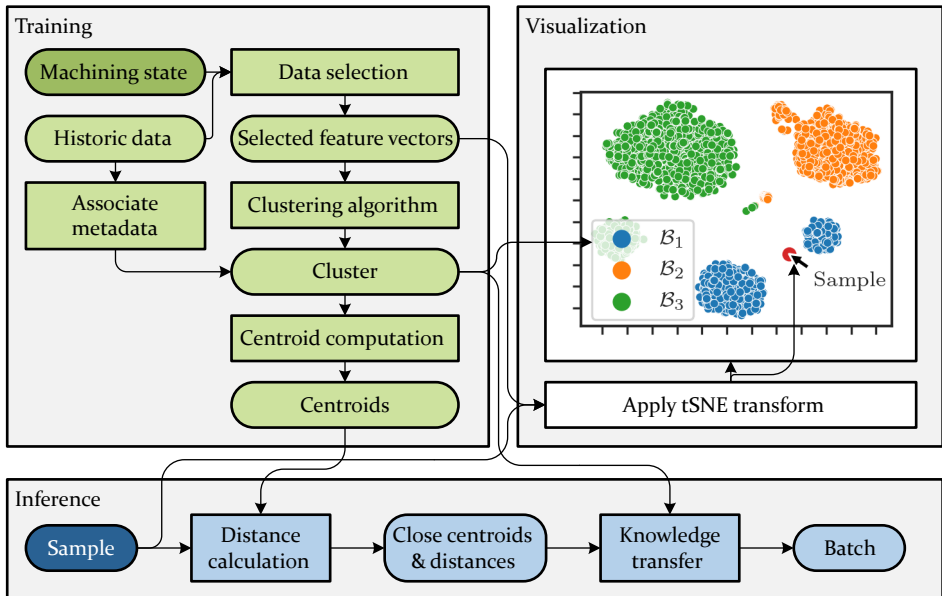
Figure 41: The clusters found are represented by the different colors and plotted using the tSNE method.

To enable a visual analysis of the data with the respective clusters found by the human operator, the high-dimensional data needs to be represented in 2D. This is achieved using the tSNE method, aggregating the feature vectors to two dimensions. The detected clusters are expressed by the color and style of each point plotted with the associated meta information shown in the legend. Furthermore, in process monitoring scenarios without any available material

batch information, the computed cluster map can be analyzed for related clusters that can be used to match experiences from the shop floor. Thereby, the clustering visualization can be used to derive necessary labels to transform the unsupervised clustering approach into the supervised classification approach.

During operation, the euclidean distances between a novel sample and each centroid are computed. The three closest clusters are considered relevant and used to transfer their associated cluster knowledge weighted by the inverse distance to the novel sample. Thereby, information about the novel sample can be derived as interpolation among the information of all close data points weighted by their similarity, with closer samples having a higher impact.

There are many algorithms for finding such clusters and assigning the samples to the respective cluster, however, most require parametrization regarding the expected amount of clusters - a requirement which can not be met in the present use case. Thus, the *evidence accumulation* algorithm [348] is used as no prior cluster count is required.

5 Smart Manufacturing System for Process Optimization Regarding Deviations among Material Batches

Process optimization methods are needed that can utilize the identified material batch to recommend corrective actions to be taken by the operator to adjust the cutting process. Thereby, batch-aware process optimization is enabled. In this chapter, this process optimization as well as the derived smart manufacturing system for process optimization regarding deviations among material batches (SMaPOMBa) are shown.

In Section 5.1, the procedure of batch-aware process optimization is detailed. Here, established tool life prediction models are adapted to model material batch-specific machinability. If such information regarding the material batch's machinability is available, the effect of changing the cutting parameters on different optimization targets can be computed.

Consecutively, given the methods proposed for *TCM*, *material identification*, and *process optimization*, specific operational strategies can be derived (Section 5.2). Next, these strategies are mapped into a service-based architecture, based on the individual methods and their interaction(Section 5.3). Finally, the prototypical implementation of the proposed smart manufacturing system is detailed (Section 5.4).

Individual services and architectures of the specific parts of the proposed smart manufacturing system were already discussed in publications by the author [P7, P11–P13]. Parts of the implementation were investigated in student's work guided by the author [S5].

5.1 Optimization of Machining Processes Regarding Material Batch Deviations

The general concept for process optimization can be seen in Figure 42. Through the previously proposed material batch identification methods, Section 4.2, the most similar behaving material batch from the past can be identified for a given to-be-optimized material. This information can then be used to find information associated to the detected batch in the *batch behavior index (BBI)* and apply it to the material currently being machined. With machinability information available, the influence of changing the cutting parameters on the expected tool life is approximated and the impact on the optimization target is computed. Thereby, the cutting process can be

improved by finding the set of cutting parameters that optimizes the selected target metric.
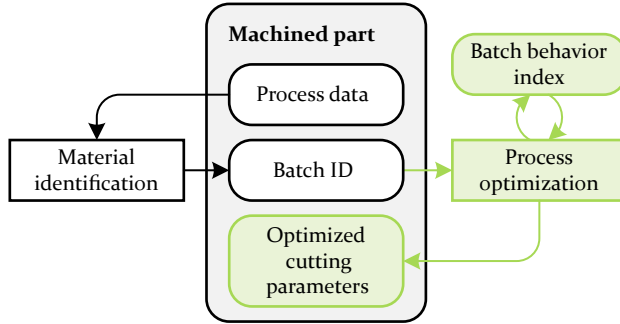
Figure 42: The ID of the material batch, identified by the material identification procedure, is used to find and transfer historic information for process optimization to the current material batch.

5.1.1   Optimization Targets

Cutting processes can be optimized towards various target metrics. In this study, the considered metrics are *total costs per part*, *production time*, *productivity*, and *net chip rate*. Furthermore, a specific maximal remaining production time can be set as a boundary condition to limit the search space. Thereby, more complex optimization targets, such as finishing a machining operation in a given time-frame at a cost optimum, can be realized. The general cost relations for turning operations, in accordance with [398], can be seen in Figure 43.
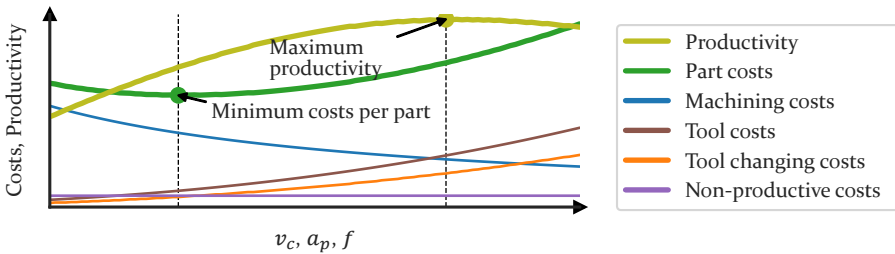
Figure 43: Cost relations in machining based on the cutting parameters, adapted from [398].

The *total costs per part* can be expressed as the sum of the machining costs, non-productive costs, tool-change costs, and tool costs. The *production time* (t_p) is defined as the sum of machining time (t_m) and tool change time (t_c).

Furthermore, the *productivity* can be calculated as the inverse of the sum of t_p and the non-productive time (t_n).

While t_n needs to be determined empirical, t_m can be found as ratio of the to-be-machined-volume (V) and the MRR and t_c can be derived by the number of tool changes (n_{tc}), the time per tool change (t_{tc}), and the expected tool life T of a cutting tool at given machining state $\mathcal{M}$ for batch $\mathcal{B}$ as:

$$t_c = n_{tc} \cdot t_{tc} = \frac{t_m}{T_{\mathcal{M};\,\mathcal{B}}} \cdot t_{tc} \tag{35}$$

Finally, the *net chip rate (NCR)* is defined as the effective material removal rate considering the non-cutting times due to tool changes. Thereby, the NCR is calculated as:

$$\mathrm{NCR} = \frac{V}{t_p} \tag{36}$$

5.1.2 Batch Behavior Index

For all optimization targets, the influence of the material batch's machinability is expressed through the batch-specific tool life. Besides the *machinability*, other relevant *miscellaneous* batch-specific information is identified with the respective stakeholders from operation and technology teams. This includes metadata on the broadest level, such as the material supplier and the date the material was machined last as well as verbose statements regarding actions taken to improve the machining behavior. Both, the batch-specific machinability and the miscellaneous information are stored in the *batch behavior index (BBI)*. Therefore, the BBI can include quantitative information such as measured tool life values from manual material characterization or qualitative information such as notes of the machine operator regarding process adjustments taken for improving the machining behavior.

For the machinability assessment, tool life models are of particular interest in this study, estimating the expected tool life for a given material and a set of cutting parameters. Among the many existing tool life models, the model proposed by Taylor in its original [52] and its extended versions [53] are especially suitable for industrial approaches due to their low number of parameters [51]. This methodology can be adapted for tool life prediction for material batches by computing *material batch-specific* coefficient parameters rather than *material grade-specific* coefficient parameters. In its original form, the expected tool life T can be computed for cutting speeds v_c given the two model parameters c_v and k (see Equation 37) [52]. In its extended version, the

model also considers the feed rate f and cutting depth a_p through additional parameters [53]. Given the material batch-specific coefficient parameters c_t, m, n, and q the expected tool life T can be computed for machining batch $\mathcal{B}$ at cutting parameters v_c, f, and a_p as seen in Equation 38. While the original version requires fewer parameters and thus less effort for set-up, the extended version has a greater scope by covering the three main cutting parameters.

$$T = c_v \cdot v_c{}^k \tag{37}$$

$$T = c_t \cdot v_c{}^m \cdot f^n \cdot a_p{}^q \tag{38}$$

Thus, known coefficient parameters k and c_v or c_t, m, n, and q for a specific material batch can be stored as entries of type *machinability* in the BBI and then used during operation to compute the expected tool life. Based on the selected model, boundary conditions that limit the scope of the model need to be considered. The coefficient parameters of the original Taylor model are limited in scope by the feed rate, cutting depth, and type of tool, while the extended version is only limited by the type of cutting tool used.

The BBI is designed as a set of entries, where each entry consists of a *key*, a *type*, a *value*, and optionally a *scope*. The key refers to the batch index for which that entry is valid. The type specifies whether the information is a machinability or a miscellaneous information while the value contains that specific information. Furthermore, if information of an entry is related to a specific cutting condition, it has to be specified as scope. As multiple behavior entries can be associated to the same material batch the key value is not unique. An example of multiple sample entries of the BBI can be seen in Table 8.

Table 8: Exemplary BBI containing different entry types.

Key	Type	Value	Scope
$\mathcal{B}_1$	Miscellaneous	Last used: *04.03.2021*	
$\mathcal{B}_2$	Machinability	k=−6.68, $c_v = 7.37 * 10^{17}$	$\mathcal{M}_{f:0.7;\ a_p:4;\ \text{tool D}}$
$\mathcal{B}_2$	Miscellaneous	"Use cutting tool type A"	

The necessary set of BBI entries can be generated during or prior to operation. To do this, existing process information acquired in the past, i.e. batch-specific parameter coefficients of a Taylor model computed during manual material characterization, can be added to the BBI with the respective material batch as the key, and the used cutting tool type, feed rate, and cutting depth as the scope. Furthermore, the proposed TCM routine can be used throughout

operation for the generation of additional entries, which are added to the BBI.

5.1.3   Parameter Recommendation

Given the identified material batch $\widehat{\mathcal{B}}$, the BBI is searched for entries with a matching key. If an entry is found that contains machinability information, such as the coefficient parameters p for either the original or the extended Taylor model, the tool life T can be computed for a potential set of cutting parameters c. Subsequently, T can be used to calculate the various optimization target metrics E for machining $\widehat{\mathcal{B}}$ at c. This approach can now be used to compute E for the current cutting parameters $\hat{c}$ and for custom cutting parameters c' defined by the user. Furthermore, the set C of all potential cutting parameter combinations can be used as parameter space to find the combination c_{ideal} that yields the extremum for the desired optimization target E^{main}.

While the optimal set of cutting parameters might provide the greatest impact on the desired optimization target, in practical scenarios other factors have to be considered, such as suggested cutting parameter limits by the tool supplier, manufacturing guidelines, or human expertise, which limit the theoretically computed optimized cutting parameters. Thus, besides calculating the ideal set of cutting parameters, visual tools are provided to the operator showing the impact on the target metrics of changing the cutting parameters. Thereby, the effects of adapting the cutting parameters can be analyzed.

Typically, the cutting speed and the feed rate are adjusted by the operator to improve the machining process. This can be carried out easily using the override functionalities of the machine tools without having to adapt the cutting program. Therefore, a visual assessment of the influence of adapting these parameters for the different optimization targets is precomputed and shown to the operator as a heat map (see Figure 44). The cutting speed is shown as the x-coordinate and the feed rate as the y-coordinate. The color shade represents the forecasted effect at each set of cutting parameters. Furthermore, the current cutting parameters and the ideal cutting parameters are shown, thereby visualizing the needed adjustments to reach a global or local optimum.

While the heat map allows an intuitive visualization of the effect of various cutting parameters on the primary optimization target, the effect on other targets might also be of interest. Therefore, a bar style visualization is used to show the effects for all optimization targets (see Figure 45). Additionally,
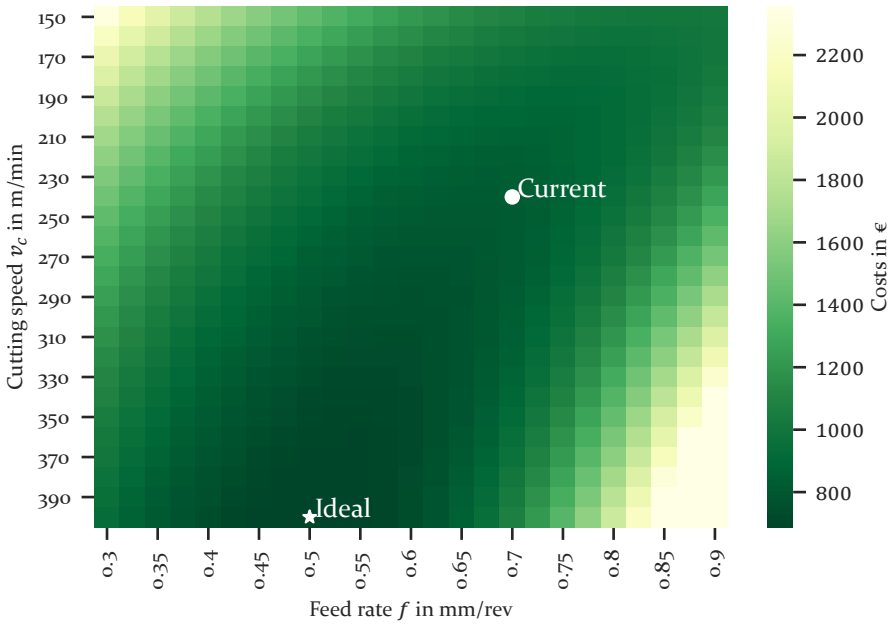
Figure 44: Visualization of the effects based on cutting parameter adjustments considering machinability influences of material batches.

user-defined parameters can be considered, allowing for the forecasting of non-ideal parameters.

The complete procedure for parameter recommendation can be seen in Algorithm 8. Given $\widehat{\mathcal{B}}$, $\mathcal{M}$, the current cutting parameters $\hat{c}$, the main optimization target E^{main}, and optionally user-defined cutting parameters c', recommendations can be generated. The BBI is queried by $\widehat{\mathcal{B}}$ to find relevant BBI entries. Entries of type miscellaneous are then directly conveyed to the operator. Furthermore, with the coefficient parameters p present, the optimization targets E are computed for $\hat{c}$, c' and C. Thereby, the ideal set of parameters c_{ideal} can be returned to the operator in combination with the computed heat map *HM* and bar plot *BP* detailing the effect of adapting the cutting parameters on the different optimization targets.

In the case of a novel material with transferred knowledge assigned, several material batch identifiers with individual weightings are predicted. Therefore, for each partially assigned material batch, the associated BBI entires are found, and the combined results are weighted based on the assigned weight of the respective material batch and returned to the user.
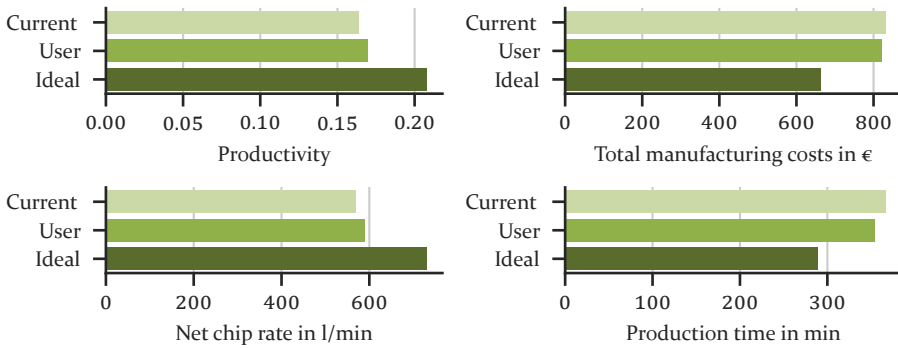
Figure 45: Visualization of the effect of current cutting parameters, custom user parameters, and the ideal recommended parameters on the various optimization targets.

Algorithm 8 Parameter recommendation

---

procedure RECOMMEND($\widehat{\mathcal{B}}, \mathcal{M}, \hat{c}, c', E^{\text{main}}$)
  $\psi \leftarrow$ SEARCH BBI($\widehat{\mathcal{B}}, \mathcal{M}$)
  DISPLAY MISCELLANEOUS ENTRIES(ψ)
  if $p \in \psi$ **then**
    for all $c \in (C \cup \hat{c} \cup c')$ **do**
      $T_c \leftarrow$ TOOL LIFE(p, c)   ▷ Estimate tool life
      $E_c \leftarrow$ COMPUTE EFFECTS(T_c, c)
    end for
    $E_{c_{\text{ideal}}} \leftarrow \max E$
    $c_{\text{ideal}} \leftarrow \arg\max E$ ▷ Find ideal c that maximize E
    $HM \leftarrow$ GENERATE HEAT MAP($E^{\text{main}}, c_{\text{ideal}}, \hat{c}, c'$)
    $BP \leftarrow$ GENERATE BAR PLOT($E_{\hat{c}}, E_{c'}, E_{c_{\text{ideal}}}$)
    return c_{ideal}, HM, BP
  end if
end procedure

5.2 Operational Routines

In this section, different routines of the smart manufacturing system are proposed, using the introduced methods for tool condition assessment, material-batch identification, and process optimization.

- The *material-batch aware parameter recommendation* routine is the central routine of the smart manufacturing system, recommending changes to the cutting process during operation based on the detected material batch. Therefore, it is only used during operation to observe process data and to infer recommended corrective actions.
- For novel material batches, an *automated material characterization* routine is provided to assess their machinability throughout operation. This

involves both the tracking of the machined volume during the cutting operation and the assessment of the tool condition before and after the machining operation. The true material characterization and model retraining takes place during non-productive time such as maintenance work.

- Similarly, a *continuous model improvement* routine is incorporated for a continuous model improvement for known material batches. As detailed for the material characterization, the machined volume is tracked during the cutting operation and the tool condition is measured before and after machining. Through this, additional ground-truth data is generated once the process is stopped, which can be used to correct and retrain the respective models.

- Finally, a *novel scene adaptation* routine is detailed, which aggregates functionalities for generating the necessary training data for novel situations. This routine is only used outside normal operation when a new scene is introduced into the TCM system.

5.2.1 Material-batch Adaptive Machining

The concept for material-batch adaptive machining is realized as recommendation system and can be seen in Figure 46. At the start of the cutting operation, the TCM system is utilized to assess the condition of the cutting tool. During machining, the data handling pipeline is used to observe process data from the machine's NC, deduce the current machining state, preprocess the process data, and aggregate the preprocessed data into information-dense features. Based on the machining state, the model storage is queried for the respective model instance matching the machining state. If no trained model is found, the respective model training routines are carried out for training the models, which can then be saved to the model storage for reusability.
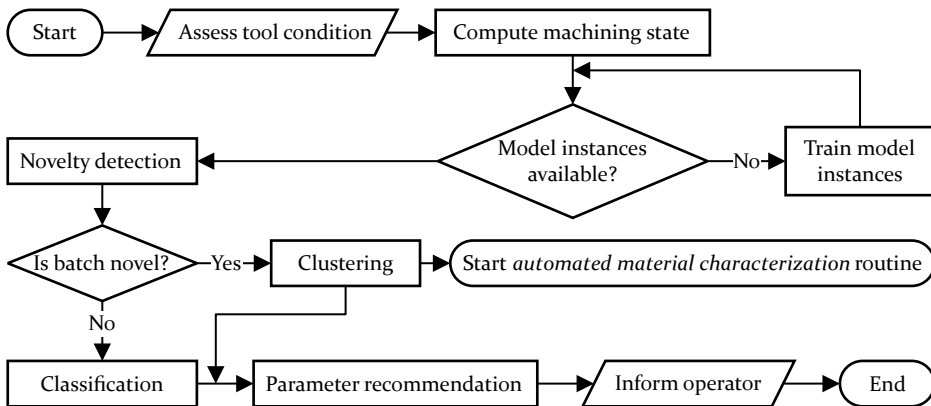
Figure 46: General procedure for adaptive machining.

With the loaded or freshly trained model, the novelty of the material currently being machined can be computed. In the case of a known material batch, it is classified using the material classification procedure. Now, the parameter optimization methods are used to calculate the expected tool life and recommend cutting parameters for optimized machining regarding the selected metric. Furthermore, verbose information is conveyed to the operator suggesting the change of the cutting parameters. In the case of a novel material being detected, the *automated material characterization* routine is initiated. Also, the cluster analysis is carried out. If ground-truth label information is available, the recommendations for each detected material batch are shown, allowing the operator to assess how the cutting process should be adapted.

5.2.2 Characterization of Novel Batches

As not all material batch variations are known prior to machining, material characterization needs to be carried out when encountering novel materials. Therefore, the *automated material characterization* routine guides the operator through the automated procedure for characterizing a novel material batch detected by the novelty detection (see Section 4.2.1). Through this, the material's machinability is determined, which allows for its integration into the material identification procedure and the proposal of optimized machining parameters.

The main task involved is to assess a material batch's machinability. As shown in Section 2.2.2, there are several approaches for describing the machinability of a material. In this work, the machinability assessment based on tool life is used as the ground truth machinability data. For this method of machinability determination, the wear of the cutting tool needs to be monitored in relation to the tool life. As the rate of tool wear typically depends on the cutting parameters, these need to be considered as well. While the tool's usage time can be derived from the metadata of the cutting operation, the tool condition can be acquired using the TCM system proposed in Chapter 3.

The general procedure of the automated material characterization routine is shown in Figure 47. The procedure can be initiated manually or by the *material batch-aware parameter recommendation* routine detecting a material batch with novel behavior. With the novel material batch detected, the operator is tasked to choose an initial set of cutting parameters c_1. Given the set of initial cutting parameters, a fresh cutting tool is exchanged and the cutting process is conducted. Throughout the machining process, the monitoring strategy as shown before is executed, stopping the process once the cutting tool is worn out. Thereby, the tuple $\mathcal{P}_1$ of ground-truth data

is yielded consisting of the selected cutting parameters c_1, the respective achieved tool life T_{c_1}, and the feature vectors X_{c_1} computed from the observed process data. By doing this, initial information about the machinability of the novel material batch $\mathcal{B}_N$ at c_1 is obtained.
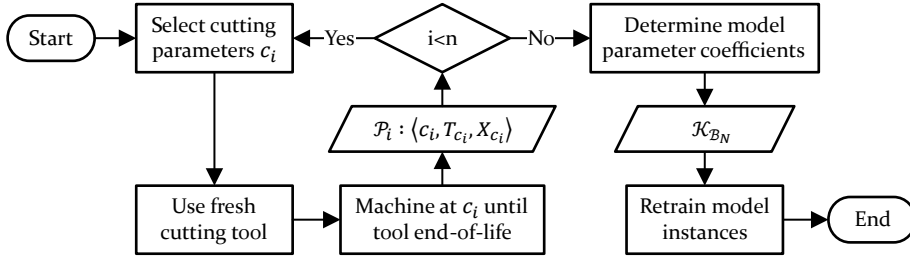
Figure 47: The automated material characterization routine requires the completion of at least two full tool cycles at different cutting parameter to determine the material batch's machinability.

However, when using the original Taylor's model, the tool life needs to be determined at least for a second set of cutting parameters c_2. Here c_2 can only vary regarding the cutting speed v_c from c_1 while the remaining cutting parameters must be kept constant. Different feed rates f and cutting depths a_p must be chosen only when using the extended Taylor model. However, in that case more support points are needed depending on the number of model parameter coefficients. Once the number i of support points $\mathcal{P}$ meets the minimum amount n of support points of the respective model, the model parameters are computed. Given the set of tool life and cutting parameters v_c, f, and a_p of all support points $\mathcal{P}$, a linear regression model can be optimized using least squared error to approximate the coefficient parameters c_t, m, n, and q of the transformed extended Taylor model (Equation 39).

$$\ln T = \ln c_t + m \ln v_c + n \ln f + q \ln a_p \tag{39}$$

The coefficient parameters can then be added as entries to the BBI. Furthermore, model instances of the novelty detection, batch classification, and clustering methods can be retrained for the investigated cutting parameters c_i.

The necessary behavior during the machining operation can be seen in Figure 48. With the material batch being detected as a batch of novel machinability, the expected tool life of the cutting tool for machining the respective batch is unknown and must be determined. Furthermore, the feature vectors need to be stored for later model training. The initial cutting parameters chosen by the operator are kept constant for the remainder of the cut to

ensure a constant machining state. The cutting process is halted at regular intervals, and the cutting tool is moved in front of the image acquisition unit. A picture of the cutting tool is taken, segmented by the proposed image segmentation model, and used to calculate the maximum flank wear width $VB_{\max}$. Furthermore, the set of all detected wear defects is shown to the operator for manual machinability assessment. In parallel, the total machining time t_m as well as the feature vectors computed from the process data are stored. Once the measured flank wear width meets a predefined threshold VB_{th}, the tool is considered worn out. The total machining time t_m up to that point is used to quantify the machinability as tool life T. Now, the set of ground-truth information $\mathcal{P}$ consisting of the tool life reached T at cutting parameters c with the observed feature vectors X is provided.
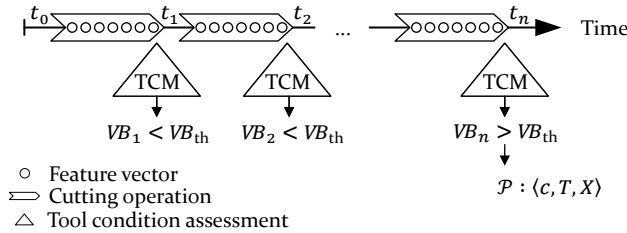
Figure 48: During the investigation period of one tool life, the cutting process is halted regularly to determine the condition of the cutting tool, stopping the process once the end-of-life criteria is reached.

5.2.3 Continuous Model Improvement

Through the *continuous model improvement* routine, the manufacturing system uses new ground truth data acquired throughout the runtime to continuously optimize its models. Thereby, both erroneous predictions can be corrected and additional support points for parameter optimization are acquired. The general concept can be seen in Figure 49. During operation, the proposed classification models are used to classify the material batch based on the available data. However, due to environmental noise and model errors, faulty predictions might occur. Preliminary studies show that such lowered prediction accuracies are encountered especially for machining states with low data volume [P11]. Independent of the material batch predicted during machining by process monitoring, after completing the cutting operation the true machinability of the workpiece can be judged using the decrease in tool condition as absolute measure for machinability. This enables the comparison of predicted machinability and actually measured machinability. With the error between both measures, the process monitoring system can then be adjusted accordingly.
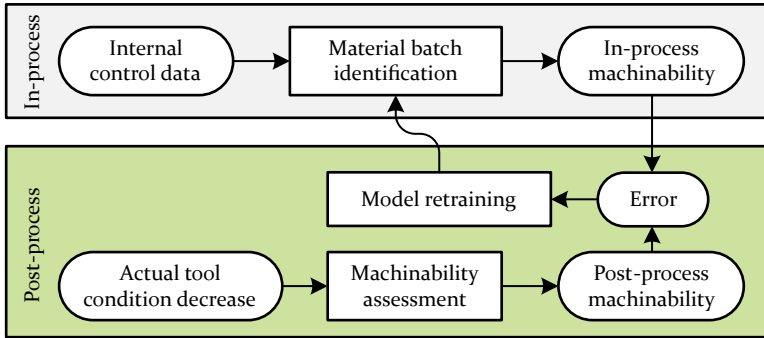
Figure 49: The error between model prediction and ground-truth machinability assessment is used to retrain the models.

The specific procedure is shown in Figure 50. It is assumed that the expected tool life $\widehat{T}$ is smaller than the machining time t_m of all parts machined from one batch so that at least one full tool life can be observed during machining. The continuous model improvement routine is autonomously running in the background during operation and does not require input from the operator. The routine enters its active state once a new cutting tool is used. Now, the machining time t_m and the cutting parameters c are tracked throughout the consecutive machining operation. Again, the material identification procedure is used to identify the predicted material batch $\widehat{\mathcal{B}}$ and recommend optimized cutting parameters c'. These are now adjusted by the operator to cutting parameters $\tilde{c}$. The cutting parameters are then kept constant until the tool reaches its end-of-life. Thereby, the total machining time t_m characterizes the true tool life T of the true material batch $\mathcal{B}$ at cutting parameters $\tilde{c}$. Given the coefficient parameters of the Taylor's model for $\widehat{\mathcal{B}}$, $\widehat{T}$ at $\tilde{c}$ can be computed. Furthermore, the calculated feature vectors X are stored temporarily for potential post-process model retraining.

Assuming that $\tilde{c}$ stayed constant during the machining time of the investigated cutting tool, T can now be compared with $\widehat{T}$ to improve prediction performance. In case both metrics are similar, with similarity defined as a configurable relative deviation, the material prediction is judged as *correctly classified*. As a result, the acquired tool life T at $\tilde{c}$ is added to the support points for machinability model generation of $\widehat{\mathcal{B}}$, the model parameter coefficients are recalculated, and the temporarily stored process data is added to the historic data. Thereby, the data volume and data variety increases.

Alternatively, if T and $\widehat{T}$ are not considered similar, it needs to be determined whether the material was actually from another batch manufactured in the past, thus a *misclassification*, or whether it is *unknown* with a novel behavior.
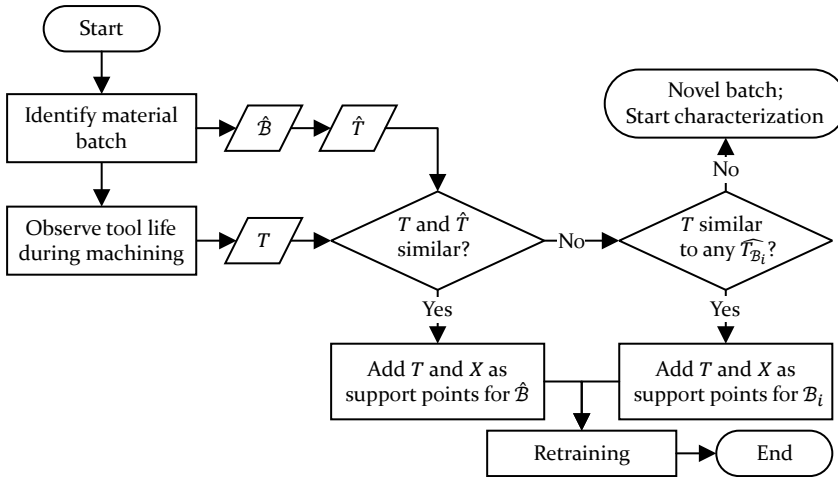
Figure 50: Depending on the error between predicted tool life $\hat{T}$ and true tool life T either model retraining or novel material characterization takes place.

For all known material batches $\mathcal{B}_i$, $i \in 1, 2, \dots, n$ the expected tool life $\widehat{T_{\mathcal{B}_i}}$ at cutting parameters $\tilde{c}$ is computed. If no $\widehat{T_{\mathcal{B}_i}}$ is similar to T based on the same similarity criteria as before, the material batch machined is considered *unknown*, and thus the error can be attributed to the novelty detection procedure. Otherwise, if similar batches are found, the error can be assigned to the material identification method as a *misclassification*. For retraining, the most similar material batch is considered the true material batch. In this case, the new ground truth data point $\langle \mathcal{B}_i, \tilde{c}, X \rangle$ is added to the support points and the model parameter coefficients are updated accordingly. Furthermore, the model instances are retrained with the new feature vectors. In case of unknown material behavior, the *automated material characterization* routine is initiated, using the data point $\langle \mathcal{B}_N, \tilde{c}, X \rangle$ as the first support point for the novel material batch $\mathcal{B}_N$. Thus, the number of necessary cutting parameters is decreased by one. Here, no model retraining happens immediately as further support points are needed, thus offloading the model retraining to the material characterization routine.

5.2.4 Effective Adaptation to New Scenes

As previously introduced, significant influences of the environment such as the cutting scenario, the machine itself, or the surrounding environment require the different ML-models to be trained for one specific situation, a *scene*. Within a scene, all samples are expected to be rather similar and only vary in the degree of tool wear for the TCM and the impact of the

material batch for process optimization. When dealing with a large amount of scenes such as when operating many machines or when encountering domain variations, see Section 3.1.2, an effective adaptation of the trained models to new scenes becomes important.

While the process monitoring system itself can be adapted to new scenes through the automated material characterization routine, a functioning TCM system is needed for tool condition assessment. Thus, the focus of new scene adaptation is on the training of the TCM system for the visual characteristics of the images acquired in the new scene. The main constraint hereby is the usage of the least amount of manual labelling effort possible. Therefore, the proposed methods for effective labeling and efficient data reuse through domain adaptation are utilized.

The concept for an effective training of the TCM system is shown in Figure 51. Here, a small amount of images from the new scene is needed. Using these images, a process expert can use the proposed tool for data annotation, which provides an initial label estimation using unsupervised learning. Doing so, the expert is tasked to correct annotation mistakes by the annotation tool, thereby allowing for the labelling of enough data in a short amount of time. While the process expert needs to be involved during data annotation, the remaining procedure happens automatically. Using the manually generated low volume dataset of annotated images, the domain adaptation model is trained to translate the existing historic image data from other scenes to match the detected shape and visual properties of the new scene. Using the trained translation model, synthetic training data is generated. Both datasets, the labelled dataset and the synthetic dataset, can then be used to train the image segmentation models.
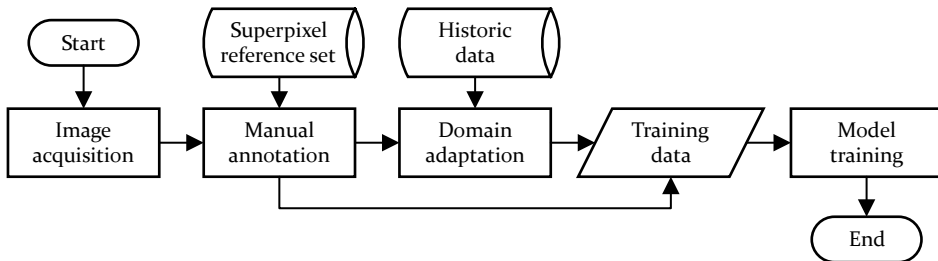
Figure 51: The TCM training routine incorporates both manual image annotation and automated synthetic data creation to generate training data for training the image segmentation algorithms.

5.3   Deduction of a Service-based Architecture

The different routines of the smart manufacturing system detailed in Section 5.2 aggregate the proposed methods for tool condition monitoring, material batch identification, and parameter recommendation into high-level functionalities commonly encountered during operation and set-up of the system. In this section, the individual methods and procedures are mapped into a service-based architecture, which is partly cloud-based and partly edge-based, with each service providing specific functionalities given the required input. Furthermore, the interfaces between the different services need to be defined. Through this, the architecture of the smart manufacturing system, which enables the execution of all proposed routines, is derived.

In Figure 52 the complete system can be seen using the *Fundamental Modeling Concept* notation. Here, a differentiation is made between agents and storage components. Agents represent active entities within the system such as sensors, services (executable scripts), and humans. Contrarily, storage components are passive objects containing various data elements that are stored over time, such as models and databases. Short-term data, such as the preprocessed feature vector or the identified material batch, are only of temporary interest at that point in time and are thus not considered storage. Furthermore, communication channels allow the transmission of information that does not need to be stored between agents. [399]

5.3.1   Storage Components

The *model storage* elements store the specific trained instances for all the different models used. This includes the image embedding models for the data annotation method, the image segmentation models, the novelty detection model, the batch classification model, and the clustering model. When models are trained with several instances, such as the scene-based image segmentation models and the machining-state-based material identification methods, the instance-defining parameter is used as a key so that the correct instance can be loaded during operation. The domain adaptation method does not have a model storage assigned, as the image translation model needs to be newly trained for each novel scene and is only needed once during initial training for the respective scene. Thus, saving the trained model for reusability is not needed.

Further image data storage components are used for the various TCM methods. These include the *superpixel reference dataset* for similarity calculation during annotation, the historic image database of micrographs and their respective annotated semantic label masks, *annotated images,* for the various scenes

Figure 52: The proposed smart manufacturing system contains many agents and storage components with specialized purposes to provide the different functionalities for set-up and operation.

encountered in the past and the *reference image* per scene used during image preprocessing for contextualization.

The process monitoring system utilizes a variety of storage components, as different types of information need to be made available for different purposes. Initially, during data preprocessing the look-up-table *G-Code to machining state* contains the mappings of the expected G-Code messages indicating the start of a cutting operation and the respective cutting parameters. Furthermore, the *baseline data* is stored as reference data for signal compensation together with the *context data*, used for context correction during preprocessing. Finally, the *initial tool condition* measured by the TCM system at the start of the cutting operation is stored to maintain a tool condition baseline throughout operation.

With the material batch detected, the parameter recommendation service utilizes both the *BBI* and the configured *business data*. The BBI is realized as a look-up-table, containing the coefficient parameters for process optimization models and miscellaneous entries indexed by the material batch ID. The business data contains relevant cost parameters needed to calculate the optimization targets and recommend optimized cutting parameters regarding the selected metric.

Finally, the derived feature vector, machining state, novelty, predicted material batch, and tool condition metrics are stored in a *buffer* for post-process evaluation. Thereby, with the knowledge of the true machinability, the model retraining service can append the observed process data with the correct machinability to the *historic process data* storage, which is persisted across machining operations and used to train the material identification models.

5.3.2 Active Components

The active components, shown as agents in Figure 52 include humans, hardware, and software services such as algorithms. The involved humans are the process experts, who are needed for annotating the cutting tool images, and the operator, who receives the recommendations from the smart manufacturing system and can thus adapt the cutting process. The primary hardware agent is the *machine's NC*, which provides a continuous data stream of control data as well as machining settings. The second hardware agent is the *camera* that is integrated into the machine tool to take pictures of the cutting tool.

The *data annotation* service takes images from the image acquisition unit and provides a frontend to the process expert for annotating the data. The respective models used for hinting at the annotation are loaded from the model storage and are updated with every intervention by the human annotator. As an output, the service provides a set of micrographs and their respective annotated semantic label masks, which are stored in the *historic image* storage.

For model training, these annotated images of a novel scene are used by the *domain adaptation* service to train the temporary image translation model. With the trained translation model, historic data is translated to match the characteristics of the novel scene, thereby creating a synthetic dataset as part of the *training dataset*.

The *image preprocessing* service appends the reference image for the respective scene, loaded from the *reference image database*, to the micrograph as described in Section 3.2.1, yielding the contextualized image. During inference, this preprocessing step is carried out for each micrograph acquired by

the *camera*, while during model training the preprocessing step is carried out for each image in the set of real and synthetic training images.

Model training services are used both for training the image segmentation and the time-series models. For image segmentation, the temporary contextualized training dataset is used for novel scenes, while the time-series models are trained using *historic process data* as well as data acquired throughout operation from the *buffer* and the *ground truth data generation* service. For computational efficiency, only specific model instances for certain machining states are trained, such as the current machining state if no prior models are available, or the machining states encountered during automated material characterization. The model training service concludes by storing the respective model instances in the *model storage* and notifying consecutive services about training completion.

During operation, images are acquired by the *image acquisition unit* once a trigger from the machine's NC is received. These images are forwarded to the image preprocessing service, appending the reference image to the micrograph. The contextualized images are then used by the *image segmentation* service. The trained image segmentation model is loaded from the *model storage* and used to evaluate the image. The prediction results are then directly analyzed by the *wear KPI calculator* yielding the desired wear metrics. Both the segmented image and the predicted wear metrics are shown to the operator using a frontend service. Furthermore, the assessed wear condition is added to the current machining state and provided as a data source.

The *data handling* service of the process monitoring system retrieves continuous process data from the machine's NC. For the data preprocessing, further data sources are needed, such as the *G-Code to machining state*, the *baseline data*, the *context data*, and the *initial tool condition*. Using the procedure shown in Section 4.1, these data sources are used to continuously yield the current machining state and the preprocessed feature vector.

The three services *novelty detection*, *material batch classification*, and *clustering* provide the respective functionalities for material identification during operation. Each service uses the current machining state to load the respective model instances from the *model storage*. If there is no model trained yet for the given machining state, the *model training* service is tasked to train and provide a new model. With the trained model loaded, the *novelty detection* algorithm evaluates the preprocessed feature vector, providing information about the material batch's *novelty*. Subsequently, either the *material batch classification* or the *clustering* service, based on the novelty information, are used to analyze the feature vector, yielding information about the estimated material batch.

The *recommendation* service uses the detected process information, such as *material batch novelty*, *detected material batch*, or *assigned material cluster*, and recommends actions (see Section 5.1). To do this, the user-selected *optimization target* as well as the *bbi* is needed. The computed recommendations are conveyed to the operator through a frontend interface. Furthermore, the assessed novelty and the detected material batch are shown in the *GUI* to the operator.

Moreover, the *ground truth data generation* module uses the tool conditions assessed before and after machining in combination with the observed chip volume at the given machining state to calculate the true machinability after the end of a machining operation. This information is provided to the *continuous improvement* service.

The *continuous improvement* service observes the prediction behavior of the smart manufacturing system. Throughout operation, the computed feature vectors and the predictions from the novelty detection, batch classification, and clustering are stored in a temporary *buffer*. At the end of the cutting operation, the predicted machinability is compared with the true machinability computed by the *ground truth data generation* module. Now, the buffered data can be added with the true label to the historic database and model retraining is executed.

5.4 Implementation

The proposed smart manufacturing system is implemented as a prototype using primarily industrial edge and cloud computing technologies. First, in Section 5.4.1 an overview of the technical systems involved is given. The proposed microservice architecture is mapped onto these systems showing how intra and inter system communication can be realized. Subsequently, the prototypical implementations are detailed. For that, the various applications are grouped into edge applications (Section 5.4.2), cloud applications (Section 5.4.3), and remaining applications running on miscellaneous hardware (Section 5.4.4).

5.4.1 Distributed Logic Execution

For implementation, several types of logic execution levels can be used. These include *edge computing*, *cloud computing*, and *miscellaneous computing*, which groups other technical systems such as personal, industrial, and embedded computers. In this study, the solutions for machine tool applications provided by *Siemens* are used primarily. For edge computing, the *Sinumerik Edge* technology is used, which integrates well with machine tools using

modern *Sinumerik* motion controls. As a cloud computing platform, the *MindSphere* platform is utilized while also incorporating *AWS* cloud computing capabilities. Furthermore, the simulation of the expected process forces is done using the computer aided manufacturing software *NX CAM*.

The high-level communication between the different levels can be seen in Figure 53. The edge device is the central element between the machine network and the internet. Through the machine network, a connection between the machine's NC and the edge device is established. Using the *Sinumerik Adapter* functionality of *Sinumerik Edge*, the various data streams from the machine tool are acquired and provided to the applications running on the edge device by publishing the data packages as messages to the data bus using the *mosquitto* [400] protocol. Furthermore, this work implements a prototypical solution, which uses an embedded linux computer as an intermediate layer for reading the microscope data.

Commercial and custom applications can be deployed on the edge device, reading from and writing to the data bus. Thus, different applications on the edge device can communicate with each other using the data bus or additionally by using *application programming interfaces (APIs)*. The edge applications can also provide GUIs using the integrated *reverse proxy* technology. Thereby, a user-interface running within an application on the edge device is mapped to an open port of the device, enabling outside access. For the communication between the edge device and cloud platforms, the *MindSphere* connector can be used to upload specific messages from the data bus, while the *FileUpload* API can be used to upload files from the edge to the cloud. The communication from the cloud to the edge is carried out manually in this work. On the cloud system, native applications can be used for device management and data visualization. Also, custom applications can be deployed using the *cloud foundry* [401] framework. The communication between the different types of data stored on the *MindSphere* platform, such as time series, events, and documents, and the custom applications, is handled by *MindSphere*'s APIs. In the prototypical phase of the proposed manufacturing system, remaining components, such as cloud computing services or personal computers of experts, are integrated on a manual file transfer basis.

With the different services and storage components defined, certain aspects that require special attention throughout implementation can be highlighted. For the three services *data annotation*, *image segmentation* (during inference), and *parameter recommendation*, a frontend element is needed to communicate with the user, such as a technology expert or machine operator. Furthermore, the services which involve model training especially for im-
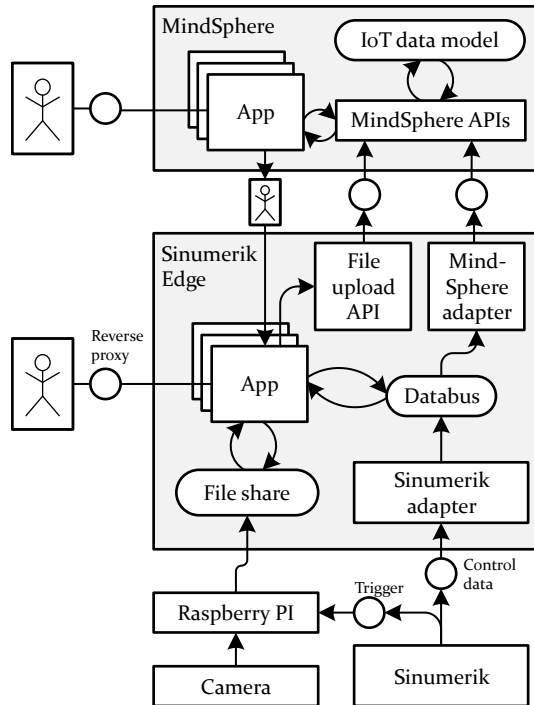
Figure 53: The different microservices can be implemented as custom applications for Sinumerik Edge and MindSphere and can communicate by using the existing communication channels.

age data, such as the *domain adaptation* service and the *image segmentation model training* services, require high computational power. During operation, both the *image segmentation* module and the *process monitoring* modules need to be connected to the NC for triggering the respective data acquisition. The *image segmentation* module also needs to be connected to the respective image hardware for image acquisition.

Based on these requirements, the distribution among platforms can be achieved (see Table 9). To agree with the computational need of the model training algorithms, cloud acceleration is used for the computationally demanding image segmentation training services. The services that are used during machining and require process data from the NC are best executed near the machine tool using edge computing. In its prototypical state, the cutting force simulation is carried out on the personal computer of the respective expert and an auxiliary device is needed for image acquisition.

Table 9: Mapping of implemented and integrated applications to computing paradigms

Edge computing	Cloud computing	Miscellaneous comput- ing
Data handling	Data annotation	Image acquisition
Novelty detection	Domain adaptation	Cutting force simulation
Batch classification	Model training[1]	
Batch clustering		
Parameter recommendation		
Data logging		
Image segmentation		
Model training[2]		

5.4.2 Edge Applications

On the Sinumerik Edge device, custom applications can be designed using the Sinumerik Edge AppSDK. The applications themselves are developed using the *Docker* [402] technology with each application potentially combining multiple specialized containers. The individual containers, their configurations, and the access to resources is specified in a *docker-compose* file. Additionally, the *metaconfig* file specifies the read and write access to the data bus running for each application on the edge device. Applications reading data from the databus are considered *consumer* applications while applications writing messages are called *producer* applications. In this work, the *Python* [403] programming language is used for backend applications and frontend applications. The Sinumerik Edge AppSDK includes libraries for data subscription to the data bus. Furthermore, a deployment pipeline exists that transforms custom docker containers into industrial applications for the *exenia* operating system, a modified version of Docker, which is running on the edge device. Applications prepared this way can be installed on individual edge devices through the respective associated MindSphere account. When the storage of time series data is required, the *influxdb* [404] technology is used as a time series database. Other objects are stored to the file system.

Data Handling

The data handling service is both a consumer and a producer application, consuming the continuous data stream provided by the *Sinumerik Adapter* and providing the current machining state and preprocessed feature vector.

---

[1] Image segmentation models
[2] Time-series models

The data handling routine operates a simple state machine to match the procedure shown in Section 4.1.1. By default, the application is in its waiting state. During the waiting state, only G-Code messages are observed and analyzed regarding the specified start trigger. Once such a trigger is observed, the application switches into the preprocessing state. In this state, the high-frequency control data is buffered to windows of fixed length, which are preprocessed and aggregated to information-dense features. In parallel, the G-Code messages are observed further. Once the end-trigger is seen, the machine switches into the waiting state. For the data alignment using DTW, the package *dtw-python* [405] is used. Furthermore, a parser is integrated for conversion of the text-based simulation data.

The four services *novelty detection*, *batch classification*, *clustering*, and *parameter optimization* follow the same service architecture. Each service has a subscription to the data bus. The novelty detection service is listening for feature vector and machining state data messages while producing novelty data messages. The material batch classification and clustering services are both listening for feature vector, machining state, and novelty messages while producing material-batch data messages. Once a message is received, the procedures shown in Sections 4.2.1, 4.2.2, and 4.2.3 are executed. The involved models are implemented in Python using the *tensorflow* [406] library when using ANNs and the *scikit-learn* [407] library for the remaining models. The calculated results are combined with the input data to form the message produced by the respective service.

The frontend *GUI* service is a sole consumer application. The application consists of a backend service, which observes the data bus for process recommendations, machining state, novelty, material batch, and cluster information and refactors the data into a format for the frontend application. The communication between frontend and backend is implemented using socket technology through the package *python-socketio* [408]. The frontend application can be seen in Figure 54. In the navigation ① the user can switch between the main process observation view and the configuration view. The configuration view (not shown) enables the setting of key-value pairs, such as the cost parameters. At the top of the screen, the current machining state is shown ② including the cutting parameters, the initial tool condition at start of the cutting operation, as well as metadata regarding the cutting operation. Below, a summary of the material identification system is seen ③ showing the predicted material batch and the computed recommendations with both concrete suggestions for optimized cutting parameters regarding the defined metric and the miscellaneous BBI entries associated to the identified material batch. Next to the summary, the effect diagram ④ is plotted showing the effect of changing the cutting parameters feed rate and cutting speed for the

selected metric as a heatmap. The bar chart style visualization showing the effect of the current, user-defined, and ideal parameters on all target metrics is visualized below ⑤. On the right side of the screen, detailed information regarding the state of the process monitoring system can be seen. The upper plot ⑥ displays the predictions of the novelty detection algorithm and the middle plot ⑦ shows the predictions of the batch classification algorithm. For the novelty detection, the novelty score is shown while the batch classification plot shows the predicted likelihood of all available batches. On the bottom, the computed cluster map with the respective labels, if available, is shown ⑧.
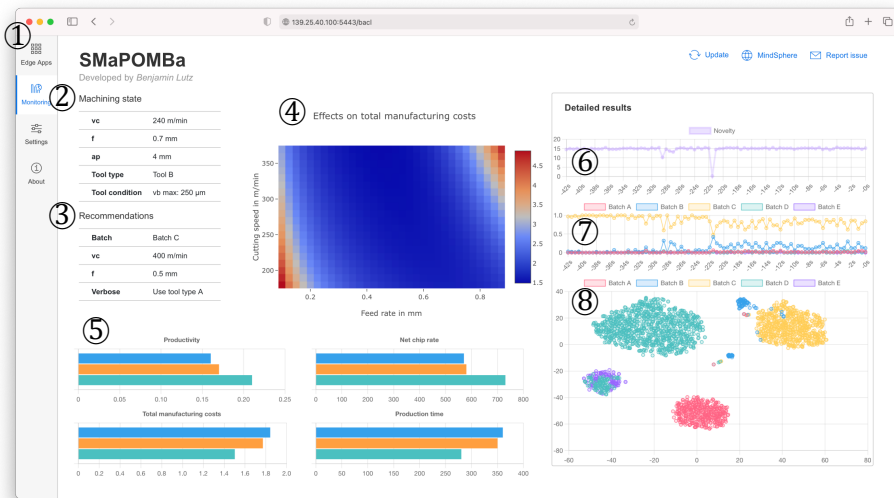
Figure 54: GUI of SMaPOMBa, showing the predicted information as well as the recommendations to the operator.

Logger

The data logger is a consumer application observing all prediction outputs. These messages with their respective timestamps are stored in a temporary buffer for post-operation retraining. The data buffer is implemented as a time series database using the *influxdb* technology.

Image Segmentation

The *image segmentation* service consists of four specialized microservices: the *GUI*, the *backend*, the *parameter* service, and the *model execution* service. The *backend* service is the central service managing the other services. It

is implemented in *Python* running in a constant loop, waiting for new image data to arrive from the *image acquisition* service. Once new image data arrives, the *model execution* service is called to analyze the image yielding the segmentation results. These are provided to the *GUI* using a web-socket connection. The *model execution* service is implemented as a web server, providing one API endpoint for inference. By separating the *backend* service from the *model execution* service, the backend service can be implemented in a light-weight fashion while the model execution service is preloaded with the necessary libraries for model execution. The image segmentation models are implemented in *tensorflow* [406]. The *GUI* provides the interface to the operator (see Figure 55). The interface shows the most recent measurements individually visualized as cards ①. Within each card, metadata such as the respective scene and timestamp of the measurement ② are shown. Below, a warning ③ appears if the tool condition surpasses configured critical thresholds, such as a flank wear width of 400 μm. At the bottom of the card, the detailed wear metrics can be found grouped by type of defect and type of metric ④. On the right-hand side of the card, the used micrograph is shown with an overlay of the detected defect classes ⑤ and a zoom functionality to enlarge regions of interest ⑥. Furthermore, a separate configuration panel is available, which can be used to set parameters of the image segmentation routine ⑦.
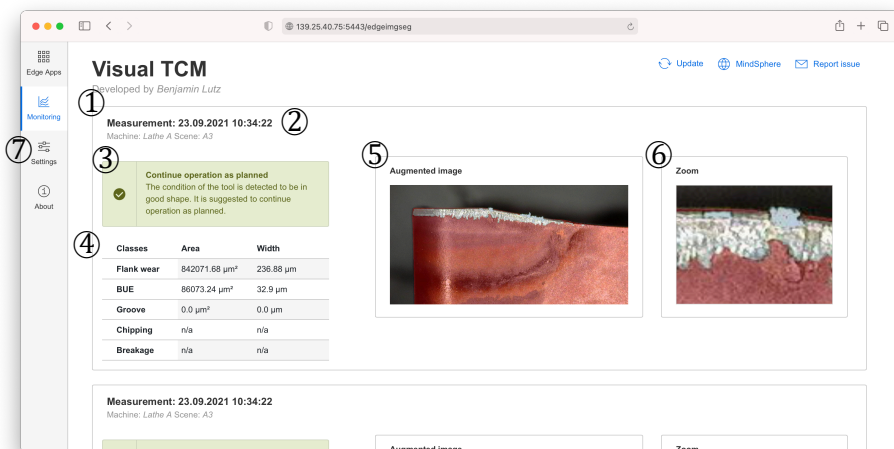
Figure 55: GUI of the visual TCM system.

5.4.3 Cloud Applications

The different services for image segmentation model training and domain adaptation are all implemented as executable scripts running on *AWS* cloud servers with an integrated graphics processing unit (GPU). The *PyTorch* framework [409] is used for the implementation of the domain adaption model [S3] while the remaining deep neural networks are implemented in *tensorflow*. Each script is scene-agnostic and can be adapted for the specifics of each scene and learning task by a configuration file. Trained segmentation models are exported in the *.h5* format, which can be imported into the image segmentation application running on the edge device for inference.

Data Annotation

As the efficient data annotation method involves user interaction, a frontend application is needed. The frontend is implemented using *VueJS* framework [410]. Through the interface, the operator can manage and create individual scenes, adapt the reference datasets, define novel class labels, and annotate images. In the annotation view, shown in Figure 56, several tools are provided to annotate images with their respective semantic regions. These tools include standard image manipulation tools such as shape-based selections and a brush tool ①, but also the proposed annotation suggestion method. Therefore, a two-step procedure is available. In an initial step the superpixels are generated ② and highlighted on the image through yellow lines. Subsequently, the metric learning-based recommendation can be used ③ to find initial estimates of the class labels. These can be corrected by the user by selecting wrongly classified superpixels individually and selecting the correct metric using the context menu on the right-hand side ④. [S5]

5.4.4 Miscellaneous Computing

The image acquisition service is implemented using a *Raspberry Pi* embedded computer for logic execution and a five megapixel USB microscope camera. The computer is connected to the machine's NC. Furthermore, the computer is connected to the edge device using the *samba server* by mounting a remote folder on the edge device to a local location on the Raspberry Pi.

The logic is running on a Raspberry Pi that is connected to the NC, the microscope camera, and the edge device. The procedure can be seen in Algorithm 9. The algorithm is running in a continuous loop, which is evaluated at the same frequency as the machine tool's cycle. The NC can issue a status once the tool is positioned in front of the camera, which is observed by the control algorithm. When the respective status bit is set, an image is grabbed from
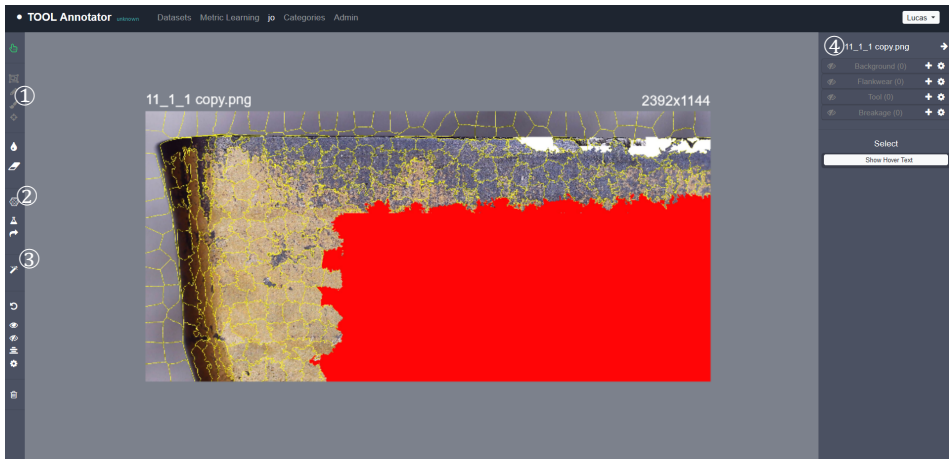
Figure 56: The image annotation user interface contains traditional image manipulation tools as well as the proposed superpixel generation and label estimation methods [S5].

the microscope camera using the *fswebcam* [411] application. This file is then renamed with the current timestamp and saved in the mounted samba folder. Thereby, the file is made available to the image analysis methods running on the edge device.

Algorithm 9 Image acquisition logic

Require: Samba folder mounted
Require: Microscope camera connected
  loop infinitely
    $b_s \leftarrow$ CHECK ANALOG INPUTS $\triangleright$ Read status bit connected to NC
    if b_s **is** set **then**
      $u \leftarrow$ GRAB IMAGE(microscope)
      file name $\leftarrow$ TIME
      SAVE IMAGE TO SAMBA(u, file name)
    end if
    WAIT(next machine cycle)
  end loop

---

6 Validation

For the validation of the proposed methods, data from various manufacturing scenarios is acquired and used. Here, the typical validation workflow for data science projects is used of dataset division into training and testing datasets to ensure the representativeness of the reported scores and to avoid model overfitting.

In Section 6.1 the different methods proposed for effective image segmentation are validated. Subsequently, the remaining methods of the smart manufacturing system are validated in Section 6.2, investigating the applicability of the proposed smart manufacturing system to typical manufacturing scenarios. Due to the fact that not all types of data are always available, only selected components are validated in each scenario.

The contents of this chapter are supported by student's work supervised by the author [S3–S5, S11]. Furthermore, the investigated validation use cases were published in parts in the publications of the author [P6–P11, P13].

6.1 Validation of Resource-efficient Image Segmentation for Cutting Tool Images

To validate the proposed methods, images from four different scenes, $\mathcal{S}_a$ - $\mathcal{S}_d$, are acquired. Images of all scenes are taken using different optical toolmaker's microscopes. The resulting images for $\mathcal{S}_a$ and $\mathcal{S}_b$ have a raw resolution of 1024 by 1280 pixels while the images for $\mathcal{S}_c$ and $\mathcal{S}_d$ are acquired at a resolution of 1144 by 2392 pixels. All images are taken in RGB color mode. $\mathcal{S}_a$ contains images of a cutting tool of type *CNMM160612RP*, $\mathcal{S}_b$ consists of cutting tool type *CNMG160612-PR4325*, $\mathcal{S}_c$ depicts an unspecified cutting tool of triangular shape, and $\mathcal{S}_d$ is of cutting tool type *FFQ4 SOMT 120516HP*. Comparing the different tools (see Figure 57), differences in geometry and coating type can be observed. Furthermore, for $\mathcal{S}_a$ and $\mathcal{S}_b$ the influence of daytime brightness is visible in the images as varying image brightness depending on the time of day the images were acquired. Contrarily, $\mathcal{S}_c$ and $\mathcal{S}_d$ are acquired in a controlled environment with fixed illumination, thus showing no external brightness effects.

In a preprocessing step all images are horizontally aligned. Additionally, the images of $\mathcal{S}_a$, $\mathcal{S}_b$, and $\mathcal{S}_c$ are cropped to an ROI with a width of 1024 pixels and a height of 512 pixels, while the images of $\mathcal{S}_d$ are cropped to an ROI of size 1100 by 2200 pixels.
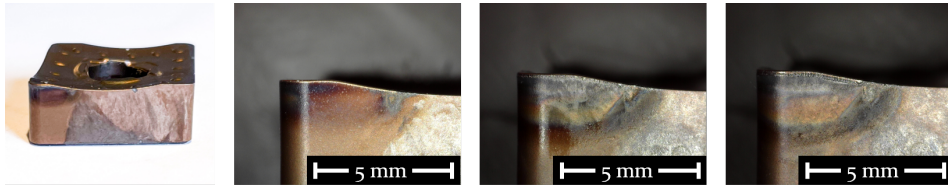
(a) Cutting tool insert for $\mathcal{S}_a$ with sample micrographs at different degrees of flank wear
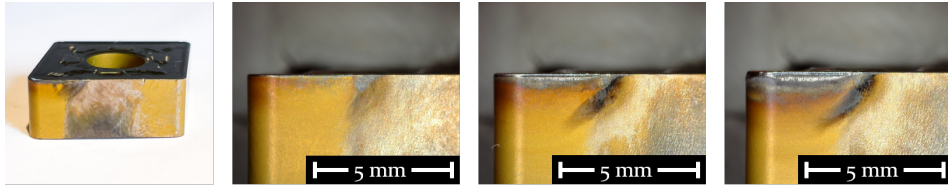
(b) Cutting tool insert for $\mathcal{S}_b$ with sample micrographs at different degrees of flank wear
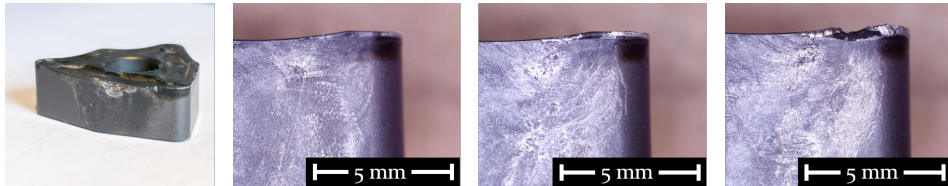
(c) Cutting tool insert for $\mathcal{S}_c$ with sample micrographs at different degrees of flank wear
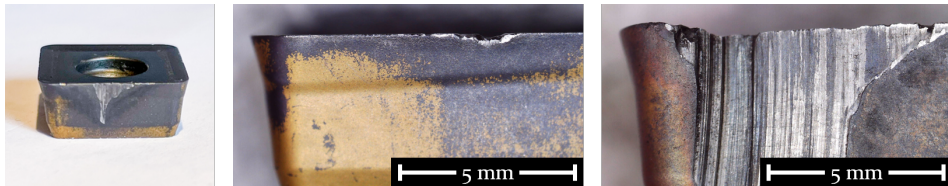
(d) Cutting tool insert for $\mathcal{S}_d$ with sample micrographs at different degrees of flank wear

Figure 57: Images of the investigated cutting tools and sample microscope image data for the various investigated scenes.

All images are annotated by process experts using traditional image manipulation software to acquire ground truth data. In this labeling process, each pixel is assigned a specific color that corresponds to the class the respective pixel belongs to. The finished masks are then exported as portable network graphics (png) images. Challenges in the labelling procedure are the similarities between the classes *flank wear* and *groove*. Furthermore, areas broken away from the cutting tool insert, which are showing background, are labelled as *catastrophic failure*. Among all scenes, the detected classes are: *background, undamaged tool body, flank wear, groove, BUE, chip notch*, and *breaking*. In

Table 10, the number of images that contain the respective defect type are shown for all scenes. The classes background and undamaged tool body are visible in all images. Defects that appear in less than five images are discarded (italic entries in Table 10). It can be seen that flank wear is present in most images. Regarding the remaining defect types, different distributions can be observed. For $\mathcal{S}_a$ and $\mathcal{S}_b$, the defect BUE is rather prominent. $\mathcal{S}_d$ however contains mostly groove, chip notch, and breaking defects.

Table 10: Class presence per defect for each scene.

	$\mathcal{S}_a$	$\mathcal{S}_b$	$\mathcal{S}_c$	$\mathcal{S}_d$
Samples showing flank wear	153	197	39	121
Samples showing groove defects	20	3	0	52
Samples showing BUE	107	110	9	2
Samples showing chip notch	22	*1*	9	63
Samples showing breaking defects	4	*1*	0	61
Total sample count	155	200	39	123

In Figure 58 the distribution of the defect sizes are shown for all investigated scenes. It can be observed that there is a wide variety of sizes for chip notch, starting at 0.003 mm^2 for $\mathcal{S}_a$ up to 7 mm^2 for $\mathcal{S}_c$. For the flank wear, all investigated scenes show similar average values between 0.3 mm^2 and 1 mm^2. The defect BUE is about one magnitude lower than the flank wear defect. The largest defect areas can be seen for the groove in $\mathcal{S}_d$ and breaking in $\mathcal{S}_a$, $\mathcal{S}_b$, and $\mathcal{S}_d$.

Among all defects, the flank wear width as a primary wear metric is investigated in greater detail (see Figure 59). For $\mathcal{S}_a$, an even distribution of the maximum flank wear width VB_{max} between values of 100 µm and 350 µm can be seen. Similarly, the average flank wear width VB_{avg} is evenly distributed with values ranging from 0 µm to 200 µm. The tools from $\mathcal{S}_b$ show a similar normal distribution for VB_{max} centered around the average value of 180 µm. Here, tools are considered worn when reaching a VB_{max} of 300 µm, thus only a few samples with higher wear values exist. For scene $\mathcal{S}_c$, there is little data for unworn tools as most images are taken of tools after they are replaced. Thus, maximum flank wear width values range mainly from 300 µm up to 750 µm, with average flank wear width values between 150 µm and 250 µm. The final scene $\mathcal{S}_d$ features both cutting tools with high and low degrees of flank wear. For most images the average wear VB_{avg} is a normal level between 0 µm and 200 µm when the tools are exchanged. However, the extreme wear
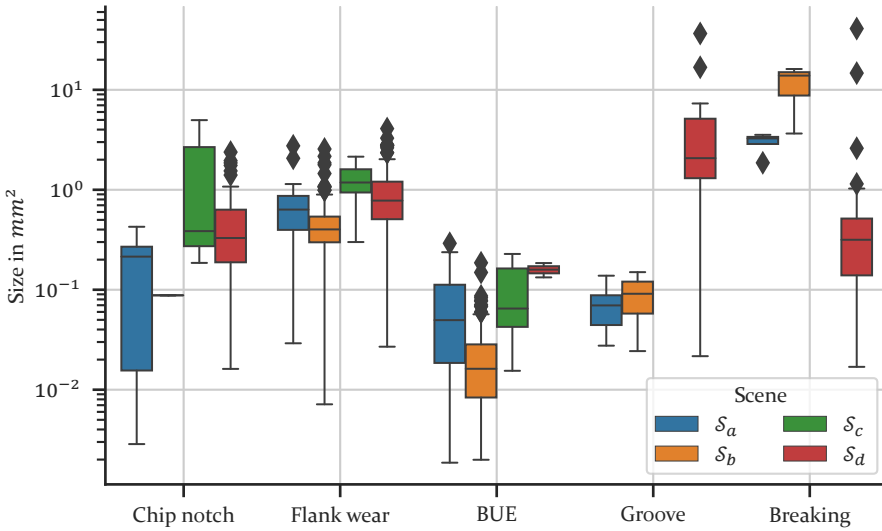
Figure 58: Distribution of defect sizes among the investigated scenes.

values range from 100 μm up to 700 μm indicting a strongly varying degree of wear among the images of the same scene.

6.1.1 Optimized Image Segmentation

For all scenes, the different image segmentation alternatives are validated. For the window-based method, a window with a height and width of 48 pixels is selected. The created windows are split into the respective subsets for training, validation, and testing on the image level. Thus, 80% of all images are selected as training images and their windows are put into the training subset. Similarly, the validation and testing subset contain 10% of all images each. For the manual CNN approach, hyperparameter optimization of the base network structure, as proposed in Section 3.2.3, is carried out with the training and validation subsets using the *tune* [412] library. Thereby, slightly different network architectures are found for $\mathcal{S}_a$, $\mathcal{S}_b$, $\mathcal{S}_c$, and $\mathcal{S}_d$. Independent of the network architecture and optimizer, model training is carried out for 200 epochs with a batch size of 16. For one-pass image segmentation, the *DeepLabV3Plus* architecture is chosen. The architecture is implemented as proposed originally. Independent of the image resolution in the respective scene, all data is resized to a common format of 1024 by 512 pixels. All algorithms are trained and optimized on the training and validation subsets and evaluated on the testing dataset using the mIoU metric. The obtained

(a) Scene $\mathcal{S}_a$

(b) Scene $\mathcal{S}_b$

(c) Scene $\mathcal{S}_c$

(d) Scene $\mathcal{S}_d$
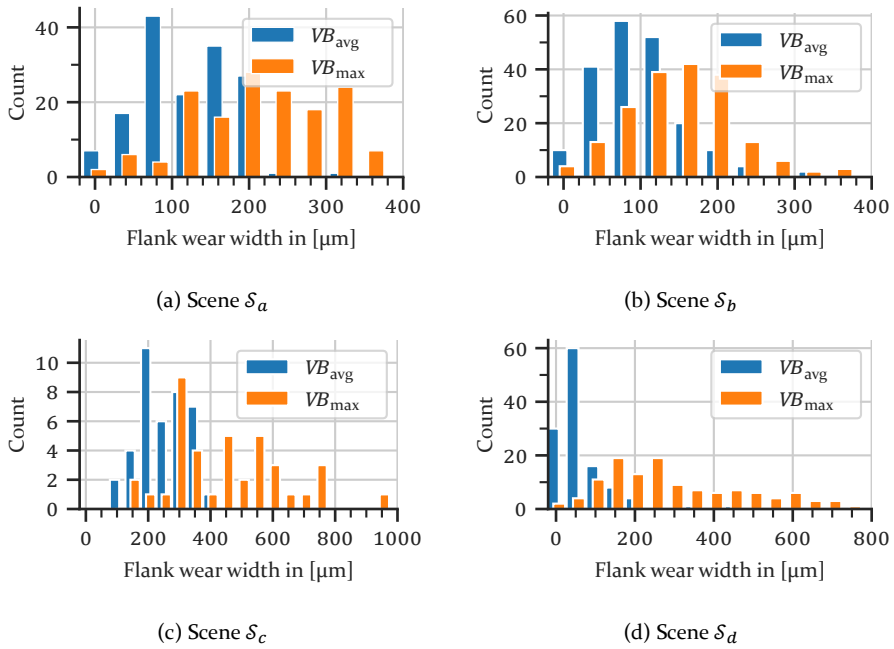
Figure 59: Measured flank wear widths.

scores are shown in Table 11. The high mIoU scores, especially for the window-based approach, show the suitability of the proposed method for semantic image segmentation of cutting tool images.

Table 11: Prediction performance in mIoU for the window-based and the one-pass segmentation alternatives for the different datasets.

	Scene $\mathcal{S}_a$	Scene $\mathcal{S}_b$	Scene $\mathcal{S}_c$	Scene $\mathcal{S}_d$
Window-based (CNN)	0.86	0.85	0.77	0.70
One-Pass Segmentation	0.70	0.92	0.63	0.71

6.1.2 Efficient Training Data Generation

For the validation of the **efficient annotation procedure**, a user study is carried out [P9]. Each user is given a short explanation about the functionalities of the labelling tool and the annotation task. Consecutively, parts of an image need to be labelled by the user with two methods. In the first method, only traditional annotation tools such as bounding box selection and the brush tool are made available. In the second method, the proposed method

of superpixel generation and deep-metric learning based suggestions can be used, thus requiring the user to only check the quality of the prediction and correct mistakes by the algorithm. To avoid bias, the order in which both methods are tested is alternated among the individual test users. For each annotation run, the time taken, the manual interactions (clicks), and the mask quality are measured. Here, the mask quality is measured as the mIoU between the user-generated mask and available ground-truth masks. In total, ten experts took part in the study, each labeling two images. [P9]

The results of the study are shown in Figure 60. It can be observed that the average labeling time per picture was reduced significantly from an average of 205 seconds for the traditional image annotation to 25 seconds for the proposed procedure. This can also be seen through the number of interactions taken by the user. In the traditional method, between 75 and 310 clicks with an average of 105 clicks were needed for the annotation of a single image. Contrarily, for the proposed method between three and 31 clicks with an average click count of 14 are recorded, which corresponds to the manual correction of wrong predictions by the underlying deep metric learning algorithm. In terms of prediction quality, the partially automated masks show higher quality than the fully manually annotated ones. Thereby, it can be seen that using such an efficient annotation tool reduces the labelling effort and increases the data quality. [P9]
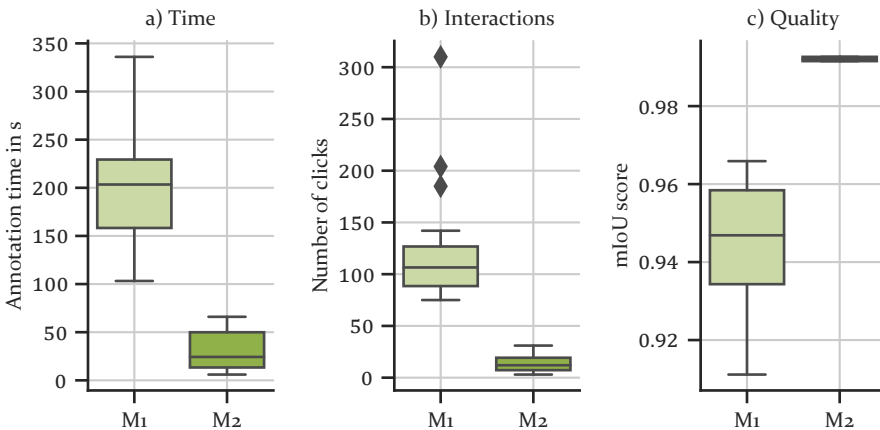
Figure 60: For the validation of the image annotation procedure the proposed method (M2) is compared to traditional image annotation (M1) through user tests, adapted from [P9].

6.1.3 Context-sensitive Data Augmentation

The available images from the different scenes are used to validate the image warping strategy for shape adaptation. In Figure 61 samples of warped images can be seen. Comparing model training on originally-shaped images to warped-to-target images, an increase of 0.11 mIoU score can be observed when using the warped dataset [S3].

(a) Scene $\mathcal{S}_a$ to scene $\mathcal{S}_b$ (b) Scene $\mathcal{S}_c$ to scene $\mathcal{S}_a$ (c) Scene $\mathcal{S}_d$ to scene $\mathcal{S}_b$

(d) Scene $\mathcal{S}_c$ to scene $\mathcal{S}_b$ (e) Scene $\mathcal{S}_d$ to scene $\mathcal{S}_a$ (f) Scene $\mathcal{S}_a$ to scene $\mathcal{S}_c$
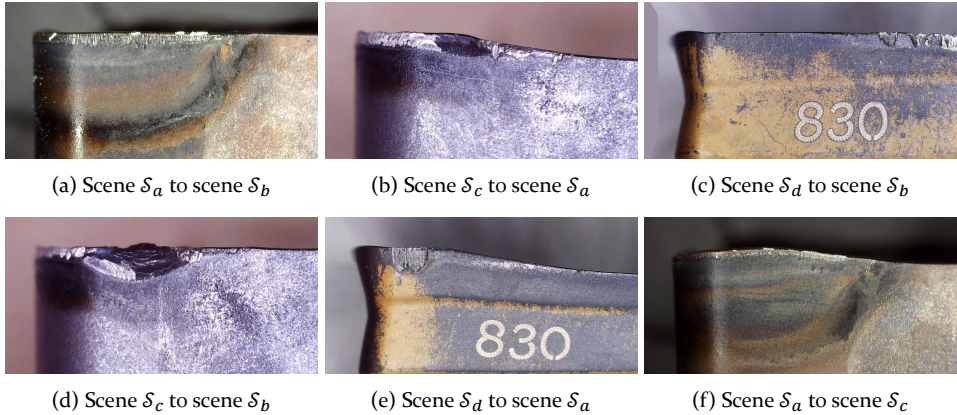
Figure 61: Sample images after being warped to the shape of the target scene.

For a quantitative validation of the domain adaptation procedure, the data from $\mathcal{S}_a$ and $\mathcal{S}_b$ are considered known, while $\mathcal{S}_d$ is considered novel. Initially, a small number n of annotated images from $\mathcal{S}_d$ is provided to train the domain adaptation models while the remaining images are used for testing. The GAN model used for visual image translation is implemented as described in Section 3.4.2 and trained for 800 epochs using the *Adam* [351] optimizer with a learning rate of 0.0002 and a momentum of 0.5 on the n training samples from provided $\mathcal{S}_d$. Using the trained generator part of the GAN model, the available image masks from $\mathcal{S}_a$ and $\mathcal{S}_b$ are used to create the synthetic datasets $\mathcal{S}_{a \to d}$ and $\mathcal{S}_{b \to d}$. Using these in combination with the n training samples provided, the *DeepLabV3Plus* image segmentation model is trained and used to evaluate its performance on the withheld dataset from $\mathcal{S}_d$. [P8]

In Figure 62, synthetic images created throughout the training of the image translation procedure are shown. It can be observed that for early epochs many artifacts are visible while the predictions from later epochs show high similarity to the original image provided.

The influence of the number n of training samples is visualized in Figure 63. It can be observed that the classes background and undamaged tool body
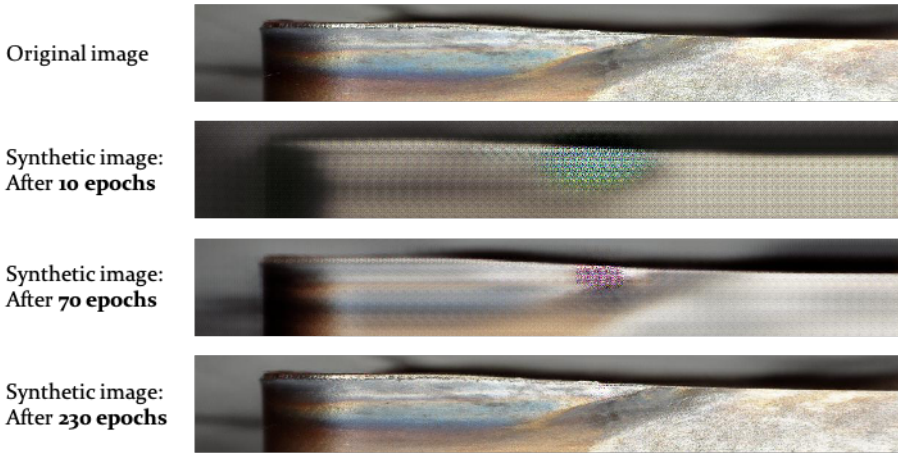
Figure 62: Improvement of synthetic image generation during model training.

can be detected well from the first image provided and reach scores of above 0.9 IoU with three or more training images. For the different investigated defects, a higher number of samples is needed for detection. The flank wear defect reaches an initial prediction accuracy of 0.4 IoU with three training images and a score of 0.7 IoU with ten images provided. For the groove defect, sufficient detection is possible with only ten training images provided. The defect BUE was not detected at all. The reason can be found in defect distribution. While the historic scenes $\mathcal{S}_a$ and $\mathcal{S}_b$ contain a significant amount of BUE, this defect is only visible in two images of $\mathcal{S}_d$. Thus, it is likely for it not be part of the n images selected for training the generator model. Moreover, the generator can only predict classes it has seen during training. [P8]

Comparing the number of annotated training data from a novel scene needed to reach a certain score, the quantitative benefit can be seen. The proposed training strategy using domain adaptation requires three annotated samples to reach a score of 0.5 mIoU while in traditional training ten images would be required. Similarly, the score of 0.7 mIoU achieved with ten annotated images by the augmentation method is reached by traditional training only when supplying 30 training samples. [P8] Thus, it can be summarized that domain adaptation enables the usage of historic training data and can reduce the labelling effort by two thirds.

6.2 Validation of the Smart Manufacturing System

To validate the remaining methods and procedures of the proposed smart manufacturing system, different experiments and operational scenarios are
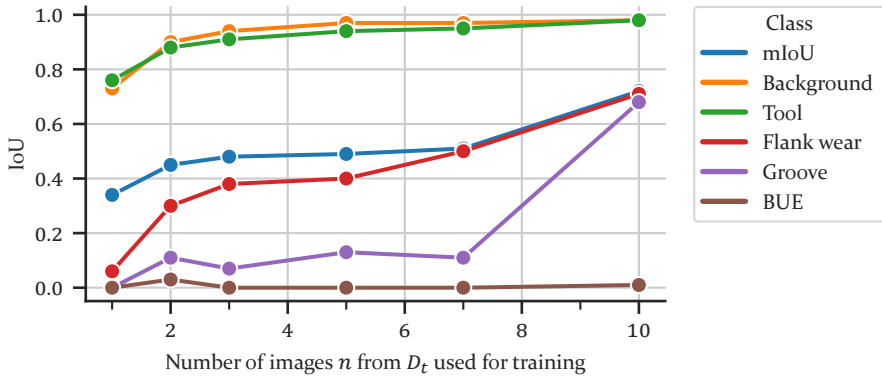
Figure 63: mIoU and IoU scores depending on the number of supplied training images, adapted from [P8].

investigated. These include the turning of multi-material parts (Section 6.2.1), the face milling of motor shafts (Section 6.2.2), the turning of gears (Section 6.2.3), and turning in an experimental setting (Section 6.2.4).

6.2.1 Machining of Multi-material Parts

With the advances of additive manufacturing, load-optimized parts can be manufactured not only in arbitrary shapes but also combining different materials optimized to the desired material properties. One such technology is wire arc additive manufacturing (WAAM), which is especially promising for the manufacturing of large volume parts, such as load-optimized support structures found in aerospace and medical equipment. Parts produced by such processes come with a rather bad surface quality, which needs to be post-processed using machining operations. With the multiple materials involved in parts manufactured this way, the material batch identification methodology proposed in this work is transferred to and evaluated for the material type identification task in this context.

A tube with an inner diameter of 57 mm, a maximum wall thickness of 12 mm, and a height of 129.5 mm is fabricated using the WAAM process. First, the lower part of the tube, $z \in [62.5 \text{ mm}, 129.5 \text{ mm}]$ is manufactured using a *AW-6060* aluminum wire (see ②, Figure 64). Then, the upper part of the tube, $z \in [0\text{mm}, 62.5\text{mm}]$, is built using an AW-5087 aluminum wire material (see ①, Figure 64). Due to material interactions in the transition zone, the exact point of transition is unknown to the operator.

Figure 64: Additively manufactured tube consisting of multiple materials.

The tube is machined using a turning process to reach the desired shape and surface quality. In total, six cuts are carried out with a cutting depth a_p of 0.458 mm. All cutting experiments are conducted at the same machining state. Throughout all experiments, the position and torque data for the main spindle, the feed drive, and the depth drive are observed and stored. Out of the six cuts acquired, the initial cut is discarded due to the extreme uneven surface finish. The remaining five cuts are referred to as cut #1, cut #2, cut #3, cut #4, and cut #5.

For the evaluation of the proposed material identification methods, the data is split into a training and testing dataset. The training dataset will be used to train the respective novelty detection and material identification models while the testing dataset will be used to benchmark these models and report the final scores. From the cuts #1, #2, and #3 the data acquired between a z of 5 mm and 65 mm are considered training data for material B, and the data observed during a z of 75 mm and 135 mm are considered training data for material A. The initial and final 5 mm are discarded due to transient response effects. Furthermore, the 10 mm near the expected material transition zone are discarded as no definite ground-truth data is available about the true material type. The remaining data from cuts #4 and #5 is then used as testing dataset.

The baseline-load for each axis is measured prior to machining and used to preprocess the signals. Furthermore, the cutting force is computed from the spindle torque using the respective diameter. Out of the 24 potential features, the recursive feature elimination method finds the ten most important features as: $\text{AVG}^C_{\text{Force}}$, $\text{STD}^C_{\text{Force}}$, $\text{AVG}^X_{\text{Torque}}$, $\text{STD}^X_{\text{Torque}}$ $\text{KUR}^X_{\text{Torque}}$, $\text{AVG}^Z_{\text{Torque}}$, $\text{STD}^Z_{\text{Force}}$, $\text{STD}^X_{\text{Acc.}}$, $\text{SKEW}^Z_{\text{Acc.}}$, and $\text{KUR}^Z_{\text{Acc.}}$. The best-performing novelty detection algorithm is found as *One-Class SVM* with the rbf kernel, a γ of 0.4, and a *nu* of 0.1. On the test-dataset the algorithm correctly classifies all samples as known. The best performing classification algorithm for material classification is found as *RF* with *19 estimators*, the *entropy* criterion for purity measurement without constraining the tree construction regarding depth and number of considered features. On the test-dataset the algorithm achieves an F1 score of 0.91. Detailed results can be seen in the confusion matrix in Table 12.

Table 12: Confusion matrix showing the materials predicted by the material classification algorithm.

	Predicted Material A	Predicted Material B
True Material A	100.0%	0.0%
True Material B	18.7%	81.3%

Furthermore, Figure 65 shows the model's predictions for the full testing cuts #4 and #5 including the transition region. In this two-class problem the probability of material B is inversely correlated to the probability of material A and is, thus, not visualized. It can be seen that for both cuts a few misclassifications appear during the initial part of the machining process while cutting the first material. Also, within the material transition zone, the probability drops to around 70%. Contrarily, the second material is classified perfectly with probabilities close to 100% for most of the remaining cutting process.

Thereby, the applicability of the proposed material batch identification procedure for the identification of different material types during machining of multi-material parts is shown. This enables the definition of material-specific cutting parameters and their suggestion to the operator during machining.

6.2.2 Face Milling of Shafts

A face milling batch production process is analyzed for the validation of the proposed procedure under limited data availability. In the investigated process, the face of shafts, used in electric motors, are machined to finish
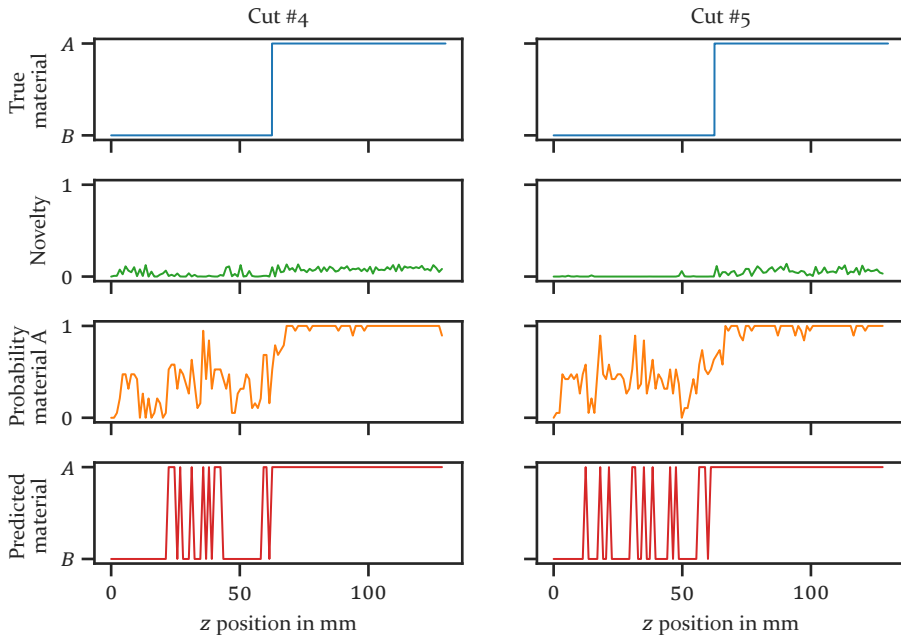
Figure 65: Prediction results of the novelty detection and material classification algorithms for the testing cuts #4 and #5.

using a face milling operation. In a preliminary process, the respective bar stock of multiple meters length is sawed to the needed dimensions with 2 mm excess on either side. During the machining operation of interest, the shafts are then machined on both sides with an initial roughing operation and a consecutive finishing operation to reach the desired dimensions with high surface quality. There are several product variations of the produced shaft, which vary in shaft diameter and base material. Independent of the variation and cutting operation, the same cutting tool is used, which consists of seven cutting tool inserts. Throughout operation, the usage time of the cutting tools is tracked. Once a critical level is reached or the condition of the tools is determined as worn, all cutting tools are replaced with fresh cutting tools, either by rotating the inserts to a fresh cutting edge or by replacing the inserts.

The cutting process is observed during normal operation for a period of three months. During the observation phase, the needed control data, the tool changes, and the runtime of each tool are logged. After completion of the observation period, the data is analyzed with the proposed methodology regarding material batch influences. As the individual cutting operations

per part are short in respect to the tool life, no ground-truth data about the true machinability of the various parts can be acquired. Furthermore, no specific information about individual material batches are available, however differences in the behavior of the materials are observed by the operators for certain days. Thus, a qualitative analysis is conducted to show that the effect of material batches can be seen through cluster analysis.

Throughout the observation period, a total of 10772 parts are processed. Among these, different product variations can be distinguished based on the shaft's diameter and the base material. The most common diameters are 32 mm with 2275 parts, 73 mm with 2103 parts and 40 mm with 1686 parts (see Figure 66 - a). 4196 parts are made out of ST60 and 11 out of 42CrMo (see Figure 66 - b). The base material information is missing for the remaining 6565 parts. Among the different diameters, the most complete dataset can be found for 32 mm diameter parts with 2243 parts of ST60. Thus, this data subset is used for the consecutive analysis. Furthermore, only data acquired at similar tool conditions is used to ensure comparability. Therefore, only cutting operations conducted with fresh cutting tools are considered. Here, fresh is defined as the cutting tool being within its initial 15% of assumed tool usage time.
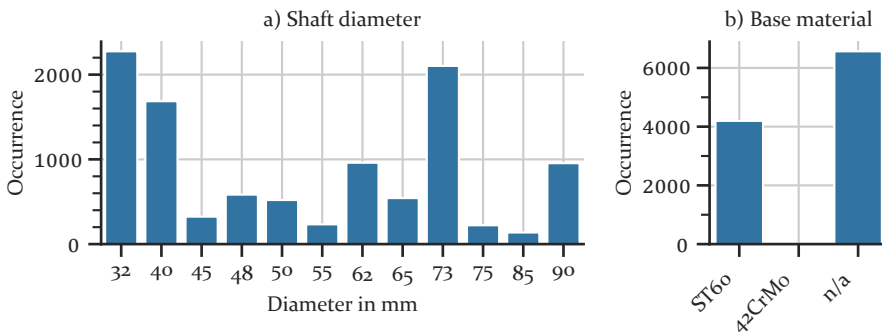
Figure 66: The observed parts vary significantly regarding its diameter and slightly regarding the base material. Only product variations with more than 100 samples are shown.

For the data preprocessing, the cutting forces are simulated using *NX Cam* and the baseline loads are determined. Both the measured and the simulated force signals are aligned by the DTW methodology. Furthermore, the signal trends F' and μ' for the signals F and μ are computed using a Butterworth lowpass filter [413] with a cutoff frequency of 15 Hz. In Figure 67, the simulated forces $\widetilde{F}$, the baseline compensated machine data F, and the computed ratio μ are shown for the spindle as well as the x and z feed drives. In general, a

good alignment between simulated and computed cutting forces can be seen throughout the cutting operation. The ratio of both signals is computed as μ indicating the influence of the material batch's machinability. It can be seen that, except for the initial signal part, μ' shows constant behavior. Thereby, the usage of simulated and observed force ratios can be validated.
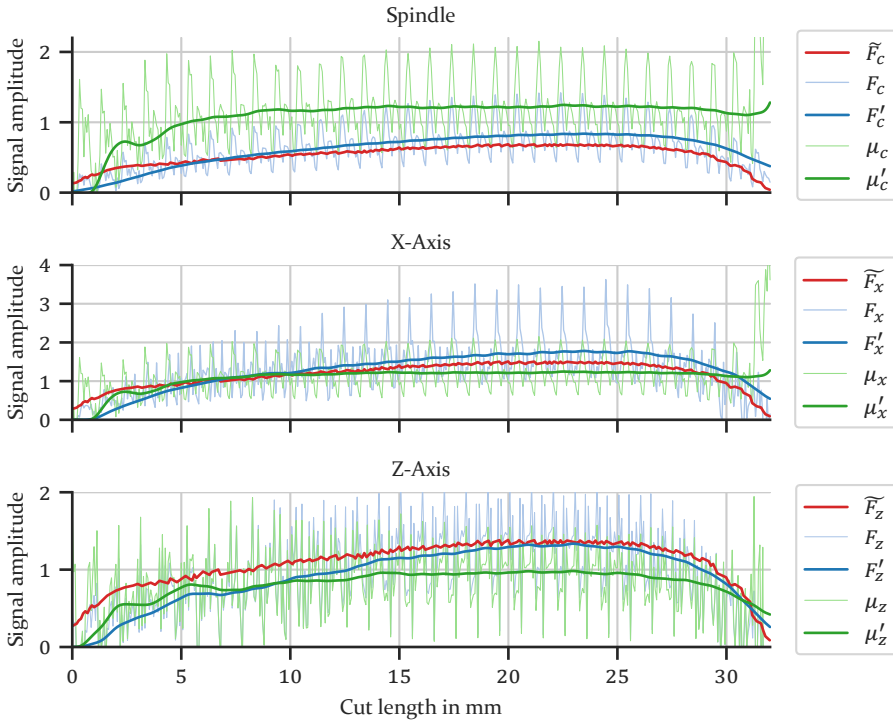
Figure 67: Simulated cutting forces $\tilde{F}$, measured force data F, and the computed batch-implying fraction μ for an exemplary cutting operation of a 32 mm diameter shaft with a fresh cutting tool.

In this scenario, no ground-truth data about each material batch is available. Thus, only the clustering approach can be validated. In Figure 68, the cluster map for the data points from 32 mm diameter parts are shown. As described, the preprocessed and compensated machine signals are aggregated to dense feature vectors. As the individual cuts are less than one second, the windowing procedure is skipped and the full cutting operation is considered a single window. The feature vectors computed this way are standardized to a mean of zero and a standard deviation of one before computing the clusters. For cluster computation, the evidence accumulation algorithm with a t value of 0.5 and a N parameter of 50 are chosen. After the iterative procedure, 17

individual clusters are found. For simplicity, clusters with less than 15 members are disregarded and aggregated as cluster *-1*. The computed clusters are highlighted by the color of their marker in the tSNE visualization. Analyzing the distributions, it can be seen that the data points are separated well by the tSNE method, and that the identified clusters match human intuition. Three clusters, cluster 6, cluster 8, and cluster 12 can be identified with no overlap to other clusters and large distances between the clusters. Among the remaining clusters, three cluster groups can be observed with their data points in proximity: Clusters 19, 21, and 22; Clusters 23 and 27; and clusters 10, 11, 25, and 26.
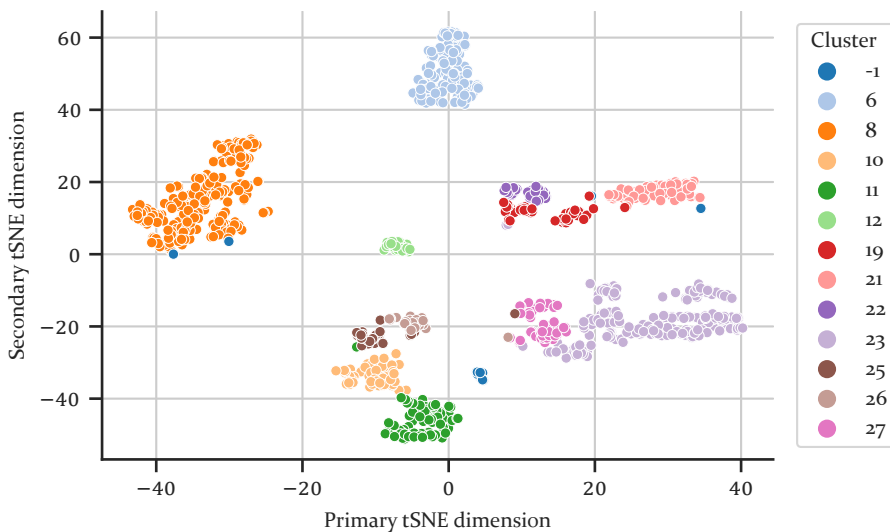
Figure 68: In the 2D visualization of the computed feature vectors at similar machining states, using the tSNE method, several clusters can be observed, which are identified by the evidence accumulation algorithm.

Considering the data selection to samples of comparable conditions, it can be inferred that remaining signal deviations can be attributed towards differences in machinability of the encountered material batches. Thus, as the clusters are found based on the similarity of process data, it can be assumed that parts within the same cluster are from the same material batch and the material batches of one cluster group might behave similar in comparison to material batches from other cluster groups.

As ground-truth data is not available for validation, the date of the respective machining processes is investigated. It can be assumed that throughout operation different material batches, e.g. from different suppliers or from

different heats, are machined. Furthermore, it can be assumed that the material is continuously delivered as needed, and then processed in a timely manner. Therefore, parts from one material batch should be machined at similar dates. Such an analysis is shown in Figure 69, plotting the ratio of the detected clusters for each day. It can be seen that parts associated to cluster 25 and 26 were mostly produced on day 33, parts of clusters 6 and 8 on day 18 and day 19, parts of clusters 10, 11, 12, 23 on days 20 and 21, and parts of clusters 19, 21 and 22 on days 30 and 31. This shows that parts belonging to one cluster were mostly machined on a single day or two consecutive days. Thus, as the detected clusters are not randomly distributed among all days but correlate with the production date, it can be concluded that the clusters found capture effects of material batches with different machinability.
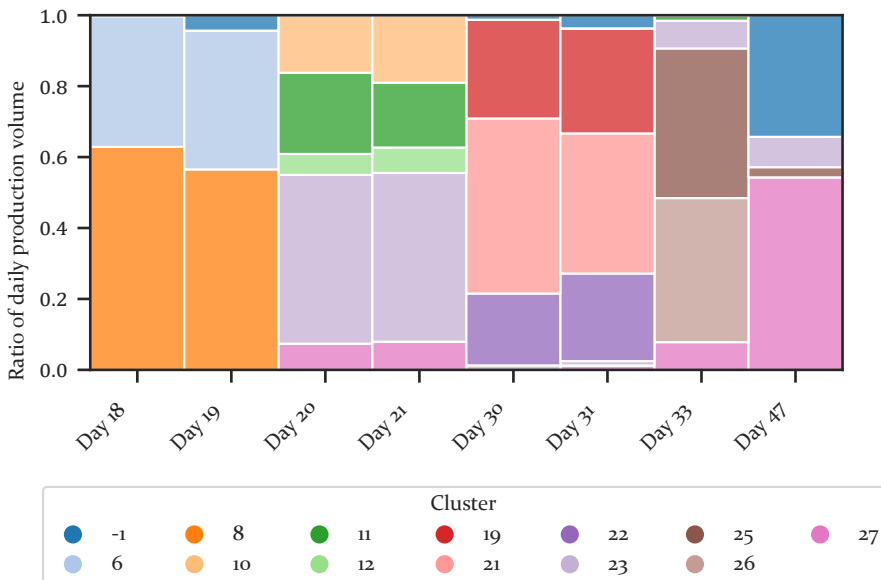
Figure 69: Distinct patterns of detected clusters can be observed in regard to the production date.

6.2.3 Small-sized Lot Production

The material identification methods are validated for a small-sized lot production use case. Medium-sized gears are preprocessed using turning operations. The production takes place in lots of six workpieces, which are processed in several roughing and finishing operations to shape the stock material to the desired geometry. Among the different lots, different product variations, varying in part diameter and part height, are manufactured. Independent

of the variation, the same base material, 18CrNiMo7-6, which is quenched and tempered, is used for all observed parts. Furthermore, all parts are machined at the same cutting parameters following similar machining programs. Machining is carried out using a vertical lathe. The processing of one lot, including planned maintenance, takes approximately eight hours. The cutting time of the investigated finishing cut is approximately three minutes. For each operation, a different type of cutting tool is used. Tools are replaced at the start of each lot or when they reach their end-of-life.

The following validation approach is chosen: During the machining process the required process data is monitored. Furthermore, at the end of each cutting operation, the flank wear width of the cutting tools is measured. Baseline data is acquired as machine data at the start of each cutting operation but before the tool engages the material. Subsequently, complete datasets are selected from the experiments, which will be used for model training and testing. The data from the first three lots will be used to train the novelty detection and material identification methods for testing. The remaining data is analyzed lot by lot, based on their chronological order. For each part within a lot, the novelty detection is carried out. If the material is detected as known, material identification is carried out. Materials detected as novel are considered a new unique material. In this case, both the novelty detection and material identification model are retrained with the so far observed data. Furthermore, for continuous improvement, all models are retrained at the end of each lot with the newly observed data.

Results

Due to the nature of using true process data, the dataset is incomplete. For the investigated finishing operation, data for eight lots with a total of 25 parts is available. The data of the first three lots, which amounts to seven parts, is used for the initial model training. The parts of the first lot are defined as batch $\mathcal{B}_1$, the second lot as batch $\mathcal{B}_2$ and the third lot as batch $\mathcal{B}_3$. Among all features the ten most important features are found as: $\text{AVG}^X_{\text{Torque}}$, $\text{STD}^X_{\text{Torque}}$, $\text{AVG}^Z_{\text{Torque}}$, $\text{STD}^Z_{\text{Torque}}$, $\text{AVG}^C_{\text{Force}}$, $\text{STD}^C_{\text{Force}}$, $\text{SKEW}^C_{\text{Force}}$, $\text{STD}^X_{\text{Acc.}}$, $\text{STD}^Z_{\text{Acc.}}$, and $\text{KUR}^Z_{\text{Acc.}}$. The novelty detection model is implemented as *One-Class SVM* with a *gamma* parameter of 0.01 and a decaying *nu* parameter based on the number of observed lots m as:

$$\text{nu} = 0.2\frac{1}{m} \tag{40}$$

The material identification algorithm is implemented as an *RF* classifier with 200 estimators and no constraints regarding tree construction.

The results of the novelty detection are shown in Figure 70 per part for all parts manufacturing during the testing phase. While the blue lines represent the computed novelty scores, the orange markers indicate detected novel situations. With a few exceptions for parts 14, 18, and 19-25, a rather steady behavior of the novelty computation can be observed. The parts 8, 12, and 20 are detected as novel, while the remaining parts are classified as known. Thus, the material of part 8 is introduced as batch B_4, the material of part 12 as batch B_5, and the material of part 20 as batch B_6 by the system.
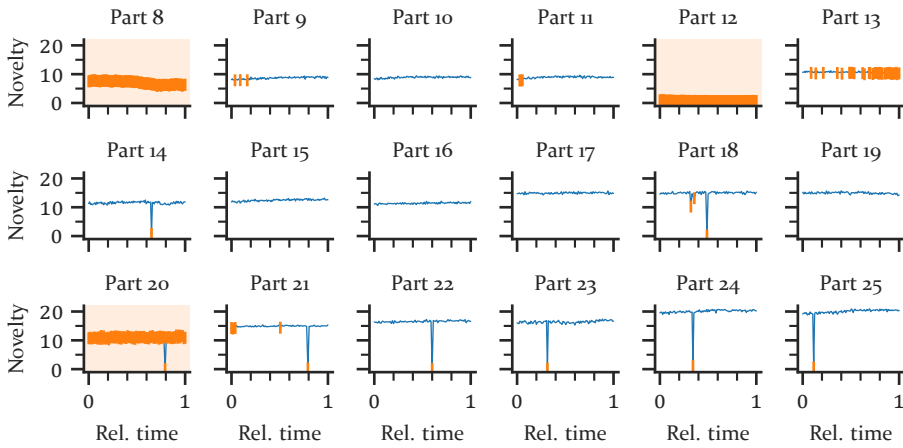
Figure 70: The novelty scores (blue line) show a rather constant behavior for each individual part. For parts 8, 12, and 20, all segments are detected as novel (orange markers).

In Figure 71, the aggregated feature vectors are shown for the training (a) and testing phase (b). It can be observed that some of the data used for testing, marked as n/a, overlaps the data used for training, while other parts form distinct clusters. After the optimization procedures, the classified samples by the algorithm are shown in Figure 71 - b, including the three novel batches identified during the testing phase.

To validate the novel materials identified, the tool degradation is observed (see Figure 72). The shown flank wear values are smoothened using a *Savitzky-Golay-Filter* [414] with a window length of three and a linear polynom. For the lots 5 and 7 the material identification algorithm identified parts belonging to two different batches, B_4 and B_5 for lot 5 and B_3 and B_6 for lot 7 (dashed lines in Figure 72). For the remaining lots, a single batch was identified each. It can be observed that batch B_1 for lot 1 shows a distinctly different behavior compared to the remaining lots, which agrees with its isolated cluster found in Figure 71. Furthermore, all lots containing batch B_4 show similar tool
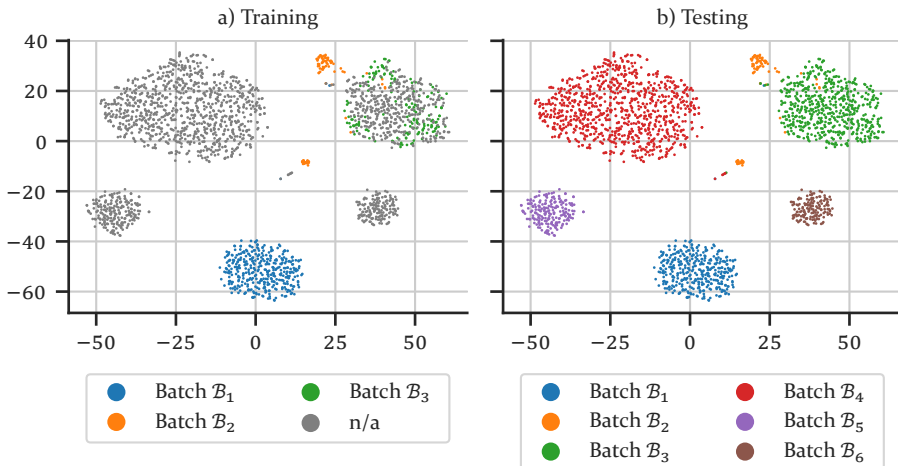
Figure 71: The extracted feature vectors from all signal segments for all parts are visualized in 2D using the tSNE method. The novel materials identified and assigned by the algorithm align well with the observable clusters.

degradation behavior. With the exception of lot 6, the same can be said about batch $\mathcal{B}_3$. The lot for batch $\mathcal{B}_3$ is closest to batch $\mathcal{B}_3$, which agrees with the overlapping clusters in the cluster map. Using this analysis, the clusters identified by the algorithm can be considered batches of different machinability. Thus, using the identified material batches as ground truth data, the accuracy of the system during the testing phase is calculated as F1 score of 0.9997.
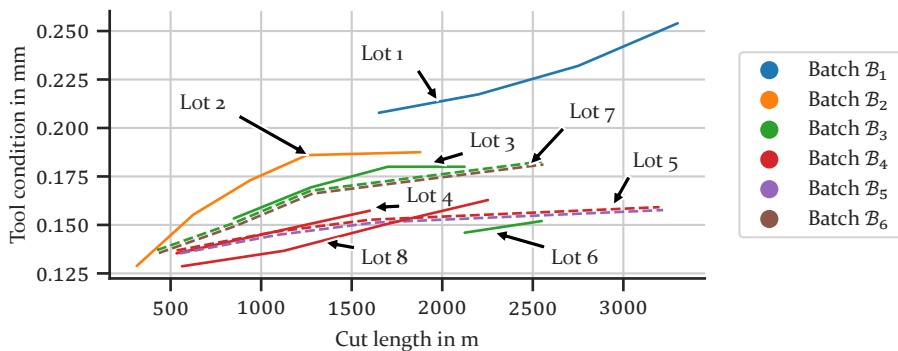
Figure 72: The observed tool condition in relation to the cut length per lot suggests that the identified material batches show different machinability.

With the small-sized lot production use case, the applicability of the proposed material identification methods to manufacturing processes is shown. The novel batches identified by the method show distinct behavior, and thus correspond to true material batches of different machinability.

6.2.4 Turning Experiments

In the final validation scenario, a turning operation is investigated in an experimental setting. Machining is carried out using a vertical lathe with indexable inserts. The lathe is equipped with a modern *Sinumerik 840D SL* control, allowing for the access of internal control data at a frequency of 500 Hz. Furthermore, a visual TCM system (see Section 6.1.1, S_A and S_B) is used to assess the tool condition in between cutting operations. Thereby, ground truth data regarding the tool life, and thus machinability, is acquired.

In this scenario, *tool life experiment sets* and *auxiliary experiment sets* are conducted with different material batches at varying cutting parameters. Each experiment set consists of multiple, consecutive cutting operations, called *cuts*. A tool life experiment set is started with a fresh cutting tool and stopped once the tool reaches its end of life. Throughout a tool life experiment, the machining state parameters cutting speed, feed rate, depth of cut, and type of cutting tool are kept constant within and in between cuts. For auxiliary experiments, these parameters are kept constant within a cut, but might vary between cuts. Thus, only the data from the tool life experiments is used for the model improvement and material characterization routines. Furthermore, auxiliary experiments are rather short with the intention of enlarging the observed parameter space. Independent of the type of experiment, all cuts within an experiment set are carried out at the same workpiece, and can thus be attributed to the same material batch. However, the diameter of the part can change in between cuts.

After removing incomplete and faulty datasets, 1040 experiments with the respective monitoring data remain. Thereby, cutting data is acquired for a variety of machining states (see Figure 73). Furthermore, among all experiments, two insert types were investigated with 576 and 464 cuts each. As tool life experiments were only carried out at cutting speeds of 180, 220, 240, 300, and 350 m/min and feed rates of 0.5 and 0.7 mm, the spikes in distribution can be explained. Furthermore, the auxiliary experiments are conducted mostly with fresh tools, explaining the deviation for the flank wear distribution.

Given the tool life experiements, the machinability of the different material batches can be determined. In Figure 74 (a) it can be seen that there are
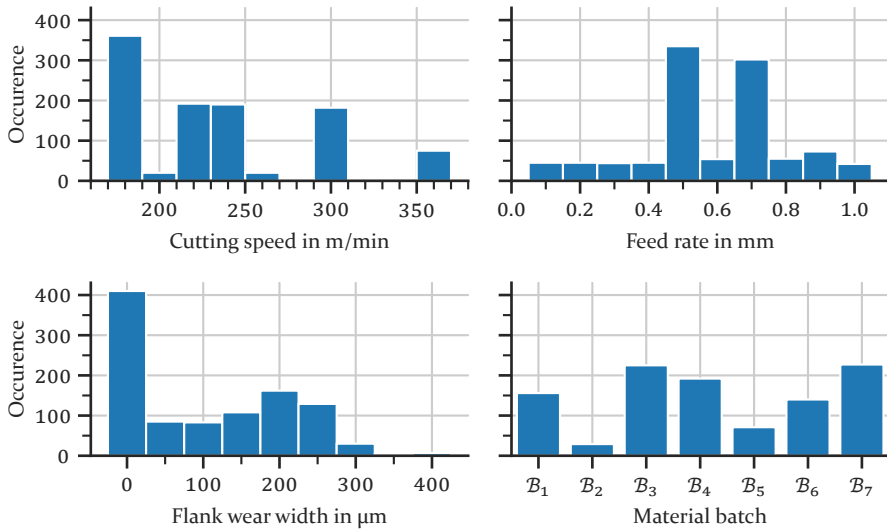
Figure 73: The conducted cutting experiments span a large parameter space.

significant differences among the material batches with B_3 having the best and B_6 having the worst machinability. Using the cost relations shown in Section 5.1, the machining costs for machining each batch at a given set of cutting parameters can be calculated. Figure 74 (b) highlights the dependency of the cutting speed on the expected machining costs for each material batch. It can be observed that the cost minimum can be found at different speeds, ranging from $296\frac{m}{min}$ for B_6 to $334\frac{m}{min}$ for B_3. Thus without the information about the material batch being machined, a one-fits-all set of cutting parameters would be selected, resulting in higher costs for each material batch. Furthermore, given this trade-off, such as using an average cutting speed of $320\frac{m}{min}$, cutting tools need to be exchanged based on the tool life of the material batch with the worst machinability to avoid tool breakage. Therefore, when machining a batch of better machinability, e.g. B_3, tools are exchanged to early resulting in up to 168 € of additional tooling costs per shift and 28 minutes of additional work for avoidable tool changes[1].

To investigate these effects, material analysis is carried out for batches B_3, B_4, B_6, and B_7[2]. This includes the analysis of microstructure, chemical composition, and hardness. The chemical composition is analyzed using a

---

[1] Assuming tooling costs of 3€ per tool, seven hours of work per shift and 30 seconds of manual labor needed for tool exchange.

[2] Due to incomplete historic data, material analysis is not available for batches B_1, B_2, and B_5

(a) Tool life analysis
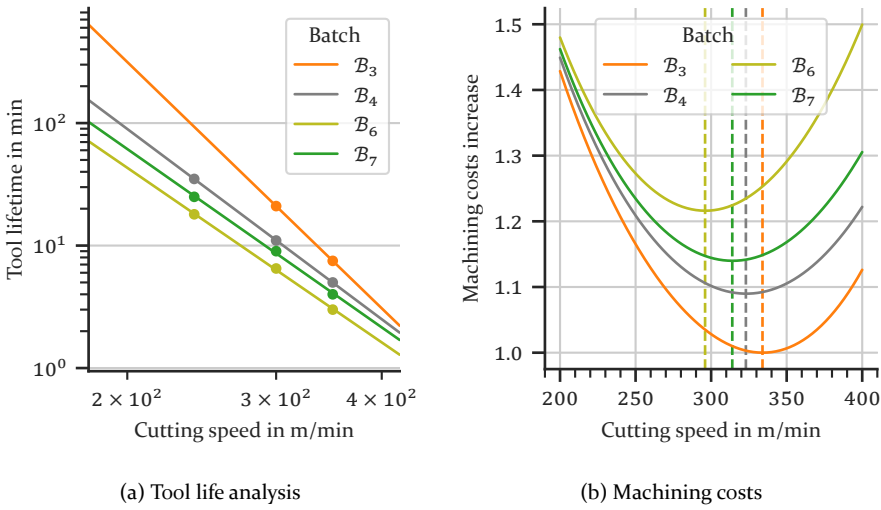
(b) Machining costs

Figure 74: Impact of material batch on expected tool life, machining costs, and ideal cutting parameters, adapted from [P11].

scanning electron microscope with centered back scatter detector. The measured chemical compositions per batch are shown in Table 13. Comparing the chemical compositions among the different batches, slight but not significant deviations can be observed.

Table 13: Chemical and mechanical analysis of the investigated samples.

	Chromium	Nickel	Molybdenum
Specification	1.75%	1.5%	0%
$\mathcal{B}_3$	1.73%	1.08%	0.04%
$\mathcal{B}_4$	1.95%	1.15%	0.13%
$\mathcal{B}_6$	2.11%	1.15%	0.11%
$\mathcal{B}_7$	1.81%	1.01%	0.03%

Furthermore, hardness measurements with a force of 30 N are conducted (Figure 75). It can be seen that batch $\mathcal{B}_3$ has the highest average hardness while the remaining batches span a rather similar hardness space. Also, while the individual measurements conducted for batch $\mathcal{B}_3$ are very precise, the measured hardness values, especially for batch $\mathcal{B}_7$, deviated significantly. Contrarily, when analyzing the microstructure of the respective samples, differences can be observed (see Figure 76). For batch $\mathcal{B}_3$, rather large grains can be seen, whereas batches $\mathcal{B}_4$, $\mathcal{B}_6$, and $\mathcal{B}_7$ have smaller grain sizes. Therefore,

a better machinability is expected for material $\mathcal{B}_3$ as larger grains lead to reduced ductility and thus reduced tensile strength.
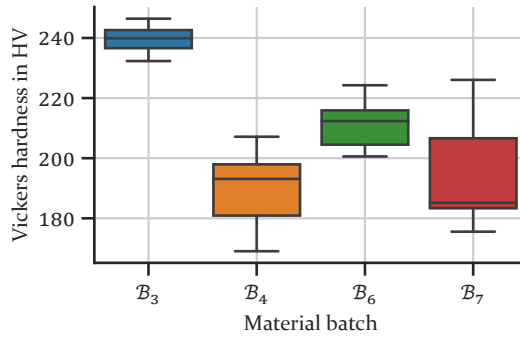
Figure 75: Hardness variations can be observed among the investigated material batches.
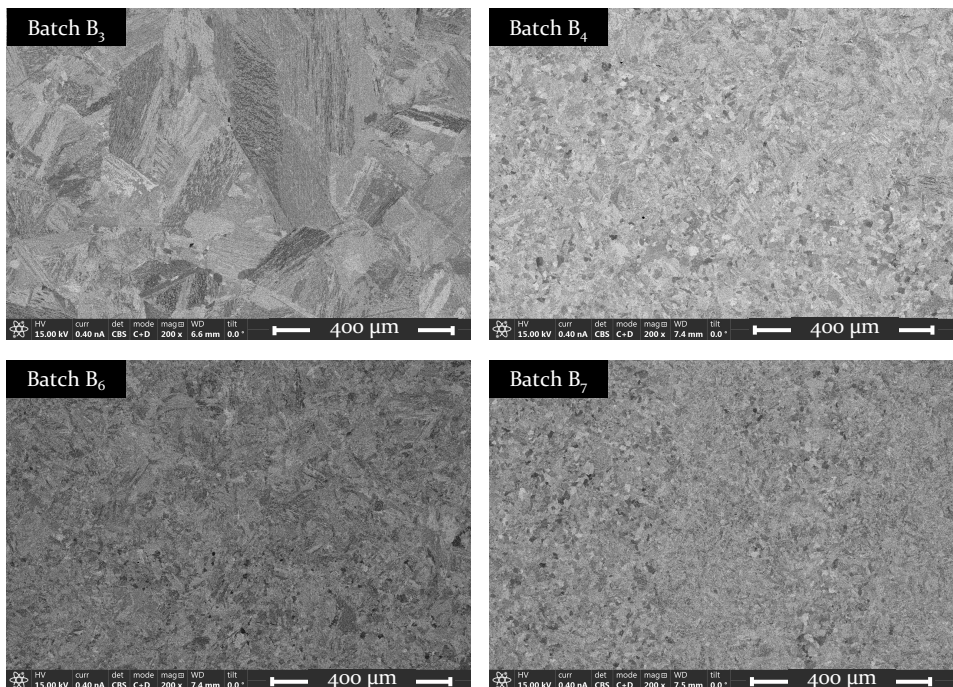
Figure 76: Differences in microstructure can be observed between the various batches investigated.

To validate the proposed methods and routines, the following procedure is chosen: all available data is split into a *training* subset and a *testing* subset. The training subset is initially provided as historic data to train the respective algorithms. The remaining data from the testing subset is now evaluated in a play-back manner. The cuts used for testing are analyzed consecutively. For each one, the recorded process data is analyzed, and the parameter recommendation routine is executed. For tool life experiments, the observed tool life is used for either model retraining or material batch characterization at the end of the respective experiment set, depending on the novelty. For this, a part is considered novel if the majority of all cuts within that experiment are detected as novel. The data separation strategy in training and testing subset is shown in Figure 77. One of the seven material batches, batch B_7, is selected as a true novel batch and not shown to the algorithm during the training phase. The data from the remaining material batches is split fairly, using 50% for model training and 50% for the testing phase. Data splitting always takes place on the experiment set level. Thus, all data from all cuts within a set of experiments are either considered training or considered testing to avoid overfitting. In total, the training dataset consists of 485 cuts while the testing set is 555 cuts large.
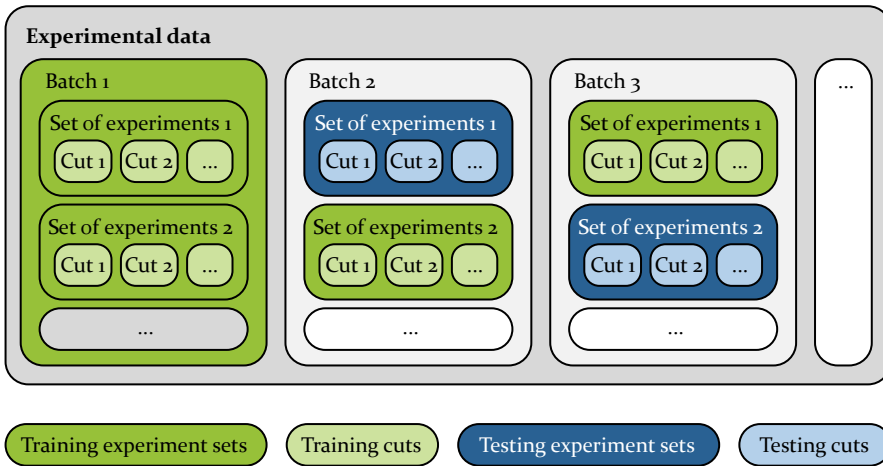
Figure 77: The acquired experimental data is split in training and testing subsets on the experiment level to avoid overfitting.

In a preliminary study [P11], the data set is investigated in regard to the optimization of the material identification method. It is found that for machining states with a high data volume of historic training data, the highest classification accuracies are achieved when using only data from that machining state, while for machining states with low data volume increased prediction

performance is seen when using broader parameters for finding relevant historic data for model training. Thus, different historic data selection strategies are used. Here, a volume of 100 samples is used as the threshold. To find relevant training data X from all available training data $\mathcal{H}$ to train a model for machining state $\mathcal{M}$ with over 100 samples, the cutting parameters of each historic sample n are compared to $\mathcal{M}$ as:

$$
\begin{aligned}
X = \{n \in \mathcal{H} \mid & (v_{c,\mathcal{M}} - 20\frac{\text{m}}{\text{min}} \leq v_{c,n} \leq v_{c,\mathcal{M}} + 20\frac{\text{m}}{\text{min}}) \wedge \\
& (f_{\mathcal{M}} - 0.05\text{mm}^{-1} \leq f_n \leq f_{\mathcal{M}} + 0.05\text{mm}^{-1}) \wedge \\
& ((VB_{\mathcal{M}}) - 50\mu\text{m} \leq VB_n \leq (VB_{\mathcal{M}} + 50\mu\text{m}) \wedge \\
& (\text{tool}_{\mathcal{M}} = \text{tool}_n)\}
\end{aligned}
$$

(41)

For machining states with less than 100 directly associated samples, the training set X is found as:

$$
\begin{aligned}
X = \{n \in \mathcal{H} \mid & (v_{c,\mathcal{M}} - 60\frac{\text{m}}{\text{min}} \leq v_{c,n} \leq v_{c,\mathcal{M}} + 60\frac{\text{m}}{\text{min}}) \wedge \\
& (f_{\mathcal{M}} - 0.15\text{mm}^{-1} \leq f_n \leq f_{\mathcal{M}} + 0.15\text{mm}^{-1}) \wedge \\
& ((VB_{\mathcal{M}} - 150\mu\text{m} \leq VB_n \leq (VB_{\mathcal{M}} + 150\mu\text{m}) \wedge \\
& (\text{tool}_{\mathcal{M}} = \text{tool}_n)\}
\end{aligned}
$$

(42)

The novelty detection is implemented as *One-Class SVM* with a *nu* of 0.25 and a *gamma* of 0.1. Furthermore, a PCA is integrated after feature standardization to aggregate the feature space to ten features. The material batch clustering procedure is implemented using the *Evidence Accumulation* method with 200 random *k-means* initializations. As labelled data is available, the distribution of material batches within each cluster is defined as cluster-related knowledge. For the classification algorithms, *RF* classifiers are selected as they show good prediction accuracies while having low computation times [P11]. The classifier is implemented with 150 estimators, the *gini* criterion for purity determination while constraining tree construction to a maximum depth of five.

Using the testing dataset the novelty detection algorithm is benchmarked. Overall, a prediction accuracy of 75.8% is reached with a high recall rate of 95.3%. The results of the batch classification method for correctly identified known materials is shown in Table 14. Samples falsely predicted as known batches are excluded, as they are already accounted for in the novelty detection metrics. For batches $\mathcal{B}_3$ and $\mathcal{B}_5$, all related cuts were sampled for the training subset. Thus, there are no true predictions for these classes. The scores are normalized for each row. Analyzing the results, it can be seen that batch

$\mathcal{B}_1$ is correctly predicted in 100% of all cases. The remaining batches have a true positive rate between 63% and 84%. The overall F1 score of the material classification system weighted by data volume per batch is 0.85.

Table 14: Confusion matrix showing the materials predicted by the material classification algorithm. The batches $\mathcal{B}_2$ and $\mathcal{B}_5$ are not present in the testing dataset.

	Predicted						
True	$\mathcal{B}_1$	$\mathcal{B}_2$	$\mathcal{B}_3$	$\mathcal{B}_4$	$\mathcal{B}_5$	$\mathcal{B}_6$	$\mathcal{B}_7$
$\mathcal{B}_1$	**100%**	0%	0%	0%	0%	0%	0%
$\mathcal{B}_3$	0%	0%	**82.6%**	0.1%	0%	12.9%	4.3%
$\mathcal{B}_4$	0%	0%	36.7%	**63.3%**	0%	0%	0%
$\mathcal{B}_6$	0%	0%	12.5%	8.3%	0%	**79.2%**	0%
$\mathcal{B}_7$	0%	0%	11.5%	4.6%	0%	0%	**84.0%**

Due to the high number materials considered novel for their respective machining state, for parameter recommendation, the transferred knowledge approach with interpolation in between clusters is used in 91.3% of all cases by the system while for the remaining cases the single batch predicted by the batch classification algorithm is used. For each cut, optimized cutting parameters $\tilde{v}_c$ and $\tilde{f}$ are proposed. In 69.7% cases, cost savings are achieved when following the algorithm's recommendations.

6.3 Summary

The results of the experiments show that there are significant differences in machinability among material batches. Further material analysis in Section 6.2.4 reveals differences in chemical composition, hardness, and microstructure among the investigated material batches. To allow efficient machining despite these deviations, a smart manufacturing system to optimize subtractive manufacturing processes regarding material batch deviations, SMaPOMBa, is introduced. Section 5.4 shows that SMaPOMBa can be implemented as a service-based software system running partly on edge devices and partly in the cloud. The results show that the chosen implementation enables the individual functionalities of the system to be used independently or together as required by the respective application. In a future evolution a direct control of the machine tool is envisioned, which is enabled by the selected design of the system.

As the tool condition is a main factor influencing process signals, an efficient TCM system is introduced allowing the accurate detection of a tools condi-

tion. The results in Section 6.1 show the complexity of wear defects among several investigated scenarios. Using the proposed window-based image segmentation approach, Section 6.1.1 shows that good segmentation results can be achieved for all scenes. Furthermore, the results stress the importance of large training data volume justifying the need for efficient training data generation methods such as assisted image labeling and synthetic training data generation. The effectiveness of the proposed assisted training data generation is shown in a user study in Section 6.1.2, proving that not only are less manual efforts needed to create the image masks, but also showing that the resulting masks are of higher quality compared to masks created in a traditional not-assisted way. Additionally, synthetic data augmentation and generation is found to be useful in Section 6.1.3, allowing the labeling efforts to be reduced by two thirds.

For the central task of material identification and classification the proposed method is shown to be useful both for the granularity of different material grades in Section 6.2.1 and of different material batches in Section 6.2.3 and 6.2.4. Furthermore, by incorporating the unsupervised clustering approach, batch associations can be found even without available ground truth data as seen in Section 6.2.2. Using the novelty detection functionality the system is well-equipped for operation with unknown amounts of material batches, as batches of novel behavior can be detected automatically as shown in Section 6.2.3. Not only are novel batches detected as such, but due to the integrated retraining capabilities, novel batches are directly introduced as a consecutively newly known batch which can be identified as known batch in subsequent machining. Combining all capabilities, the results in Section 6.2.4 show that even in a complex application with many machining states and thus models to be trained, the suggested parameters by the recommendation module would lead to optimized cutting in most cases.

Due to the choice of relying primarily on NC signals as data source for material identification, the approach can easily be scaled to new machine tools. This is further supported by the data preprocessing routines, striving after machine agnostic evaluation models. With the availability of routines for automated material characterization and model retraining human interaction is only needed for annotating training data during TCM training and selecting unique cutting parameters during material characterization.

In summary, the conducted validation experiments support the effectiveness of the proposed methods and the designed smart manufacturing system for process optimization regarding deviations among material batches.

7   Summary and Outlook

Process optimization is needed in subtractive manufacturing to find ideal cutting parameters allowing for machining at maximal MRR with minimal tool degradation. This is especially important when dealing with parts of varying machinability, such as during the post-processing of additively manufactured multi-material parts or when significant effects of the material batch are present. Here, specific ideal parameters need to be found for each material and material batch encountered to enable fully-optimized machining. However, existing approaches in industry and research fall short when solving the problem of material batch-aware process optimization in its entirety. Traditional control-based approaches are limited to the control of the cutting process based on system feedback, such as the measured cutting force or vibration, but do not provide semantic information about the material batch currently being machined. Therefore, sophisticated process optimization, such as the transfer and application of historic batch-specific processing knowledge is not possible. More advanced scientific approaches for semantic material classification do not allow for the detection of material batches nor do the respective system architectures contain the capabilities needed for operational use in changing environments, such as TCM for integrating tool condition information. Furthermore, such material identification approaches all require the number of to-be-identified material classes to be known and can not handle novel materials. Existing TCM approaches encountered in industry are often in-process, which are prone to noise and provide limited wear information compared to the proposed method. Contrarily, direct approaches found in literature mostly utilize ML for image processing but require large amounts of manually annotated training data. Thus, this thesis addresses the optimization problem by proposing a smart manufacturing system to solve it holistically, integrating capabilities for material batch detection, the recommendation of optimized cutting parameters, the handling of novel material batches, and a TCM system with related methods for effective model training.

The proposed smart manufacturing system utilizes both internal control data and images of the cutting tool for the initial assessment of the condition of the cutting tool, the subsequent in situ identification of the machined material batch, and the final recommendation of optimized process parameters. Thereby, different routines are enabled for process optimization throughout machining, the incorporation of material batches with novel behavior, continuous model improvement, and efficient adaptation to new machining scenarios.

The assessment of the condition of the cutting tool is essential for any process monitoring, as the cutting tool's condition significantly influences the obtained control signals. In this work, the usage of semantic image segmentation models in particular was found to be a promising analysis procedure. Through these models, not only is the primary defect metric of flank wear made available, but a detailed analysis of many defect classes regarding their presence, location, and size are also given. Due to specific characteristics of the TCM domain, such as the low training data volume and defect scarcity, special image segmentation and training methods are needed. The proposed window-based approach, which integrates reference image data for global context, outperforms state-of-the-art image segmentation networks for the TCM domain.

Furthermore, while there is a variety of novel network architectures proposed in literature, the training data generation remains a necessary task that often limits the adoption of such data-driven approaches due to its high resource demands. As a solution, the proposed methodology in this work supports the image annotation process and allows the data transfer from historic scenarios to novel ones. To support the annotation process, a method is proposed for dividing the image into small subregions of constant class labels using a superpixel-based approach and a consecutive deep metric learning to find an initial label guess by comparing the embedded superpixels to a reference dataset. Thereby, the tasks conducted by the human expert are shifted from pixel-wise annotation to the correction of faulty guesses. This procedure is implemented as a web-based application to enable its usage by the respective experts. Secondly, the transfer of data between different scenarios is investigated. There are many factors influencing the visual appearance within a scenario leading to the effect that images from the same scenario are rather similar while images from different scenarios are rather distinct. Therefore, the highest prediction performances are achieved when training distinct model instances for each scenario. To still be able to reuse data from other scenarios, a method is proposed for adapting the image data from a source scenario to match a target scenario. This involves the adaption of the shape of the visible cutting tool by image warping and the adaptation of the visual appearance by GAN-based mask-to-image translation.

The identification of the material batch currently being machined is based on the internal control data of the NC, which can be accessed using an edge device. This data includes position and current values for all machining axes. Due to the high number of signals and data points, a preprocessing routine containing dimensionality reduction and feature extraction is carried out to reduce the continuous data stream to dense feature vectors. Besides, the event data is analyzed regarding the machine control instructions to

obtain information about the current cutting operation. This information in combination with the condition of the cutting tool is defined as the machining state. As the different machining states have a significant impact on the observed features, specific instances of the respective analysis models used are trained for each unique machining state. These models can be split into three categories: novelty detection, batch classification, and batch clustering. Initially, the novelty detection algorithm is used to find novel material batches that do not behave like any material batch encountered in the past. If this is the case, the batch clustering approach is used and the material batch characterization routine is triggered. Otherwise, the batch classification alternative is chosen. For batch clustering, available process data at that machining state is analyzed in an unsupervised manner to find clusters. These can then be used to transfer knowledge from individual samples in the nearest cluster to the novel data point. In batch classification, supervised learning models are trained, which allow for the mapping from input feature vector to material batch.

With the material batch identified, information associated with the historic batches can be transferred to the current operation. In this work, such batch behavior information includes both machinability and miscellaneous data, ranging from basic information to sophisticated machinability information through model coefficient parameters. If such parameters are available for an identified material batch, the expected tool life can be computed and thus a mapping between cutting parameters and optimization targets, such as costs or productivity, can be established. This allows for the deduction of optimized parameters as well as a general forecast of the expected effects when adapting the cutting parameters. While the impact of such an optimization strongly depends on the deviations in machinability present for the given application, in this study cutting parameters had to be adjusted by up to 10% resulting in cost savings, with further potential of saving up to 200 € in tooling costs and 20 minutes in labor per shift when using batch-specific tool exchange cycles.

To enable operational usage, the individual methods are combined into four routines for specific purposes. The parameter recommendation routine combines the image segmentation methods for tool condition assessment, the material batch identification alternatives, and the final parameter recommendation to provide the operator insight into the machining process in regard to material batch deviations throughout operation. The novel material characterization routine is used when a material batch with novel behavior is detected and involves the assessment of tool life throughout operation by regularly monitoring the tool condition using the TCM system. Similarly, ground truth tool life information acquired by the TCM system at constant machining states can be used to judge the predicted machinability with the

actual machinability and retrain all material identification models accordingly. Finally, the novel scene routine aggregates methods when adapting the procedure to a new environment. This mainly involves the methods for efficient image segmentation model training to enable TCM. Through these routines, most situations encountered in operational use can be handled. By using the proposed service-based architecture, which utilizes both edge and cloud computing, task-specific computing power allocation is enabled. Intensive tasks such as model training can be carried out in the cloud using the advantages of scalable and on-demand hardware, while the process monitoring tasks close to the machine are carried out on local edge devices, reducing latency and enabling usage even without a cloud connection.

Looking into the future, the proposed smart manufacturing system should be extended to further reduce the current dependencies on human interaction. For this purpose, control access to the machine tool must be established by the system, whereby new sets of cutting parameters could be automatically trasferred to the machine. In regard to the manual selection of cutting parameter sets for automated material characterization, the field of *reinforcement learning* seems promising to dynamically suggest the most information yielding set of parameters to be investigated next. Furthermore, the integration of a *condition monitoring* module offers the chance to automatically detect the current machining state. This could replace the manual setup of start and end triggers in the G-Code. Such a superordinate machining state detection system also offers the potential to reduce system complexity as the number of state-specific models needed could be reduced by grouping similar machining states together. In this context, it would also be helpful to refine the different ML-models, especially the material identification and novelty detection models, for state-independent usage. This could be realized on the one hand by extending the data preprocessing to compensate any state-induced signal influence, or on the other hand by considering the machining state as further inputs of the respective model. In order to handle the additional model complexity for the latter case, the training phase of the system should to be optimized through adaptive data collection for maximizing the information gain during data acquisition. Another application for *reinforcement learning* algorithms can be seen in the process optimization routine. Here, agent-based methods offer the potential to investigate different parameter combinations to find an ideal parameter set even with non-linear system behavior. With respect to the human understanding of the decisions made by the smart optimization system, the field of *causal reasoning* shows additional potential to reveal understandable correlations between process patterns and deduced reactions for parameter optimization.

8 Zusammenfassung

In der spanenden Fertigung gilt es, durch Prozessoptimierung ideale Schnittparameter zu finden, welche eine Bearbeitung mit maximalem Zerspanvolumen bei minimalem Werkzeugverschleiß ermöglichen. Dies ist insbesondere bei der Bearbeitung von Halbzeugen aus Materialien unterschiedlicher Zerspanbarkeit herausfordernd, wie beispielsweise bei großen Einflüssen der Materialcharge oder dem Nachbearbeiten additiv hergestellter Multimaterial-Bauteile. In solchen Situationen müssen für jedes Material und jede Materialcharge spezifische Schnittparameter gefunden werden, um eine optimale Zerspanung zu erreichen. Ganzheitlichen Lösungen der chargenbewussten Prozessoptimierung in Industrie und Forschung weisen heute Schwächen auf. Traditionelle Ansätze der Regelungstechnik beschränken sich auf die Regelung des Bearbeitungsprozesses durch Überwachung einer Regelgröße des Systems, wie etwa der Schnittkraft oder der Vibration. Das Bereitstellen von Information über der sich in Bearbeitung befindenden Charge steht hierbei nicht im Fokus. Aus diesem Grund ist das Übertragen chargenspezifischer Prozessierungserfahrung aus der Vergangenheit nicht möglich. Wissenschaftliche Ansätze der datengetriebenen Materialerkennung hingegen sind weder für das Erkennen spezifischer Materialchargen noch für den operativen Betrieb ausgelegt. So mangelt es den jeweiligen Systemarchitekturen unter anderem an Fähigkeiten zur Berücksichtigung des kontinuierlichen Verschleißes des eingesetzten Werkzeugs. Ebenfalls erfordern existierende Ansätze eine definierte Anzahl an zu erkennenden Materialien, die initial bekannt sein muss und sind somit nicht in der Lage, mit neuen Materialien und Materialchargen umzugehen. Für die Erfassung des Verschleißzustandes werden vornehmlich die Verfahren des Maschinellen Lernens untersucht. Solche Ansätze benötigen allerdings eine große Anzahl manuell annotierter Trainingsdaten. Aus diesen Gründen adressiert diese Arbeit das Problem der chargenbewussten Prozessoptimierung durch die Einführung eines intelligenten Fertigungsassistenzsystems mit integrierten Fähigkeiten zur Erkennung der Materialcharge, der Ableitung optimierter Schnittparameter, der Berücksichtigung unbekannter Materialchargen sowie der Werkzeugzustandsüberwachung mit effizientem Modelltraining.

Das konzipierte System nutzt hierfür sowohl interne Steuerungssignale als auch Bilddaten der Schneidwerkzeuge für die Bestimmung des Werkzeugzustands, die anschließende in situ Erkennung der sich in Bearbeitung befindenden Materialcharge und die finale Ausgabe optimierter Schnittbedingungen. Basierend auf den Fähigkeiten des Systems lassen sich vier operative Routinen definieren: Die Optimierung der Schnittparameter während der

Bearbeitung, die Integration unbekannter Materialchargen, die kontinuierliche Selbstverbesserung der Modelle und das effektive Anpassen des Systems an neue Einsatzbedingungen.

Für die Bewertung des Verschleißzustands des Schneidwerkzeugs wird in dieser Arbeit die Methode der semantischen Bildsegmentierung verwendet. Der erforschte Ansatz beinhaltet ein Raster-basiertes Segmentierungsverfahren im Zusammenspiel mit einem Referenzbild für die Integration von Kontextinformationen. Somit ist es möglich, nicht nur den Freiflächenverschleiß, sondern auch weitere Verschleißarten zu erfassen, wodurch der detaillierte Verschleißzustand mit Häufigkeit, Größe und Lage der verschiedenen Verschleißtypen bestimmt werden kann.

Neben dem Segmentierungsmodell stellt die Erforschung effektiver Trainingsmethoden einen zentralen Aspekt zur industriellen Adaption lernender Systeme dar. Der erforschte Ansatz zur effektiven Trainingsdatengenerierung beinhaltet sowohl eine Methode zur Optimierung des Annotationsprozesses, sowie einen Ansatz zum Übertrag existierender Daten auf neue Anwendungsfälle. Zur Optimierung der Bildannotation wird das zu annotierende Bild in kleine Regionen gleicher Klasse durch Verwendung von Superpixeln aufgeteilt. Durch Deep Metric Learning wird nun ein initialer Vorschlag für jede Region durch Vergleich mit einem Referenzdatensatz generiert. Demnach muss der Experte nur falsche Vorschläge korrigieren und nicht komplette Bilder annotieren. Das resultierende web-basierte Annotationstool zeigt eine signifikante Verbesserung in der Effektivität im Vergleich zu etablierten Ansätzen. Bei der Untersuchung verschiedener Anwendungsszenarien zeigt sich weiterhin, dass aufgrund der Vielzahl von Einflussfaktoren Bilder innerhalb eines Szenarios eine hohe Ähnlichkeit aufweisen, Bilder unterschiedlicher Szenarien hingegen teils stark voneinander abweichen. Aus diesem Grund gilt es, für jedes Szenario ein spezifisches Segmentierungsmodell zu trainieren. Um trotzdem vorhandene Trainingsdaten für mehrere Szenarien nutzen zu können, wird ein Prozessschritt eingeführt, welcher die Adaption dieser Daten auf das jeweilige Zielszenario ermöglicht. Dieser beinhaltet die Anpassung der Form des sichtbaren Schneidwerkzeugs durch Bildverzerrung und die Anpassung der visuellen Ausprägung durch generative Verfahren der Bildübersetzung.

Die Erkennung der aktuellen Materialcharge erfolgt über die Auswertung der internen Signale der numerischen Steuerung. Diese Daten beinhalten Positions- und Stromdaten aller Bearbeitungsachsen. Aufgrund der großen Zahl von Signalen und Messwerten erfolgt eine Datenvorverarbeitung zur Reduktion der Komplexität und Extraktion zentraler Kenngrößen. Durch die Überwachung der Ereignisdaten können zusätzlich die Schnittbedingungen

ausgewertet werden. Auf Basis der Schnittbedingungen und dem Verschleiß-grad des Werkzeugs wird der Bearbeitungszustand definiert, welcher den Einsatzbereich der Modelle zur Materialerkennung bestimmt. Initial wird der Neuigkeitserkennungsalgorithmus verwendet, um unbekannte Chargen zu erkennen. Ist dies der Fall, wird der Chargen Clustering Ansatz verwendet und es wird die automatische Chargencharakterisierungsroutine gestartet. Andernfalls wird die Chargenklassifikation verwendet. Für das Chargen Clustering wird unüberwachtes Lernen eingesetzt. Die Grundlage hierfür bildet das Zusammenfassen historischer Prozessdaten zu Clustern ähnlichen Verhaltens. Darauf basierend werden naheliegende Cluster zum aktuellen Bearbeitungspunkt gesucht und assoziiertes Wissen übertragen. Für die Klassifikation hingegen wird überwachtes Lernen verwendet. Die hier verwendeten Modelle ermöglichen es, basierend auf den Prozessdaten eine spezifische Charge der Vergangenheit zu identifizieren, welche der aktuell sich in Bearbeitung befindenden Charge am meisten ähnelt.

Mit bekannter Materialcharge kann nun die historische Erfahrung der jeweiligen Chargen auf die aktuelle Bearbeitung übertragen werden. In dieser Arbeit sind dies sowohl Information über die Zerspanbarkeit als auch weitere Daten, wie spezifische Standzeitenmodelle. Damit ist es möglich, für die identifizierte Materialcharge die zur erwartende Standzeit zu berechnen und dadurch den Zusammenhang zwischen den Schnittbedingungen und dem gewählten Optimierungsziel, wie Kostenminimierung oder Produktivitäts-maximierung, zu ermitteln. Der vorgestellte Ansatz erlaubt insofern sowohl das Ableiten optimierter Schnittparameter als auch die generelle Vorhersage der zu erwartenden Auswirkung bei Anpassung der Schnittparameter. Zwar hängt die Auswirkung einer solchen Optimierung stark von der Stärke der Abweichung der Zerspanbarkeit der verschiedenen Chargen ab, eine exemplarische Berechnung zeigt jedoch das Einsparungspotential bei Optimierung der Schnittparameter von bis zu 10% der Bearbeitungskosten.

Die Forschungsarbeiten fließen im intelligenten Fertigungsassistenzsystem *SMaPOMBa* zusammen, welches die erforschten Methoden zu folgenden vier, bislang nicht verfügbaren, Routinen für den operativen Betrieb kombiniert. Als erstes nutzt die Parameteroptimierungsroutine die Methoden der Bildsegmentierung zur Erfassung des Verschleißzustandes, die Chargenerkennungsansätze zur Identifizierung der Materialcharge und das Vorschlagssystem zur Bereitstellung optimierter Schnittparameter für den Bediener. Als zweites wird die Chargencharakterisierungsroutine verwendet, wenn eine unbekannte Charge detektiert wird und beinhaltet die Ermittlung der Standzeit während der Bearbeitung. Ähnlich verhält sich die dritte Routine zur kontinuierlichen Modellverbesserung, welche durch die tatsächlichen Standzeiten, welche mit fortschreitender Bearbeitung erfasst

werden, einen Abgleich der Modellvorhersagen mit der Realität ermöglicht, und bei Abweichungen ein Neutrainieren anstößt. Als viertes dient die Routine für neuartige Szenen der effektiven Anpassung des Systems auf neue Bearbeitungsszenarien. Durch die vorgestellte service-basierte Systemarchitektur, welche sowohl auf Cloud- als auch Edge-Computing aufbaut, kann zudem aufgabenspezifische Rechenleistungsallokation erfolgen. Aufwändige Aufgaben wie das Trainieren eines Modelles werden so in der Cloud ausgeführt, während die Prozessüberwachung mit geringer Latenz auf lokalen Edge-Geräten verortet ist.

Zukünftig bietet es sich an, das vorgestellte Assistenzsystem hinsichtlich der benötigten menschlichen Interaktion weiterzuentwickeln. Für diesen Zweck gilt es, optimierte Parameter automatisch an die Maschine zu übertragen. In Bezug auf die manuelle Auswahl der Schnittparameter für die automatische Chargencharakterisierung bietet das Gebiet des *Reinforcement Learning* vielversprechende Ansätze zur dynamischen Auswahl des am besten geeigneten Parametersatzes. Weiterhin ist es zielführend, das manuelle Setzen von Start- und Endmarken in den Bearbeitungsanweisungen abzulösen. Dafür ist es notwendig, ein *Condition Monitoring* Modul zu integrieren, welches den aktuellen Bearbeitungszustand automatisch ermittelt. Ein solch übergeordnetes Bearbeitungszustandserfassungssystem bietet zudem das Potential, Systemkomplexität durch Gruppieren ähnlicher Zustände zu reduzieren und somit die Anzahl der zustand-spezifischen Modelle zu minimieren. In diesem Zusammenhang ist es weiterhin sinnvoll, die verschiedenen Modelle hinsichtlich zustandsunabhängiger Einsetzbarkeit weiterzuentwickeln. Dies kann zum einen durch die Berücksichtigung des Zustands als Modellvariable erfolgen oder alternativ durch eine Ausweitung der Datenvorverarbeitung zur Kompensation sämtlicher Zustandseinflüsse geschehen. Im Hinblick auf die Bestimmung idealer Schnittparameter findet sich ein weiterer Ansatz für *Reinforcement Learning*. Hier würden Agenten-basierte Ansätze das Potential bieten, verschiedene Kombinationen von Schnittparametern zu untersuchen, um auch bei nicht-linearem Systemverhalten ein Optimum zu finden. In Bezug auf die menschliche Nachvollziehbarkeit der getroffenen Entscheidungen eines solch intelligenten Assistenzsystems ist ebenfalls das Feld von *Causal Reasoning* potentialversprechend, um Korrelationen zwischen Prozessmustern und den daraus abgeleiteten Reaktionen der Parameteroptimierung besser zu verstehen.

Bibliography

[1]   Denkena, Berend; Bergmann, Benjamin; Breidenstein, Bernd; Prasan-
        than, Vannila, and Witt, Matthias. "Analysis of Potentials to Improve
        the Machining of Hybrid Workpieces". *Production Engineering* 13.1
        (Feb. 2019), pp. 11–19.

[2]   Jemielniak, Krzysztof and Kosmol, Jan. "Tool and Process Monitoring
        – State of Art and Future Prospects". *Scientific Papers of the Inst. of
        Mech. Engng. and Automation of the Technical Univ. of Wroclaw* 61
        (1995), pp. 90–112.

[3]   Siepmann, Jens P.; Wortberg, Johannes, and Heinzler, Felix A. "Analy-
        sis of Batch-Related Influences on Injection Molding Processes
        Viewed in the Context of Electro Plating Quality Demands". *PRO-
        CEEDINGS OF PPS-31: The 31st International Conference of the Poly-
        mer Processing Society – Conference Papers*. Jeju Island, Korea, 2016,
        p. 040010.

[4]   Zaeh, M. F.; Schnoes, F.; Obst, B., and Hartmann, D. "Combined
        Offline Simulation and Online Adaptation Approach for the Accu-
        racy Improvement of Milling Robots". *CIRP Annals* 69.1 (Jan. 2020),
        pp. 337–340.

[5]   Evans, Mark. "Incorporating Specific Batch Characteristics Such
        as Chemistry, Heat Treatment, Hardness and Grain Size into the
        Wilshire Equations for Safe Life Prediction in High Temperature
        Applications: An Application to 12Cr Stainless Steel Bars for Tur-
        bine Blades". *Applied Mathematical Modelling* 40.23-24 (Jan. 2016),
        pp. 10342–10359.

[6]   Fyllingen, Ø.; Hopperstad, O. S., and Langseth, M. "Robustness Study
        on the Behaviour of Top-Hat Thin-Walled High-Strength Steel Sec-
        tions Subjected to Axial Crushing". *International Journal of Impact
        Engineering* 36.1 (Jan. 2009), pp. 12–24.

[7]   Šuchmann, Pavel and Martinek, Petr. "Influence of Small Deviations
        in Steel Chemical Composition on Hardenability". *Proceedings of
        Materials Science & Technology 2014*. Vol. 1. Jan. 2014, pp. 493–499.

[8]   Goppold, Cindy; Urlau, Franz; Pinder, Thomas; Herwig, Patrick,
        and Lasagni, Andrés F. "Experimental Investigation of Cutting Per-
        formance for Different Material Compositions of Cr/Ni-steel with
        $1\,\mu$m Laser Radiation". *Journal of Laser Applications* 30.3 (Jan. 2018),
        p. 031501.

[9]   Denkena, Berend; Bergmann, Benjamin, and Witt, Matthias. "Automatic Process Parameter Adaption for a Hybrid Workpiece during Cylindrical Operations". *The International Journal of Advanced Manufacturing Technology* 95.1 (Mar. 2018), pp. 311–316.

[10]   Neugebauer, Reimund; Ben-Hanan, Uri; Ihlenfeldt, Steffen; Wabner, Markus, and Stoll, Andrea. "Acoustic Emission as a Tool for Identifying Drill Position in Fiber-Reinforced Plastic and Aluminum Stacks". *International Journal of Machine Tools and Manufacture* 57 (June 2012), pp. 20–26.

[11]   Krüger, Jörg; Fleischer, Jürgen; Franke, Jörg, and Groche, Peter. *WGP-Standpunkt KI in Der Produktion*. Hannover: WGP Wissenschaftliche Gesellschaft für Produktionstechnik e.V., Sept. 2019.

[12]   Kißkalt, Dominik; Fleischmann, Hans; Kreitlein, Sven; Knott, Manuel, and Franke, Jörg. "A Novel Approach for Data-Driven Process and Condition Monitoring Systems on the Example of Mill-Turn Centers". *Production Engineering* 12.3-4 (June 2018), pp. 525–533.

[13]   Kim, Dong-Hyeon; Kim, Thomas J. Y.; Wang, Xinlin; Kim, Mincheol; Quan, Ying-Jun; Oh, Jin Woo; Min, Soo-Hong; Kim, Hyungjung; Bhandari, Binayak; Yang, Insoon, and Ahn, Sung-Hoon. "Smart Machining Process Using Machine Learning: A Review and Perspective on Machining Industry". *International Journal of Precision Engineering and Manufacturing-Green Technology* 5.4 (Aug. 2018), pp. 555–568.

[14]   Bähr, Rüdiger. "Urformen". *Dubbel*. Berlin, Heidelberg: Springer Berlin Heidelberg, 2018, pp. 1384–1408.

[15]   Ruge, Jürgen and Wohlfahrt, Helmut. *Technologie der Werkstoffe: Herstellung, Verarbeitung, Einsatz; mit 68 Tabellen*. 8., überarb. und erw. Aufl. Studium Technik. Wiesbaden: Vieweg, 2007.

[16]   Weißbach, Wolfgang; Dahms, Michael, and Jaroschek, Christoph. *Werkstoffe und ihre Anwendungen*. Wiesbaden: Springer Fachmedien Wiesbaden, 2018.

[17]   Götze, Jens and Göbbels, Matthias. "Vom Erz zum Stahl". *Einführung in die Angewandte Mineralogie*. Berlin, Heidelberg: Springer Berlin Heidelberg, 2017, pp. 253–264.

[18]   Tanzi, Maria Cristina; Farè, Silvia, and Candiani, Gabriele. "Organization, Structure, and Properties of Materials". *Foundations of Biomaterials Engineering*. Elsevier, 2019, pp. 3–103.

[19]   Liewald, Mathias and Wagner, Stefan. "Umformen". *Dubbel*. Berlin, Heidelberg: Springer Berlin Heidelberg, 2018, pp. 1409–1429.

[20] Wagner, Stefan; Denkena, Berend, and Liewald, Mathias. "Trennen". *Dubbel*. Berlin, Heidelberg: Springer Berlin Heidelberg, 2018, pp. 1430–1462.

[21] Schneider, George. "Chapter 2. Metal Removal Methods". *Cutting-Tool-Applications*. Nelson Pub., 2002.

[22] Bergner, Oliver; Dambacher, Michael; Gresens, Thomas; Liesch, Thomas; Morgner, Dietmar; Pflug, Alexander; Wieneke, Falko, and Verlag Europa-Lehrmittel Nourney, Vollmer GmbH & Co. *Fachkunde Zerspantechnik*. 2019.

[23] *DIN 8580: Fertigungsverfahren – Begriffe, Einteilung. Deutsches Institut für Normung (Hrsg.), Berlin: Beuth Verlag, 2003.*

[24] Klocke, Fritz and König, Wilfried. *Fertigungsverfahren 1 Drehen, Fräsen, Bohren*. 8. Berlin: Springer-Verlag, 2002.

[25] Rodríguez, J. M.; Carbonell, J. M., and Jonsén, P. "Numerical Methods for the Modelling of Chip Formation". *Archives of Computational Methods in Engineering* 27.2 (Apr. 2020), pp. 387–412.

[26] Klocke, Fritz. *Fertigungsverfahren 1: Zerspanung mit geometrisch bestimmter Schneide*. VDI-Buch. Berlin, Heidelberg: Springer Berlin Heidelberg, 2018.

[27] Brezocnik, Miran; Kovacic, Miha, and Psenicnik, Matej. "Prediction of Steel Machinability by Genetic Programming". *Journal of Achievements in Materials and Manufacturing Engineering* 16.1-2 (Jan. 2006), p. 107113.

[28] Schneider, George. "Chapter 3. Machinability of Metals". *Cutting-Tool-Applications*. Nelson Pub., 2002.

[29] Kirsch-Racine, A.; Bomont-Arzur, A., and Confente, M. "Calcium Treatment of Medium Carbon Steel Grades for Machinability Enhancement: From the Theory to Industrial Practice". *Revue de Métallurgie* 104.12 (Dec. 2007), pp. 591–597.

[30] Lou, D.; Cui, K., and Jia, Y. "Study on the Machinability of Resulfurized Composite Free-Cutting Steels". *Journal of Materials Engineering and Performance* 6.2 (Apr. 1997), pp. 215–218.

[31] Bletton, O.; Duet, R., and Pedarre, P. "Influence of Oxide Nature on the Machinability of 316L Stainless Steels". *Wear* 139.2 (Aug. 1990), pp. 179–193.

[32] Anmark, Niclas; Karasev, Andrey, and Jönsson, Pär Göran. "The Effect of Different Non-Metallic Inclusions on the Machinability of Steels". *Materials (Basel, Switzerland)* 8.2 (Feb. 2015), pp. 751–783.

[33]   Abouridouane, Mustapha; Laschet, Gottfried; Kripak, Viktor; Dierdorf, Jens; Prahl, Ulrich; Wirtz, Guido, and Bergs, Thomas. "Microstructure-Based Approach to Predict the Machinability of the Ferritic-Pearlitic Steel C60 by Cutting Operations". *Procedia CIRP* 82 (2019), pp. 107–112.

[34]   Demir, Halil. "The Effects of Microalloyed Steel Pre-Heat Treatment on Microstructure and Machinability". *The International Journal of Advanced Manufacturing Technology* 35.9 (Jan. 2008), pp. 1041–1046.

[35]   Olovsjö, Stefan; Hammersberg, Peter; Avdovic, Pajazit; Ståhl, Jan-Eric, and Nyborg, Lars. "Methodology for Evaluating Effects of Material Characteristics on Machinability—Theory and Statistics-Based Modelling Applied on Alloy 718". *The International Journal of Advanced Manufacturing Technology* 59.1 (Mar. 2012), pp. 55–66.

[36]   Jeon, Soon-Hyeok; Kim, Soon-Tae; Lee, In-Sung, and Park, Yong-Soo. "Effects of Sulfur Addition on Pitting Corrosion and Machinability Behavior of Super Duplex Stainless Steel Containing Rare Earth Metals: Part 2". *Corrosion Science* 52.10 (Oct. 2010), pp. 3537–3547.

[37]   Freitas, Vera Lúcia de Araújo; Albuquerque, Victor Hugo C. de; Silva, Edgard de Macedo; Silva, Antonio Almeida, and Tavares, João Manuel R. S. "Nondestructive Characterization of Microstructures and Determination of Elastic Properties in Plain Carbon Steel Using Ultrasonic Measurements". *Materials Science and Engineering: A* 527.16 (June 2010), pp. 4431–4437.

[38]   Ozcatalbas, Yusuf and Ercan, Fevzi. "The Effects of Heat Treatment on the Machinability of Mild Steels". *Journal of Materials Processing Technology* 136.1 (May 2003), pp. 227–238.

[39]   Chandrasekaran, H. and M'Saoubi, R. "Improved Machinability in Hard Milling and Strategies for Steel Development". *CIRP Annals* 55.1 (2006), pp. 93–96.

[40]   Dong, Z.; Hu, W., and Xue, D. "New Production Cost-Tolerance Models for Tolerance Synthesis". *Journal of Engineering for Industry* 116.2 (May 1994), pp. 199–206.

[41]   Bergs, Thomas; Klocke, Fritz, and Baier, Stefan. *Analyse Der Zerspanbarkeit von Stranggepressten Zinkknetlegierungen Und Entwicklung Angepasster Werkzeuge Und Bearbeitungsstrategien Für Das Drehen Und Bohren*. IGF Schlussbericht. Jan. 2019.

[42]   Evans, Mark. "Accounting for Batch to Batch Variation When Predicting the Safe Life of Materials Operating at High Temperatures: An Application to 1Cr1Mo0.25V Steels Using the Theta Methodology". *Metallurgical and Materials Transactions A* 44.5 (May 2013), pp. 2431–2444.

[43]   Schnoes, F. and Zaeh, M.F. "Model-Based Planning of Machining Operations for Industrial Robots". *Procedia CIRP* 82 (2019), pp. 497–502.

[44]   Madić, Miloš; Radenković, Goran, and Radovanović, Miroslav. "Evaluation of ANN-BP and ANN-GA Models Performance in Predicting Mechanical Properties and Machinability of Cast Copper Alloys". *Strojarstvo* 54.2 (2012), pp. 169–174.

[45]   Diógenes, Alysson; Hoff, Eduardo, and Fernandes, Celso. "Grain Size Measurement by Image Analysis: An Application in the Ceramic and in the Metallic Industries" (Jan. 2005).

[46]   Marin, Florin Bogdan; Potecaşu, Florentina; Marin, Mihaela, and Alexandru, Petrică. "Automatic Grain Size Determination in Microstructures Using Computer Vision Algorithm Based on Support Vector Machine (SVM)". *Advanced Materials Research* 1143 (2017), pp. 194–199.

[47]   Teti, R. and La Commare, U. "Cutting Conditions and Work Material State Identification through Acoustic Emission Methods". *CIRP Annals* 41.1 (Jan. 1992), pp. 89–92.

[48]   Kothuru, Achyuth; Nooka, Sai Prasad, and Liu, Rui. "Audio-Based Tool Condition Monitoring in Milling of the Workpiece Material with the Hardness Variation Using Support Vector Machines and Convolutional Neural Networks". *Journal of Manufacturing Science and Engineering* 140.11 (Nov. 2018), p. 111006.

[49]   Wan, Yi; Cheng, Kai; Zhanqiang, Liu, and Ye, Hongtao. "An Investigation on Machinability Assessment of Difficult-to-Cut Materials Based on Radar Charts". *Proceedings of the Institution of Mechanical Engineers, Part B: Journal of Engineering Manufacture* 227 (Dec. 2013), pp. 1916–1920.

[50]   *Zerspantechnik: Prozesse, Werkzeuge, Technologien ; mit 45 Tabellen.* 12., vollst. überarb. und erw. Aufl. Studium. Wiesbaden: Vieweg + Teubner, 2008.

[51]   Johansson, Daniel; Hägglund, Sören; Bushlya, Volodymyr, and Ståhl, Jan-Eric. "Assessment of Commonly Used Tool Life Models in Metal Cutting". *Procedia Manufacturing* 11 (2017), pp. 602–609.

[52]   Taylor, Frederick Winslow. *On the Art of Cutting Metals*. Vol. 23. American Society of Mechanical Engineers, Jan. 1906.

[53]   Dos Santos, A.L.B.; Duarte, M.A.V.; Abrão, A.M., and Machado, A.R. "An Optimisation Procedure to Determine the Coefficients of the Extended Taylor's Equation in Machining". *International Journal of Machine Tools and Manufacture* 39.1 (Jan. 1999), pp. 17–31.

[54]   Colding, Bertil N. *The Machining Productivity Mountain and Its Wall of Optimum Productivity*. Society of Manufacturing Engineers, 1980.

[55]   Strafford, K.N. and Audy, J. "Indirect Monitoring of Machinability in Carbon Steels by Measurement of Cutting Forces". *Journal of Materials Processing Technology* 67.1-3 (May 1997), pp. 150–156.

[56]   Lian, M.; Liu, H.; Zhou, L.; Zhang, T.; Liu, B., and Wang, Y. "Ultrasonic Roughness Measurement Based on Scattering Attenuation". *Surface Topography: Metrology and Properties* 7.1 (Jan. 2019), p. 015001.

[57]   Persson, Ulf. "Surface Roughness Measurement on Machined Surfaces Using Angular Speckle Correlation". *Journal of Materials Processing Technology* 180.1 (Dec. 2006), pp. 233–238.

[58]   Jawahir, I. S. "The Chip Control Factor in Machinability Assessments: Recent Trends". *Journal of Mechanical Working Technology* 17 (Aug. 1988), pp. 213–224.

[59]   Jawahir, I.S.; Qureshi, N., and Arsecularatne, J.A. "On the Interrelationships of Some Machinability Parameters in Finish Turning with Cermet Chip Forming Tool Inserts". *International Journal of Machine Tools and Manufacture* 32.5 (Oct. 1992), pp. 709–723.

[60]   Fang, X.D. and Jawahir, I.S. "On Predicting Chip Breakability in Machining of Steels with Carbide Tool Inserts Having Complex Chip Groove Geometries". *Journal of Materials Processing Technology* 28.1-2 (Sept. 1991), pp. 37–47.

[61]   Fang, X. D. and Jawahir, I. S. "Predicting Total Machining Performance in Finish Turning Using Integrated Fuzzy-Set Models of the Machinability Parameters". *International Journal of Production Research* 32.4 (Apr. 1994), pp. 833–849.

[62]   Wang, X.; Da, Z. J.; Balaji, A. K., and Jawahir, I. S. "Performance-Based Optimal Selection of Cutting Conditions and Cutting Tools in Multipass Turning Operations Using Genetic Algorithms". *International Journal of Production Research* 40.9 (Jan. 2002), pp. 2053–2065.

[63]   Jawahir, I.S.; Balaji, A.K.; Rouch, K.E., and Baker, J.R. "Towards Integration of Hybrid Models for Optimized Machining Performance in Intelligent Manufacturing Systems". *Journal of Materials Processing Technology* 139.1-3 (Aug. 2003), pp. 488–498.

[64]   Piuri, Vincenzo and Scotti, Fabio. "Design of an Automatic Wood Types Classification System by Using Fluorescence Spectra". *IEEE Transactions on Systems, Man, and Cybernetics, Part C (Applications and Reviews)* 40.3 (May 2010), pp. 358–366.

[65]   Denkena, Berend; Bergmann, Benjamin, and Witt, Matthias. "Material Identification Based on Machine-Learning Algorithms for Hybrid Workpieces during Cylindrical Operations". *Journal of Intelligent Manufacturing* 30.6 (Aug. 2019), pp. 2449–2456.

[66]   Strese, Matti; Brudermueller, Lara; Kirsch, Jonas, and Steinbach, Eckehard. "Haptic Material Analysis and Classification Inspired by Human Exploratory Procedures". *IEEE Transactions on Haptics* 13.2 (Apr. 2020), pp. 404–424.

[67]   Lopez-Caudana, Edgar; Quiroz, Omar; Rodríguez, Adriana; Yépez, Luis, and Ibarra, David. "Classification of Materials by Acoustic Signal Processing in Real Time for NAO Robots". *International Journal of Advanced Robotic Systems* 14.4 (July 2017).

[68]   Neumann, Michael; Nottensteiner, Korbinian; Kossyk, Ingo, and Marton, Zoltan-Csaba. "Material Classification through Knocking and Grasping by Learning of Structure-Borne Sound under Changing Acoustic Conditions". *2018 IEEE 14th International Conference on Automation Science and Engineering (CASE)*. Munich: IEEE, Aug. 2018, pp. 1269–1275.

[69]   Liu, H.; Sun, F.; Fang, B., and Lu, S. "Multimodal Measurements Fusion for Surface Material Categorization". *IEEE Transactions on Instrumentation and Measurement* 67.2 (Feb. 2018), pp. 246–256.

[70]   Penumuru, Durga Prasad; Muthuswamy, Sreekumar, and Karumbu, Premkumar. "Identification and Classification of Materials Using Machine Vision and Machine Learning in the Context of Industry 4.0". *Journal of Intelligent Manufacturing* 31.5 (June 2020), pp. 1229–1241.

[71]   Aujeszky, Tamas; Korres, Georgios, and Eid, Mohamad. "Material Classification with Laser Thermography and Machine Learning". *Quantitative InfraRed Thermography Journal* 16.2 (Apr. 2019), pp. 181–202.

[72]   Saponaro, Philip; Sorensen, Scott; Kolagunda, Abhishek, and Kambhamettu, Chandra. "Material Classification with Thermal Imagery". *2015 IEEE Conference on Computer Vision and Pattern Recognition (CVPR)*. Boston, MA, USA: IEEE, June 2015, pp. 4649–4656.

[73]   Narayanan, Barath Narayanan; Beigh, Kelly; Duning, Solomon, and Erdahl, Dathan. "Automated Material Identification and Segmentation Using Deep Learning for Laser Powder Bed Fusion". *Applications of Machine Learning 2020*. Vol. 11511. International Society for Optics and Photonics, Aug. 2020, 115110P.

[74]   Xie, Yu; Chen, Chuhao; Wu, Dezhi; Xi, Wenming, and Liu, Houde. "Human-Touch-Inspired Material Recognition for Robotic Tactile Sensing". *Applied Sciences* 9.12 (Jan. 2019), p. 2537.

[75]   Schnabel, T; Zimmer, B; Petutschnigg, A J, and Schönberger, S. "An Approach to Classify Thermally Modified Hardwoods by Color". *FOREST PRODUCTS JOURNAL* 57.9 (2007), p. 6.

[76]   Sousa, Wilza Carla Santos e; Barbosa, Lucas de Jesus; Soares, Alvaro Augusto Vieira; Goulart, Selma Lopes, and Protásio, Thiago de Paula. "Wood Colorimetry for the Characterization of Amazonian Tree Species: A Subsidy for a More Efficient Classification". *CERNE* 25.4 (Dec. 2019), pp. 451–462.

[77]   Liu, H. and Sun, F. "Material Identification Using Tactile Perception: A Semantics-Regularized Dictionary Learning Method". *IEEE/ASME Transactions on Mechatronics* 23.3 (June 2018), pp. 1050–1058.

[78]   Kerr, Emmett; McGinnity, T. M., and Coleman, Sonya. "Material Classification Based on Thermal and Surface Texture Properties Evaluated against Human Performance". *2014 13th International Conference on Control Automation Robotics & Vision (ICARCV)*. Singapore: IEEE, Dec. 2014, pp. 444–449.

[79]   Bhattacharjee, Tapomayukh; Wade, Joshua, and Kemp, Charles. "Material Recognition from Heat Transfer given Varying Initial Conditions and Short-Duration Contact" (July 2015).

[80]   Gómez Eguíluz, A.; Rañó, I.; Coleman, S. A., and McGinnity, T. M. "Multimodal Material Identification through Recursive Tactile Sensing". *Robotics and Autonomous Systems* 106 (Aug. 2018), pp. 130–139.

[81]   Kaboli, Mohsen and Cheng, Gordon. "Robust Tactile Descriptors for Discriminating Objects from Textural Properties via Artificial Robotic Skin". *IEEE Transactions on Robotics* 34.4 (Aug. 2018), pp. 985–1003.

[82]   Romano, Joseph M. and Kuchenbecker, Katherine J. "Methods for Robotic Tool-Mediated Haptic Surface Recognition". *2014 IEEE Haptics Symposium (HAPTICS)*. Houston, TX, USA: IEEE, Feb. 2014, pp. 49–56.

[83]   Denkena, Berend; Bergmann, Benjamin; Handrup, Miriam, and Witt, Matthias. "Material Identification during Turning by Neural Network". *Journal of Machine Engineering* 20.2 (June 2020), pp. 65–76.

[84]   Eschelbacher, Sarah; Duntschew, Jonas, and Möhring, Hans-Christian. "Recognition of Wood and Wood-Based Materials during Machining Using Acoustic Emission". *Production at the Leading Edge of Technology*. Berlin, Heidelberg: Springer, 2019, pp. 317–325.

[85]   Demir, Hasan. "Classification of Texture Images Cased on the Histogram of Oriented Gradients Using Support Vector Machines". *Istanbul University - Journal of Electrical & Electronics Engineering* 18.1 (2018), pp. 90–94.

[86]   Kramer, N. "In-Process Identification of Material-Properties by Acoustic Emission Signals". *CIRP Annals* 56.1 (Jan. 2007), pp. 331–334.

[87]   Strese, Matti; Schuwerk, Clemens; Iepure, Albert, and Steinbach, Eckehard. "Multimodal Feature-Based Surface Material Classification". *IEEE Transactions on Haptics* 10.2 (Apr. 2017), pp. 226–239.

[88]   Ji, Mengqi; Fang, Lu; Zheng, Haitian; Strese, Matti, and Steinbach, Eckehard. "Preprocessing-Free Surface Material Classification Using Convolutional Neural Networks Pretrained by Sparse Autoencoder". *2015 IEEE 25th International Workshop on Machine Learning for Signal Processing (MLSP)*. Boston, MA, USA: IEEE, Sept. 2015, pp. 1–6.

[89]   Renganathan, Prasanth; Karthi, Prabu; Mouleeswaran, Senthilkumar; Vijayan, Krishnaraj, and mani R, Raja. "Identification of Drill Position in CFRP/Titanium Alloy Stacks Using Acoustic Emission Signals". *International Conference on Advances in Materials, Manufacturing and Applications (AMMA 2015)*. Apr. 2015.

[90]   Tou, Jing Yi; Tay, Yong Haur, and Lau, Phooi Yee. "A Comparative Study for Texture Classification Techniques on Wood Species Recognition Problem". *2009 Fifth International Conference on Natural Computation*. Tianjian, China: IEEE, 2009, pp. 8–12.

[91]   Varma, M. and Zisserman, A. "A Statistical Approach to Material Classification Using Image Patch Exemplars". *IEEE Transactions on Pattern Analysis and Machine Intelligence* 31.11 (Nov. 2009), pp. 2032–2047.

[92]   Zheng, Haitian; Fang, Lu; Ji, Mengqi; Strese, Matti; Ozer, Yigitcan, and Steinbach, Eckehard. "Deep Learning for Surface Material Classification Using Haptic and Visual Information". *IEEE Transactions on Multimedia* 18.12 (Dec. 2016), pp. 2407–2416.

[93]   Dai, Tian-hong; Wang, Ke-qi, and Yang, Shao-chun. "Research on Wooden Board Classification Based on Color and Texture Features". 2008.

[94]   Strese, Matti; Lee, Jun-Yong; Schuwerk, Clemens; Han, Qingfu; Kim, Hyoung-Gook, and Steinbach, Eckehard. "A Haptic Texture Database for Tool-Mediated Texture Recognition and Classification". *2014 IEEE International Symposium on Haptic, Audio and Visual Environments and Games (HAVE) Proceedings*. Richardson, TX, USA: IEEE, Oct. 2014, pp. 118–123.

[95]   Caputo, B.; Hayman, E., and Mallikarjuna, P. "Class-Specific Material Categorisation". *Tenth IEEE International Conference on Computer Vision (ICCV'05) Volume 1*. Beijing, China: IEEE, 2005, 1597–1604 Vol. 2.

[96]   Jamali, N and Sammut, C. "Majority Voting: Material Classification by Tactile Sensing Using Surface Texture". *IEEE Transactions on Robotics* 27.3 (June 2011), pp. 508–521.

[97]   Strese, Matti; Schuwerk, Clemens, and Steinbach, Eckehard. "Surface Classification Using Acceleration Signals Recorded during Human Freehand Movement". *2015 IEEE World Haptics Conference (WHC)*. Evanston, IL: IEEE, June 2015, pp. 214–219.

[98]   Xiong, P.; He, K.; Song, A., and Liu, P. X. "A Novel Multi-Modal One-Shot Learning Method for Texture Recognition". *IEEE Access* 7 (2019), pp. 182538–182547.

[99]   Bell, Sean; Upchurch, Paul; Snavely, Noah, and Bala, Kavita. "Material Recognition in the Wild with the Materials in Context Database". *Proceedings of the IEEE Conference on Computer Vision and Pattern Recognition*. 2015, pp. 3479–3487.

[100]   Lin, Ye; Chen, Dan; Liang, Shijia; Xu, Zhezhuang; Qiu, Yang; Zhang, Jiahao, and Liu, Xinxiang. "Color Classification of Wooden Boards Based on Machine Vision and the Clustering Algorithm". *Applied Sciences* 10.19 (Sept. 2020), p. 6816.

[101] Pardo, Andrea; Majeed, Mohammed, and Heinemann, Robert. "Process Signals Characterisation to Enable Adaptive Drilling of Aerospace Stacks". *Procedia CIRP*. 13th CIRP Conference on Intelligent Computation in Manufacturing Engineering, 17-19 July 2019, Gulf of Naples, Italy 88 (Jan. 2020), pp. 479–484.

[102] Liu, H.; Song, X.; Bimbo, J.; Seneviratne, L., and Althoefer, K. "Surface Material Recognition through Haptic Exploration Using an Intelligent Contact Sensing Finger". *2012 IEEE/RSJ International Conference on Intelligent Robots and Systems*. Oct. 2012, pp. 52–57.

[103] Aujeszky, Tamas; Korres, Georgios, and Eid, Mohamad. "A Framework for Thermographic Material Characterization Using Multichannel Neural Network". *IEEE Transactions on Instrumentation and Measurement* 69.9 (Sept. 2020), pp. 7061–7071.

[104] LeCun, Yann; Bengio, Yoshua, and Hinton, Geoffrey. "Deep Learning". *Nature* 521.7553 (May 2015), pp. 436–444.

[105] Prabukarthi, A.; Senthilkumar, M., and Krishnaraj, V. "Prominence in Understanding the Position of Drill Tool Using Acoustic Emission Signals During Drilling of CFRP/Ti6Al4V Stacks:" *Advances in Chemical and Materials Engineering*. IGI Global, 2020, pp. 214–230.

[106] Noll, Reinhard; Fricke-Begemann, Cord; Connemann, Sven; Meinhardt, Christoph, and Sturm, Volker. "LIBS Analyses for Industrial Applications – an Overview of Developments from 2014 to 2018". *Journal of Analytical Atomic Spectrometry* 33.6 (2018), pp. 945–956.

[107] Hull, Michael W. "Accuracy, Precision, and Confidence in X-ray Fluorescence for Positive Material Identification". *The NDT Technician* 16.1 (2017), pp. 1–6.

[108] Seelenbinder, John and Rein, Alan. "Positive Material Identification: Qualification, Composition Verification and Counterfeit Detection of Polymeric Material Using Mobile FTIR Spectrometers". *Danbury, USA* (2014).

[109] Sher Afgan, Muhammad; Hou, Zongyu, and Wang, Zhe. "Quantitative Analysis of Common Elements in Steel Using a Handheld μ-LIBS Instrument". *Journal of Analytical Atomic Spectrometry* 32.10 (2017), pp. 1905–1915.

[110] Brooks, Leslie and Gaustad, Gabrielle. "Positive Material Identification (PMI) Capabilities in the Metals Secondary Industry: An Analysis of XRF and LIBS Handheld Analyzers". *Light Metals 2019*. The Minerals, Metals & Materials Series. Cham: Springer International Publishing, 2019, pp. 1375–1380.

[111]   Valenti, Michael. "Machine Tools Get Smarter". *Mechanical Engineering* 117.11 (1995), pp. 70–75.

[112]   Zheng, P.; wang, H.; Sang, Z.; Zhong, R.Y.; Liu, Y.; Liu, C.; Mubarok, K.; Yu, S., and Xu, X. "Smart Manufacturing Systems for Industry 4.0: Conceptual Framework, Scenarios, and Future Perspectives". *Frontiers of Mechanical Engineering* 13.2 (2018), pp. 137–150.

[113]   Kang, Hyoung Seok; Lee, Ju Yeon; Choi, SangSu; Kim, Hyun; Park, Jun Hee; Son, Ji Yeon; Kim, Bo Hyun, and Noh, Sang Do. "Smart Manufacturing: Past Research, Present Findings, and Future Directions". *International Journal of Precision Engineering and Manufacturing-Green Technology* 3.1 (Jan. 2016), pp. 111–128.

[114]   Wang, B.; Tao, F.; Fang, X.; Liu, C.; Liu, Y., and Freiheit, T. "Smart Manufacturing and Intelligent Manufacturing: A Comparative Review". *Engineering* (2020).

[115]   Kusiak, Andrew. "Smart Manufacturing". *International Journal of Production Research* 56.1-2 (Jan. 2018), pp. 508–517.

[116]   Mittal, Sameer; Khan, Muztoba Ahmad; Romero, David, and Wuest, Thorsten. "Smart Manufacturing: Characteristics, Technologies and Enabling Factors". *Proceedings of the Institution of Mechanical Engineers, Part B: Journal of Engineering Manufacture* 233.5 (Apr. 2019), pp. 1342–1361.

[117]   Zhao, Yaoyao Fiona and Xu, Xun. "Enabling Cognitive Manufacturing through Automated On-Machine Measurement Planning and Feedback". *Advanced Engineering Informatics*. The Cognitive Factory 24.3 (Aug. 2010), pp. 269–284.

[118]   Liu, Changqing; Li, Yingguang, and Hao, Xiaozhong. "An Adaptive Machining Approach Based on In-Process Inspection of Interim Machining States for Large-Scaled and Thin-Walled Complex Parts". *The International Journal of Advanced Manufacturing Technology* 90.9 (June 2017), pp. 3119–3128.

[119]   Wojcicki, J. and Bianchi, G. "A Smart Spindle Component Concept as a Standalone Measurement System for Industry 4.0 Machine Tools". *2020 IEEE International Workshop on Metrology for Industry 4.0 and IoT, MetroInd 4.0 and IoT 2020 - Proceedings*. 2020, pp. 278–282.

[120]   Shirase, K. "CAM-CNC Integration for Innovative Intelligent Machine Tool". *Proceedings of the 8th International Conference on Leading Edge Manufacturing in 21st Century, LEM 2015*. 2015.

[121] Shirase, K. and Nakamoto, K. "Simulation Technologies for the Development of an Autonomous and Intelligent Machine Tool". *International Journal of Automation Technology* 7.1 (2013), pp. 6–15.

[122] Tong, Xin; Liu, Qiang; Pi, Shiwei, and Xiao, Yao. "Real-Time Machining Data Application and Service Based on IMT Digital Twin". *Journal of Intelligent Manufacturing* 31.5 (Jan. 2019), pp. 1113–1132.

[123] Rigal, J.-F. and Mabrouki, T. "A Smart Machining Systems Application to Reduce the Machining Costs within a Multi-Process Production". *International Journal of Mechatronics and Manufacturing Systems* 2.5-6 (2009), pp. 505–514.

[124] Park, H.-S.; Qi, B.; Dang, D.-V., and Park, D.Y. "Development of Smart Machining System for Optimizing Feedrates to Minimize Machining Time". *Journal of Computational Design and Engineering* 5.3 (2018), pp. 299–304.

[125] Mourtzis, Dimitris. "Machine Tool 4.0 in the Era of Digital Manufacturing". *Proceedings of the 32nd European Modeling & Simulation Symposium (EMSS 2020)*. CAL-TEK srl, Sept. 2020, pp. 416–429.

[126] Liu, C.; Vengayil, H.; Zhong, R.Y., and Xu, X. "A Systematic Development Method for Cyber-Physical Machine Tools". *Journal of Manufacturing Systems* 48 (2018), pp. 13–24.

[127] Corbett, J. "Smart Machine Tools". *Proceedings of the Institution of Mechanical Engineers. Part I: Journal of Systems and Control Engineering* 212.3 (1998), pp. 203–213.

[128] Jeon, Byeongwoo; Yoon, Joo-Sung; Um, Jumyung, and Suh, Suk-Hwan. "The Architecture Development of Industry 4.0 Compliant Smart Machine Tool System (SMTS)". *Journal of Intelligent Manufacturing* (Jan. 2020).

[129] Denkena, Berend; Bergmann, Benjamin, and Witt, Matthias. "Feeling Machine for Process Monitoring of Turning Hybrid Solid Components". *Metals* 10.7 (July 2020), p. 930.

[130] Cao, H.; Zhang, X., and Chen, X. "The Concept and Progress of Intelligent Spindles: A Review". *International Journal of Machine Tools and Manufacture* 112 (2017), pp. 21–52.

[131] Desforges, X.; Habbadi, A., and Archimède, B. "Design Methodology for Smart Actuator Services for Machine Tool and Machining Control and Monitoring". *Robotics and Computer-Integrated Manufacturing* 27.6 (2011), pp. 963–976.

[132] Wang, C.; Cheng, K., and Rakowski, R. "Development of Smart Tooling Concepts Applied to Ultraprecision Machining". *Journal of Micro and Nano-Manufacturing* 5.2 (2017).

[133] Wang, Chao; Ghani, Saiful BC; Cheng, Kai, and Rakowski, Richard. "Adaptive Smart Machining Based on Using Constant Cutting Force and a Smart Cutting Tool". *Proceedings of the Institution of Mechanical Engineers, Part B: Journal of Engineering Manufacture* 227.2 (Feb. 2013), pp. 249–253.

[134] Cho, Dong-Woo; Lee, Sang Jo, and Chu, Chong Nam. "The State of Machining Process Monitoring Research in Korea". *International Journal of Machine Tools and Manufacture* 39.11 (Nov. 1999), pp. 1697–1715.

[135] Byrne, G.; Dornfeld, D.; Inasaki, I.; Ketteler, G.; König, W., and Teti, R. "Tool Condition Monitoring (TCM) — The Status of Research and Industrial Application". *CIRP Annals* 44.2 (Jan. 1995), pp. 541–567.

[136] Abellan-Nebot, Jose Vicente and Romero Subirón, Fernando. "A Review of Machining Monitoring Systems Based on Artificial Intelligence Process Models". *The International Journal of Advanced Manufacturing Technology* 47.1-4 (Jan. 2010), pp. 237–257.

[137] Oliveira, J F G; Ferraz Júnior, F; Coelho, R T, and Silva, E J. "Architecture for Machining Process and Production Monitoring Based in Open Computer Numerical Control". *Proceedings of the Institution of Mechanical Engineers, Part B: Journal of Engineering Manufacture* 222.12 (Dec. 2008), pp. 1605–1612.

[138] Teti, R.; Jemielniak, K.; O'Donnell, G., and Dornfeld, D. "Advanced Monitoring of Machining Operations". *CIRP Annals - Manufacturing Technology* 59.2 (Jan. 2010), pp. 717–739.

[139] Dey, S. and Stori, J.A. "A Bayesian Network Approach to Root Cause Diagnosis of Process Variations". *International Journal of Machine Tools and Manufacture* 45.1 (Jan. 2005), pp. 75–91.

[140] Weck, Manfred and Brecher, Christian. *Werkzeugmaschinen, Fertigungssysteme. 3: Mechatronische Systeme, Vorschubantriebe, Prozessdiagnose*. 6., neu bearb. Aufl. VDI[-Buch]. Berlin Heidelberg New York: Springer, 2006.

[141] Liang, Steven Y. and Shih, Albert J. *Analysis of Machining and Machine Tools*. Springer US, 2016.

[142] Smith, S. and Tlusty, J. "Current Trends in High-Speed Machining". *Journal of Manufacturing Science and Engineering* 119.4B (Nov. 1997), pp. 664–666.

[143]   Kurada, S. and Bradley, C. "A Review of Machine Vision Sensors for Tool Condition Monitoring". *Computers in Industry* 34.1 (Oct. 1997), pp. 55–72.

[144]   García-Ordás, María Teresa; Alegre-Gutiérrez, Enrique; Alaiz-Rodríguez, Rocío, and González-Castro, Víctor. "Tool Wear Monitoring Using an Online, Automatic and Low Cost System Based on Local Texture". *Mechanical Systems and Signal Processing* 112 (Nov. 2018), pp. 98–112.

[145]   Teti, R. "Machining of Composite Materials". *CIRP Annals - Manufacturing Technology* 51.2 (Jan. 2002), pp. 611–634.

[146]   Fernández-Robles, Laura; Azzopardi, George; Alegre, Enrique, and Petkov, Nicolai. "Cutting Edge Localisation in an Edge Profile Milling Head". *Computer Analysis of Images and Patterns*. Vol. 9257. Cham: Springer International Publishing, 2015, pp. 336–347.

[147]   Siddhpura, A and Paurobally, R. "A Review of Flank Wear Prediction Methods for Tool Condition Monitoring in a Turning Process". *The International Journal of Advanced Manufacturing Technology* 65.1-4 (2013), p. 23.

[148]   Zhou, Yuqing and Xue, Wei. "Review of Tool Condition Monitoring Methods in Milling Processes". *The International Journal of Advanced Manufacturing Technology* 96.5 (Jan. 2018), p. 25092523.

[149]   Li, Yingguang; Mou, Wenping; Li, Jingjing; Liu, Changqing, and Gao, James. "An Automatic and Accurate Method for Tool Wear Inspection Using Grayscale Image Probability Algorithm Based on Bayesian Inference". *Robotics and Computer-Integrated Manufacturing* 68 (Apr. 2021), p. 102079.

[150]   Dutta, S.; Pal, S. K.; Mukhopadhyay, S., and Sen, R. "Application of Digital Image Processing in Tool Condition Monitoring: A Review". *CIRP Journal of Manufacturing Science and Technology* 6.3 (Jan. 2013), pp. 212–232.

[151]   Devillez, A.; Lesko, S., and Mozer, W. "Cutting Tool Crater Wear Measurement with White Light Interferometry". *Wear* 256.1 (Jan. 2004), pp. 56–65.

[152]   Sommer, Karl; Heinz, Rudolf, and Schöfer, Jörg. *Verschleiß metallischer Werkstoffe*. Wiesbaden: Springer Fachmedien Wiesbaden, 2014.

[153]   Bittès, G. "Contribution à La Connaissance Des Mécanismes Fondamentaux Liés à l'usinabilité Des Aciers de Construction Mécanique". *Université de Toulon* (1993).

[154]   Telle, Rainer. *Werkstoffentwicklung und Materialverhalten moderner Schneidkeramiken*. Kontakt & Studium 370. Ehningen, 1993.

[155]   Habig, Karl-Heinz. *Verschleiss Und Härte von Werkstoffen*. München; Wien: Hanser, 1980.

[156]   Erinski, Dobri P. "Untersuchungen über den Einfluß des Werkstoffgefüges auf das Zerspanverhalten von Al-Si-Gußlegierungen". PhD thesis. Aachen, 1990.

[157]   Bahr, B.; Motavalli, S., and Arfi, T. "Sensor Fusion for Monitoring Machine Tool Conditions". *International Journal of Computer Integrated Manufacturing* 10.5 (Jan. 1997), pp. 314–323.

[158]   Medeossi, F; Sorgato, M; Savio, E; Bruschi, S, et al. "Micro-milling tool wear monitoring through a novel method for burrs evaluation". *Proceedings of the 16th International Conference of the European Society for Precision Engineering and Nanotechnology, EUSPEN 2016*. euspen. 2017, pp. 153–154.

[159]   Zhang, Guoqing; To, Suet, and Xiao, Gaobo. "Novel Tool Wear Monitoring Method in Ultra-Precision Raster Milling Using Cutting Chips". *Precision Engineering* 38.3 (July 2014), pp. 555–560.

[160]   Aghazadeh, Fatemeh; Tahan, Antoine, and Thomas, Marc. "Tool Condition Monitoring Using Spectral Subtraction and Convolutional Neural Networks in Milling Process". *The International Journal of Advanced Manufacturing Technology* 98.9 (Oct. 2018), pp. 3217–3227.

[161]   Binsaeid, S.; Asfour, S.; Cho, S., and Onar, A. "Machine Ensemble Approach for Simultaneous Detection of Transient and Gradual Abnormalities in End Milling Using Multisensor Fusion". *Journal of Materials Processing Technology* 209.10 (Jan. 2009), pp. 4728–4738.

[162]   Shen, Z.-G.; He, N., and Li, L. "An Intelligent Monitoring System for High-Speed Milling Process". *Harbin Gongye Daxue Xuebao/Journal of Harbin Institute of Technology* 42.7 (Jan. 2010), pp. 1158–11621167.

[163]   René de Jesús, R.-T.; Gilberto, H.-R.; Iván, T.-V., and Carlos, J.-C.J. "Driver Current Analysis for Sensorless Tool Breakage Monitoring of CNC Milling Machines". *International Journal of Machine Tools and Manufacture* 43.15 (Jan. 2003), pp. 1529–1534.

[164]   Tansel, I. N.; Li, M.; Demetgul, M.; Bickraj, K.; Kaya, B., and Ozcelik, B. "Detecting Chatter and Estimating Wear from the Torque of End Milling Signals by Using Index Based Reasoner (IBR)". *International Journal of Advanced Manufacturing Technology* 58.1-4 (Jan. 2012), pp. 109–118.

[165]   Dutta, Samik; Pal, Surjya, and Sen, Ranjan. "Tool Condition Monitoring in Turning by Applying Machine Vision". *Journal of Manufacturing Science and Engineering* 138 (Oct. 2015).

[166]   Danesh, Mahdi and Khalili, Khalil. "Determination of Tool Wear in Turning Process Using Undecimated Wavelet Transform and Textural Features". *Procedia Technology*. 8th International Conference Interdisciplinarity in Engineering, INTER-ENG 2014, 9-10 October 2014, Tirgu Mures, Romania 19 (Jan. 2015), pp. 98–105.

[167]   Cho, Sohyung; Binsaeid, Sultan, and Asfour, Shihab. "Design of Multisensor Fusion-Based Tool Condition Monitoring System in End Milling". *The International Journal of Advanced Manufacturing Technology* 46.5-8 (Jan. 2010), pp. 681–694.

[168]   Ghosh, N.; Ravi, Y. B.; Patra, A.; Mukhopadhyay, S.; Paul, S.; Mohanty, A. R., and Chattopadhyay, A. B. "Estimation of Tool Wear during CNC Milling Using Neural Network-Based Sensor Fusion". *Mechanical Systems and Signal Processing* 21.1 (Jan. 2007), pp. 466–479.

[169]   García-Ordás, María Teresa; Alegre, Enrique; González-Castro, Víctor, and Alaiz-Rodríguez, Rocío. "A Computer Vision Approach to Analyze and Classify Tool Wear Level in Milling Processes Using Shape Descriptors and Machine Learning Techniques". *The International Journal of Advanced Manufacturing Technology* 90.5 (May 2017), pp. 1947–1961.

[170]   Dai, Y. and Zhu, K. "A Machine Vision System for Micro-Milling Tool Condition Monitoring". *Precision Engineering* 52 (Jan. 2018), pp. 183–191.

[171]   Sick, Bernhard. "ON-LINE AND INDIRECT TOOL WEAR MONITORING IN TURNING WITH ARTIFICIAL NEURAL NETWORKS: A REVIEW OF MORE THAN A DECADE OF RESEARCH". *Mechanical Systems and Signal Processing* 16.4 (July 2002), pp. 487–546.

[172]   Zhu, Kunpeng; Wong, Yoke San, and Hong, Geok Soon. "Wavelet Analysis of Sensor Signals for Tool Condition Monitoring: A Review and Some New Results". *International Journal of Machine Tools and Manufacture* 49.7 (June 2009), pp. 537–553.

[173]   Yu, Jianbo and Zhou, Junjie. "A Machine Vision Method for Non-Contact Tool Wear Inspection". *2020 Chinese Automation Congress (CAC)*. Nov. 2020, pp. 1239–1243.

[174]   Ruitao Peng; Pang, Haolin; Jiang, Haojian, and Hu, Yunbo. "Study of Tool Wear Monitoring Using Machine Vision". *Automatic Control and Computer Sciences* 54.3 (May 2020), pp. 259–270.

[175]   Bagga, P. J.; Makhesana, M. A., and Patel, K. M. "A Novel Approach of Combined Edge Detection and Segmentation for Tool Wear Measurement in Machining". *Production Engineering* 15.3-4 (June 2021), pp. 519–533.

[176]   Du, Daxi; Sun, Jianfei; Yang, Sen, and Chen, Wuyi. "An Investigation on Measurement and Evaluation of Tool Wear Based on 3D Topography". *International Journal of Manufacturing Research* 13.2 (Jan. 2018), pp. 168–182.

[177]   Kou, Rui; Lian, Shiwei; Xie, Nan; Lu, Beier, and Liu, Xuemei. *Image-Based Tool Condition Monitoring Based on Convolution Neural Network in Turning Process*. Preprint. In Review, May 2021.

[178]   Yamashina, Hajime and Okumura, Susumu. "A Machine Vision System for Measuring Wear and Chipping of Drilling Tools". *Journal of Intelligent Manufacturing* 7.4 (Aug. 1996), pp. 319–327.

[179]   Niranjan Prasad, K and Ramamoorthy, B. "Tool Wear Evaluation by Stereo Vision and Prediction by Artificial Neural Network". *Journal of Materials Processing Technology* 112.1 (May 2001), pp. 43–52.

[180]   Liu, Jian Cheng and Xiong, Guang Xi. "Study on Volumetric Tool Wear Measurement Using Image Processing". *Applied Mechanics and Materials* 670-671 (2014), pp. 1194–1199.

[181]   Zhu, Aibin; He, Dayong; Zhao, Jianwei, and Wu, Hongling. "Online Tool Wear Condition Monitoring Using Binocular Vision". *Insight - Non-Destructive Testing and Condition Monitoring* 59.4 (Apr. 2017), pp. 203–210.

[182]   Szydłowski, Michał; Powałka, Bartosz; Matuszak, Marcin, and Kochmański, Paweł. "Machine Vision Micro-Milling Tool Wear Inspection by Image Reconstruction and Light Reflectance". *Precision Engineering* 44 (Apr. 2016), pp. 236–244.

[183]   Weckenmann, A. and Nalbantic, K. "Precision Measurement of Cutting Tools with Two Matched Optical 3D-Sensors". *CIRP Annals* 52.1 (Jan. 2003), pp. 443–446.

[184]   Dawson, Ty G. and Kurfess, Thomas R. "Quantification of Tool Wear Using White Light Interferometry and Three-Dimensional Computational Metrology". *International Journal of Machine Tools and Manufacture* 45.4 (Apr. 2005), pp. 591–596.

[185]   Zapico, P.; Blanco, D.; Cuervo, C.; Valiño, G., and Rico, J. C. "Cutting-Tool Wear Characterization by Means of Conoscopic Holography". *Procedia Manufacturing*. Manufacturing Engineering Society International Conference 2017, MESIC 2017, 28-30 June 2017, Vigo (Pontevedra), Spain 13 (Jan. 2017), pp. 13–20.

[186]   Jeon, Seongkyul; Stepanick, Christopher K.; Zolfaghari, Abolfazl A., and Lee, ChaBum. "Knife-Edge Interferometry for Cutting Tool Wear Monitoring". *Precision Engineering* 50 (Oct. 2017), pp. 354–360.

[187]   Lee, ChaBum. "Precision Cutting Tool Wear Monitoring Method by Knife-Edge Diffraction Interferometry". *Volume 3: Manufacturing Equipment and Systems*. College Station, Texas, USA: American Society of Mechanical Engineers, June 2018, V003T02A026.

[188]   Jurkovic, J.; Korosec, M., and Kopac, J. "New Approach in Tool Wear Measuring Technique Using CCD Vision System". *International Journal of Machine Tools and Manufacture* 45.9 (July 2005), pp. 1023–1030.

[189]   Wang, Zhongren; Li, Bo, and Zhou, Yuebin. "Fast 3D Reconstruction of Tool Wear Based on Monocular Vision and Multi-Color Structured Light Illuminator". *International Symposium on Optoelectronic Technology and Application 2014: Image Processing and Pattern Recognition*. Vol. 9301. International Society for Optics and Photonics, Nov. 2014, p. 93011D.

[190]   Wang, W. H.; Wong, Y. S., and Hong, G. S. "3D Measurement of Crater Wear by Phase Shifting Method". *Wear* 261.2 (July 2006), pp. 164–171.

[191]   Čerče, Luka; Pušavec, Franci, and Kopač, Janez. "3D Cutting Tool-Wear Monitoring in the Process". *Journal of Mechanical Science and Technology* 29.9 (Sept. 2015), pp. 3885–3895.

[192]   Čerče, L.; Pušavec, F., and Kopac, J. "A New Approach to Spatial Tool Wear Analysis and Monitoring" (2015).

[193]   Yu, Zhanjiang; Zhang, Linshuai; Xia, Kui; Zhang, Liuxin, and Yu, Huadong. "Tool Wear Inspection Method for Small Lathe". *2014 IEEE International Conference on Mechatronics and Automation*. Aug. 2014, pp. 1161–1165.

[194]   Zhang, Jilin; Zhang, Chen; Guo, Song, and Zhou, Laishui. "Research on Tool Wear Detection Based on Machine Vision in End Milling Process". *Production Engineering* 6.4-5 (2012), p. 7.

[195]   Fong, Ka Mun; Wang, Xin; Kamaruddin, Shahrul, and Ismadi, Mohd-Zulhilmi. "Investigation on Universal Tool Wear Measurement Technique Using Image-Based Cross-Correlation Analysis". *Measurement* 169 (Feb. 2021), p. 108489.

[196]   Thakre, Avinash A; Lad, Aniruddha V, and Mala, Kiran. "Measurements of Tool Wear Parameters Using Machine Vision System". *Modelling and Simulation in Engineering* (2019), p. 10.

[197]   Soleimani, Seyfollah; Sukumaran, Jacob; Kumcu, Asli; De Baets, Patrick, and Philips, Wilfried. "Quantifying Abrasion and Micro-Pits in Polymer Wear Using Image Processing Techniques". *Wear* 319.1 (Nov. 2014), pp. 123–137.

[198]   Su, J. C.; Huang, C. K., and Tarng, Y. S. "An Automated Flank Wear Measurement of Microdrills Using Machine Vision". *Journal of Materials Processing Technology* 180.1 (Dec. 2006), pp. 328–335.

[199]   Zhu, Kunpeng and Yu, Xiaolong. "The Monitoring of Micro Milling Tool Wear Conditions by Wear Area Estimation". *Mechanical Systems and Signal Processing* 93 (Sept. 2017), pp. 80–91.

[200]   Fadare, David and Oni, Abayomi. "Development and Application of a Machine Vision System for Measurement of Tool Wear". *Journal of Engineering and Applied Sciences* 4 (Jan. 2009).

[201]   D'Addona, D. M.; Matarazzo, D.; Ullah, A. M. M. Sharif, and Teti, R. "Tool Wear Control through Cognitive Paradigms". *Procedia CIRP*. 9th CIRP Conference on Intelligent Computation in Manufacturing Engineering - CIRP ICME '14 33 (Jan. 2015), pp. 221–226.

[202]   Kwon, Yongjin and Fischer, Gary W. "A Novel Approach to Quantifying Tool Wear and Tool Life Measurements for Optimal Tool Management". *International Journal of Machine Tools and Manufacture* 43.4 (Mar. 2003), pp. 359–368.

[203]   Lanzetta, M. "A New Flexible High-Resolution Vision Sensor for Tool Condition Monitoring". *Journal of Materials Processing Technology* 119.1-3 (Jan. 2001), pp. 73–82.

[204]   Sun, Wei-Heng and Yeh, Syh-Shiuh. "Using the Machine Vision Method to Develop an On-machine Insert Condition Monitoring System for Computer Numerical Control Turning Machine Tools". *Materials* 11.10 (Jan. 2018), p. 1977.

[205]   Kim, Jeon-Ha; Moon, Deok-Kyu; Lee, Deuk-Woo; Kim, Jeong-suk; Kang, Myung-Chang, and Kim, Kwang Ho. "Tool Wear Measuring Technique on the Machine Using CCD and Exclusive Jig". *Journal of Materials Processing Technology*. AFDM 2002 S.I. 130-131 (Dec. 2002), pp. 668–674.

[206]   Yang, Zeqing; Liu, Libing; Peng, Kai; Li, Shanshan; Zhang, Junfeng, and Gai, Liya. "Monitoring Method of High-speed Tool Wear Level Based on Machine Vision". *International Journal of Signal Processing, Image Processing and Pattern Recognition* 10 (June 2017), pp. 23–38.

[207]   Shahabi, H. H. and Ratnam, M. M. "On-Line Monitoring of Tool Wear in Turning Operation in the Presence of Tool Misalignment". *The International Journal of Advanced Manufacturing Technology* 38.7-8 (Sept. 2008), pp. 718–727.

[208]   Shahabi, H H and Ratnam, M M. "In-Cycle Monitoring of Tool Nose Wear and Surface Roughness of Turned Parts Using Machine Vision". *Int J Adv Manuf Technol* (2009), p. 10.

[209]   Miao, Huihui; Zhao, Zhibin; Sun, Chuang; Li, Bing, and Yan, Ruqiang. "A U-Net-Based Approach for Tool Wear Area Detection and Identification". *IEEE Transactions on Instrumentation and Measurement* 70 (2021), pp. 1–10.

[210]   Zhang, Chen and Zhang, Jilin. "On-Line Tool Wear Measurement for Ball-End Milling Cutter Based on Machine Vision". *Computers in Industry* 64.6 (Aug. 2013), pp. 708–719.

[211]   Wang, W.; Wong, Y. S., and Hong, G. S. "Flank Wear Measurement by Successive Image Analysis". *Computers in Industry*. Machine Vision Special Issue 56.8 (Dec. 2005), pp. 816–830.

[212]   Wu, Xuefeng; Liu, Yahui; Zhou, Xianliang, and Mou, Aolei. "Automatic Identification of Tool Wear Based on Convolutional Neural Network in Face Milling Process". *Sensors* 19.18 (Jan. 2019), p. 3817.

[213]   Lins, Romulo Gonçalves; Guerreiro, Bruno; Marques de Araujo, Paulo Ricardo, and Schmitt, Robert. "In-Process Tool Wear Measurement System Based on Image Analysis for CNC Drilling Machines". *IEEE Transactions on Instrumentation and Measurement* 69.8 (Aug. 2020), pp. 5579–5588.

[214]   D'Addona, D. M. and Teti, R. "Image Data Processing via Neural Networks for Tool Wear Prediction". *Procedia CIRP*. Eighth CIRP Conference on Intelligent Computation in Manufacturing Engineering 12 (Jan. 2013), pp. 252–257.

[215]   Moldovan, Ovidiu Gheorghe; Dzitac, Simona; Moga, Ioan; Vesse-lenyi, Tiberiu, and Dzitac, Ioan. "Tool-Wear Analysis Using Image Processing of the Tool Flank". *Symmetry* 9.12 (Dec. 2017), p. 296.

[216]   Giusti, F.; Santochi, M., and Tantussi, G. "A Flexible Tool Wear Sensor for NC Lathes". *CIRP Annals* 33.1 (Jan. 1984), pp. 229–232.

[217]   Giusti, F.; Santochi, M., and Tantussi, G. "On-Line Sensing of Flank and Crater Wear of Cutting Tools". *CIRP Annals* 36.1 (Jan. 1987), pp. 41–44.

[218]   Yu, Xiaolong; Lin, Xin; Dai, Yiquan, and Zhu, Kunpeng. "Image Edge Detection Based Tool Condition Monitoring with Morphological Component Analysis". *ISA Transactions* 69 (July 2017), pp. 315–322.

[219]   Sawangsri, Worapong and Wattanasinbumrung, Pakanun. "A Model Approach for In-Process Tool Condition Monitoring in CNC Turning Using Machine Vision". *International Journal on Interactive Design and Manufacturing (IJIDeM)* 16.4 (2022), pp. 1439–1456.

[220]   Mehta, Soham; Singh, Rajput Anurag; Mohata, Yugalkishore, and Kiran, M B. "Measurement and Analysis of Tool Wear Using Vision System". *2019 IEEE 6th International Conference on Industrial Engineering and Applications (ICIEA)*. Apr. 2019, pp. 45–49.

[221]   Castejón, M.; Alegre, E.; Barreiro, J., and Hernández, L. K. "On-Line Tool Wear Monitoring Using Geometric Descriptors from Digital Images". *International Journal of Machine Tools and Manufacture* 47.12 (Oct. 2007), pp. 1847–1853.

[222]   Liang, Y.-T. and Chiou, Y.-C. *Taguchi Analysis of Milling Wear Automatic Monitoring System Based on Machine Vision Technique*. Vol. 5579 LNAI. 22nd International Conference on Industrial, Engineering and Other Applications of Applied Intelligent Systems, IEA/AIE 2009. Tainan, Jan. 2009.

[223]   Fernández-Robles, L.; Charro, N.; Sánchez-González, L.; Pérez, H.; Castejón-Limas, M., and Alfonso-Cendón, J. *Tool Wear Estimation and Visualization Using Image Sensors in Micro Milling Manufacturing*. Vol. 10870 LNAI. 13th International Conference on Hybrid Artificial Intelligent Systems, HAIS 2018. Springer Verlag, Jan. 2018.

[224]   Ong, Pauline; Lee, Woon Kiow, and Lau, Raymond Jit Hoo. "Tool Condition Monitoring in CNC End Milling Using Wavelet Neural Network Based on Machine Vision". *The International Journal of Advanced Manufacturing Technology* 104.1 (Sept. 2019), pp. 1369–1379.

[225]   Liang, Yu-Teng and Chiou, Yih-Chih. *An Effective Drilling Wear Measurement Based on Visual Inspection Technique*. Vol. 2006. Jan. 2006.

[226] Liang, Yu-Teng and Chiou, Yih-Chih. "Automation Tool Wear System Based on Validated Corner Detection and Taguchi's Method". *Advanced Science Letters* 4.6-7 (July 2011), pp. 2059–2065.

[227] Liang, Yu-Teng and Chiou, Yih-Chih. "Vision-Based Automatic Tool Wear Monitoring System". *2008 7th World Congress on Intelligent Control and Automation*. June 2008, pp. 6031–6035.

[228] Yuan, Qiaoling; Ji, Shi Ming, and Zhang, Li. "Study of Monitoring the Abrasion of Metal Cutting Tools Based on Digital Image Technology". 5642 (Jan. 2005), pp. 397–402.

[229] Atli, A. V.; Urhan, Oguzhan; Erturk, Sarp, and Sönmez, M. "A Computer Vision-Based Fast Approach to Drilling Tool Condition Monitoring". *Proceedings of The Institution of Mechanical Engineers Part B-journal of Engineering Manufacture - PROC INST MECH ENG B-J ENG MA* 220 (Sept. 2006), pp. 1409–1415.

[230] Fernández-Robles, Laura; Sánchez-González, Lidia; Díez-González, Javier; Castejón-Limas, Manuel, and Pérez, Hilde. "Use of Image Processing to Monitor Tool Wear in Micro Milling". *Neurocomputing* 452 (Sept. 2021), pp. 333–340.

[231] Duan, Guifang; Chen, Yen-Wei, and Sukegawa, Takeshi. "Automatic Optical Flank Wear Measurement of Microdrills Using Level Set for Cutting Plane Segmentation". *Machine Vision and Applications* 21.5 (Aug. 2010), pp. 667–676.

[232] Kim, Hyun-ho; Chung, Siyon; Kim, Seung-chul; Jee, Won-ho, and Chung, Sung-chong. *Condition Monitoring of Micro-Drilling Processes on Glass by Using Machine Vision*. 2006.

[233] Sortino, M. "Application of Statistical Filtering for Optical Detection of Tool Wear". *International Journal of Machine Tools and Manufacture* 43.5 (Apr. 2003), pp. 493–497.

[234] Wang, W. H.; Hong, G. S., and Wong, Y. S. "Flank Wear Measurement by a Threshold Independent Method with Sub-Pixel Accuracy". *International Journal of Machine Tools and Manufacture* 46.2 (Feb. 2006), pp. 199–207.

[235] Kurada, S. and Bradley, C. "A Machine Vision System for Tool Wear Assessment". *Tribology International* 30.4 (Apr. 1997), pp. 295–304.

[236] Kerr, David; Pengilley, James, and Garwood, Robert. "Assessment and Visualisation of Machine Tool Wear Using Computer Vision". *The International Journal of Advanced Manufacturing Technology* 28 (2006), pp. 781–791.

[237] Alegre, Enrique; Aláiz, Rocío; Barreiro, Joaquín, and Viñuela, Mavilo. "Tool Insert Wear Classification Using Statistical Descriptors and Neuronal Networks". *Progress in Pattern Recognition, Image Analysis and Applications*. Vol. 3773. Berlin, Heidelberg: Springer Berlin Heidelberg, 2005, pp. 786–793.

[238] Xiong, Si Chang; Dong, Ling Ping, and Wen, Dong Hui. "Tool Wear Image Segmentation Based on Markov Random Field Model". *Advanced Materials Research* 102-104 (2010), pp. 600–604.

[239] Li, Lihong and An, Qingbin. "An In-Depth Study of Tool Wear Monitoring Technique Based on Image Segmentation and Texture Analysis". *Measurement* 79 (Feb. 2016), pp. 44–52.

[240] Hou, Qiulin; Sun, Jie, and Huang, Panling. "A Novel Algorithm for Tool Wear Online Inspection Based on Machine Vision". *The International Journal of Advanced Manufacturing Technology* 101.9 (Apr. 2019), pp. 2415–2423.

[241] Duan, Guifang; Wang, Hongcui; Liu, Zhenyu, and Chen, Yen-Wei. "A Machine Learning-Based Framework for Automatic Visual Inspection of Microdrill Bits in PCB Production". *IEEE Transactions on Systems, Man, and Cybernetics, Part C (Applications and Reviews)* 42.6 (Nov. 2012), pp. 1679–1689.

[242] Chethan, Y. D.; Ravindra, H. V.; gowda, Y. T. Krishne, and Kumar, S. Bharath. "Machine Vision for Tool Status Monitoring in Turning Inconel 718 Using Blob Analysis". *Materials Today: Proceedings*. 4th International Conference on Materials Processing and Characterzation 2.4 (Jan. 2015), pp. 1841–1848.

[243] García-Ordás, M. T.; Alegre-Gutiérrez, E.; González-Castro, V., and Alaiz-Rodríguez, R. "Combining Shape and Contour Features to Improve Tool Wear Monitoring in Milling Processes". *International Journal of Production Research* 56.11 (Jan. 2018), pp. 3901–3913.

[244] Alegre, Enrique; Alaiz-Rodríguez, Rocío; Barreiro, Joaquín, and Ruiz, Jonatan. "Use of Contour Signatures and Classification Methods to Optimize the Tool Life in Metal Machining". *Estonian Journal of Engineering* 15.1 (2009), p. 3.

[245] Xiong, Guangxi; Liu, Jiancheng, and Avila, Adrian. "Cutting Tool Wear Measurement by Using Active Contour Model Based Image Processing". *2011 IEEE International Conference on Mechatronics and Automation*. Aug. 2011, pp. 670–675.

[246] Schmitt, R.; Cai, Y., and Pavim, A. *Machine Vision System for Inspecting Flank Wear on Cutting Tools*. Vol. 3. 1. 2012, pp. 37–31.

[247] Barreiro, J.; Castejón, M.; Alegre, E., and Hernández, L. K. "Use of Descriptors Based on Moments from Digital Images for Tool Wear Monitoring". *International Journal of Machine Tools and Manufacture* 48.9 (July 2008), pp. 1005–1013.

[248] Zhi, Gaofeng; He, Dedao; Sun, Weifang; Zhou, Yuqing; Pan, Xiaoming, and Gao, Chen. "An Edge-Labeling Graph Neural Network Method for Tool Wear Condition Monitoring Using Wear Image with Small Samples". *Measurement Science and Technology* 32.6 (Apr. 2021), p. 064006.

[249] Liang, Yu-Teng; Chiou, Yih-Chih, and Louh, Chien-Jiong. *Automatic Wear Measurement of Ti-based Coatings Milling via Image Registration*. Jan. 2005, pp. 88–91.

[250] Ramzi, Raiminor; Bakar, Elmi Abu, and Mahmod, M. F. "Drill Bit Flank Wear Monitoring System in Composite Drilling Process Using Image Processing". *10th International Conference on Robotics, Vision, Signal Processing and Power Applications*. Lecture Notes in Electrical Engineering. Singapore: Springer, 2019, pp. 551–557.

[251] Chethan, Y. D.; Ravindra, H. V.; Gowda, Y. T. Krishne, and Kumar, G. D. Mohan. "Parametric Optimization in Drilling EN-8 Tool Steel and Drill Wear Monitoring Using Machine Vision Applied with Taguchi Method". *Procedia Materials Science*. International Conference on Advances in Manufacturing and Materials Engineering, ICAMME 2014 5 (Jan. 2014), pp. 1442–1449.

[252] Otieno, Andrew; Pedapati, Chandhana; Wan, Xiaonan, and Zhang, Haiyan. "Imaging and Wear Analysis of Micro-tools Using Machine Vision". *Proceedings of the IJME Conference*. 2006, p. 9.

[253] Sharma, Ekta; Shivali; Jyotsna; Mahapatra, Prasant, and Doegar, Amit. "Tool Condition Monitoring Using the Chain Code Technique, Pixel Matching and Morphological Operations". *2017 3rd International Conference on Computational Intelligence Communication Technology (CICT)*. Feb. 2017, pp. 1–6.

[254] Pfeifer, T. and Wiegers, L. "Reliable Tool Wear Monitoring by Optimized Image and Illumination Control in Machine Vision". *Measurement* 28.3 (Oct. 2000), pp. 209–218.

[255] Rehorn, Adam G; Jiang, Jin, and Orban, Peter E. "State-of-the-Art Methods and Results in Tool Condition Monitoring: A Review". *The International Journal of Advanced Manufacturing Technology* 26 (2005), pp. 693–710.

[256] Takuma, Masanori; Shibasaka, T.; Yamamoto, Akio, and Teshima, T. "A Study on Tool Management System in Turning (1st Report)" (1994).

[257] Klancnik, S.; Ficko, M.; Balic, J., and Pahole, I. "Computer Vision-Based Approach to End Mill Tool Monitoring". *International Journal of Simulation Modelling* 14.4 (Jan. 2015), pp. 571–583.

[258] Yang, Min-yang and Kwon, Oh-dal. "A Tool Condition Recognition System Using Image Processing". *Control Engineering Practice* 6.11 (Nov. 1998), pp. 1389–1395.

[259] D'Addona, Doriana M.; Ullah, A. M. M. Sharif, and Matarazzo, D. "Tool-Wear Prediction and Pattern-Recognition Using Artificial Neural Network and DNA-based Computing". *Journal of Intelligent Manufacturing* 28.6 (Aug. 2017), pp. 1285–1301.

[260] Li, Pengyang; Li, Yan; Yang, Mingshun; Zheng, Jianming, and Yuan, Qilong. "Monitoring Technology Research of Tool Wear Condition Based on Machine Vision". *2008 7th World Congress on Intelligent Control and Automation*. June 2008, pp. 2783–2787.

[261] Marei, Mohamed; Zaatari, Shirine El, and Li, Weidong. "Transfer Learning Enabled Convolutional Neural Networks for Estimating Health State of Cutting Tools". *Robotics and Computer-Integrated Manufacturing* 71 (Oct. 2021), p. 102145.

[262] Mikołajczyk, T.; Nowicki, K.; Kłodowski, A., and Pimenov, D. Yu. "Neural Network Approach for Automatic Image Analysis of Cutting Edge Wear". *Mechanical Systems and Signal Processing* 88 (May 2017), pp. 100–110.

[263] Mikołajczyk, T.; Nowicki, K.; Bustillo, A., and Yu Pimenov, D. "Predicting Tool Life in Turning Operations Using Neural Networks and Image Processing". *Mechanical Systems and Signal Processing* 104 (May 2018), pp. 503–513.

[264] Bergs, Thomas; Holst, Carsten; Gupta, Pranjul, and Augspurger, Thorsten. "Digital Image Processing with Deep Learning for Automated Cutting Tool Wear Detection". *Procedia Manufacturing* 48 (2020), pp. 947–958.

[265] Holst, Carsten; Yavuz, Taha Berk; Gupta, Pranjul; Ganser, Philipp, and Bergs, Thomas. "Deep Learning and Rule-Based Image Processing Pipeline for Automated Metal Cutting Tool Wear Detection and Measurement". *IFAC-PapersOnLine* 55 (Jan. 2022), pp. 534–539.

[266] Treiss, Alexander; Walk, Jannis, and Kühl, Niklas. "An Uncertainty-based Human-in-the-loop System for Industrial Tool Wear Analysis". *Machine Learning and Knowledge Discovery in Databases. Applied Data Science and Demo Track: European Conference, ECML PKDD 2020, Ghent, Belgium, September 14-18, 2020, Proceedings, Part V*. Springer. 2021, pp. 85–100.

[267] Ren, Huanrong; Guo, Wei; Jiang, Pingyu, and Wan, Xu. "An Integrated Approach of Active Incremental Fine-Tuning, SegNet, and CRF for Cutting Tool Wearing Areas Segmentation with Small Samples". *Knowledge-Based Systems* 218 (Apr. 2021), p. 106838.

[268] Deng, Jia; Dong, Wei; Socher, Richard; Li, Li-Jia; Li, Kai, and Fei-Fei, Li. "ImageNet: A Large-Scale Hierarchical Image Database". *2009 IEEE Conference on Computer Vision and Pattern Recognition*. June 2009, pp. 248–255.

[269] Liu, Y.; Hu, Xiao-Feng, and Jin, J. "Remaining Useful Life Prediction of Cutting Tools Based on Deep Adversarial Transfer Learning". *ICCPR* (2019).

[270] Zhao, Zhibin; Zhang, Qiyang; Yu, Xiaolei; Sun, Chuang; Wang, Shibin; Yan, Ruqiang, and Chen, Xuefeng. "Unsupervised Deep Transfer Learning for Intelligent Fault Diagnosis: An Open Source and Comparative Study". *arXiv:1912.12528 [cs, eess]* (Dec. 2019).

[271] Wang, Lizhe; von Laszewski, Gregor; Younge, Andrew; He, Xi; Kunze, Marcel; Tao, Jie, and Fu, Cheng. "Cloud Computing: A Perspective Study". *New Generation Computing* 28.2 (Apr. 2010), pp. 137–146.

[272] Hayes, Brian. "Cloud Computing". *Communications of the ACM* 51.7 (July 2008), p. 911.

[273] Sultan, Nabil. "Cloud Computing for Education: A New Dawn?" *International Journal of Information Management* 30.2 (Apr. 2010), pp. 109–116.

[274] Vouk, Mladen A. "Cloud Computing – Issues, Research and Implementations". *Journal of computing and information technology* 16.4 (2008), pp. 235–246.

[275] Georgakopoulos, Dimitrios; Jayaraman, Prem Prakash; Fazia, Maria; Villari, Massimo, and Ranjan, Rajiv. "Internet of Things and Edge Cloud Computing Roadmap for Manufacturing". *IEEE Cloud Computing* 3.4 (July 2016), pp. 66–73.

[276]   Armbrust, Michael; Fox, Armando; Griffith, Rean; Joseph, Anthony D.; Katz, Randy; Konwinski, Andy; Lee, Gunho; Patterson, David; Rabkin, Ariel; Stoica, Ion, and Zaharia, Matei. "A View of Cloud Computing". *Communications of the ACM* 53.4 (Apr. 2010), pp. 50–58.

[277]   Rani, Dimpi and Ranjan, Rajiv Kumar. "A Comparative Study of SaaS, PaaS and IaaS in Cloud Computing". *International Journal of Advanced Research in Computer Science and Software Engineering* 4.6 (2014), p. 5.

[278]   Wu, Wei-Wen; Lan, Lawrence W., and Lee, Yu-Ting. "Exploring Decisive Factors Affecting an Organization's SaaS Adoption: A Case Study". *International Journal of Information Management* 31.6 (Dec. 2011), pp. 556–563.

[279]   Oliveira, Tiago; Thomas, Manoj, and Espadanal, Mariana. "Assessing the Determinants of Cloud Computing Adoption: An Analysis of the Manufacturing and Services Sectors". *Information & Management* 51.5 (July 2014), pp. 497–510.

[280]   Lou, P.; Liu, S.; Hu, J.; Li, R.; Xiao, Z., and Yan, J. "Intelligent Machine Tool Based on Edge-Cloud Collaboration". *IEEE Access* 8 (2020), pp. 139953–139965.

[281]   Shi, Weisong; Cao, Jie; Zhang, Quan; Li, Youhuizi, and Xu, Lanyu. "Edge Computing: Vision and Challenges". *IEEE Internet of Things Journal* 3.5 (Oct. 2016), pp. 637–646.

[282]   Satyanarayanan, Mahadev; Bahl, Paramvir; Caceres, Ramon, and Davies, Nigel. "The Case for VM-Based Cloudlets in Mobile Computing". *IEEE Pervasive Computing* 8.4 (Oct. 2009), pp. 14–23.

[283]   Bonomi, Flavio; Milito, Rodolfo; Zhu, Jiang, and Addepalli, Sateesh. "Fog Computing and Its Role in the Internet of Things". *Proceedings of the First Edition of the MCC Workshop on Mobile Cloud Computing - MCC '12*. Helsinki, Finland: ACM Press, 2012, p. 13.

[284]   Abbas, Nasir; Zhang, Yan; Taherkordi, Amir, and Skeie, Tor. "Mobile Edge Computing: A Survey". *IEEE Internet of Things Journal* 5.1 (Feb. 2018), pp. 450–465.

[285]   Khan, Wazir Zada; Ahmed, Ejaz; Hakak, Saqib; Yaqoob, Ibrar, and Ahmed, Arif. "Edge Computing: A Survey". *Future Generation Computer Systems* 97 (Aug. 2019), pp. 219–235.

[286]   Shi, Weisong and Dustdar, Schahram. "The Promise of Edge Computing". *Computer* 49.5 (May 2016), pp. 78–81.

[287]   Chen, Baotong; Wan, Jiafu; Celesti, Antonio; Li, Di; Abbas, Haider, and Zhang, Qin. "Edge Computing in IoT-Based Manufacturing". *IEEE Communications Magazine* 56.9 (Sept. 2018), pp. 103–109.

[288]   Satyanarayanan, Mahadev. "The Emergence of Edge Computing". *Computer* 50.1 (Jan. 2017), pp. 30–39.

[289]   Ahmed, Arif and Ahmed, Ejaz. "A Survey on Mobile Edge Computing". *2016 10th International Conference on Intelligent Systems and Control (ISCO)*. Coimbatore, India: IEEE, Jan. 2016, pp. 1–8.

[290]   Liu, B.; Zhang, Y.; Zhang, G., and Zheng, P. "Edge-Cloud Orchestration Driven Industrial Smart Product-Service Systems Solution Design Based on CPS and IIoT". *Advanced Engineering Informatics* 42 (2019).

[291]   Zhang, J.; Deng, C.; Zheng, P.; Xu, X., and Ma, Z. "Development of an Edge Computing-Based Cyber-Physical Machine Tool". *Robotics and Computer-Integrated Manufacturing* 67 (2021).

[292]   Vater, J.; Harscheidt, L., and Knoll, A. "A Reference Architecture Based on Edge and Cloud Computing for Smart Manufacturing". *Proceedings - International Conference on Computer Communications and Networks, ICCCN*. Vol. 2019-July. 2019.

[293]   Lee, K.-T.; Lee, Y.-S., and Yoon, H. "Development of Edge-based Deep Learning Prediction Model for Defect Prediction in Manufacturing Process". *ICTC 2019 - 10th International Conference on ICT Convergence: ICT Convergence Leading the Autonomous Future*. 2019, pp. 248–250.

[294]   MacKenzie, C Matthew; Laskey, Ken; McCabe, Francis; Brown, Peter F; Metz, Rebekah, and Hamilton, Booz Allen. "Reference model for service oriented architecture 1.0". *OASIS standard* 12.S18 (2006), pp. 1–31.

[295]   Niknejad, Naghmeh; Ismail, Waidah; Ghani, Imran; Nazari, Behzad, and Bahari, Mahadi. "Understanding Service-Oriented Architecture (SOA): A Systematic Literature Review and Directions for Further Investigation". *Information Systems* (2020), p. 27.

[296]   Fuchs, Jonathan; Oks, Sascha Julian, and Franke, Jörg. "Platform-Based Service Composition for Manufacturing: A Conceptualization". *Procedia CIRP* 81 (Jan. 2019), pp. 541–546.

[297]   Newman, Sam. *Building Microservices: Designing Fine-Grained Systems*. First Edition. Beijing Sebastopol, CA: O'Reilly Media, 2015.

[298]   Fuchs, J.; Herrmann, H.; Oks, S. J.; Sjarov, M., and Franke, J. "Increasing Efficiency in Maintenance Processes Through Modular Service Bundles". *Production at the Leading Edge of Technology*. Berlin, Heidelberg: Springer Berlin Heidelberg, 2021, pp. 439–447.

[299]   Schäffer, Eike; Mayr, Andreas; Fuchs, Jonathan; Sjarov, Martin; Vorndran, Johannes, and Franke, Jörg. "Microservice-Based Architecture for Engineering Tools Enabling a Collaborative Multi-User Configuration of Robot-Based Automation Solutions". *Procedia CIRP* 86 (Oct. 2019), pp. 86–91.

[300]   Schäffer, Eike Wolfram. "Web- and knowledge-based engineering configurator for robot-centric automation solutionsWeb- und wissensbasierter Engineering-Konfigurator für roboterzentrierte Automatisierungslösungen". PhD thesis. FAU University Press, 2021.

[301]   Ghosh, Swarnendu; Das, Nibaran; Das, Ishita, and Maulik, Ujjwal. "Understanding Deep Learning Techniques for Image Segmentation". *ACM Computing Surveys* 52.4 (Sept. 2019), pp. 1–35.

[302]   Schwenzer, Max. "Big Data Magic : Revolutioniert Maschinelles Lernen Die Zerspanung?" RWTH-2018-231728 (2018).

[303]   Yu, Lean; Wang, Shouyang, and Lai, K.K. "An Integrated Data Preparation Scheme for Neural Network Data Analysis". *IEEE Transactions on Knowledge and Data Engineering* 18.2 (Feb. 2006), pp. 217–230.

[304]   Zhang, Shichao; Zhang, Chengqi, and Yang, Qiang. "Data Preparation for Data Mining". *Applied Artificial Intelligence* 17.5-6 (May 2003), pp. 375–381.

[305]   Witten, Ian H.; Frank, Eibe; Hall, Mark A., and Pal, Christopher J. *Data Mining: Practical Machine Learning Tools and Techniques*. Morgan Kaufmann, Jan. 2016.

[306]   Lepot, Mathieu; Aubin, Jean-Baptiste, and Clemens, François H. L. R. "Interpolation in Time Series: An Introductive Overview of Existing Methods, Their Performance Criteria and Uncertainty Assessment". *Water* 9.10 (Oct. 2017), p. 796.

[307]   Berndt, Donald J and Clifford, James. "Using Dynamic Time Warping to Find Patterns in Time Series." *KDD Workshop*. Vol. 10. 1994, pp. 359–370.

[308]   Petitjean, François; Ketterlin, Alain, and Gançarski, Pierre. "A Global Averaging Method for Dynamic Time Warping, with Applications to Clustering". *Pattern Recognition* 44.3 (Mar. 2011), pp. 678–693.

[309] Shapira Weber, Ron A; Eyal, Matan; Skafte, Nicki; Shriki, Oren, and Freifeld, Oren. "Diffeomorphic Temporal Alignment Nets". *Advances in Neural Information Processing Systems*. Vol. 32. Curran Associates, Inc., 2019.

[310] Ratanamahatana, Chotirat Ann and Keogh, Eamonn. "Making Time-series Classification More Accurate Using Learned Constraints". *Proceedings of the 2004 SIAM International Conference on Data Mining*. Society for Industrial and Applied Mathematics, Apr. 2004, pp. 11–22.

[311] Nargesian, Fatemeh; Samulowitz, Horst; Khurana, Udayan; Khalil, Elias B., and Turaga, Deepak. "Learning Feature Engineering for Classification". *Proceedings of the Twenty-Sixth International Joint Conference on Artificial Intelligence*. Melbourne, Australia: International Joint Conferences on Artificial Intelligence Organization, Aug. 2017, pp. 2529–2535.

[312] Hong, G.S.; Rahman, M., and Zhou, Q. "Using Neural Network for Tool Condition Monitoring Based on Wavelet Decomposition". *International Journal of Machine Tools and Manufacture* 36.5 (May 1996), pp. 551–566.

[313] Quan, Y.; Zhou, M., and Luo, Z. "On-Line Robust Identification of Tool-Wear via Multi-Sensor Neural-Network Fusion". *Engineering Applications of Artificial Intelligence* 6.11 (1998), pp. 717–722.

[314] Jemielniak, Krzysztof; Kwiatkowski, Leszek, and Wrzosek, Paweł. "Diagnosis of Tool Wear Based on Cutting Forces and Acoustic Emission Measures as Inputs to a Neural Network". *Journal of Intelligent Manufacturing* 9 (Oct. 1998), pp. 447–455.

[315] Scheffer, C. and Heyns, P. S. "An Industrial Tool Wear Monitoring System for Interrupted Turning". *Mechanical Systems and Signal Processing* 18.5 (Sept. 2004), pp. 1219–1242.

[316] Kohavi, Ron and John, George H. "Wrappers for Feature Subset Selection". *Artificial Intelligence* 97.1-2 (Dec. 1997), pp. 273–324.

[317] Van Der Maaten, Laurens; Postma, Eric, and Van den Herik, Jaap. "Dimensionality Reduction: A Comparative". *Journal of machine learning research : JMLR* 10.66-71 (2009), p. 13.

[318] Golub, G. H. and Reinsch, C. "Singular Value Decomposition and Least Squares Solutions". *Linear Algebra*. Berlin, Heidelberg: Springer Berlin Heidelberg, 1971, pp. 134–151.

[319] Wold, Svante; Esbensen, Kim, and Geladi, Paul. "Principal Component Analysis". *Chemometrics and intelligent laboratory systems* 2.1-3 (1987), pp. 37–52.

[320]   Van der Maaten, Laurens and Hinton, Geoffrey. "Visualizing Data Using T-SNE." *Journal of machine learning research* 9.11 (2008).

[321]   Russell, Stuart and Norvig, Peter. "Artificial Intelligence: A Modern Approach" (2002).

[322]   Samuel, A. L. "Some Studies in Machine Learning Using the Game of Checkers". *IBM Journal of Research and Development* 3.3 (July 1959), pp. 210–229.

[323]   Cunningham, P; Cord, M, and Delany, S. "Chapter 2. Supervised Learning". *Machine Learning Techniques for Multimedia. Springer-Verlag Berlin Heidelberg*, pp. 21–46.

[324]   Murphy, Kevin P. *Machine Learning: A Probabilistic Perspective*. Adaptive Computation and Machine Learning Series. Cambridge, MA: MIT Press, 2012.

[325]   Sutton, Richard S and Barto, Andrew G. *Reinforcement Learning: An Introduction*. MIT press, 2018.

[326]   Suárez-Díaz, Juan Luis; García, Salvador, and Herrera, Francisco. "A Tutorial on Distance Metric Learning: Mathematical Foundations, Algorithms, Experimental Analysis, Prospects and Challenges (with Appendices on Mathematical Background and Detailed Algorithms Explanation)". *arXiv:1812.05944 [cs, stat]* (Aug. 2020). eprint: 1812.05944.

[327]   Settles, Burr. "Active Learning Literature Survey" (2009), p. 47.

[328]   Quinlan, J. R. "Induction of Decision Trees". *Machine Learning* 1.1 (Mar. 1986), pp. 81–106.

[329]   Kotsiantis, S. B. "Decision Trees: A Recent Overview". *Artificial Intelligence Review* 39.4 (Apr. 2013), pp. 261–283.

[330]   Hastie, Trevor; Tibshirani, Robert, and Friedman, Jerome. *The Elements of Statistical Learning*. Springer Series in Statistics. New York, NY: Springer New York, 2009.

[331]   Quinlan, J Ross. "C 4.5: Programs for Machine Learning". *The Morgan Kaufmann Series in Machine Learning* (1993).

[332]   Breiman, L; Friedman, JH; Olshen, R, and Stone, CJ. "Classification and Regression Trees" (1984).

[333]   Schapire, Robert E. "The Boosting Approach to Machine Learning: An Overview". *Nonlinear Estimation and Classification*. Vol. 171. New York, NY: Springer New York, 2003, pp. 149–171.

[334]   Breiman, Leo. "Bagging Predictors". *Machine Learning* 24.2 (Aug. 1996), pp. 123–140.

[335]   Breiman, Leo. "Random Forests". *Machine Learning* 45.1 (Oct. 2001), pp. 5–32.

[336]   Freund, Yoav and Schapire, Robert E. "A Decision-Theoretic Generalization of On-Line Learning and an Application to Boosting". *Journal of Computer and System Sciences* 55.1 (Aug. 1997), pp. 119–139.

[337]   Chen, Tianqi and Guestrin, Carlos. "XGBoost: A Scalable Tree Boosting System". *Proceedings of the 22nd ACM SIGKDD International Conference on Knowledge Discovery and Data Mining*. San Francisco California USA: ACM, Aug. 2016, pp. 785–794.

[338]   Elith, J.; Leathwick, J. R., and Hastie, T. "A Working Guide to Boosted Regression Trees". *Journal of Animal Ecology* 77.4 (2008), pp. 802–813.

[339]   Liu, Fei Tony; Ting, Kai Ming, and Zhou, Zhi-Hua. "Isolation Forest". *2008 Eighth IEEE International Conference on Data Mining*. Dec. 2008, pp. 413–422.

[340]   Vapnik, Vladimir and Chervonenkis, Alexey. *Theory of Pattern Recognition*. 1974.

[341]   Widodo, Achmad and Yang, Bo-Suk. "Support Vector Machine in Machine Condition Monitoring and Fault Diagnosis". *Mechanical Systems and Signal Processing* (2007), p. 15.

[342]   Suykens, J.A.K. and Vandewalle, J. "Least Squares Support Vector Machine Classifiers". *Neural Processing Letters* 9.3 (1999), pp. 293–300.

[343]   Erfani, Sarah M.; Rajasegarar, Sutharshan; Karunasekera, Shanika, and Leckie, Christopher. "High-Dimensional and Large-Scale Anomaly Detection Using a Linear One-Class SVM with Deep Learning". *Pattern Recognition* 58 (Oct. 2016), pp. 121–134.

[344]   Tax, David M.J. and Duin, Robert P.W. "Support Vector Data Description". *Machine Learning* 54.1 (Jan. 2004), pp. 45–66.

[345]   Yean, Choong Wen; Khairunizam, Wan; Omar, Mohammad Iqbal; Murugappan, Murugappan; Zheng, Bong Siao; Bakar, Shahriman Abu; Razlan, Zuradzman Mohamad, and Ibrahim, Zunaidi. "Analysis of The Distance Metrics of KNN Classifier for EEG Signal in Stroke Patients". *2018 International Conference on Computational Approach in Smart Systems Design and Applications (ICASSDA)*. Aug. 2018, pp. 1–4.

[346]   MacQueen, James. "Some Methods for Classification and Analysis of Multivariate Observations". *Proceedings of the Fifth Berkeley Symposium on Mathematical Statistics and Probability*. Vol. 1. 1967, pp. 281–297.

[347]   Grygorash, Oleksandr; Zhou, Yan, and Jorgensen, Zach. "Minimum Spanning Tree Based Clustering Algorithms". *2006 18th IEEE International Conference on Tools with Artificial Intelligence (ICTAI'06)*. Nov. 2006, pp. 73–81.

[348]   Fred, A.L.N. and Jain, A.K. "Data Clustering Using Evidence Accumulation". *Object Recognition Supported by User Interaction for Service Robots*. Vol. 4. Quebec City, Que., Canada: IEEE Comput. Soc, 2002, pp. 276–280.

[349]   Goodfellow, Ian; Bengio, Yoshua, and Courville, Aaron. *Deep Learning*. MIT press, 2016.

[350]   Sharma, Siddharth; Sharma, Simone; Scholar, UG, and Athaiya, Anidhya. "Activation Functions in Neural Networks". *International Journal of Engineering Applied Sciences and Technology* 4.12 (2020), pp. 310–316.

[351]   Kingma, Diederik P. and Ba, Jimmy. *Adam: A Method for Stochastic Optimization*. Tech. rep. Dec. 2014.

[352]   Studer, Stefan; Bui, Thanh Binh; Drescher, Christian; Hanuschkin, Alexander; Winkler, Ludwig; Peters, Steven, and Müller, Klaus-Robert. "Towards CRISP-ML(Q): A Machine Learning Process Model with Quality Assurance Methodology". *Machine Learning and Knowledge Extraction* 3.2 (Apr. 2021), pp. 392–413. arXiv: 2003.05155.

[353]   Wirth, Rüdiger and Hipp, Jochen. "CRISP-DM: Towards a Standard Process Model for Data Mining". 1 (2000), pp. 29–39.

[354]   Papadopoulos, Dim P.; Clarke, Alasdair D. F.; Keller, Frank, and Ferrari, Vittorio. "Training Object Class Detectors from Eye Tracking Data". *Computer Vision – ECCV 2014*. Vol. 8693. Cham: Springer International Publishing, 2014, pp. 361–376.

[355]   Boykov, Y.Y. and Jolly, M.-P. "Interactive Graph Cuts for Optimal Boundary & Region Segmentation of Objects in N-D Images". *Proceedings Eighth IEEE International Conference on Computer Vision. ICCV 2001*. Vol. 1. Vancouver, BC, Canada: IEEE Comput. Soc, 2001, pp. 105–112.

[356]   Lin, Di; Dai, Jifeng; Jia, Jiaya; He, Kaiming, and Sun, Jian. "ScribbleSup: Scribble-Supervised Convolutional Networks for Semantic Segmentation". *2016 IEEE Conference on Computer Vision and Pattern Recognition (CVPR)*. Las Vegas, NV, USA: IEEE, June 2016, pp. 3159–3167.

[357] Maninis, K.-K.; Caelles, S.; Pont-Tuset, J., and Van Gool, L. "Deep Extreme Cut: From Extreme Points to Object Segmentation". *2018 IEEE/CVF Conference on Computer Vision and Pattern Recognition*. Salt Lake City, UT, USA: IEEE, June 2018, pp. 616–625.

[358] Benenson, Rodrigo; Popov, Stefan, and Ferrari, Vittorio. "Large-Scale Interactive Object Segmentation With Human Annotators". *2019 IEEE/CVF Conference on Computer Vision and Pattern Recognition (CVPR)*. Long Beach, CA, USA: IEEE, June 2019, pp. 11692–11701.

[359] Bragantini, Jordão; Falcão, Alexandre, and Najman, Laurent. "Rethinking Interactive Image Segmentation: Feature Space Annotation". *arXiv:2101.04378 [cs]* (Jan. 2021).

[360] Wolpert, David H. "The Lack of A Priori Distinctions Between Learning Algorithms". *Neural Computation* 8.7 (Oct. 1996), pp. 1341–1390.

[361] Kohavi, Ron and John, George H. "Automatic Parameter Selection by Minimizing Estimated Error". *Machine Learning Proceedings 1995*. Elsevier, 1995, pp. 304–312.

[362] Bergstra, James and Bengio, Yoshua. "Random Search for Hyper-Parameter Optimization." *Journal of machine learning research* 13.2 (2012).

[363] Shahriari, Bobak; Swersky, Kevin; Wang, Ziyu; Adams, Ryan P., and de Freitas, Nando. "Taking the Human Out of the Loop: A Review of Bayesian Optimization". *Proceedings of the IEEE* 104.1 (Jan. 2016), pp. 148–175.

[364] *Automated Machine Learning: Methods, Systems, Challenges*. The Springer Series on Challenges in Machine Learning. Cham: Springer International Publishing, 2019.

[365] Zoph, Barret and Le, Quoc V. "Neural Architecture Search with Reinforcement Learning". *arXiv:1611.01578 [cs]* (Feb. 2017).

[366] Ebadi, Ashkan; Gauthier, Yvan; Tremblay, Stéphane, and Paul, Patrick. "How Can Automated Machine Learning Help Business Data Science Teams?" *2019 18th IEEE International Conference On Machine Learning And Applications (ICMLA)*. Dec. 2019, pp. 1186–1191.

[367] LeCun, Yann; Bengio, Yoshua; Bottou, Léon, and Haffner, Patrick. "Gradient-Based Learning Applied to Document Recognition". *Proceedings of the IEEE* (Jan. 1998), pp. 2278–2324.

[368] O'Shea, Keiron and Nash, Ryan. "An Introduction to Convolutional Neural Networks". *arXiv:1511.08458 [cs]* (Dec. 2015).

[369]   Albawi, Saad; Mohammed, Tareq Abed, and Al-Zawi, Saad. "Under-
standing of a Convolutional Neural Network". *2017 International Con-
ference on Engineering and Technology (ICET)*. Aug. 2017, pp. 1–6.

[370]   Ronneberger, Olaf; Fischer, Philipp, and Brox, Thomas. *U-Net: Con-
volutional Networks for Biomedical Image Segmentation*. Tech. rep.
May 2015.

[371]   Zhou, Zongwei; Siddiquee, Md Mahfuzur Rahman; Tajbakhsh, Nima,
and Liang, Jianming. "UNet++: A Nested U-Net Architecture for Med-
ical Image Segmentation". *Deep Learning in Medical Image Analysis
and Multimodal Learning for Clinical Decision Support : 4th Inter-
national Workshop, DLMIA 2018, and 8th International Workshop,
ML-CDS 2018, held in conjunction with MICCAI 2018, Granada, Spain,
S* 11045 (Sept. 2018), pp. 3–11.

[372]   Oktay, Ozan; Schlemper, Jo; Folgoc, Loic Le; Lee, Matthew; Hein-
rich, Mattias; Misawa, Kazunari; Mori, Kensaku; McDonagh, Steven;
Hammerla, Nils Y.; Kainz, Bernhard; Glocker, Ben, and Rueckert,
Daniel. "Attention U-Net: Learning Where to Look for the Pancreas".
arXiv:1804.03999 [cs] (May 2018).

[373]   He, Kaiming; Zhang, Xiangyu; Ren, Shaoqing, and Sun, Jian. "Deep
Residual Learning for Image Recognition". *Proceedings of the IEEE
conference on computer vision and pattern recognition*. 2016, pp. 770–
778.

[374]   Chaurasia, Abhishek and Culurciello, Eugenio. "LinkNet: Exploiting
Encoder Representations for Efficient Semantic Segmentation" (Jan.
2017), pp. 1–4.

[375]   Zhou, Bolei; Khosla, Aditya; Lapedriza, Agata; Oliva, Aude, and
Torralba, Antonio. "Object Detectors Emerge in Deep Scene CNNs".
arXiv:1412.6856 [cs] (Apr. 2015).

[376]   Zhao, Hengshuang; Shi, Jianping; Qi, Xiaojuan; Wang, Xiaogang, and
Jia, Jiaya. "Pyramid Scene Parsing Network". *2017 IEEE Conference
on Computer Vision and Pattern Recognition (CVPR)*. Honolulu, HI:
IEEE, July 2017, pp. 6230–6239.

[377]   Holschneider, Matthias; Kronland-Martinet, Richard; Morlet, Jean,
and Tchamitchian, Ph. "A Real-Time Algorithm for Signal Analysis
with the Help of the Wavelet Transform". *Wavelets*. Springer, 1990,
pp. 286–297.

[378]   Chen, Liang-Chieh; Papandreou, George; Schroff, Florian, and Adam,
Hartwig. "Rethinking Atrous Convolution for Semantic Image Seg-
mentation". *arXiv:1706.05587 [cs]* (Dec. 2017).

[379]   Chen, Liang-Chieh; Zhu, Yukun; Papandreou, George; Schroff, Florian, and Adam, Hartwig. "Encoder-Decoder with Atrous Separable Convolution for Semantic Image Segmentation". *Computer Vision – ECCV 2018*. Vol. 11211. Cham: Springer International Publishing, 2018, pp. 833–851.

[380]   Goodfellow, Ian J.; Pouget-Abadie, Jean; Mirza, Mehdi; Xu, Bing; Warde-Farley, David; Ozair, Sherjil; Courville, Aaron, and Bengio, Yoshua. "Generative Adversarial Networks". *Advances in neural information processing systems* 27 (2014).

[381]   Shrivastava, Ashish; Pfister, Tomas; Tuzel, Oncel; Susskind, Joshua; Wang, Wenda, and Webb, Russell. "Learning from Simulated and Unsupervised Images through Adversarial Training" (2017), pp. 2107–2116.

[382]   Mirza, Mehdi and Osindero, Simon. "Conditional Generative Adversarial Nets". *arXiv:1411.1784 [cs, stat]* (Nov. 2014).

[383]   Isola, Phillip; Zhu, Jun-Yan; Zhou, Tinghui, and Efros, Alexei A. "Image-to-Image Translation with Conditional Adversarial Networks". *Proceedings of the IEEE conference on computer vision and pattern recognition*. 2017, pp. 1125–1134.

[384]   Radford, Alec; Metz, Luke, and Chintala, Soumith. "Unsupervised Representation Learning with Deep Convolutional Generative Adversarial Networks". *arXiv:1511.06434 [cs]* (Jan. 2016).

[385]   Ioffe, Sergey and Szegedy, Christian. "Batch Normalization: Accelerating Deep Network Training by Reducing Internal Covariate Shift". *International conference on machine learning*. pmlr. 2015, pp. 448–456.

[386]   Wang, Ting-Chun; Liu, Ming-Yu; Zhu, Jun-Yan; Tao, Andrew; Kautz, Jan, and Catanzaro, Bryan. "High-Resolution Image Synthesis and Semantic Manipulation with Conditional GANs". *Proceedings of the IEEE conference on computer vision and pattern recognition*. 2018, pp. 8798–8807.

[387]   Thoma, Martin. "A Survey of Semantic Segmentation". *arXiv:1602.06541 [cs]* (May 2016).

[388]   Wong, Y.S.; Yuen, W.K.; Lee, K.S., and Bradley, C. "Machine vision monitoring of tool wear". *Sensors and Controls for Intelligent Machining, Agile Manufacturing, and Mechatronics*. Vol. 3518. 1998, pp. 17–24.

[389]   Feurer, Matthias; Klein, Aaron; Eggensperger, Katharina; Springen-berg, Jost; Blum, Manuel, and Hutter, Frank. "Efficient and Robust Automated Machine Learning". *Advances in neural information processing systems* 28 (2015), p. 9.

[390]   Jin, Haifeng; Song, Qingquan, and Hu, Xia. "Auto-Keras: An Efficient Neural Architecture Search System". *Proceedings of the 25th ACM SIGKDD International Conference on Knowledge Discovery & Data Mining*. ACM. 2019, pp. 1946–1956.

[391]   Jampani, Varun; Sun, Deqing; Liu, Ming-Yu; Yang, Ming-Hsuan, and Kautz, Jan. "Superpixel Sampling Networks". *Computer Vision – ECCV 2018*. Vol. 11211. Cham: Springer International Publishing, 2018, pp. 363–380.

[392]   Achanta, Radhakrishna; Shaji, Appu; Smith, Kevin; Lucchi, Aurelien; Fua, Pascal, and Süsstrunk, Sabine. "SLIC Superpixels Compared to State-of-the-Art Superpixel Methods". *IEEE Transactions on Pattern Analysis and Machine Intelligence* 34.11 (Nov. 2012), pp. 2274–2282.

[393]   Milbich, Timo; Roth, Karsten; Brattoli, Biagio, and Ommer, Björn. "Sharing Matters for Generalization in Deep Metric Learning". *IEEE Transactions on Pattern Analysis and Machine Intelligence* (2020), pp. 1–1. arXiv: 2004.05582.

[394]   Zhuang, Fuzhen; Qi, Zhiyuan; Duan, Keyu; Xi, Dongbo; Zhu, Yongchun; Zhu, Hengshu; Xiong, Hui, and He, Qing. "A Comprehensive Survey on Transfer Learning". *Proceedings of the IEEE* 109.1 (Jan. 2021), pp. 43–76.

[395]   Boris, N. "Delaunay. Sur La Sphere Vide". *Izvestia Akademia Nauk SSSR, VII Seria, Otdelenie Matematicheskii i Estestvennyka Nauk* 7 (1934), pp. 793–800.

[396]   Canny, John. "A Computational Approach to Edge Detection". *IEEE Transactions on Pattern Analysis and Machine Intelligence* PAMI-8.6 (Nov. 1986), pp. 679–698.

[397]   Shannon, C.E. "Communication in the Presence of Noise". *Proceedings of the IRE* 37.1 (Jan. 1949), pp. 10–21.

[398]   Neugebauer, R.; Drossel, W.; Wertheim, R.; Hochmuth, C., and Dix, M. "Resource and Energy Efficiency in Machining Using High-Performance and Hybrid Processes". *Procedia CIRP* 1 (2012), pp. 3–16.

[399]   Knöpfel, Andreas; Gröne, Bernhard, and Tabeling, Peter. "Fundamental Modeling Concepts". *Effective Communication of IT Systems, England* 51 (2005).

[400] Light, Roger A. "Mosquitto: Server and Client Implementation of the MQTT Protocol". *Journal of Open Source Software* 2.13 (2017), p. 265.

[401] *Cloud Foundry – Open Source Cloud Native Application Delivery*. https://www.cloudfoundry.org/. (Visited on 09/21/2021).

[402] *Docker CE*. Docker. Sept. 2021. (Visited on 09/28/2021).

[403] *This Is Python Version 3.11.0 Alpha 0*. Python. Sept. 2021. (Visited on 09/28/2021).

[404] *InfluxDB*. InfluxData. Sept. 2021. (Visited on 09/28/2021).

[405] Giorgino, Toni. "Computing and Visualizing Dynamic Time Warping Alignments in R: The Dtw Package". *Journal of Statistical Software* 31.7 (2009).

[406] Abadi, Martín; Agarwal, Ashish; Barham, Paul; Brevdo, Eugene; Chen, Zhifeng; Citro, Craig; Corrado, Greg S.; Davis, Andy; Dean, Jeffrey; Devin, Matthieu; Ghemawat, Sanjay; Goodfellow, Ian; Harp, Andrew; Irving, Geoffrey; Isard, Michael; Jia, Yangqing; Jozefowicz, Rafal; Kaiser, Lukasz; Kudlur, Manjunath; Levenberg, Josh; Mané, Dan; Monga, Rajat; Moore, Sherry; Murray, Derek; Olah, Chris; Schuster, Mike; Shlens, Jonathon; Steiner, Benoit; Sutskever, Ilya; Talwar, Kunal; Tucker, Paul; Vanhoucke, Vincent; Vasudevan, Vijay; Viégas, Fernanda; Vinyals, Oriol; Warden, Pete; Wattenberg, Martin; Wicke, Martin; Yu, Yuan, and Zheng, Xiaoqiang. *TensorFlow: Large-scale Machine Learning on Heterogeneous Systems*. Jan. 2015.

[407] Pedregosa, F.; Varoquaux, G.; Gramfort, A.; Michel, V.; Thirion, B.; Grisel, O.; Blondel, M.; Prettenhofer, P.; Weiss, R.; Dubourg, V.; Vanderplas, J.; Passos, A.; Cournapeau, D.; Brucher, M.; Perrot, M., and Duchesnay, E. "Scikit-Learn: Machine Learning in Python". *Journal of Machine Learning Research* 12 (2011), pp. 2825–2830.

[408] Grinberg, Miguel. *Python-Socketio*. Sept. 2021. (Visited on 09/21/2021).

[409] Paszke, Adam; Gross, Sam; Massa, Francisco; Lerer, Adam; Bradbury, James; Chanan, Gregory; Killeen, Trevor; Lin, Zeming; Gimelshein, Natalia; Antiga, Luca, et al. "PyTorch: An Imperative Style, High-Performance Deep Learning Library". *Advances in neural information processing systems* 32 (2019), p. 12.

[410] *Vue.Js*. https://vuejs.org/#. (Visited on 08/14/2021).

[411] *Ubuntu Manpage: Fswebcam - Small and Simple Webcam for *nix*. http://manpages.ubuntu.com/manpages/bionic/man1/fswebcam.1.html. (Visited on 09/21/2021).

[412]   Liaw, Richard; Liang, Eric; Nishihara, Robert; Moritz, Philipp; Gonzalez, Joseph E, and Stoica, Ion. "Tune: A Research Platform for Distributed Model Selection and Training". *arXiv preprint arXiv:1807.05118* (2018).

[413]   Butterworth, Stephen. "On the Theory of Filter Amplifiers". *Wireless Engineer* 7.6 (1930), pp. 536–541.

[414]   Savitzky, Abraham and Golay, Marcel JE. "Smoothing and Differentiation of Data by Simplified Least Squares Procedures." *Analytical chemistry* 36.8 (1964), pp. 1627–1639.

Own publications referring to this work

[P1] Lutz, Benjamin; Kisskalt, Dominik; Regulin, Daniel; Hauser, Tobias, and Franke, Jörg. "Material Identification for Smart Manufacturing Systems: A Review". *2021 4th IEEE International Conference on Industrial Cyber-Physical Systems (ICPS)*. May 2021, 353 bibrangedash 360.

[P2] Mayr, Andreas; Kißkalt, Dominik; Meiners, Moritz; Lutz, Benjamin; Schäfer, Franziska; Seidel, Reinhardt; Selmaier, Andreas; Fuchs, Jonathan; Metzner, Maximilian; Blank, Andreas, and Franke, Jörg. "Machine Learning in Production – Potentials, Challenges and Exemplary Applications". *Procedia CIRP* 86 (Jan. 2019), pp. 49–54.

[P3] Lutz, Benjamin and Regulin, Daniel. "Determining the level of wear of a tool". WO2021023514A1. Feb. 2021.

[P4] Lutz, Benjamin Samuel and Regulin, Daniel. "Method to Train a Neural Network to Detect a Tool Status from Images, Method of Machining and/or Manufacturing, and Installation". US20220067913A1. Mar. 2022.

[P5] Janisch, Lucas and Lutz, Benjamin Samuel. "Methods and Systems for Generating Segmentation Masks". WO2023072744A1. May 2023.

[P6] Lutz, Benjamin; Reisch, Raven; Kisskalt, Dominik; Avci, Behiye; Regulin, Daniel; Knoll, Alois, and Franke, Jörg. "Benchmark of Automated Machine Learning with State-of-the-Art Image Segmentation Algorithms for Tool Condition Monitoring". *Procedia Manufacturing*. 30th International Conference on Flexible Automation and Intelligent Manufacturing (FAIM2021) 51 (Jan. 2020), pp. 215–221.

[P7] Lutz, Benjamin; Kisskalt, Dominik; Regulin, Daniel; Reisch, Raven; Schiffler, Andreas, and Franke, Jörg. "Evaluation of Deep Learning for Semantic Image Segmentation in Tool Condition Monitoring". *2019 18th IEEE International Conference On Machine Learning And Applications (ICMLA)*. Boca Raton, FL, USA: IEEE, Dec. 2019, pp. 2008–2013.

[P8] Lutz, Benjamin; Kisskalt, Dominik; Regulin, Daniel; Aybar, Burak, and Franke, Jörg. "Automated Domain Adaptation in Tool Condition Monitoring Using Generative Adversarial Networks". *2021 IEEE 17th International Conference on Automation Science and Engineering (CASE)*. Aug. 2021, pp. 1326–1331.

[P9] Lutz, Benjamin; Janisch, Lucas; Kisskalt, Dominik; Regulin, Daniel, and Franke, Jörg. "Interactive Image Segmentation Using Superpixels and Deep Metric Learning for Tool Condition Monitoring". *Procedia CIRP* 118 (2023), pp. 459–464.

[P10] Lutz, Benjamin; Howell, Philip; Regulin, Daniel; Engelmann, Bastian, and Franke, Jörg. "Towards Material-Batch-Aware Tool Condition Monitoring". *Journal of Manufacturing and Materials Processing* 5.4 (Sept. 2021), p. 103.

[P11] Lutz, Benjamin; Kisskalt, Dominik; Mayr, Andreas; Regulin, Daniel; Pantano, Matteo, and Franke, Jörg. "In-Situ Identification of Material Batches Using Machine Learning for Machining Operations". *Journal of Intelligent Manufacturing* 32 (2021), pp. 1485–1495.

[P12] Lutz, Benjamin Samuel and Regulin, Daniel. "Verfahren zur subtraktiven Bearbeitung eines Materials, Steuerungseinrichtung und Fertigungsanlage". DE102020201077A1. July 2021.

[P13] Lutz, Benjamin; Kisskalt, Dominik; Regulin, Daniel, and Franke, Jörg. "AI-based Approach for Predicting the Machinability under Consideration of Material Batch Deviations in Turning Processes". *Procedia CIRP* 93 (2020), pp. 1382–1387.

Students' theses referring to this work

[S1]   Roider, Christoph. "Systematische Analyse von Datengetriebenen Lösungsansätzen zur Berücksichtigung Material-Spezifischer Abweichungen in der Subtraktiven Fertigung". Bachelor Thesis. Erlangen: Friedrich-Alexander-Universität Erlangen-Nürnberg, Sept. 2020.

[S2]   Rester, Robin. "Identifikation und Analyse von Lösungen der automatisierten Materialerkennung in der intelligenten Fertigung". Bachelor Thesis. Erlangen: Friedrich-Alexander-Universität Erlangen-Nürnberg, Aug. 2021.

[S3]   Aybar, Burak. "GAN Based Image-to-Image Translation for Domain Adaptation in Tool Condition Monitoring". Master Thesis. Munich: Technische Universität München, Mar. 2021.

[S4]   Avci, Behiye. "Deep Learning Based Industrial Process Data Analysis and Optimization". Master Thesis. Technische Universität München, Apr. 2020.

[S5]   Janisch, Lucas. "Conception and Implementation of an Active Learning Approach to Generate Multi-Class Annotated Data Using Deep Learning Methods". Master Thesis. Erlangen: Friedrich-Alexander-Universität Erlangen-Nürnberg, 2021.

[S6]   Haigis, Natalja. "Vergleich der Systemarchitekturen intelligenter Werkzeugmaschinen zur Befähigung simulationsgestützter Lernverfahren". Master Thesis. Erlangen: Friedrich-Alexander-Universität Erlangen-Nürnberg.

[S7]   Hahnkamp, Manuel. "Analyse von Einflussfaktoren auf die visuelle Ausprägung bei der Werkzeugzustandsüberwachung von Schneidwerkzeugen". Project Thesis. Erlangen: Friedrich-Alexander-Universität Erlangen-Nürnberg.

[S8]   Krishna, Ajay. "Machine Learning Based Optimization and Time-Series Analysis for Smart Manufacturing Processes". Master Thesis. Hochschule Furtwangen University, May 2021.

[S9]   Schmidt, Timon. "Konzipierung und Implementierung eines lernenden Verfahrens zur Erkennung und Identifizierung von Bauteilen". Bachelor Thesis. Erlangen: Friedrich-Alexander-Universität Erlangen-Nürnberg, May 2020.

[S10] Qin, Chao. "Konzpetionierung und Implentierung eines Deep Learning Verfahrens zur semantischen Segmentierung von Schweißnähten". Master Thesis. Erlangen: Friedrich-Alexander-Universität Erlangen-Nürnberg, May 2020.

[S11]   Khaldi, Anass. "Cloud-Based Process Optimization of Additive and Subtractive Manufacturing through Artificial Intelligence". Master Thesis. Technische Hochschule Ulm, Feb. 2020.

Reihenübersicht

Koordination der Reihe (Stand 2023):
Geschäftsstelle Maschinenbau, Dr.-Ing. Oliver Kreis, www.mb.fau.de/diss/

Im Rahmen der Reihe sind bisher die nachfolgenden Bände erschienen.

Band 1 – 52
Fertigungstechnik – Erlangen
ISSN 1431-6226
Carl Hanser Verlag, München

Band 53 – 307
Fertigungstechnik – Erlangen
ISSN 1431-6226
Meisenbach Verlag, Bamberg

ab Band 308
FAU Studien aus dem Maschinenbau
ISSN 2625-9974
FAU University Press, Erlangen

Die Zugehörigkeit zu den jeweiligen Lehrstühlen ist wie folgt
gekennzeichnet:

Lehrstühle:

FAPS	Lehrstuhl für Fertigungsautomatisierung und Produktionssystematik
FMT	Lehrstuhl für Fertigungsmesstechnik
KTmfk	Lehrstuhl für Konstruktionstechnik
LFT	Lehrstuhl für Fertigungstechnologie
LGT	Lehrstuhl für Gießereitechnik
LPT	Lehrstuhl für Photonische Technologien
REP	Lehrstuhl für Ressourcen- und Energieeffiziente Produktionsmaschinen

Band 1: Andreas Hemberger
Innovationspotentiale in der rechnerintegrierten Produktion durch wissensbasierte Systeme
FAPS, 208 Seiten, 107 Bilder. 1988.
ISBN 3-446-15234-2.

Band 2: Detlef Classe
Beitrag zur Steigerung der Flexibilität automatisierter Montagesysteme durch Sensorintegration und erweiterte Steuerungskonzepte
FAPS, 194 Seiten, 70 Bilder. 1988.
ISBN 3-446-15529-5.

Band 3: Friedrich-Wilhelm Nolting
Projektierung von Montagesystemen
FAPS, 201 Seiten, 107 Bilder, 1 Tab.
1989.ISBN 3-446-15541-4.

Band 4: Karsten Schlüter
Nutzungsgradsteigerung von Montagesystemen durch den Einsatz der Simulationstechnik
FAPS, 177 Seiten, 97 Bilder. 1989.
ISBN 3-446-15542-2.

Band 5: Shir-Kuan Lin
Aufbau von Modellen zur Lageregelung von Industrierobotern
FAPS, 168 Seiten, 46 Bilder. 1989.
ISBN 3-446-15546-5.

Band 6: Rudolf Nuss
Untersuchungen zur Bearbeitungsqualität im Fertigungssystem Laserstrahlschneiden
LFT, 206 Seiten, 115 Bilder, 6 Tab.
1989. ISBN 3-446-15783-2.

Band 7: Wolfgang Scholz
Modell zur datenbankgestützten Planung automatisierter Montageanlagen
FAPS, 194 Seiten, 89 Bilder. 1989.
ISBN 3-446-15825-1.

Band 8: Hans-Jürgen Wißmeier
Beitrag zur Beurteilung des Bruchverhaltens von Hartmetall-Fließpreßmatrizen
LFT, 179 Seiten, 99 Bilder, 9 Tab.
1989. ISBN 3-446-15921-5.

Band 9: Rainer Eisele
Konzeption und Wirtschaftlichkeit von Planungssystemen in der Produktion
FAPS, 183 Seiten, 86 Bilder. 1990.
ISBN 3-446-16107-4.

Band 10: Rolf Pfeiffer
Technologisch orientierte Montageplanung am Beispiel der Schraubtechnik
FAPS, 216 Seiten, 102 Bilder, 16 Tab. 1990. ISBN 3-446-16161-9.

Band 11: Herbert Fischer
Verteilte Planungssysteme zur Flexibilitätssteigerung der rechnerintegrierten Teilefertigung
FAPS, 201 Seiten, 82 Bilder. 1990.
ISBN 3-446-16105-8.

Band 12: Gerhard Kleineidam
CAD/CAP: Rechnergestützte Montagefeinplanung
FAPS, 203 Seiten, 107 Bilder. 1990.
ISBN 3-446-16112-0.

Band 13: Frank Vollertsen
Pulvermetallurgische Verarbeitung eines übereutektoiden verschleißfesten Stahls
LFT, XIII u. 217 Seiten, 67 Bilder, 34 Tab. 1990.
ISBN 3-446-16133-3.

Band 14: Stephan Biermann
Untersuchungen zur Anlagen- und Prozeßdiagnostik für das Schneiden mit CO_2-Hochleistungslasern
LFT, VIII u. 170 Seiten, 93 Bilder, 4 Tab. 1991. ISBN 3-446-16269-0.

Band 15: Uwe Geißler
Material- und Datenfluß in einer flexiblen Blechbearbeitungszelle
LFT, 124 Seiten, 41 Bilder, 7 Tab.
1991. ISBN 3-446-16358-1.

Band 16: Frank Oswald Hake
Entwicklung eines rechnergestützten Diagnosesystems für automatisierte Montagezellen
FAPS, XIV u. 166 Seiten, 77 Bilder.
1991. ISBN 3-446-16428-6.

Band 17: Herbert Reichel
Optimierung der Werkzeugbereitstellung durch rechnergestützte Arbeitsfolgenbestimmung
FAPS, 198 Seiten, 73 Bilder, 2 Tab.
1991. ISBN 3-446-16453-7.

Band 18: Josef Scheller
Modellierung und Einsatz von Softwaresystemen für rechnergeführte Montagezellen
FAPS, 198 Seiten, 65 Bilder. 1991.
ISBN 3-446-16454-5.

Band 19: Arnold vom Ende
Untersuchungen zum Biegeumforme mit elastischer Matrize
LFT, 166 Seiten, 55 Bilder, 13 Tab.
1991. ISBN 3-446-16493-6.

Band 20: Joachim Schmid
Beitrag zum automatisierten Bearbeiten von Keramikguß mit Industrierobotern
FAPS, XIV u. 176 Seiten, 111 Bilder, 6 Tab. 1991.
ISBN 3-446-16560-6.

Band 21: Egon Sommer
Multiprozessorsteuerung für kooperierende Industrieroboter in Montagezellen
FAPS, 188 Seiten, 102 Bilder. 1991.
ISBN 3-446-17062-6.

Band 22: Georg Geyer
Entwicklung problemspezifischer Verfahrensketten in der Montage
FAPS, 192 Seiten, 112 Bilder. 1991.
ISBN 3-446-16552-5.

Band 23: Rainer Flohr
Beitrag zur optimalen Verbindungstechnik in der Oberflächenmontage (SMT)
FAPS, 186 Seiten, 79 Bilder. 1991.
ISBN 3-446-16568-1.

Band 24: Alfons Rief
Untersuchungen zur Verfahrensfolge Laserstrahlschneiden und -schweißen in der Rohkarosseriefertigung
LFT, VI u. 145 Seiten, 58 Bilder, 5 Tab. 1991. ISBN 3-446-16593-2.

Band 25: Christoph Thim
Rechnerunterstützte Optimierung von Materialflußstrukturen in der Elektronikmontage durch Simulation
FAPS, 188 Seiten, 74 Bilder. 1992.
ISBN 3-446-17118-5.

Band 26: Roland Müller
CO_2-Laserstrahlschneiden von kurzglasverstärkten Verbundwerkstoffen
LFT, 141 Seiten, 107 Bilder, 4 Tab.
1992. ISBN 3-446-17104-5.

Band 27: Günther Schäfer
Integrierte Informationsverarbeitung bei der Montageplanung
FAPS, 195 Seiten, 76 Bilder. 1992.
ISBN 3-446-17117-7.

Band 28: Martin Hoffmann
Entwicklung einerCAD/CAM-Prozeßkette für die Herstellung von Blechbiegeteilen
LFT, 149 Seiten, 89 Bilder. 1992.
ISBN 3-446-17154-1.

Band 29: Peter Hoffmann
Verfahrensfolge Laserstrahlschneiden und –schweißen: Prozeßführung und Systemtechnik in der 3D-Laserstrahlbearbeitung von Blechformteilen
LFT, 186 Seiten, 92 Bilder, 10 Tab.
1992. ISBN 3-446-17153-3.

Band 30: Olaf Schrödel
Flexible Werkstattsteuerung mit objektorientierten Softwarestrukturen
FAPS, 180 Seiten, 84 Bilder. 1992.
ISBN 3-446-17242-4.

Band 31: Hubert Reinisch
Planungs- und Steuerungswerkzeuge zur impliziten Geräteprogrammierung in Roboterzellen
FAPS, XI u. 212 Seiten, 112 Bilder.
1992. ISBN 3-446-17380-3.

Band 32: Brigitte Bärnreuther
Ein Beitrag zur Bewertung des Kommunikationsverhaltens von Automatisierungsgeräten in flexiblen Produktionszellen
FAPS, XI u. 179 Seiten, 71 Bilder.
1992. ISBN 3-446-17451-6.

Band 33: Joachim Hutfless
Laserstrahlregelung und Optikdiagnostik in der Strahlführung einer CO2-Hochleistungslaseranlage
LFT, 175 Seiten, 70 Bilder, 17 Tab.
1993. ISBN 3-446-17532-6.

Band 34: Uwe Günzel
Entwicklung und Einsatz eines Simula-tionsverfahrens für operative undstrategische Probleme der Produktionsplanung und -steuerung
FAPS, XIV u. 170 Seiten, 66 Bilder,
5 Tab. 1993. ISBN 3-446-17604-7.

Band 35: Bertram Ehmann
Operatives Fertigungscontrolling durch Optimierung auftragsbezogener Bearbeitungsabläufe in der Elektronikfertigung
FAPS, XV u. 167 Seiten, 114 Bilder.
1993. ISBN 3-446-17658-6.

Band 36: Harald Kolléra
Entwicklung eines benutzerorientierten Werkstattprogrammiersystems für das Laserstrahlschneiden
LFT, 129 Seiten, 66 Bilder, 1 Tab.
1993. ISBN 3-446-17719-1.

Band 37: Stephanie Abels
Modellierung und Optimierung von Montageanlagen in einem integrierten Simulationssystem
FAPS, 188 Seiten, 88 Bilder. 1993.
ISBN 3-446-17731-0.

Band 38: Robert Schmidt-Hebbel
Laserstrahlbohren durchflußbestimmender Durchgangslöcher
LFT, 145 Seiten, 63 Bilder, 11 Tab.
1993. ISBN 3-446-17778-7.

Band 39: Norbert Lutz
Oberflächenfeinbearbeitung keramischer Werkstoffe mit XeCl-Excimerlaserstrahlung
LFT, 187 Seiten, 98 Bilder, 29 Tab.
1994. ISBN 3-446-17970-4.

Band 40: Konrad Grampp
Rechnerunterstützung bei Test und Schulung an Steuerungssoftware von SMD-Bestücklinien
FAPS, 178 Seiten, 88 Bilder. 1995.
ISBN 3-446-18173-3.

Band 41: Martin Koch
Wissensbasierte Unterstützung derAngebotsbearbeitung in der Investitionsgüterindustrie
FAPS, 169 Seiten, 68 Bilder. 1995.
ISBN 3-446-18174-1.

Band 42: Armin Gropp
Anlagen- und Prozeßdiagnostik beim Schneiden mit einem gepulsten Nd:YAG-Laser
LFT, 160 Seiten, 88 Bilder, 7 Tab.
1995. ISBN 3-446-18241-1.

Band 43: Werner Heckel
Optische 3D-Konturerfassung und on-line Biegewinkelmessung mit dem Lichtschnittverfahren
LFT, 149 Seiten, 43 Bilder, 11 Tab.
1995. ISBN 3-446-18243-8.

Band 44: Armin Rothhaupt
Modulares Planungssystem zur Optimierung der Elektronikfertigung
FAPS, 180 Seiten, 101 Bilder. 1995.
ISBN 3-446-18307-8.

Band 45: Bernd Zöllner
Adaptive Diagnose in der Elektronikproduktion
FAPS, 195 Seiten, 74 Bilder, 3 Tab.
1995. ISBN 3-446-18308-6.

Band 46: Bodo Vormann
Beitrag zur automatisierten Handhabungsplanung komplexer Blechbiegeteile
LFT, 126 Seiten, 89 Bilder, 3 Tab.
1995. ISBN 3-446-18345-0.

Band 47: Peter Schnepf
Zielkostenorientierte Montageplanung
FAPS, 144 Seiten, 75 Bilder. 1995.
ISBN 3-446-18397-3.

Band 48: Rainer Klotzbücher
Konzept zur rechnerintegrierten Materialversorgung in flexiblen Fertigungssystemen
FAPS, 156 Seiten, 62 Bilder. 1995.
ISBN 3-446-18412-0.

Band 49: Wolfgang Greska
Wissensbasierte Analyse undKlassifizierung von Blechteilen
LFT, 144 Seiten, 96 Bilder. 1995.
ISBN 3-446-18462-7.

Band 50: Jörg Franke
Integrierte Entwicklung neuer Produkt- und Produktionstechnologien für räumliche spritzgegossene Schaltungsträger (3-D MID)
FAPS, 196 Seiten, 86 Bilder, 4 Tab.
1995. ISBN 3-446-18448-1.

Band 51: Franz-Josef Zeller
Sensorplanung und schnelle Sensorregelung für Industrieroboter
FAPS, 190 Seiten, 102 Bilder, 9 Tab.
1995. ISBN 3-446-18601-8.

Band 52: Michael Solvie
Zeitbehandlung und Multimedia-Unterstützung in Feldkommunikationssystemen
FAPS, 200 Seiten, 87 Bilder, 35 Tab. 1996. ISBN 3-446-18607-7.

Band 53: Robert Hopperdietzel
Reengineering in der Elektro- und Elektronikindustrie
FAPS, 180 Seiten, 109 Bilder, 1 Tab.
1996. ISBN 3-87525-070-2.

Band 54: Thomas Rebhahn
Beitrag zur Mikromaterialbearbeitung mit Excimerlasern - Systemkomponenten und Verfahrensoptimierungen
LFT, 148 Seiten, 61 Bilder, 10 Tab. 1996. ISBN 3-87525-075-3.

Band 55: Henning Hanebuth
Laserstrahlhartlöten mit Zweistrahltechnik
LFT, 157 Seiten, 58 Bilder, 11 Tab. 1996. ISBN 3-87525-074-5.

Band 56: Uwe Schönherr
Steuerung und Sensordatenintegration für flexible Fertigungszellen mitkooperierenden Robotern
FAPS, 188 Seiten, 116 Bilder, 3 Tab. 1996. ISBN 3-87525-076-1.

Band 57: Stefan Holzer
Berührungslose Formgebung mitLaserstrahlung
LFT, 162 Seiten, 69 Bilder, 11 Tab. 1996. ISBN 3-87525-079-6.

Band 58: Markus Schultz
Fertigungsqualität beim 3D-Laserstrahlschweißen vonBlechformteilen
LFT, 165 Seiten, 88 Bilder, 9 Tab. 1997. ISBN 3-87525-080-X.

Band 59: Thomas Krebs
Integration elektromechanischer CA-Anwendungen über einem STEP-Produktmodell
FAPS, 198 Seiten, 58 Bilder, 8 Tab. 1997. ISBN 3-87525-081-8.

Band 60: Jürgen Sturm
Prozeßintegrierte Qualitätssicherung in der Elektronikproduktion
FAPS, 167 Seiten, 112 Bilder, 5 Tab. 1997. ISBN 3-87525-082-6.

Band 61: Andreas Brand
Prozesse und Systeme zur Bestückung räumlicher elektronischer Baugruppen (3D-MID)
FAPS, 182 Seiten, 100 Bilder. 1997. ISBN 3-87525-087-7.

Band 62: Michael Kauf
Regelung der Laserstrahlleistung und der Fokusparameter einer CO2-Hochleistungslaseranlage
LFT, 140 Seiten, 70 Bilder, 5 Tab. 1997. ISBN 3-87525-083-4.

Band 63: Peter Steinwasser
Modulares Informationsmanagement in der integrierten Produkt- und Prozeßplanung
FAPS, 190 Seiten, 87 Bilder. 1997. ISBN 3-87525-084-2.

Band 64: Georg Liedl
Integriertes Automatisierungskonzept für den flexiblen Materialfluß in der Elektronikproduktion
FAPS, 196 Seiten, 96 Bilder, 3 Tab. 1997. ISBN 3-87525-086-9.

Band 65: Andreas Otto
Transiente Prozesse beim Laserstrahlschweißen
LFT, 132 Seiten, 62 Bilder, 1 Tab. 1997. ISBN 3-87525-089-3.

Band 66: Wolfgang Blöchl
Erweiterte Informationsbereitstellung an offenen CNC-Steuerungen zur Prozeß- und Programmoptimierung
FAPS, 168 Seiten, 96 Bilder. 1997. ISBN 3-87525-091-5.

Band 67: Klaus-Uwe Wolf
Verbesserte Prozeßführung und Prozeßplanung zur Leistungs- und Qualitätssteigerung beim Spulenwickeln
FAPS, 186 Seiten, 125 Bilder. 1997. ISBN 3-87525-092-3.

Band 68: Frank Backes
Technologieorientierte Bahnplanung für die 3D-Laserstrahlbearbeitung
LFT, 138 Seiten, 71 Bilder, 2 Tab. 1997. ISBN 3-87525-093-1.

Band 69: Jürgen Kraus
Laserstrahlumformen von Profilen
LFT, 137 Seiten, 72 Bilder, 8 Tab. 1997. ISBN 3-87525-094-X.

Band 70: Norbert Neubauer
Adaptive Strahlführungen für CO2-Laseranlagen
LFT, 120 Seiten, 50 Bilder, 3 Tab. 1997. ISBN 3-87525-095-8.

Band 71: Michael Steber
Prozeßoptimierter Betrieb flexibler Schraubstationen in der automatisierten Montage
FAPS, 168 Seiten, 78 Bilder, 3 Tab. 1997. ISBN 3-87525-096-6.

Band 72: Markus Pfestorf
Funktionale 3D-Oberflächenkenngrößen in der Umformtechnik
LFT, 162 Seiten, 84 Bilder, 15 Tab. 1997. ISBN 3-87525-097-4.

Band 73: Volker Franke
Integrierte Planung und Konstruktion von Werkzeugen für die Biegebearbeitung
LFT, 143 Seiten, 81 Bilder. 1998. ISBN 3-87525-098-2.

Band 74: Herbert Scheller
Automatisierte Demontagesysteme und recyclinggerechte Produktgestaltung elektronischer Baugruppen
FAPS, 184 Seiten, 104 Bilder, 17 Tab. 1998. ISBN 3-87525-099-0.

Band 75: Arthur Meßner
Kaltmassivumformung metallischer Kleinstteile – Werkstoffverhalten, Wirkflächenreibung, Prozeßauslegung
LFT, 164 Seiten, 92 Bilder, 14 Tab. 1998. ISBN 3-87525-100-8.

Band 76: Mathias Glasmacher
Prozeß- und Systemtechnik zum Laserstrahl-Mikroschweißen
LFT, 184 Seiten, 104 Bilder, 12 Tab. 1998. ISBN 3-87525-101-6.

Band 77: Michael Schwind
Zerstörungsfreie Ermittlung mechanischer Eigenschaften von Feinblechen mit dem Wirbelstromverfahren
LFT, 124 Seiten, 68 Bilder, 8 Tab. 1998. ISBN 3-87525-102-4.

Band 78: Manfred Gerhard
Qualitätssteigerung in der Elektronikproduktion durch Optimierung der Prozeßführung beim Löten komplexer Baugruppen
FAPS, 179 Seiten, 113 Bilder, 7 Tab. 1998. ISBN 3-87525-103-2.

Band 79: Elke Rauh
Methodische Einbindung der Simulation in die betrieblichen Planungs- und Entscheidungsabläufe
FAPS, 192 Seiten, 114 Bilder, 4 Tab. 1998. ISBN 3-87525-104-0.

Band 80: Sorin Niederkorn
Meßeinrichtung zur Untersuchung der Wirkflächenreibung bei umformtechnischen Prozessen
LFT, 99 Seiten, 46 Bilder, 6 Tab. 1998. ISBN 3-87525-105-9.

Band 81: Stefan Schuberth
Regelung der Fokuslage beim Schweißen mit CO2-Hochleistungslasern unter Einsatz von adaptiven Optiken
LFT, 140 Seiten, 64 Bilder, 3 Tab. 1998. ISBN 3-87525-106-7.

Band 82: Armando Walter Colombo
Development and Implementation of Hierarchical Control Structures of Flexible Production Systems Using High Level Petri Nets
FAPS, 216 Seiten, 86 Bilder. 1998. ISBN 3-87525-109-1.

Band 83: Otto Meedt
Effizienzsteigerung bei Demontage und Recycling durch flexible Demontagetechnologien und optimierte Produktgestaltung
FAPS, 186 Seiten, 103 Bilder. 1998. ISBN 3-87525-108-3.

Band 84: Knuth Götz
Modelle und effiziente Modellbildung zur Qualitätssicherung in der Elektronikproduktion
FAPS, 212 Seiten, 129 Bilder, 24 Tab. 1998. ISBN 3-87525-112-1.

Band 85: Ralf Luchs
Einsatzmöglichkeiten leitender Klebstoffe zur zuverlässigen Kontaktierung elektronischer Bauelemente in der SMT
FAPS, 176 Seiten, 126 Bilder, 30 Tab. 1998. ISBN 3-87525-113-7.

Band 86: Frank Pöhlau
Entscheidungsgrundlagen zur Einführung räumlicher spritzgegossener Schaltungsträger (3-D MID)
FAPS, 144 Seiten, 99 Bilder. 1999. ISBN 3-87525-114-8.

Band 87: Roland T. A. Kals
Fundamentals on the miniaturization of sheet metal working processes
LFT, 128 Seiten, 58 Bilder, 11 Tab. 1999. ISBN 3-87525-115-6.

Band 88: Gerhard Luhn
Implizites Wissen und technisches Handeln am Beispiel der Elektronikproduktion
FAPS, 252 Seiten, 61 Bilder, 1 Tab. 1999. ISBN 3-87525-116-4.

Band 89: Axel Sprenger
Adaptives Streckbiegen von Aluminium-Strangpreßprofilen
LFT, 114 Seiten, 63 Bilder, 4 Tab. 1999. ISBN 3-87525-117-2.

Band 90: Hans-Jörg Pucher
Untersuchungen zur Prozeßfolge Umformen, Bestücken und Laserstrahllöten von Mikrokontakten
LFT, 158 Seiten, 69 Bilder, 9 Tab. 1999. ISBN 3-87525-119-9.

Band 91: Horst Arnet
Profilbiegen mit kinematischer Gestalterzeugung
LFT, 128 Seiten, 67 Bilder, 7 Tab. 1999. ISBN 3-87525-120-2.

Band 92: Doris Schubart
Prozeßmodellierung und Technologieentwicklung beim Abtragen mit CO2-Laserstrahlung
LFT, 133 Seiten, 57 Bilder, 13 Tab. 1999. ISBN 3-87525-122-9.

Band 93: Adrianus L. P. Coremans
Laserstrahlsintern von Metallpulver - Prozeßmodellierung, Systemtechnik, Eigenschaften laserstrahlgesinterter Metallkörper
LFT, 184 Seiten, 108 Bilder, 12 Tab. 1999. ISBN 3-87525-124-5.

Band 94: Hans-Martin Biehler
Optimierungskonzepte für Qualitätsdatenverarbeitung und Informationsbereitstellung in der Elektronikfertigung
FAPS, 194 Seiten, 105 Bilder. 1999. ISBN 3-87525-126-1.

Band 95: Wolfgang Becker
Oberflächenausbildung und tribologische Eigenschaften excimerlaserstrahlbearbeiteter Hochleistungskeramiken
LFT, 175 Seiten, 71 Bilder, 3 Tab. 1999. ISBN 3-87525-127-X.

Band 96: Philipp Hein
Innenhochdruck-Umformen von Blechpaaren: Modellierung, Prozeßauslegung und Prozeßführung
LFT, 129 Seiten, 57 Bilder, 7 Tab. 1999. ISBN 3-87525-128-8.

Band 97: Gunter Beitinger
Herstellungs- und Prüfverfahren für thermoplastische Schaltungsträger
FAPS, 169 Seiten, 92 Bilder, 20 Tab. 1999. ISBN 3-87525-129-6.

Band 98: Jürgen Knoblach
Beitrag zur rechnerunterstützten verursachungsgerechten Angebotskalkulation von Blechteilen mit Hilfe wissensbasierter Methoden
LFT, 155 Seiten, 53 Bilder, 26 Tab. 1999. ISBN 3-87525-130-X.

Band 99: Frank Breitenbach
Bildverarbeitungssystem zur Erfassung der Anschlußgeometrie elektronischer SMT-Bauelemente
LFT, 147 Seiten, 92 Bilder, 12 Tab. 2000. ISBN 3-87525-131-8.

Band 100: Bernd Falk
Simulationsbasierte Lebensdauervorhersage für Werkzeuge der Kaltmassivumformung
LFT, 134 Seiten, 44 Bilder, 15 Tab. 2000. ISBN 3-87525-136-9.

Band 101: Wolfgang Schlögl
Integriertes Simulationsdaten-Management für Maschinenentwicklung und Anlagenplanung
FAPS, 169 Seiten, 101 Bilder, 20 Tab. 2000. ISBN 3-87525-137-7.

Band 102: Christian Hinsel
Ermüdungsbruchversagen hartstoffbeschichteter Werkzeugstähle in der Kaltmassivumformung
LFT, 130 Seiten, 80 Bilder, 14 Tab. 2000. ISBN 3-87525-138-5.

Band 103: Stefan Bobbert
Simulationsgestützte Prozessauslegung für das Innenhochdruck-Umformen von Blechpaaren
LFT, 123 Seiten, 77 Bilder. 2000. ISBN 3-87525-145-8.

Band 104: Harald Rottbauer
Modulares Planungswerkzeug zum Produktionsmanagement in der Elektronikproduktion
FAPS, 166 Seiten, 106 Bilder. 2001. ISBN 3-87525-139-3.

Band 105: Thomas Hennige
Flexible Formgebung von Blechen durch Laserstrahlumformen
LFT, 119 Seiten, 50 Bilder. 2001. ISBN 3-87525-140-7.

Band 106: Thomas Menzel
Wissensbasierte Methoden für die rechnergestützte Charakterisierung und Bewertung innovativer Fertigungsprozesse
LFT, 152 Seiten, 71 Bilder. 2001. ISBN 3-87525-142-3.

Band 107: Thomas Stöckel
Kommunikationstechnische Integration der Prozeßebene in Produktionssysteme durch Middleware-Frameworks
FAPS, 147 Seiten, 65 Bilder, 5 Tab. 2001. ISBN 3-87525-143-1.

Band 108: Frank Pitter
Verfügbarkeitssteigerung von Werkzeugmaschinen durch Einsatz mechatronischer Sensorlösungen
FAPS, 158 Seiten, 131 Bilder, 8 Tab. 2001. ISBN 3-87525-144-X.

Band 109: Markus Korneli
Integration lokaler CAP-Systeme in einen globalen Fertigungsdatenverbund
FAPS, 121 Seiten, 53 Bilder, 11 Tab. 2001. ISBN 3-87525-146-6.

Band 110: Burkhard Müller
Laserstrahljustieren mit Excimer-Lasern - Prozeßparameter und Modelle zur Aktorkonstruktion
LFT, 128 Seiten, 36 Bilder, 9 Tab. 2001. ISBN 3-87525-159-8.

Band 111: Jürgen Göhringer
Integrierte Telediagnose via Internet zum effizienten Service von Produktionssystemen
FAPS, 178 Seiten, 98 Bilder, 5 Tab. 2001. ISBN 3-87525-147-4.

Band 112: Robert Feuerstein
Qualitäts- und kosteneffiziente Integration neuer Bauelementetechnologien in die Flachbaugruppenfertigung
FAPS, 161 Seiten, 99 Bilder, 10 Tab. 2001. ISBN 3-87525-151-2.

Band 113: Marcus Reichenberger
Eigenschaften und Einsatzmöglichkeiten alternativer Elektroniklote in der Oberflächenmontage (SMT)
FAPS, 165 Seiten, 97 Bilder, 18 Tab. 2001. ISBN 3-87525-152-0.

Band 114: Alexander Huber
Justieren vormontierter Systeme mit dem Nd:YAG-Laser unter Einsatz von Aktoren
LFT, 122 Seiten, 58 Bilder, 5 Tab. 2001. ISBN 3-87525-153-9.

Band 115: Sami Krimi
Analyse und Optimierung von Montagesystemen in der Elektronikproduktion
FAPS, 155 Seiten, 88 Bilder, 3 Tab. 2001. ISBN 3-87525-157-1.

Band 116: Marion Merklein
Laserstrahlumformen von Aluminiumwerkstoffen - Beeinflussung der Mikrostruktur und der mechanischen Eigenschaften
LFT, 122 Seiten, 65 Bilder, 15 Tab. 2001. ISBN 3-87525-156-3.

Band 117: Thomas Collisi
Ein informationslogistisches Architekturkonzept zur Akquisition simulationsrelevanter Daten
FAPS, 181 Seiten, 105 Bilder, 7 Tab. 2002. ISBN 3-87525-164-4.

Band 118: Markus Koch
Rationalisierung und ergonomische Optimierung im Innenausbau durch den Einsatz moderner Automatisierungstechnik
FAPS, 176 Seiten, 98 Bilder, 9 Tab. 2002. ISBN 3-87525-165-2.

Band 119: Michael Schmidt
Prozeßregelung für das Laserstrahl-Punktschweißen in der Elektronikproduktion
LFT, 152 Seiten, 71 Bilder, 3 Tab. 2002. ISBN 3-87525-166-0.

Band 120: Nicolas Tiesler
Grundlegende Untersuchungen zum Fließpressen metallischer Kleinstteile
LFT, 126 Seiten, 78 Bilder, 12 Tab. 2002. ISBN 3-87525-175-X.

Band 121: Lars Pursche
Methoden zur technologieorientierten Programmierung für die 3D-Lasermikrobearbeitung
LFT, 111 Seiten, 39 Bilder, 0 Tab. 2002. ISBN 3-87525-183-0.

Band 122: Jan-Oliver Brassel
Prozeßkontrolle beim Laserstrahl-Mikroschweißen
LFT, 148 Seiten, 72 Bilder, 12 Tab. 2002. ISBN 3-87525-181-4.

Band 123: Mark Geisel
Prozeßkontrolle und -steuerung beim Laserstrahlschweißen mit den Methoden der nichtlinearen Dynamik
LFT, 135 Seiten, 46 Bilder, 2 Tab. 2002. ISBN 3-87525-180-6.

Band 124: Gerd Eßer
Laserstrahlunterstützte Erzeugung metallischer Leiterstrukturen auf Thermoplastsubstraten für die MID-Technik
LFT, 148 Seiten, 60 Bilder, 6 Tab. 2002. ISBN 3-87525-171-7.

Band 125: Marc Fleckenstein
Qualität laserstrahl-gefügter Mikroverbindungen elektronischer Kontakte
LFT, 159 Seiten, 77 Bilder, 7 Tab. 2002. ISBN 3-87525-170-9.

Band 126: Stefan Kaufmann
Grundlegende Untersuchungen zum Nd:YAG- Laserstrahlfügen von Silizium für Komponenten der Optoelektronik
LFT, 159 Seiten, 100 Bilder, 6 Tab. 2002. ISBN 3-87525-172-5.

Band 127: Thomas Fröhlich
Simultanes Löten von Anschlußkontakten elektronischer Bauelemente mit Diodenlaserstrahlung
LFT, 143 Seiten, 75 Bilder, 6 Tab. 2002. ISBN 3-87525-186-5.

Band 128: Achim Hofmann
Erweiterung der Formgebungs-
grenzen beim Umformen von Alu-
miniumwerkstoffen durch den
Einsatz prozessangepasster Plati-
nen
LFT, 113 Seiten, 58 Bilder, 4 Tab.
2002. ISBN 3-87525-182-2.

Band 129: Ingo Kriebitzsch
3 - D MID Technologie in der Au-
tomobilelektronik
FAPS, 129 Seiten, 102 Bilder, 10
Tab. 2002. ISBN 3-87525-169-5.

Band 130: Thomas Pohl
Fertigungsqualität und Umform-
barkeit laserstrahlgeschweißter
Formplatinen aus Aluminiumle-
gierungen
LFT, 133 Seiten, 93 Bilder, 12 Tab.
2002. ISBN 3-87525-173-3.

Band 131: Matthias Wenk
Entwicklung eines konfigurierba-
ren Steuerungssystems für die fle-
xible Sensorführung von Industrie-
robotern
FAPS, 167 Seiten, 85 Bilder, 1 Tab.
2002. ISBN 3-87525-174-1.

Band 132: Matthias Negendanck
Neue Sensorik und Aktorik für Be-
arbeitungsköpfe zum Laserstrahl-
schweißen
LFT, 116 Seiten, 60 Bilder, 14 Tab.
2002. ISBN 3-87525-184-9.

Band 133: Oliver Kreis
Integrierte Fertigung - Verfahrens-
integration durch Innenhoch-
druck-Umformen, Trennen und
Laserstrahlschweißen in einem
Werkzeug sowie ihre tele- und
multimediale Präsentation
LFT, 167 Seiten, 90 Bilder, 43 Tab.
2002. ISBN 3-87525-176-8.

Band 134: Stefan Trautner
Technische Umsetzung produkt-
bezogener Instrumente der Um-
weltpolitik bei Elektro- und Elekt-
ronikgeräten
FAPS, 179 Seiten, 92 Bilder, 11 Tab.
2002. ISBN 3-87525-177-6.

Band 135: Roland Meier
Strategien für einen produktorien-
tierten Einsatz räumlicher spritz-
gegossener Schaltungsträger (3-D
MID)
FAPS, 155 Seiten, 88 Bilder, 14 Tab.
2002. ISBN 3-87525-178-4.

Band 136: Jürgen Wunderlich
Kostensimulation - Simulationsba-
sierte Wirtschaftlichkeitsregelung
komplexer Produktionssysteme
FAPS, 202 Seiten, 119 Bilder, 17 Tab.
2002. ISBN 3-87525-179-2.

Band 137: Stefan Novotny
Innenhochdruck-Umformen von
Blechen aus Aluminium- und Mag-
nesiumlegierungen bei erhöhter
Temperatur
LFT, 132 Seiten, 82 Bilder, 6 Tab.
2002. ISBN 3-87525-185-7.

Band 138: Andreas Licha
Flexible Montageautomatisierung
zur Komplettmontage flächenhaf-
ter Produktstrukturen durch ko-
operierende Industrieroboter
FAPS, 158 Seiten, 87 Bilder, 8 Tab.
2003. ISBN 3-87525-189-X.

Band 139: Michael Eisenbarth
Beitrag zur Optimierung der Auf-
bau- und Verbindungstechnik für
mechatronische Baugruppen
FAPS, 207 Seiten, 141 Bilder, 9 Tab.
2003. ISBN 3-87525-190-3.

Band 140: Frank Christoph
Durchgängige simulationsge-
stützte Planung von Fertigungs-
einrichtungen der Elektronikpro-
duktion
FAPS, 187 Seiten, 107 Bilder, 9 Tab.
2003. ISBN 3-87525-191-1.

Band 141: Hinnerk Hagenah
Simulationsbasierte Bestimmung
der zu erwartenden Maßhaltigkeit
für das Blechbiegen
LFT, 131 Seiten, 36 Bilder, 26 Tab.
2003. ISBN 3-87525-192-X.

Band 142: Ralf Eckstein
Scherschneiden und Biegen metal-
lischer Kleinstteile - Materialein-
fluss und Materialverhalten
LFT, 148 Seiten, 71 Bilder, 19 Tab.
2003. ISBN 3-87525-193-8.

**Band 143: Frank H. Meyer-
Pittroff**
Excimerlaserstrahlbiegen dünner
metallischer Folien mit homoge-
ner Lichtlinie
LFT, 138 Seiten, 60 Bilder, 16 Tab.
2003. ISBN 3-87525-196-2.

Band 144: Andreas Kach
Rechnergestützte Anpassung von
Laserstrahlschneidbahnen
an Bauteilabweichungen
LFT, 139 Seiten, 69 Bilder, 11 Tab.
2004. ISBN 3-87525-197-0.

Band 145: Stefan Hierl
System- und Prozeßtechnik für das
simultane Löten mit Diodenlaser-
strahlung von elektronischen Bau-
elementen
LFT, 124 Seiten, 66 Bilder, 4 Tab.
2004. ISBN 3-87525-198-9.

Band 146: Thomas Neudecker
Tribologische Eigenschaften kera-
mischer Blechumformwerkzeuge-
Einfluss einer Oberflächenendbe-
arbeitung mittels Excimerlaser-
strahlung
LFT, 166 Seiten, 75 Bilder, 26 Tab.
2004. ISBN 3-87525-200-4.

Band 147: Ulrich Wenger
Prozessoptimierung in der Wickel-
technik durch innovative maschi-
nenbauliche und regelungstechni-
sche Ansätze
FAPS, 132 Seiten, 88 Bilder, 0 Tab.
2004. ISBN 3-87525-203-9.

Band 148: Stefan Slama
Effizienzsteigerung in der Montage
durch marktorientierte Monta-
gestrukturen und erweiterte Mitar-
beiterkompetenz
FAPS, 188 Seiten, 125 Bilder, 0 Tab.
2004. ISBN 3-87525-204-7.

Band 149: Thomas Wurm
Laserstrahljustieren mittels Akto-
ren-Entwicklung von Konzepten
und Methoden für die rechnerun-
terstützte Modellierung und Opti-
mierung von komplexen Aktorsys-
temen in der Mikrotechnik
LFT, 122 Seiten, 51 Bilder, 9 Tab.
2004. ISBN 3-87525-206-3.

Band 150: Martino Celeghini
Wirkmedienbasierte Blechumformung: Grundlagenuntersuchungen zum Einfluss von Werkstoff und Bauteilgeometrie
LFT, 146 Seiten, 77 Bilder, 6 Tab. 2004. ISBN 3-87525-207-1.

Band 151: Ralph Hohenstein
Entwurf hochdynamischer Sensor- und Regelsysteme für die adaptiveLaserbearbeitung
LFT, 282 Seiten, 63 Bilder, 16 Tab. 2004. ISBN 3-87525-210-1.

Band 152: Angelika Hutterer
Entwicklung prozessüberwachender Regelkreise für flexible Formgebungsprozesse
LFT, 149 Seiten, 57 Bilder, 2 Tab. 2005. ISBN 3-87525-212-8.

Band 153: Emil Egerer
Massivumformen metallischer Kleinstteile bei erhöhter Prozesstemperatur
LFT, 158 Seiten, 87 Bilder, 10 Tab. 2005. ISBN 3-87525-213-6.

Band 154: Rüdiger Holzmann
Strategien zur nachhaltigen Optimierung von Qualität und Zuverlässigkeit in der Fertigung hochintegrierter Flachbaugruppen
FAPS, 186 Seiten, 99 Bilder, 19 Tab. 2005. ISBN 3-87525-217-9.

Band 155: Marco Nock
Biegeumformen mit Elastomerwerkzeugen Modellierung, Prozessauslegung und Abgrenzung des Verfahrens am Beispiel des Rohrbiegens
LFT, 164 Seiten, 85 Bilder, 13 Tab. 2005. ISBN 3-87525-218-7.

Band 156: Frank Niebling
Qualifizierung einer Prozesskette zum Laserstrahlsintern metallischer Bauteile
LFT, 148 Seiten, 89 Bilder, 3 Tab. 2005. ISBN 3-87525-219-5.

Band 157: Markus Meiler
Großserientauglichkeit trockenschmierstoffbeschichteter Aluminiumbleche im Presswerk Grundlegende Untersuchungen zur Tribologie, zum Umformverhalten und Bauteilversuche
LFT, 104 Seiten, 57 Bilder, 21 Tab. 2005. ISBN 3-87525-221-7.

Band 158: Agus Sutanto
Solution Approaches for Planning of Assembly Systems in Three-Dimensional Virtual Environments
FAPS, 169 Seiten, 98 Bilder, 3 Tab. 2005. ISBN 3-87525-220-9.

Band 159: Matthias Boiger
Hochleistungssysteme für die Fertigung elektronischer Baugruppen auf der Basis flexibler Schaltungsträger
FAPS, 175 Seiten, 111 Bilder, 8 Tab. 2005. ISBN 3-87525-222-5.

Band 160: Matthias Pitz
Laserunterstütztes Biegen höchstfester Mehrphasenstähle
LFT, 120 Seiten, 73 Bilder, 11 Tab. 2005. ISBN 3-87525-223-3.

Band 161: Meik Vahl
Beitrag zur gezielten Beeinflussung des Werkstoffflusses beim Innenhochdruck-Umformen von Blechen
LFT, 165 Seiten, 94 Bilder, 15 Tab. 2005. ISBN 3-87525-224-1.

Band 162: Peter K. Kraus
Plattformstrategien - Realisierung einer varianz- und kostenoptimierten Wertschöpfung
FAPS, 181 Seiten, 95 Bilder, 0 Tab. 2005. ISBN 3-87525-226-8.

Band 163: Adrienn Cser
Laserstrahlschmelzabtrag - Prozessanalyse und -modellierung
LFT, 146 Seiten, 79 Bilder, 3 Tab. 2005. ISBN 3-87525-227-6.

Band 164: Markus C. Hahn
Grundlegende Untersuchungen zur Herstellung von Leichtbauverbundstrukturen mit Aluminiumschaumkern
LFT, 143 Seiten, 60 Bilder, 16 Tab. 2005. ISBN 3-87525-228-4.

Band 165: Gordana Michos
Mechatronische Ansätze zur Optimierung von Vorschubachsen
FAPS, 146 Seiten, 87 Bilder, 17 Tab. 2005. ISBN 3-87525-230-6.

Band 166: Markus Stark
Auslegung und Fertigung hochpräziser Faser-Kollimator-Arrays
LFT, 158 Seiten, 115 Bilder, 11 Tab. 2005. ISBN 3-87525-231-4.

Band 167: Yurong Zhou
Kollaboratives Engineering Management in der integrierten virtuellen Entwicklung der Anlagen für die Elektronikproduktion
FAPS, 156 Seiten, 84 Bilder, 6 Tab. 2005. ISBN 3-87525-232-2.

Band 168: Werner Enser
Neue Formen permanenter und lösbarer elektrischer Kontaktierungen für mechatronische Baugruppen
FAPS, 190 Seiten, 112 Bilder, 5 Tab. 2005. ISBN 3-87525-233-0.

Band 169: Katrin Melzer
Integrierte Produktpolitik bei elektrischen und elektronischen Geräten zur Optimierung des Product-Life-Cycle
FAPS, 155 Seiten, 91 Bilder, 17 Tab. 2005. ISBN 3-87525-234-9.

Band 170: Alexander Putz
Grundlegende Untersuchungen zur Erfassung der realen Vorspannung von armierten Kaltfließpresswerkzeugen mittels Ultraschall
LFT, 137 Seiten, 71 Bilder, 15 Tab. 2006. ISBN 3-87525-237-3.

Band 171: Martin Prechtl
Automatisiertes Schichtverfahren für metallische Folien - System- und Prozesstechnik
LFT, 154 Seiten, 45 Bilder, 7 Tab. 2006. ISBN 3-87525-238-1.

Band 172: Markus Meidert
Beitrag zur deterministischen Lebensdauerabschätzung von Werkzeugen der Kaltmassivumformung
LFT, 131 Seiten, 78 Bilder, 9 Tab. 2006. ISBN 3-87525-239-X.

Band 173: Bernd Müller
Robuste, automatisierte Montagesysteme durch adaptive Prozessführung und montageübergreifende Fehlerprävention am Beispiel flächiger Leichtbauteile
FAPS, 147 Seiten, 77 Bilder, 0 Tab. 2006. ISBN 3-87525-240-3.

Band 174: Alexander Hofmann
Hybrides Laserdurchstrahlschweißen von Kunststoffen
LFT, 136 Seiten, 72 Bilder, 4 Tab. 2006. ISBN 978-3-87525-243-9.

Band 175: Peter Wölflick
Innovative Substrate und Prozesse
mit feinsten Strukturen für blei-
freie Mechatronik-Anwendungen
FAPS, 177 Seiten, 148 Bilder, 24
Tab. 2006.
ISBN 978-3-87525-246-0.

Band 176: Attila Komlodi
Detection and Prevention of Hot
Cracks during Laser Welding of
Aluminium Alloys Using Advanced
Simulation Methods
LFT, 155 Seiten, 89 Bilder, 14 Tab.
2006. ISBN 978-3-87525-248-4.

Band 177: Uwe Popp
Grundlegende Untersuchungen
zum Laserstrahlstrukturieren von
Kaltmassivumformwerkzeugen
LFT, 140 Seiten, 67 Bilder, 16 Tab.
2006. ISBN 978-3-87525-249-1.

Band 178: Veit Rückel
Rechnergestützte Ablaufplanung
und Bahngenerierung Für koope-
rierende Industrieroboter
FAPS, 148 Seiten, 75 Bilder, 7 Tab.
2006. ISBN 978-3-87525-250-7.

Band 179: Manfred Dirscherl
Nicht-thermische Mikrojustier-
technik mittels ultrakurzer Laser-
pulse
LFT, 154 Seiten, 69 Bilder, 10 Tab.
2007. ISBN 978-3-87525-251-4.

Band 180: Yong Zhuo
Entwurf eines rechnergestützten
integrierten Systems für Konstruk-
tion und Fertigungsplanung räum-
licher spritzgegossener Schal-
tungsträger (3D-MID)
FAPS, 181 Seiten, 95 Bilder, 5 Tab.
2007. ISBN 978-3-87525-253-8.

Band 181: Stefan Lang
Durchgängige Mitarbeiterinforma-
tion zur Steigerung von Effizienz
und Prozesssicherheit in der Pro-
duktion
FAPS, 172 Seiten, 93 Bilder. 2007.
ISBN 978-3-87525-257-6.

Band 182: Hans-Joachim Krauß
Laserstrahlinduzierte Pyrolyse prä-
keramischer Polymere
LFT, 171 Seiten, 100 Bilder. 2007.
ISBN 978-3-87525-258-3.

Band 183: Stefan Junker
Technologien und Systemlösungen
für die flexibel automatisierte Be-
stückung permanent erregter Läu-
fer mit oberflächenmontierten
Dauermagneten
FAPS, 173 Seiten, 75 Bilder. 2007.
ISBN 978-3-87525-259-0.

Band 184: Rainer Kohlbauer
Wissensbasierte Methoden für die
simulationsgestützte Auslegung
wirkmedienbasierter Blechum-
formprozesse
LFT, 135 Seiten, 50 Bilder. 2007.
ISBN 978-3-87525-260-6.

Band 185: Klaus Lamprecht
Wirkmedienbasierte Umformung
tiefgezogener Vorformen unter be-
sonderer Berücksichtigung maßge-
schneiderter Halbzeuge
LFT, 137 Seiten, 81 Bilder. 2007.
ISBN 978-3-87525-265-1.

Band 186: Bernd Zolleiß
Optimierte Prozesse und Systeme
für die Bestückung mechatroni-
scherBaugruppen
FAPS, 180 Seiten, 117 Bilder. 2007.
ISBN 978-3-87525-266-8.

Band 187: Michael Kerausch
Simulationsgestützte Prozessausle-
gung für das Umformen lokal wär-
mebehandelter Aluminiumplati-
nen
LFT, 146 Seiten, 76 Bilder, 7 Tab.
2007. ISBN 978-3-87525-267-5.

Band 188: Matthias Weber
Unterstützung der Wandlungsfä-
higkeit von Produktionsanlagen
durch innovative Softwaresysteme
FAPS, 183 Seiten, 122 Bilder, 3 Tab.
2007. ISBN 978-3-87525-269-9.

Band 189: Thomas Frick
Untersuchung der prozessbestim-
menden Strahl-Stoff-Wechselwir-
kungen beim Laserstrahlschwei-
ßen von Kunststoffen
LFT, 104 Seiten, 62 Bilder, 8 Tab.
2007. ISBN 978-3-87525-268-2.

Band 190: Joachim Hecht
Werkstoffcharakterisierung und
Prozessauslegung für die wirk-
medienbasierte Doppelblech-Um-
formung von Magnesiumlegierun-
gen
LFT, 107 Seiten, 91 Bilder, 2 Tab.
2007. ISBN 978-3-87525-270-5.

Band 191: Ralf Völkl
Stochastische Simulation zur
Werkzeuglebensdaueroptimierung
und Präzisionsfertigung in der
Kaltmassivumformung
LFT, 178 Seiten, 75 Bilder, 12 Tab.
2008. ISBN 978-3-87525-272-9.

Band 192: Massimo Tolazzi
Innenhochdruck-Umformen ver-
stärkter Blech-Rahmenstrukturen
LFT, 164 Seiten, 85 Bilder, 7 Tab.
2008. ISBN 978-3-87525-273-6.

Band 193: Cornelia Hoff
Untersuchung der Prozesseinfluss-
größen beim Presshärten des
höchstfesten Vergütungsstahls
22MnB5
LFT, 133 Seiten, 92 Bilder, 5 Tab.
2008. ISBN 978-3-87525-275-0.

Band 194: Christian Alvarez
Simulationsgestützte Methoden
zur effizienten Gestaltung von Löt-
prozessen in der Elektronikpro-
duktion
FAPS, 149 Seiten, 86 Bilder, 8 Tab.
2008. ISBN 978-3-87525-277-4.

Band 195: Andreas Kunze
Automatisierte Montage von mak-
romechatronischen Modulen zur
flexiblen Integration in hybride
Pkw-Bordnetzsysteme
FAPS, 160 Seiten, 90 Bilder, 14 Tab.
2008.
ISBN 978-3-87525-278-1.

Band 196: Wolfgang Hußnätter
Grundlegende Untersuchungen
zur experimentellen Ermittlung
und zur Modellierung von Fließ-
ortkurven bei erhöhten Tempera-
turen
LFT, 152 Seiten, 73 Bilder, 21 Tab.
2008. ISBN 978-3-87525-279-8.

Band 197: Thomas Bigl
Entwicklung, angepasste Herstellungsverfahren und erweiterte Qualitätssicherung von einsatzgerechten elektronischen Baugruppen
FAPS, 175 Seiten, 107 Bilder, 14 Tab. 2008.
ISBN 978-3-87525-280-4.

Band 198: Stephan Roth
Grundlegende Untersuchungen zum Excimerlaserstrahl-Abtragen unter Flüssigkeitsfilmen
LFT, 113 Seiten, 47 Bilder, 14 Tab. 2008. ISBN 978-3-87525-281-1.

Band 199: Artur Giera
Prozesstechnische Untersuchungen zum Rührreibschweißen metallischer Werkstoffe
LFT, 179 Seiten, 104 Bilder, 36 Tab. 2008. ISBN 978-3-87525-282-8.

Band 200: Jürgen Lechler
Beschreibung und Modellierung des Werkstoffverhaltens von presshärtbaren Bor-Manganstählen
LFT, 154 Seiten, 75 Bilder, 12 Tab. 2009. ISBN 978-3-87525-286-6.

Band 201: Andreas Blankl
Untersuchungen zur Erhöhung der Prozessrobustheit bei der Innenhochdruck-Umformung von flächigen Halbzeugen mit vor- bzw. nachgeschalteten Laserstrahlfügeoperationen
LFT, 120 Seiten, 68 Bilder, 9 Tab. 2009. ISBN 978-3-87525-287-3.

Band 202: Andreas Schaller
Modellierung eines nachfrageorientierten Produktionskonzeptes für mobile Telekommunikationsgeräte
FAPS, 120 Seiten, 79 Bilder, 0 Tab. 2009. ISBN 978-3-87525-289-7.

Band 203: Claudius Schimpf
Optimierung von Zuverlässigkeitsuntersuchungen, Prüfabläufen und Nacharbeitsprozessen in der Elektronikproduktion
FAPS, 162 Seiten, 90 Bilder, 14 Tab. 2009.
ISBN 978-3-87525-290-3.

Band 204: Simon Dietrich
Sensoriken zur Schwerpunktslagebestimmung der optischen Prozessemissionen beim Laserstrahltiefschweißen
LFT, 138 Seiten, 70 Bilder, 5 Tab. 2009. ISBN 978-3-87525-292-7.

Band 205: Wolfgang Wolf
Entwicklung eines agentenbasierten Steuerungssystems zur Materialflussorganisation im wandelbaren Produktionsumfeld
FAPS, 167 Seiten, 98 Bilder. 2009. ISBN 978-3-87525-293-4.

Band 206: Steffen Polster
Laserdurchstrahlschweißen transparenter Polymerbauteile
LFT, 160 Seiten, 92 Bilder, 13 Tab. 2009. ISBN 978-3-87525-294-1.

Band 207: Stephan Manuel Dörfler
Rührreibschweißen von walzplattiertem Halbzeug und Aluminiumblech zur Herstellung flächiger Aluminiumschaum-Sandwich-Verbundstrukturen
LFT, 190 Seiten, 98 Bilder, 5 Tab. 2009. ISBN 978-3-87525-295-8.

Band 208: Uwe Vogt
Seriennahe Auslegung von Aluminium Tailored Heat Treated Blanks
LFT, 151 Seiten, 68 Bilder, 26 Tab. 2009. ISBN 978-3-87525-296-5.

Band 209: Till Laumann
Qualitative und quantitative Bewertung der Crashtauglichkeit von höchstfesten Stählen
LFT, 117 Seiten, 69 Bilder, 7 Tab. 2009. ISBN 978-3-87525-299-6.

Band 210: Alexander Diehl
Größeneffekte bei Biegeprozessen- Entwicklung einer Methodik zur Identifikation und Quantifizierung
LFT, 180 Seiten, 92 Bilder, 12 Tab. 2010. ISBN 978-3-87525-302-3.

Band 211: Detlev Staud
Effiziente Prozesskettenauslegung für das Umformen lokal wärmebehandelter und geschweißter Aluminiumbleche
LFT, 164 Seiten, 72 Bilder, 12 Tab. 2010. ISBN 978-3-87525-303-0.

Band 212: Jens Ackermann
Prozesssicherung beim Laserdurchstrahlschweißen thermoplastischer Kunststoffe
LPT, 129 Seiten, 74 Bilder, 13 Tab. 2010. ISBN 978-3-87525-305-4.

Band 213: Stephan Weidel
Grundlegende Untersuchungen zum Kontaktzustand zwischen Werkstück und Werkzeug bei umformtechnischen Prozessen unter tribologischen Gesichtspunkten
LFT, 144 Seiten, 67 Bilder, 11 Tab. 2010. ISBN 978-3-87525-307-8.

Band 214: Stefan Geißdörfer
Entwicklung eines mesoskopischen Modells zur Abbildung von Größeneffekten in der Kaltmassivumformung mit Methoden der FE-Simulation
LFT, 133 Seiten, 83 Bilder, 11 Tab. 2010. ISBN 978-3-87525-308-5.

Band 215: Christian Matzner
Konzeption produktspezifischer Lösungen zur Robustheitssteigerung elektronischer Systeme gegen die Einwirkung von Betauung im Automobil
FAPS, 165 Seiten, 93 Bilder, 14 Tab. 2010. ISBN 978-3-87525-309-2.

Band 216: Florian Schüßler
Verbindungs- und Systemtechnik für thermisch hochbeanspruchte und miniaturisierte elektronische Baugruppen
FAPS, 184 Seiten, 93 Bilder, 18 Tab. 2010.
ISBN 978-3-87525-310-8.

Band 217: Massimo Cojutti
Strategien zur Erweiterung der Prozessgrenzen bei der Innhochdruck-Umformung von Rohren und Blechpaaren
LFT, 125 Seiten, 56 Bilder, 9 Tab. 2010. ISBN 978-3-87525-312-2.

Band 218: Raoul Plettke
Mehrkriterielle Optimierung komplexer Aktorsysteme für das Laserstrahljustieren
LFT, 152 Seiten, 25 Bilder, 3 Tab. 2010. ISBN 978-3-87525-315-3.

Band 219: Andreas Dobroschke
Flexible Automatisierungslösungen für die Fertigung wickeltechnischer Produkte
FAPS, 184 Seiten, 109 Bilder, 18 Tab. 2011.
ISBN 978-3-87525-317-7.

Band 220: Azhar Zam
Optical Tissue Differentiation for Sensor-Controlled Tissue-Specific Laser Surgery
LPT, 99 Seiten, 45 Bilder, 8 Tab. 2011. ISBN 978-3-87525-318-4.

Band 221: Michael Rösch
Potenziale und Strategien zur Optimierung des Schablonendruckprozesses in der Elektronikproduktion
FAPS, 192 Seiten, 127 Bilder, 19 Tab. 2011.
ISBN 978-3-87525-319-1.

Band 222: Thomas Rechtenwald
Quasi-isothermes Laserstrahlsintern von Hochtemperatur-Thermoplasten - Eine Betrachtung werkstoff-prozessspezifischer Aspekte am Beispiel PEEK
LPT, 150 Seiten, 62 Bilder, 8 Tab. 2011. ISBN 978-3-87525-320-7.

Band 223: Daniel Craiovan
Prozesse und Systemlösungen für die SMT-Montage optischer Bauelemente auf Substrate mit integrierten Lichtwellenleitern
FAPS, 165 Seiten, 85 Bilder, 8 Tab. 2011. ISBN 978-3-87525-324-5.

Band 224: Kay Wagner
Beanspruchungsangepasste Kaltmassivumformwerkzeuge durch lokal optimierte Werkzeugoberflächen
LFT, 147 Seiten, 103 Bilder, 17 Tab. 2011. ISBN 978-3-87525-325-2.

Band 225: Martin Brandhuber
Verbesserung der Prognosegüte des Versagens von Punktschweißverbindungen bei höchstfesten Stahlgüten
LFT, 155 Seiten, 91 Bilder, 19 Tab. 2011. ISBN 978-3-87525-327-6.

Band 226: Peter Sebastian Feuser
Ein Ansatz zur Herstellung von pressgehärteten Karosseriekomponenten mit maßgeschneiderten mechanischen Eigenschaften: Temperierte Umformwerkzeuge. Prozessfenster, Prozesssimuation und funktionale Untersuchung
LFT, 195 Seiten, 97 Bilder, 60 Tab. 2012. ISBN 978-3-87525-328-3.

Band 227: Murat Arbak
Material Adapted Design of Cold Forging Tools Exemplified by Powder Metallurgical Tool Steels and Ceramics
LFT, 109 Seiten, 56 Bilder, 8 Tab. 2012. ISBN 978-3-87525-330-6.

Band 228: Indra Pitz
Beschleunigte Simulation des Laserstrahlumformens von Aluminiumblechen
LPT, 137 Seiten, 45 Bilder, 27 Tab. 2012. ISBN 978-3-87525-333-7.

Band 229: Alexander Grimm
Prozessanalyse und -überwachung des Laserstrahlhartlötens mittels optischer Sensorik
LPT, 125 Seiten, 61 Bilder, 5 Tab. 2012. ISBN 978-3-87525-334-4.

Band 230: Markus Kaupper
Biegen von höhenfesten Stahlblechwerkstoffen - Umformverhalten und Grenzen der Biegbarkeit
LFT, 160 Seiten, 57 Bilder, 10 Tab. 2012. ISBN 978-3-87525-339-9.

Band 231: Thomas Kroiß
Modellbasierte Prozessauslegung für die Kaltmassivumformung unter Brücksichtigung der Werkzeug- und Pressenauffederung
LFT, 169 Seiten, 50 Bilder, 19 Tab. 2012. ISBN 978-3-87525-341-2.

Band 232: Christian Goth
Analyse und Optimierung der Entwicklung und Zuverlässigkeit räumlicher Schaltungsträger (3D-MID)
FAPS, 176 Seiten, 102 Bilder, 22 Tab. 2012.
ISBN 978-3-87525-340-5.

Band 233: Christian Ziegler
Ganzheitliche Automatisierung mechatronischer Systeme in der Medizin am Beispiel Strahlentherapie
FAPS, 170 Seiten, 71 Bilder, 19 Tab. 2012. ISBN 978-3-87525-342-9.

Band 234: Florian Albert
Automatisiertes Laserstrahllöten und -reparaturlöten elektronischer Baugruppen
LPT, 127 Seiten, 78 Bilder, 11 Tab. 2012. ISBN 978-3-87525-344-3.

Band 235: Thomas Stöhr
Analyse und Beschreibung des mechanischen Werkstoffverhaltens von presshärtbaren Bor-Mangan-stählen
LFT, 118 Seiten, 74 Bilder, 18 Tab. 2013. ISBN 978-3-87525-346-7.

Band 236: Christian Kägeler
Prozessdynamik beim Laserstrahlschweißen verzinkter Stahlbleche im Überlappstoß
LPT, 145 Seiten, 80 Bilder, 3 Tab. 2013. ISBN 978-3-87525-347-4.

Band 237: Andreas Sulzberger
Seriennahe Auslegung der Prozesskette zur wärmeunterstützten Umformung von Aluminiumblechwerkstoffen
LFT, 153 Seiten, 87 Bilder, 17 Tab. 2013. ISBN 978-3-87525-349-8.

Band 238: Simon Opel
Herstellung prozessangepasster Halbzeuge mit variabler Blechdicke durch die Anwendung von Verfahren der Blechmassivumformung
LFT, 165 Seiten, 108 Bilder, 27 Tab. 2013. ISBN 978-3-87525-350-4.

Band 239: Rajesh Kanawade
In-vivo Monitoring of Epithelium Vessel and Capillary Density for the Application of Detection of Clinical Shock and Early Signs of Cancer Development
LPT, 124 Seiten, 58 Bilder, 15 Tab. 2013. ISBN 978-3-87525-351-1.

Band 240: Stephan Busse
Entwicklung und Qualifizierung eines Schneidclinchverfahrens
LFT, 119 Seiten, 86 Bilder, 20 Tab. 2013. ISBN 978-3-87525-352-8.

Band 241: Karl-Heinz Leitz
Mikro- und Nanostrukturierung
mit kurz und ultrakurz gepulster
Laserstrahlung
LPT, 154 Seiten, 71 Bilder, 9 Tab.
2013. ISBN 978-3-87525-355-9.

Band 242: Markus Michl
Webbasierte Ansätze zur ganzheit-
lichen technischen Diagnose
FAPS, 182 Seiten, 62 Bilder, 20 Tab.
2013.
ISBN 978-3-87525-356-6.

Band 243: Vera Sturm
Einfluss von Chargenschwankun-
gen auf die Verarbeitungsgrenzen
von Stahlwerkstoffen
LFT, 113 Seiten, 58 Bilder, 9 Tab.
2013. ISBN 978-3-87525-357-3.

Band 244: Christian Neudel
Mikrostrukturelle und mecha-
nisch-technologische Eigenschaf-
ten widerstandspunktgeschweiß-
ter Aluminium-Stahl-Verbindun-
gen für den Fahrzeugbau
LFT, 178 Seiten, 171 Bilder, 31 Tab.
2014. ISBN 978-3-87525-358-0.

Band 245: Anja Neumann
Konzept zur Beherrschung der
Prozessschwankungen im Press-
werk
LFT, 162 Seiten, 68 Bilder, 15 Tab.
2014. ISBN 978-3-87525-360-3.

**Band 246: Ulf-Hermann Quen-
tin**
Laserbasierte Nanostrukturierung
mit optisch positionierten Mikro-
linsen
LPT, 137 Seiten, 89 Bilder, 6 Tab.
2014. ISBN 978-3-87525-361-0.

Band 247: Erik Lamprecht
Der Einfluss der Fertigungsverfah-
ren auf die Wirbelstromverluste
von Stator-Einzelzahnblechpake-
ten für den Einsatz in Hybrid- und
Elektrofahrzeugen
FAPS, 148 Seiten, 138 Bilder, 4 Tab.
2014. ISBN 978-3-87525-362-7.

Band 248: Sebastian Rösel
Wirkmedienbasierte Umformung
von Blechhalbzeugen unter An-
wendung magnetorheologischer
Flüssigkeiten als kombiniertes
Wirk- und Dichtmedium
LFT, 148 Seiten, 61 Bilder, 12 Tab.
2014. ISBN 978-3-87525-363-4.

Band 249: Paul Hippchen
Simulative Prognose der Geomet-
rie indirekt pressgehärteter Karos-
seriebauteile für die industrielle
Anwendung
LFT, 163 Seiten, 89 Bilder, 12 Tab.
2014. ISBN 978-3-87525-364-1.

Band 250: Martin Zubeil
Versagensprognose bei der Pro-
zesssimulation von Biegeumform-
und Falzverfahren
LFT, 171 Seiten, 90 Bilder, 5 Tab.
2014. ISBN 978-3-87525-365-8.

Band 251: Alexander Kühl
Flexible Automatisierung der Sta-
torenmontage mit Hilfe einer uni-
versellen ambidexteren Kinematik
FAPS, 142 Seiten, 60 Bilder, 26 Tab.
2014.
ISBN 978-3-87525-367-2.

Band 252: Thomas Albrecht
Optimierte Fertigungstechnolo-
gien für Rotoren getriebeintegrier-
ter PM-Synchronmotoren von
Hybridfahrzeugen
FAPS, 198 Seiten, 130 Bilder, 38
Tab. 2014.
ISBN 978-3-87525-368-9.

Band 253: Florian Risch
Planning and Production Concepts
for Contactless Power Transfer
Systems for Electric Vehicles
FAPS, 185 Seiten, 125 Bilder, 13 Tab.
2014.
ISBN 978-3-87525-369-6.

Band 254: Markus Weigl
Laserstrahlschweißen von Misch-
verbindungen aus austenitischen
und ferritischen korrosionsbestän-
digen Stahlwerkstoffen
LPT, 184 Seiten, 110 Bilder, 6 Tab.
2014. ISBN 978-3-87525-370-2.

Band 255: Johannes Noneder
Beanspruchungserfassung für die
Validierung von FE-Modellen zur
Auslegung von Massivumform-
werkzeugen
LFT, 161 Seiten, 65 Bilder, 14 Tab.
2014. ISBN 978-3-87525-371-9.

Band 256: Andreas Reinhardt
Ressourceneffiziente Prozess- und
Produktionstechnologie für fle-
xible Schaltungsträger
FAPS, 123 Seiten, 69 Bilder, 19 Tab.
2014. ISBN 978-3-87525-373-3.

Band 257: Tobias Schmuck
Ein Beitrag zur effizienten Gestal-
tung globaler Produktions- und
Logistiknetzwerke mittels Simula-
tion
FAPS, 151 Seiten, 74 Bilder. 2014.
ISBN 978-3-87525-374-0.

Band 258: Bernd Eichenhüller
Untersuchungen der Effekte und
Wechselwirkungen charakteristi-
scher Einflussgrößen auf das Um-
formverhalten bei Mikroumform-
prozessen
LFT, 127 Seiten, 29 Bilder, 9 Tab.
2014. ISBN 978-3-87525-375-7.

Band 259: Felix Lütteke
Vielseitiges autonomes Transport-
system basierend auf Weltmo-
dellerstellung mittels Datenfusion
von Deckenkameras und Fahr-
zeugsensoren
FAPS, 152 Seiten, 54 Bilder, 20 Tab.
2014.
ISBN 978-3-87525-376-4.

Band 260: Martin Grüner
Hochdruck-Blechumformung mit
formlos festen Stoffen als Wirkme-
dium
LFT, 144 Seiten, 66 Bilder, 29 Tab.
2014. ISBN 978-3-87525-379-5.

Band 261: Christian Brock
Analyse und Regelung des Laser-
strahltiefschweißprozesses durch
Detektion der Metalldampffackel-
position
LPT, 126 Seiten, 65 Bilder, 3 Tab.
2015. ISBN 978-3-87525-380-1.

Band 262: Peter Vatter
Sensitivitätsanalyse des 3-Rollen-
Schubbiegens auf Basis der Finite
Elemente Methode
LFT, 145 Seiten, 57 Bilder, 26 Tab.
2015. ISBN 978-3-87525-381-8.

Band 263: Florian Klämpfl
Planung von Laserbestrahlungen
durch simulationsbasierte Opti-
mierung
LPT, 169 Seiten, 78 Bilder, 32 Tab.
2015. ISBN 978-3-87525-384-9.

Band 264: Matthias Domke
Transiente physikalische Mechanismen bei der Laserablation von dünnen Metallschichten
LPT, 133 Seiten, 43 Bilder, 3 Tab. 2015. ISBN 978-3-87525-385-6.

Band 265: Johannes Götz
Community-basierte Optimierung des Anlagenengineerings
FAPS, 177 Seiten, 80 Bilder, 30 Tab. 2015.
ISBN 978-3-87525-386-3.

Band 266: Hung Nguyen
Qualifizierung des Potentials von Verfestigungseffekten zur Erweiterung des Umformvermögens aushärtbarer Aluminiumlegierungen
LFT, 137 Seiten, 57 Bilder, 16 Tab. 2015. ISBN 978-3-87525-387-0.

Band 267: Andreas Kuppert
Erweiterung und Verbesserung von Versuchs- und Auswertetechniken für die Bestimmung von Grenzformänderungskurven
LFT, 138 Seiten, 82 Bilder, 2 Tab. 2015. ISBN 978-3-87525-388-7.

Band 268: Kathleen Klaus
Erstellung eines Werkstofforientierten Fertigungsprozessfensters zur Steigerung des Formgebungsvermögens von Alumi-niumlegierungen unter Anwendung einer zwischengeschalteten Wärmebehandlung
LFT, 154 Seiten, 70 Bilder, 8 Tab. 2015. ISBN 978-3-87525-391-7.

Band 269: Thomas Svec
Untersuchungen zur Herstellung von funktionsoptimierten Bauteilen im partiellen Presshärtprozess mittels lokal unterschiedlich temperierter Werkzeuge
LFT, 166 Seiten, 87 Bilder, 15 Tab. 2015. ISBN 978-3-87525-392-4.

Band 270: Tobias Schrader
Grundlegende Untersuchungen zur Verschleißcharakterisierung beschichteter Kaltmassivumformwerkzeuge
LFT, 164 Seiten, 55 Bilder, 11 Tab. 2015. ISBN 978-3-87525-393-1.

Band 271: Matthäus Brela
Untersuchung von Magnetfeld-Messmethoden zur ganzheitlichen Wertschöpfungsoptimierung und Fehlerdetektion an magnetischen Aktoren
FAPS, 170 Seiten, 97 Bilder, 4 Tab. 2015. ISBN 978-3-87525-394-8.

Band 272: Michael Wieland
Entwicklung einer Methode zur Prognose adhäsiven Verschleißes an Werkzeugen für das direkte Presshärten
LFT, 156 Seiten, 84 Bilder, 9 Tab. 2015. ISBN 978-3-87525-395-5.

Band 273: René Schramm
Strukturierte additive Metallisierung durch kaltaktives Atmosphärendruckplasma
FAPS, 136 Seiten, 62 Bilder, 15 Tab. 2015. ISBN 978-3-87525-396-2.

Band 274: Michael Lechner
Herstellung beanspruchungsangepasster Aluminiumblechhalbzeuge durch eine maßgeschneiderte Variation der Abkühlgeschwindigkeit nach Lösungsglühen
LFT, 136 Seiten, 62 Bilder, 15 Tab. 2015. ISBN 978-3-87525-397-9.

Band 275: Kolja Andreas
Einfluss der Oberflächenbeschaffenheit auf das Werkzeugeinsatzverhalten beim Kaltfließpressen
LFT, 169 Seiten, 76 Bilder, 4 Tab. 2015. ISBN 978-3-87525-398-6.

Band 276: Marcus Baum
Laser Consolidation of ITO Nanoparticles for the Generation of Thin Conductive Layers on Transparent Substrates
LPT, 158 Seiten, 75 Bilder, 3 Tab. 2015. ISBN 978-3-87525-399-3.

Band 277: Thomas Schneider
Umformtechnische Herstellung dünnwandiger Funktionsbauteile aus Feinblech durch Verfahren der Blechmassivumformung
LFT, 188 Seiten, 95 Bilder, 7 Tab. 2015. ISBN 978-3-87525-401-3.

Band 278: Jochen Merhof
Sematische Modellierung automatisierter Produktionssysteme zur Verbesserung der IT-Integration zwischen Anlagen-Engineering und Steuerungsebene
FAPS, 157 Seiten, 88 Bilder, 8 Tab. 2015. ISBN 978-3-87525-402-0.

Band 279: Fabian Zöller
Erarbeitung von Grundlagen zur Abbildung des tribologischen Systems in der Umformsimulation
LFT, 126 Seiten, 51 Bilder, 3 Tab. 2016. ISBN 978-3-87525-403-7.

Band 280: Christian Hezler
Einsatz technologischer Versuche zur Erweiterung der Versagensvorhersage bei Karosseriebauteilen aus höchstfesten Stählen
LFT, 147 Seiten, 63 Bilder, 44 Tab. 2016. ISBN 978-3-87525-404-4.

Band 281: Jochen Bönig
Integration des Systemverhaltens von Automobil-Hochvoltleitungen in die virtuelle Absicherung durch strukturmechanische Simulation
FAPS, 177 Seiten, 107 Bilder, 17 Tab. 2016.
ISBN 978-3-87525-405-1.

Band 282: Johannes Kohl
Automatisierte Datenerfassung für diskret ereignisorientierte Simulationen in der energieflexiblen Fabrik
FAPS, 160 Seiten, 80 Bilder, 27 Tab. 2016.
ISBN 978-3-87525-406-8.

Band 283: Peter Bechtold
Mikroschockwellenumformung mittels ultrakurzer Laserpulse
LPT, 155 Seiten, 59 Bilder, 10 Tab. 2016. ISBN 978-3-87525-407-5.

Band 284: Stefan Berger
Laserstrahlschweißen thermoplastischer Kohlenstofffaserverbundwerkstoffe mit spezifischem Zusatzdraht
LPT, 118 Seiten, 68 Bilder, 9 Tab. 2016. ISBN 978-3-87525-408-2.

Band 285: Martin Bornschlegl
Methods-Energy Measurement -
Eine Methode zur Energieplanung
für Fügeverfahren im Karosserie-
bau
FAPS, 136 Seiten, 72 Bilder, 46 Tab.
2016.
ISBN 978-3-87525-409-9.

Band 286: Tobias Rackow
Erweiterung des Unterneh-
menscontrollings um die Dimen-
sion Energie
FAPS, 164 Seiten, 82 Bilder, 29 Tab.
2016.
ISBN 978-3-87525-410-5.

Band 287: Johannes Koch
Grundlegende Untersuchungen
zur Herstellung zyklisch-symmet-
rischer Bauteile mit Nebenform-
elementen durch Blechmassivum-
formung
LFT, 125 Seiten, 49 Bilder, 17 Tab.
2016. ISBN 978-3-87525-411-2.

**Band 288: Hans Ulrich Vierzig-
mann**
Beitrag zur Untersuchung der tri-
bologischen Bedingungen in der
Blechmassivumformung - Bereit-
stellung von tribologischen Mo-
dellversuchen und Realisierung
von Tailored Surfaces
LFT, 174 Seiten, 102 Bilder, 34 Tab.
2016. ISBN 978-3-87525-412-9.

Band 289: Thomas Senner
Methodik zur virtuellen Absiche-
rung der formgebenden Operation
des Nasspressprozesses von Ge-
lege-Mehrschichtverbunden
LFT, 156 Seiten, 96 Bilder, 21 Tab.
2016. ISBN 978-3-87525-414-3.

Band 290: Sven Kreitlein
Der grundoperationsspezifische
Mindestenergiebedarf als Refe-
renzwert zur Bewertung der Ener-
gieeffizienz in der Produktion
FAPS, 185 Seiten, 64 Bilder, 30 Tab.
2016.
ISBN 978-3-87525-415-0.

Band 291: Christian Roos
Remote-Laserstrahlschweißen ver-
zinkter Stahlbleche in Kehlnahtge-
ometrie
LPT, 123 Seiten, 52 Bilder, 0 Tab.
2016. ISBN 978-3-87525-416-7.

**Band 292: Alexander Kahrima-
nidis**
Thermisch unterstützte Umfor-
mung von Aluminiumblechen
LFT, 165 Seiten, 103 Bilder, 18 Tab.
2016. ISBN 978-3-87525-417-4.

Band 293: Jan Tremel
Flexible Systems for Permanent
Magnet Assembly and Magnetic
Rotor Measurement / Flexible Sys-
teme zur Montage von Permanent-
magneten und zur Messung mag-
netischer Rotoren
FAPS, 152 Seiten, 91 Bilder, 12 Tab.
2016. ISBN 978-3-87525-419-8.

Band 294: Ioannis Tsoupis
Schädigungs- und Versagensver-
halten hochfester Leichtbauwerk-
stoffe unter Biegebeanspruchung
LFT, 176 Seiten, 51 Bilder, 6 Tab.
2017. ISBN 978-3-87525-420-4.

Band 295: Sven Hildering
Grundlegende Untersuchungen
zum Prozessverhalten von Silizium
als Werkzeugwerkstoff für das
Mikroscherschneiden metallischer
Folien
LFT, 177 Seiten, 74 Bilder, 17 Tab.
2017. ISBN 978-3-87525-422-8.

**Band 296: Sasia Mareike Hert-
weck**
Zeitliche Pulsformung in der La-
sermikromaterialbearbeitung –
Grundlegende Untersuchungen
und Anwendungen
LPT, 146 Seiten, 67 Bilder, 5 Tab.
2017. ISBN 978-3-87525-423-5.

Band 297: Paryanto
Mechatronic Simulation Approach
for the Process Planning of En-
ergy-Efficient Handling Systems
FAPS, 162 Seiten, 86 Bilder, 13 Tab.
2017. ISBN 978-3-87525-424-2.

Band 298: Peer Stenzel
Großserientaugliche Nadelwickel-
technik für verteilte Wicklungen
im Anwendungsfall der E-Trakti-
onsantriebe
FAPS, 239 Seiten, 147 Bilder, 20
Tab. 2017.
ISBN 978-3-87525-425-9.

Band 299: Mario Lušić
Ein Vorgehensmodell zur Erstel-
lung montageführender Werkerin-
formationssysteme simultan zum
Produktentstehungsprozess
FAPS, 174 Seiten, 79 Bilder, 22 Tab.
2017.
ISBN 978-3-87525-426-6.

Band 300: Arnd Buschhaus
Hochpräzise adaptive Steuerung
und Regelung robotergeführter
Prozesse
FAPS, 202 Seiten, 96 Bilder, 4 Tab.
2017. ISBN 978-3-87525-427-3.

Band 301: Tobias Laumer
Erzeugung von thermoplastischen
Werkstoffverbunden mittels si-
multanem, intensitätsselektivem
Laserstrahlschmelzen
LPT, 140 Seiten, 82 Bilder, 0 Tab.
2017. ISBN 978-3-87525-428-0.

Band 302: Nora Unger
Untersuchung einer thermisch un-
terstützten Fertigungskette zur
Herstellung umgeformter Bauteile
aus der höherfesten Aluminiumle-
gierung EN AW-7020
LFT, 142 Seiten, 53 Bilder, 8 Tab.
2017. ISBN 978-3-87525-429-7.

Band 303: Tommaso Stellin
Design of Manufacturing Processes
for the Cold Bulk Forming of Small
Metal Components from Metal
Strip
LFT, 146 Seiten, 67 Bilder, 7 Tab.
2017. ISBN 978-3-87525-430-3.

Band 304: Bassim Bachy
Experimental Investigation, Mode-
ling, Simulation and Optimization
of Molded Interconnect Devices
(MID) Based on Laser Direct
Structuring (LDS) / Experimentelle
Untersuchung, Modellierung, Si-
mulation und Optimierung von
Molded Interconnect Devices
(MID) basierend auf Laser Direkt-
strukturierung (LDS)
FAPS, 168 Seiten, 120 Bilder, 26
Tab. 2017.
ISBN 978-3-87525-431-0.

Band 305: Michael Spahr
Automatisierte Kontaktierungsver-
fahren für flachleiterbasierte Pkw-
Bordnetzsysteme
FAPS, 197 Seiten, 98 Bilder, 17 Tab.
2017. ISBN 978-3-87525-432-7.

Band 306: Sebastian Suttner
Charakterisierung und Modellierung des spannungszustandsabhängigen Werkstoffverhaltens der Magnesiumlegierung AZ31B für die numerische Prozessauslegung
LFT, 150 Seiten, 84 Bilder, 19 Tab. 2017. ISBN 978-3-87525-433-4.

Band 307: Bhargav Potdar
A reliable methodology to deduce thermo-mechanical flow behaviour of hot stamping steels
LFT, 203 Seiten, 98 Bilder, 27 Tab. 2017. ISBN 978-3-87525-436-5.

Band 308: Maria Löffler
Steuerung von Blechmassivumformprozessen durch maßgeschneiderte tribologische Systeme
LFT, viii u. 166 Seiten, 90 Bilder, 5 Tab. 2018. ISBN 978-3-96147-133-1.

Band 309: Martin Müller
Untersuchung des kombinierten Trenn- und Umformprozesses beim Fügen artungleicher Werkstoffe mittels Schneidclinchverfahren
LFT, xi u. 149 Seiten, 89 Bilder, 6 Tab. 2018.
ISBN 978-3-96147-135-5.

Band 310: Christopher Kästle
Qualifizierung der Kupfer-Drahtbondtechnologie für integrierte Leistungsmodule in harschen Umgebungsbedingungen
FAPS, xii u. 167 Seiten, 70 Bilder, 18 Tab. 2018.
ISBN 978-3-96147-145-4.

Band 311: Daniel Vipavc
Eine Simulationsmethode für das 3-Rollen-Schubbiegen
LFT, xiii u. 121 Seiten, 56 Bilder, 17 Tab. 2018. ISBN 978-3-96147-147-8.

Band 312: Christina Ramer
Arbeitsraumüberwachung und autonome Bahnplanung für ein sicheres und flexibles Roboter-Assistenzsystem in der Fertigung
FAPS, xiv u. 188 Seiten, 57 Bilder, 9 Tab. 2018.
ISBN 978-3-96147-153-9.

Band 313: Miriam Rauer
Der Einfluss von Poren auf die Zuverlässigkeit der Lötverbindungen von Hochleistungs-Leuchtdioden
FAPS, xii u. 209 Seiten, 108 Bilder, 21 Tab. 2018.
ISBN 978-3-96147-157-7.

Band 314: Felix Tenner
Kamerabasierte Untersuchungen der Schmelze und Gasströmungen beim Laserstrahlschweißen verzinkter Stahlbleche
LPT, xxiii u. 184 Seiten, 94 Bilder, 7 Tab. 2018.
ISBN 978-3-96147-160-7.

Band 315: Aarief Syed-Khaja
Diffusion Soldering for High-temperature Packaging of Power Electronics
FAPS, x u. 202 Seiten, 144 Bilder, 32 Tab. 2018.
ISBN 978-3-87525-162-1.

Band 316: Adam Schaub
Grundlagenwissenschaftliche Untersuchung der kombinierten Prozesskette aus Umformen und Additive Fertigung
LFT, xi u. 192 Seiten, 72 Bilder, 27 Tab. 2019.
ISBN 978-3-96147-166-9.

Band 317: Daniel Gröbel
Herstellung von Nebenformelementen unterschiedlicher Geometrie an Blechen mittels Fließpressverfahren der Blechmassivumformung
LFT, x u. 165 Seiten, 96 Bilder, 13 Tab. 2019. ISBN 978-3-96147-168-3.

Band 318: Philipp Hildenbrand
Entwicklung einer Methodik zur Herstellung von Tailored Blanks mit definierten Halbzeugeigenschaften durch einen Taumelprozess
LFT, ix u. 153 Seiten, 77 Bilder, 4 Tab. 2019. ISBN 978-3-96147-174-4.

Band 319: Tobias Konrad
Simulative Auslegung der Spann- und Fixierkonzepte im Karosserierohbau: Bewertung der Baugruppenmaßhaltigkeit unter Berücksichtigung schwankender Einflussgrößen
LFT, x u. 203 Seiten, 134 Bilder, 32 Tab. 2019.
ISBN 978-3-96147-176-8.

Band 320: David Meinel
Architektur applikationsspezifischer Multi-Physics-Simulationskonfiguratoren am Beispiel modularer Triebzüge
FAPS, xii u. 166 Seiten, 82 Bilder, 25 Tab. 2019.
ISBN 978-3-96147-184-3.

Band 321: Andrea Zimmermann
Grundlegende Untersuchungen zum Einfluss fertigungsbedingter Eigenschaften auf die Ermüdungsfestigkeit kaltmassivumgeformter Bauteile
LFT, ix u. 160 Seiten, 66 Bilder, 5 Tab. 2019.
ISBN 978-3-96147-190-4.

Band 322: Christoph Amann
Simulative Prognose der Geometrie nassgepresster Karosseriebauteile aus Gelege-Mehrschichtverbunden
LFT, xvi u. 169 Seiten, 80 Bilder, 13 Tab. 2019.
ISBN 978-3-96147-194-2.

Band 323: Jennifer Tenner
Realisierung schmierstofffreier Tiefziehprozesse durch maßgeschneiderte Werkzeugoberflächen
LFT, x u. 187 Seiten, 68 Bilder, 13 Tab. 2019.
ISBN 978-3-96147-196-6.

Band 324: Susan Zöller
Mapping Individual Subjective Values to Product Design
KTmfk, xi u. 223 Seiten, 81 Bilder, 25 Tab. 2019.
ISBN 978-3-96147-202-4.

Band 325: Stefan Lutz
Erarbeitung einer Methodik zur semiempirischen Ermittlung der Umwandlungskinetik durchhärtender Wälzlagerstähle für die Wärmebehandlungssimulation
LFT, xiv u. 189 Seiten, 75 Bilder, 32 Tab. 2019.
ISBN 978-3-96147-209-3.

Band 326: Tobias Gnibl
Modellbasierte Prozesskettenabbildung rührreibgeschweißter Aluminiumhalbzeuge zur umformtechnischen Herstellung höchstfester Leichtbau-strukturteile
LFT, xii u. 167 Seiten, 68 Bilder, 17 Tab. 2019.
ISBN 978-3-96147-217-8.

Band 327: Johannes Bürner
Technisch-wirtschaftliche Optionen zur Lastflexibilisierung durch intelligente elektrische Wärmespeicher
FAPS, xiv u. 233 Seiten, 89 Bilder, 27 Tab. 2019.
ISBN 978-3-96147-219-2.

Band 328: Wolfgang Böhm
Verbesserung des Umformverhaltens von mehrlagigen Aluminiumblechwerkstoffen mit ultrafeinkörnigem Gefüge
LFT, ix u. 160 Seiten, 88 Bilder, 14 Tab. 2019.
ISBN 978-3-96147-227-7.

Band 329: Stefan Landkammer
Grundsatzuntersuchungen, mathematische Modellierung und Ableitung einer Auslegungsmethodik für Gelenkantriebe nach dem Spinnenbeinprinzip
LFT, xii u. 200 Seiten, 83 Bilder, 13 Tab. 2019.
ISBN 978-3-96147-229-1.

Band 330: Stephan Rapp
Pump-Probe-Ellipsometrie zur Messung transienter optischer Materialeigen-schaften bei der Ultrakurzpuls-Lasermaterialbearbeitung
LPT, xi u. 143 Seiten, 49 Bilder, 2 Tab. 2019.
ISBN 978-3-96147-235-2.

Band 331: Michael Scholz
Intralogistics Execution System mit integrierten autonomen, servicebasierten Transportentitäten
FAPS, xi u. 195 Seiten, 55 Bilder, 11 Tab. 2019.
ISBN 978-3-96147-237-6.

Band 332: Eva Bogner
Strategien der Produktindividualisierung in der produzierenden Industrie im Kontext der Digitalisierung
FAPS, ix u. 201 Seiten, 55 Bilder, 28 Tab. 2019.
ISBN 978-3-96147-246-8.

Band 333: Daniel Benjamin Krüger
Ein Ansatz zur CAD-integrierten muskuloskelettalen Analyse der Mensch-Maschine-Interaktion
KTmfk, x u. 217 Seiten, 102 Bilder, 7 Tab. 2019.
ISBN 978-3-96147-250-5.

Band 334: Thomas Kuhn
Qualität und Zuverlässigkeit laserdirektstrukturierter mechatronisch integrierter Baugruppen (LDS-MID)
FAPS, ix u. 152 Seiten, 69 Bilder, 12 Tab. 2019.
ISBN: 978-3-96147-252-9.

Band 335: Hans Fleischmann
Modellbasierte Zustands- und Prozessüberwachung auf Basis sozio-cyber-physischer Systeme
FAPS, xi u. 214 Seiten, 111 Bilder, 18 Tab. 2019.
ISBN: 978-3-96147-256-7.

Band 336: Markus Michalski
Grundlegende Untersuchungen zum Prozess- und Werkstoffverhalten bei schwingungsüberlagerter Umformung
LFT, xii u. 197 Seiten, 93 Bilder, 11 Tab. 2019.
ISBN: 978-3-96147-270-3.

Band 337: Markus Brandmeier
Ganzheitliches ontologiebasiertes Wissensmanagement im Umfeld der industriellen Produktion
FAPS, xi u. 255 Seiten, 77 Bilder, 33 Tab. 2020.
ISBN: 978-3-96147-275-8.

Band 338: Stephan Purr
Datenerfassung für die Anwendung lernender Algorithmen bei der Herstellung von Blechformteilen
LFT, ix u. 165 Seiten, 48 Bilder, 4 Tab. 2020.
ISBN: 978-3-96147-281-9.

Band 339: Christoph Kiener
Kaltfließpressen von gerad- und schrägverzahnten Zahnrädern
LFT, viii u. 151 Seiten, 81 Bilder, 3 Tab. 2020.
ISBN 978-3-96147-287-1.

Band 340: Simon Spreng
Numerische, analytische und empirische Modellierung des Heißcrimpprozesses
FAPS, xix u. 204 Seiten, 91 Bilder, 27 Tab. 2020.
ISBN 978-3-96147-293-2.

Band 341: Patrik Schwingenschlögl
Erarbeitung eines Prozessverständnisses zur Verbesserung der tribologischen Bedingungen beim Presshärten
LFT, x u. 177 Seiten, 81 Bilder, 8 Tab. 2020.
ISBN 978-3-96147-297-0.

Band 342: Emanuela Affronti
Evaluation of failure behaviour of sheet metals
LFT, ix u. 136 Seiten, 57 Bilder, 20 Tab. 2020.
ISBN 978-3-96147-303-8.

Band 343: Julia Degner
Grundlegende Untersuchungen zur Herstellung hochfester Aluminiumblechbauteile in einem kombinierten Umform- und Abschreckprozess
LFT, x u. 172 Seiten, 61 Bilder, 9 Tab. 2020.
ISBN 978-3-96147-307-6.

Band 344: Maximilian Wagner
Automatische Bahnplanung für die Aufteilung von Prozessbewegungen in synchrone Werkstück- und Werkzeugbewegungen mittels Multi-Roboter-Systemen
FAPS, xxi u. 181 Seiten, 111 Bilder, 15 Tab. 2020.
ISBN 978-3-96147-309-0.

Band 345: Stefan Härter
Qualifizierung des Montageprozesses hochminiaturisierter elektronischer Bauelemente
FAPS, ix u. 194 Seiten, 97 Bilder, 28 Tab. 2020.
ISBN 978-3-96147-314-4.

Band 346: Toni Donhauser
Ressourcenorientierte Auftragsregelung in einer hybriden Produktion mittels betriebsbegleitender Simulation
FAPS, xix u. 242 Seiten, 97 Bilder, 17 Tab. 2020.
ISBN 978-3-96147-316-8.

Band 347: Philipp Amend
Laserbasiertes Schmelzkleben von Thermoplasten mit Metallen
LPT, xv u. 154 Seiten, 67 Bilder. 2020. ISBN 978-3-96147-326-7.

Band 348: Matthias Ehlert
Simulationsunterstützte funktionale Grenzlagenabsicherung
KTmfk, xvi u. 300 Seiten, 101 Bilder, 73 Tab. 2020.
ISBN 978-3-96147-328-1.

Band 349: Thomas Sander
Ein Beitrag zur Charakterisierung und Auslegung des Verbundes von Kunststoffsubstraten mit harten Dünnschichten
KTmfk, xiv u. 178 Seiten, 88 Bilder, 21 Tab. 2020.
ISBN 978-3-96147-330-4.

Band 350: Florian Pilz
Fließpressen von Verzahnungselementen an Blechen
LFT, x u. 170 Seiten, 103Bilder, 4 Tab. 2020.
ISBN 978-3-96147-332-8.

Band 351: Sebastian Josef Katona
Evaluation und Aufbereitung von Produktsimulationen mittels abweichungsbehafteter Geometriemodelle
KTmfk, ix u. 147 Seiten, 73 Bilder, 11 Tab. 2020.
ISBN 978-3-96147-336-6.

Band 352: Jürgen Herrmann
Kumulatives Walzplattieren. Bewertung der Umformeigenschaften mehrlagiger Blechwerkstoffe der ausscheidungshärtbaren Legierung AA6014
LFT, x u. 157 Seiten, 64 Bilder, 5 Tab. 2020.
ISBN 978-3-96147-344-1.

Band 353: Christof Küstner
Assistenzsystem zur Unterstützung der datengetriebenen Produktentwicklung
KTmfk, xii u. 219 Seiten, 63 Bilder, 14 Tab. 2020.
ISBN 978-3-96147-348-9.

Band 354: Tobias Gläßel
Prozessketten zum Laserstrahlschweißen von flachleiterbasierten Formspulenwicklungen für automobile Traktionsantriebe
FAPS, xiv u. 206 Seiten, 89 Bilder, 11 Tab. 2020.
ISBN 978-3-96147-356-4.

Band 355: Andreas Meinel
Experimentelle Untersuchung der Auswirkungen von Axialschwingungen auf Reibung und Verschleiß in Zylinderrol-lenlagern
KTmfk, xii u. 162 Seiten, 56 Bilder, 7 Tab. 2020.
ISBN 978-3-96147-358-8.

Band 356: Hannah Riedle
Haptische, generische Modelle weicher anatomischer Strukturen für die chirurgische Simulation
FAPS, xxx u. 179 Seiten, 82 Bilder, 35 Tab. 2020.
ISBN 978-3-96147-367-0.

Band 357: Maximilian Landgraf
Leistungselektronik für den Einsatz dielektrischer Elastomere in aktorischen, sensorischen und integrierten sensomotorischen Systemen
FAPS, xxiii u. 166 Seiten, 71 Bilder, 10 Tab. 2020.
ISBN 978-3-96147-380-9.

Band 358: Alireza Esfandyari
Multi-Objective Process Optimization for Overpressure Reflow Soldering in Electronics Production
FAPS, xviii u. 175 Seiten, 57 Bilder, 23 Tab. 2020.
ISBN 978-3-96147-382-3.

Band 359: Christian Sand
Prozessübergreifende Analyse komplexer Montageprozessketten mittels Data Mining
FAPS, XV u. 168 Seiten, 61 Bilder, 12 Tab. 2021.
ISBN 978-3-96147-398-4.

Band 360: Ralf Merkl
Closed-Loop Control of a Storage-Supported Hybrid Compensation System for Improving the Power Quality in Medium Voltage Networks
FAPS, xxvii u. 200 Seiten, 102 Bilder, 2 Tab. 2021.
ISBN 978-3-96147-402-8.

Band 361: Thomas Reitberger
Additive Fertigung polymerer optischer Wellenleiter im Aerosol-Jet-Verfahren
FAPS, xix u. 141 Seiten, 65 Bilder, 11 Tab. 2021.
ISBN 978-3-96147-400-4.

Band 362: Marius Christian Fechter
Modellierung von Vorentwürfen in der virtuellen Realität mit natürlicher Fingerinteraktion
KTmfk, x u. 188 Seiten, 67 Bilder, 19 Tab. 2021.
ISBN 978-3-96147-404-2.

Band 363: Franziska Neubauer
Oberflächenmodifizierung und Entwicklung einer Auswertemethodik zur Verschleißcharakterisierung im Presshärteprozess
LFT, ix u. 177 Seiten, 42 Bilder, 6 Tab. 2021.
ISBN 978-3-96147-406-6.

Band 364: Eike Wolfram Schäffer
Web- und wissensbasierter Engineering-Konfigurator für roboterzentrierte Automatisierungslösungen
FAPS, xxiv u. 195 Seiten, 108 Bilder, 25 Tab. 2021.
ISBN 978-3-96147-410-3.

Band 365: Daniel Gross
Untersuchungen zur kohlenstoffdioxidbasierten kryogenen Minimalmengenschmierung
REP, xii u. 184 Seiten, 56 Bilder, 18 Tab. 2021.
ISBN 978-3-96147-412-7.

Band 366: Daniel Junker
Qualifizierung laser-additiv gefertigter Komponenten für den Einsatz im Werkzeugbau der Massivumformung
LFT, vii u. 142 Seiten, 62 Bilder, 5 Tab. 2021.
ISBN 978-3-96147-416-5.

Band 367: Tallal Javied
Totally Integrated Ecology Management for Resource Efficient and Eco-Friendly Production
FAPS, xv u. 160 Seiten, 60 Bilder, 13 Tab. 2021.
ISBN 978-3-96147-418-9.

Band 368: David Marco Hochrein
Wälzlager im Beschleunigungsfeld – Eine Analysestrategie zur Bestimmung des Reibungs-, Axialschub- und Temperaturverhaltens von Nadelkränzen –
KTmfk, xiii u. 279 Seiten, 108 Bilder, 39 Tab. 2021.
ISBN 978-3-96147-420-2.

Band 369: Daniel Gräf
Funktionalisierung technischer Oberflächen mittels prozessüberwachter aerosolbasierter Drucktechnologie
FAPS, xxii u. 175 Seiten, 97 Bilder, 6 Tab. 2021.
ISBN 978-3-96147-433-2.

Band 370: Andreas Gröschl
Hochfrequent fokusabstandsmodulierte Konfokalsensoren für die Nanokoordinatenmesstechnik
FMT, x u. 144 Seiten, 98 Bilder, 6 Tab. 2021.
ISBN 978-3-96147-435-6.

Band 371: Johann Tüchsen
Konzeption, Entwicklung und Einführung des Assistenzsystems D-DAS für die Produktentwicklung elektrischer Motoren
KTmfk, xii u. 178 Seiten, 92 Bilder, 12 Tab. 2021.
ISBN 978-3-96147-437-0.

Band 372: Max Marian
Numerische Auslegung von Oberflächenmikrotexturen für geschmierte tribologische Kontakte
KTmfk, xviii u. 276 Seiten, 85 Bilder, 45 Tab. 2021.
ISBN 978-3-96147-439-4.

Band 373: Johannes Strauß
Die akustooptische Strahlformung in der Lasermaterialbearbeitung
LPT, xvi u. 113 Seiten, 48 Bilder. 2021. ISBN 978-3-96147-441-7.

Band 374: Martin Hohmann
Machine learning and hyper spectral imaging: Multi Spectral Endoscopy in the Gastro Intestinal Tract towards Hyper Spectral Endoscopy
LPT, x u. 137 Seiten, 62 Bilder, 29 Tab. 2021.
ISBN 978-3-96147-445-5.

Band 375: Timo Kordaß
Lasergestütztes Verfahren zur selektiven Metallisierung von epoxidharzbasierten Duromeren zur Steigerung der Integrationsdichte für dreidimensionale mechatronische Package-Baugruppen
FAPS, xviii u. 198 Seiten, 92 Bilder, 24 Tab. 2021.
ISBN 978-3-96147-443-1.

Band 376: Philipp Kestel
Assistenzsystem für den wissensbasierten Aufbau konstruktionsbegleitender Finite-Elemente-Analysen
KTmfk, xviii u. 209 Seiten, 57 Bilder, 17 Tab. 2021.
ISBN 978-3-96147-457-8.

Band 377: Martin Lerchen
Messverfahren für die pulverbettbasierte additive Fertigung zur Sicherstellung der Konformität mit geometrischen Produktspezifikationen
FMT, x u. 150 Seiten, 60 Bilder, 9 Tab. 2021.
ISBN 978-3- 96147-463-9.

Band 378: Michael Schneider
Inline-Prüfung der Permeabilität in weichmagnetischen Komponenten
FAPS, xxii u. 189 Seiten, 79 Bilder, 14 Tab. 2021.
ISBN 978-3-96147-465-3.

Band 379: Tobias Sprügel
Sphärische Detektorflächen als Unterstützung der Produktentwicklung zur Datenanalyse im Rahmen des Digital Engineering
KTmfk, xiii u. 213 Seiten, 84 Bilder, 33 Tab. 2021.
ISBN 978-3-96147-475-2.

Band 380: Tom Häfner
Multipulseffekte beim Mikro-Materialabtrag von Stahllegierungen mit Pikosekunden-Laserpulsen
LPT, xxviii u. 159 Seiten, 57 Bilder, 13 Tab. 2021.
ISBN 978-3-96147-479-0.

Band 381: Björn Heling
Einsatz und Validierung virtueller Absicherungsmethoden für abweichungs-behaftete Mechanismen im Kontext des Robust Design
KTmfk, xi u. 169 Seiten, 63 Bilder, 27 Tab. 2021.
ISBN 978-3-96147-487-5.

Band 382: Tobias Kolb
Laserstrahl-Schmelzen von Metallen mit einer Serienanlage – Prozesscharakterisierung und Erweiterung eines Überwachungssystems
LPT, xv u. 170 Seiten, 128 Bilder, 16 Tab. 2021.
ISBN 978-3-96147-491-2.

Band 383: Mario Meinhardt
Widerstandselementschweißen mit gestauchten Hilfsfügeelementen - Umformtechnische Wirkzusammenhänge zur Beeinflussung der Verbindungsfestigkeit
LFT, xii u. 189 Seiten, 87 Bilder, 4 Tab. 2022.
ISBN 978-3-96147-473-8.

Band 384: Felix Bauer
Ein Beitrag zur digitalen Auslegung von Fügeprozessen im Karosseriebau mit Fokus auf das Remote-Laserstrahlschweißen unter Einsatz flexibler Spanntechnik
LFT, xi u. 185 Seiten, 74 Bilder, 12 Tab. 2022.
ISBN 978-3-96147-498-1.

Band 385: Jochen Zeitler
Konzeption eines rechnergestützten Konstruktionssystems für optomechatronische Baugruppen
FAPS, xix u. 172 Seiten, 88 Bilder, 11 Tab. 2022.
ISBN 978-3-96147-499-8.

Band 386: Vincent Mann
Einfluss von Strahloszillation auf das Laserstrahlschweißen hochfester Stähle
LPT, xiii u. 172 Seiten, 103 Bilder, 18 Tab. 2022.
ISBN 978-3-96147-503-2.

Band 387: Chen Chen
Skin-equivalent opto-/elastofluidic in-vitro microphysiological vascular models for translational studies of optical biopsies
LPT, xx u. 126 Seiten, 60 Bilder, 10 Tab. 2022.
ISBN 978-3-96147-505-6.

Band 388: Stefan Stein
Laser drop on demand joining as bonding method for electronics assembly and packaging with high thermal requirements
LPT, x u. 112 Seiten, 54 Bilder, 10 Tab. 2022.
ISBN 978-3-96147-507-0

Band 389: Nikolaus Urban
Untersuchung des Laserstrahlschmelzens von Neodym-Eisen-Bor zur additiven Herstellung von Permanentmagneten
FAPS, x u. 174 Seiten, 88 Bilder, 18 Tab. 2022.
ISBN 978-3-96147-501-8.

Band 390: Yiting Wu
Großflächige Topographiemessungen mit einem Weißlichtinterferenzmikroskop und einem metrologischen Rasterkraftmikroskop
FMT, xii u. 142 Seiten, 68 Bilder, 11 Tab. 2022.
ISBN: 978-3-96147-513-1.

Band 391: Thomas Papke
Untersuchungen zur Umformbarkeit hybrider Bauteile aus Blechgrundkörper und additiv gefertigter Struktur
LFT, xii u. 194 Seiten, 71 Bilder, 16 Tab. 2022.
ISBN 978-3-96147-515-5.

Band 392: Bastian Zimmermann
Einfluss des Vormaterials auf die mehrstufige Kaltumformung vom Draht
LFT, xi u. 182 Seiten, 36 Bilder, 6 Tab. 2022.
ISBN 978-3-96147-519-3.

Band 393: Harald Völkl
Ein simulationsbasierter Ansatz zur Auslegung additiv gefertigter FLM-Faserverbundstrukturen
KTmfk, xx u. 204 Seiten, 95 Bilder, 22 Tab. 2022.
ISBN 978-3-96147-523-0.

Band 394: Robert Schulte
Auslegung und Anwendung prozessangepasster Halbzeuge für Verfahren der Blechmassivumformung
LFT, x u. 163 Seiten, 93 Bilder, 5 Tab. 2022.
ISBN 978-3-96147-525-4.

Band 395: Philipp Frey
Umformtechnische Strukturierung metallischer Einleger im Folgeverbund für mediendichte Kunststoff-Metall-Hybridbauteile
LFT, ix u. 180 Seiten, 83 Bilder, 7 Tab. 2022.
ISBN 978-3-96147-534-6.

Band 396: Thomas Johann Luft
Komplexitätsmanagement in der Produktentwicklung - Holistische Modellierung, Analyse, Visualisierung und Bewertung komplexer Systeme
KTmfk, xiii u. 510 Seiten, 166 Bilder, 16 Tab. 2022.
ISBN 978-3-96147-540-7.

Band 397: Li Wang
Evaluierung der Einsetzbarkeit des lasergestützten Verfahrens zur selektiven Metallisierung für die Verbesserung passiver Intermodulation in Hochfrequenzanwendungen
FAPS, xxii u.151 Seiten, 72 Bilder, 22 Tab. 2022.
ISBN 978-3-96147-542-1.

Band 398: Sebastian Reitelshöfer
Der Aerosol-Jet-Druck Dielektrischer Elastomere als additives Fertigungsverfahren für elastische mechatronische Komponenten
FAPS, xxv u. 206 Seiten, 87 Bilder, 13 Tab. 2022.
ISBN 978-3-96147-547-6.

Band 399: Alexander Meyer
Selektive Magnetmontage zur Verringerung des Rastmomentes permanenterregter Synchronmotoren
FAPS, xv u. 164 Seiten, 90 Bilder, 18 Tab. 2022.
ISBN 978-3-96147-555-1.

Band 400: Rong Zhao
Design verschleißreduzierender amorpher Kohlenstoffschichtsysteme für trockene tribologische Gleitkontakte
KTmfk, x u. 148 Seiten, 69 Bilder, 14 Tab. 2022.
ISBN 978-3-96147-557-5.

Band 401: Christian P. J. Schwarzer
Kupfersintern als Fügetechnologie für Leistungselektronik
FAPS, xxvii u. 234 Seiten, 125 Bilder, 24 Tab. 2022.
ISBN 978-3-96147-566-7.

Band 402: Alexander Horn
Grundlegende Untersuchungen zur Gradierung der mechanischen Eigenschaften pressgehärteter Bauteile durch eine örtlich begrenzte Aufkohlung
LFT, xii u. 204 Seiten, 58 Bilder, 6 Tab. 2022.
ISBN 978-3-96147-568-1.

Band 403: Artur Klos
Werkstoff- und umformtechnische Bewertung von hochfesten Aluminiumblechwerkstoffen für den Karosseriebau
LFT, x u. 192 Seiten, 73 Bilder, 12 Tab. 2022.
ISBN 978-3-96147-572-8.

Band 404: Harald Schmid
Ganzheitliche Erarbeitung eines Prozessverständnisses von Tiefziehprozessen mit Ziehsicken auf Basis mechanischer und tribologischer Analysen
LFT, xiii u. 211 Seiten, 78 Bilder, 5 Tab. 2022.
ISBN 978-3-96147-577-3.

Band 405: Johannes Henneberg
Blechmassivumformung von Funktionsbauteilen aus Bandmaterial
LFT, viii u. 176 Seiten, 101 Bilder, 2 Tab. 2022.
ISBN 978-3-96147-579-7.

Band 406: Anton Schmailzl
Festigkeits- und zeitoptimierte Prozessführung beim quasi-simultanen Laser-Durchstrahlschweißen
LPT, xiii u. 157 Seiten, 84 Bilder, 7 Tab. 2022.
ISBN 978-3-96147-583-4.

Band 407: Alexander Wolf
Modellierung und Vorhersage menschlichen Interaktionsverhaltens zur Analyse der Mensch-Produkt Interaktion
KTmfk, x u. 207 Seiten, 69 Bilder, 10 Tab. 2022.
ISBN 978-3-96147-585-8.

Band 408: Tim Weikert
Modifikationen amorpher Kohlenstoffschichten zur Anpassung der Reibungsbedingungen und zur Erhöhung des Verschleißschutzes
KTmfk, xvii u. 258 Seiten, 91 Bilder, 9 Tab. 2022.
ISBN 978-3-96147-589-6.

Band 409: Stefan Götz
Frühzeitiges konstruktionsbegleitendes Toleranzmanagement
KTmfk, ix u. 276 Seiten, 127 Bilder, 13 Tab. 2022.
ISBN 978-3-96147-593-3.

Band 410: Markus Hubert
Einsatzpotenziale der Rotationsschneidtechnologie in der Verarbeitung von metallischen Funktionsfolien für mechatronische Produkte
FAPS, xviii u. 139 Seiten, 86 Bilder, 7 Tab. 2022.
ISBN 978-3-96147-603-9.

Band 411: Manfred Vogel
Grundlagenuntersuchungen und Erarbeitung einer Methodik zur Herstellung maßgeschneiderter Halbzeuge auf Basis eines neuartigen flexiblen Walzprozesses
LFT, ix u. 176 Seiten, 61 Bilder, 11 Tab. 2022.
ISBN 978-3-96147-605-3.

Band 412: Michael Weigelt
Multidimensionale Optionenanalyse alternativer Antriebskonzepte für die individuelle Langstreckenmobilität
FAPS, xv u. 222 Seiten, 89 Bilder, 38 Tab. 2022.
ISBN 978-3-96147-607-7.

Band 413: Frank Bodendorf
Machine Learning im Cost Engineering des Supply Managements
FAPS, xiii u. 165 Seiten, 75 Bilder, 13 Tab. 2023.
ISBN 978-3-96147-609-1.

Band 414: Maximilian Metzner
Planung und Simulation taktiler, intelligenter und kollaborativer Roboterfähigkeiten in der Montage
FAPS, xix u. 174 Seiten, 72 Bilder, 3 Tab. 2023.
ISBN 978-3-96147-611-4.

Band 415: Tina Buker
Ein Ansatz zur Reduktion produktinduzierter Nutzerstigmatisierung durch Förderung einer gleichermaßen gebrauchstauglichen wie emotionalen Produktgestalt
KTmfk, x u. 236 Seiten, 54 Bilder, 44 Tab. 2022.
ISBN 978-3-96147-613-8.

Band 416: Marlene Kuhn
Model-based Traceability System Development for Complex Manufacturing Applying Blockchain and Graphs
FAPS, xv u. 167 Seiten, 63 Bilder, 10 Tab. 2022.
ISBN 978-3-96147-615-2.

Band 417: Benjamin Lengenfelder
Remote photoacoustic sensing using speckle-analysis for biomedical imaging
LPT, xv u. 124 Seiten, 86 Bilder, 10 Tab. 2023.
ISBN 978-3-96147-617-6.

Band 418: Benjamin Pohrer
Analyse des Zusammenhangs zwischen dem tribochemischen Aufbau von Grenzschichten und der Ausbildung von White Etching Crack-Schäden
KTmfk, xv u. 258 Seiten, 103 Bilder, 10 Tab. 2023.
ISBN 978-3-96147- 621-3.

Band 419: Matthias Friedlein
Zuverlässigkeitsmethoden zur Beschleunigung von Qualifizierungsuntersuchungen für Steckkontakte
FAPS, xxv u. 162 Seiten, 98 Bilder, 7 Tab. 2023.
ISBN 978-3-96147-625-1.

Band 420: Thomas Stoll
Laser Powder Bed Fusion von Kupfer auf Aluminiumoxid-Keramiken
FAPS, xxvii u. 236 Seiten, 103 Bilder, 11 Tab. 2023.
ISBN 978-3-96147-631-2.

Band 421: Eric Eschner
Relation of Particle Motion and Process Zone Formation as a Basis for Sensing Approaches within PBF-LB/M
LPT, xiv u. 143 Seiten, 87 Bilder, 0 Tab. 2023.
ISBN 978-3-96147-633-6.

Band 422: Fanuel Mehari
Laser-induced Breakdown Spectroscopy (LIBS) as a diagnostics tool for biological tissue analysis.
LPT, xv u. 145 Seiten, 68 Bilder, 12 Tab. 2023.
ISBN 978-3-96147-641-1.

Band 423: Uwe Leicht
Ultraschallüberlagertes Umformen und Verstemmen von Stahlwerkstoffen
LFT, xi u. 165 Seiten, 65 Bilder, 6 Tab. 2023.
ISBN 978-3-96147-643-5.

Band 424: Thomas Braun
Potenzialanalyse der plasmabasierten, strukturierten Metallisierung thermoaktiver Oberflächen im industriellen Hausbau
FAPS, xvii u. 152 Seiten, 72 Bilder, 11 Tab. 2023.
ISBN 978-3-96147-653-4.

Band 425: Reinhardt Seidel
Modellbasierte Optimierung des Selektivwellenlötprozesses
FAPS, xxii u. 167 Seiten, 73 Bilder, 23 Tab. 2023.
ISBN: 978-3-96147-651-0.

Band 426: Matthias Lenzen
Maßgeschneiderte Werkstoffcharakterisierung für die numerische Auslegung von Blechumformprozessen
LFT, xi u. 187 Seiten, 77 Bilder, 13 Tab. 2023.
ISBN: 978-3-96147-663-3.

Band 427: Matthias Graser
Analyse lokaler Kurzzeitwärmebehandlungsmethoden zur Verbesserung des Umformverhaltens und der Bauteileigenschaften von Aluminiumstrangpresshohlprofilen
LFT, xi u. 169 Seiten, 81 Bilder, 1 Tab. 2023.
ISBN: 978-3-96147-666-4.

Band 428: Markus Lieret
Sicheres autonomes Flugroboter-
system für den Einsatz im Produk-
tions- und Logistikumfeld
FAPS, xix u. 198 Seiten, 54 Bilder,
7 Tab. 2023.
ISBN 978-3-96147-668-8.

Band 429: Petar Vukovic
Simulation komplexer Kommuni-
kationssysteme in der Fertigungs-
automatisierung
FAPS, xiv u. 163 Seiten, 57 Bilder, 21
Tab. 2023.
ISBN 978-3-96147-673-2.

Band 430: Fabian Knieps
Finite Elemente Simulation dünns-
ter Verpackungsstähle: Entwick-
lung einer geeigneten Charakteri-
sierungs- und Validierungsstrate-
gie
LFT, xix, 189 Seiten, 122 Bilder, 17
Tab. 2023
ISBN 978-3-96147-689-3

Band 431: Julian Seßner
Multimodale Bildsegmentierung
gering strukturierter Umgebungen
für die Navigation am Beispiel
eines Assistenzsystems für sehbe-
einträchtigte Personen
FAPS, xxv, 203 Seiten, 57 Bilder, 25
Tab. 2023
ISBN 978-3-96147-697-8

Band 431: Benjamin Samuel Lutz
Smart Manufacturing System for
Process Optimization Regarding
Deviations among Material
Batches
FAPS, xix, 208 Seiten, 77 Bilder, 14
Tab. 2024
ISBN 978-3-96147-703-6

Kurzzusammenfassung

Aufgrund der Fortschritte digitaler Technologien strebt die subtraktive Fertigung nach intelligenten Werkzeugmaschinen, welche eine datengetriebene Selbstoptimierung ermöglichen. Als Beitrag zur Erreichung dieses Ziels wird in dieser Arbeit ein Ansatz zur Berücksichtigung der Einflüsse von Materialchargen vorgestellt.

Das beschriebene System nutzt dabei Bilder der verwendeten Schneidwerkzeuge, um deren Zustand zu erfassen. Es werden Methoden für die semantische Bildsegmentierung vorgeschlagen, durch welche die unterschiedlichen Verschleißdefekte erkannt und vermessen werden können. Zusätzlich werden neuartige Ansätze zur Generierung neuer sowie zur Adaption existierender Trainingsdaten auf neue Anwendungsfälle dargestellt.

Die Erkennung der Materialcharge während der Bearbeitung erfolgt anhand interner Steuerungssignale. Im Rahmen einer Signalvorverarbeitung werden dabei die hochfrequenten Signale zu charakteristischen Kennwerten aggregiert. Ein Algorithmus bewertet nun den Neuheitsgrad der aktuellen Charge. Ist diese bekannt wird eine Klassifizierung durchgeführt, andernfalls kommt ein Clusteralgorithmus zum Einsatz.

Mit diesen Informationen kann nun historisches Wissen für die Berechnung optimierter, chargen-spezifischer Schnittparameter verwendet werden. Zusätzlich ermöglicht das vorgestellte System das automatische Charakterisieren neuartiger Chargen, das kontinuierliche Verbessern der Modelle, sowie die effektive Anpassung an neue Anwendungsfälle.

With the recent advances in digital technologies, the subtractive manufacturing industry is striving for smart machine tools, capable of data-driven self-optimization. As a building block, this work proposes an approach for incorporating awareness regarding the material and its batch-specific characteristics for process optimization.

The proposed smart manufacturing system utilizes cutting tool images for an initial condition assessment. Methods are proposed for the semantic segmentation of the defect classes encountered in tool condition monitoring, enabling a detailed analysis regarding their presence, location, and size.

Furthermore, novel methods are proposed that support the image annotation process and the adaptation of existing training data to new scenes.

During machining, internal control data is used for material batch identification. The high-frequency control data is preprocessed, error-compensated, and aggregated into features. Using a novelty detection algorithm, unknown batches are identified. Subsequently, a classification algorithm is used to classify known batches, whereas a clustering approach is used to analyze unknown batches.

In a final step, historic process knowledge is used to compute optimized cutting parameters, thus enabling batch-adaptive machining. Furthermore, operational routines are proposed for the automated incorporation of material batches with novel behavior, continuous model improvement, and efficient adaptation to new machining scenarios.

9 783961 477036